AVANCES EN LA COMPRENSIÓN DE LA FUNCIÓN DE VTRNA2-1/NC886/SNC886S EN CÁNCER DE PRÓSTATA

Tesis de Doctorado

Programa de Desarrollo de las Ciencias Básicas (PEDECIBA)

Área Biología, Subárea Biología Celular y Molecular

Rafael Sebastián Fort Canobra

Laboratorio de Interacciones Moleculares

Facultad de Ciencias – Universidad de la República

Orientadora: Dra. María Ana Duhagon

Co-orientador: Dr. José Roberto Sotelo Silveira

Tribunal de Tesis:

Dr. Alfonso Cayota (Presidente)

Dr. Gustavo Folle

Dr. José Badano

CONTENIDO

RESUMEN

VtRNA2-1 es un ARN no codificante mediano cuya identidad ha sido controversial, siendo inicialmente anotado como hsa-mir-886, un precursor de microARNs (hsa-miR-886-3p y hsa-miR-886-5p), y luego como vtRNA2-1, al ser catalogado como un miembro de la familia de los ARN de tipo bóveda, en inglés "vault" ARNs (vtRNAs). Los vtRNAs son ARNs no codificantes que forman parte de la partícula vault, el complejo ribonucleoproteico más grande de la célula, compuesto por las proteínas MVP, TEP1 y PARP4 y por los vtRNAs del locus 1 (vtRNA1-1, vtRNA1-2 y vtRNA1-3). A pesar de que vtRNA2-1 procede evolutivamente de los vtRNAs, su función no estaría asociada a este complejo, encontrándose otras funciones relacionadas con la modulación de la actividad de las proteínas PKR y OAS1. Estos trabajos sugirieron su reclasificación como non-coding RNA 886 (nc886), dado que su función no estaría relacionada a los vtRNAs. Esta tesis estudió la función de vtRNA2-1/nc886 en cáncer de próstata. Determinamos que vtRNA2-1/nc886 actúa como un gen supresor de tumor de esta enfermedad y que se encuentra reprimido en la neoplasia debido a un incremento de la metilación en su promotor. En base al estudio de datos de metilación de grandes cohortes de cáncer de próstata, tales como la de adenocarcinoma de próstata del proyecto Atlas Genómico del Cáncer (PRAD-TCGA), observamos que el aumento en la metilación del promotor de vtRNA2-1/nc886 se encuentra asociado con un peor pronóstico clínico, reflejado por su asociación con una mayor puntuación de Gleason, un mayor valor de estadificación T y mayor recurrencia bioquímica. Asimismo, el aumento en la metilación del promotor de vtRNA2-1/nc886 conlleva a un concomitante descenso de su expresión y el resultante incremento de características neoplásicas. Evaluamos los efectos de la sobreexpresión estable de vtRNA2-1/nc886 respecto a un ARN control en líneas celulares tumorales de próstata (DU145 y LNCaP) y observamos una disminución en la viabilidad celular y de la capacidad invasiva *in vitro*, así como una disminución del crecimiento tumoral *in vivo*. Adicionalmente, determinamos la asociación entre la represión de vtRNA2-1/nc886 y la desrepresión de una firma molecular asociada a la proliferación celular en tumores de pacientes. Por otro lado, hemos mostrado que vtRNA2-1/nc886 puede funcionar como un precursor de pequeños ARNs no codificantes de tipo microARNs, como también ha sido evidenciado para otros vtRNAs. Determinamos que estos pequeños ARNs no codificantes derivados de vtRNA2-1/nc886 (snc886-3p/hsa-miR-886-3p y snc886-5p/hsa-miR-886-5p) serían producidos por el procesamiento específico de DICER y se asociarían al complejo RISC. El estudio de diferentes sets de datos públicos demostró que snc886-3p/hsa-miR-886-3p posee un patrón de expresión de tipo supresor de tumor en cáncer de próstata al igual que su precursor vtRNA2-1/nc886. Concordantemente, la sobreexpresión *in vitro* de snc886-3p/hsa-miR-886-3p en las líneas celulares DU145, LNCaP y PC3 reveló una

disminución de la viabilidad celular, un aumento de la apoptosis temprana y alteraciones del ciclo celular. La búsqueda de posibles genes blancos de acción utilizando microarreglos de expresión génica de células DU145 que sobreexpresan snc886-3p/hsa-miR-886-3p, reveló un enriquecimiento en ARNs mensajeros reprimidos que poseen sitios complementarios a la semilla de snc886-3p/hsa-miR-886-3p (6nt-kmer seed) en el 3´-UTR. Estos posibles genes blanco de acción directa están asociados a procesos celulares como el ciclo celular y la apoptosis. Los mismos también configuran una firma de expresión génica que se asocia con características clínicas de la enfermedad, incluida la capacidad de predecir la sobrevida libre de enfermedad de los pacientes. Finalmente, a través del metaanálisis de estudios transcriptómicos de pequeños ARNs no codificantes disponibles en bases de datos públicas, encontramos que durante la carcinogénesis ocurriría no solo una disminución de snc886-3p/hsa-miR-886-3p sino un aumento de snc886-5p/hsa-miR-886-5p. Estos resultados junto con la correlación de los niveles de snc886-5p/hsa-miR-886-5p y la clínica sugieren que podría actuar como oncogén en la próstata. El conjunto de nuestros datos indica que vtRNA2-1/nc886 ejerce su función principalmente mediante su transcrito de ARN de tamaño completo, pero también dando origen a 2 microARNs, uno supresor de tumor y otro que podría ser oncogénico; estos microARNs disminuyen y aumentan durante la carcinogénesis respectivamente. Teniendo en cuenta este complejo escenario, hipotetizamos que vtRNA2-1/nc886 podría generar así un triple impacto molecular, que probablemente involucre vías diferentes en el cáncer de próstata.

Motivados por la existencia de pocos datos masivos de expresión para los vtRNAs, y la comprensión de que la regulación de la cromatina es un factor determinante de la expresión de los transcritos de la ARN polimerasa III, estudiamos los datos de “The assay for transposase-accessible chromatin using sequencing” (ATAC-seq) y de metilación del promotor (microarreglos de metilación) para los 4 vtRNAs en el conjunto de muestras disponibles en el set Pan-Cáncer del TCGA. Confirmamos que los niveles de metilación del promotor de los vtRNAs representan una buena aproximación a los niveles de accesibilidad de la cromatina determinados por ATAC-seq. Producto de los análisis realizados, evidenciamos un perfil de accesibilidad a la cromatina y de metilación del promotor específico para cada vtRNA, y una posible co-regulación de la transcripción. El vtRNA1-1, y en menor medida el vtRNA1-3, presentan un estado de accesibilidad a la cromatina ubicua y constante en los diferentes tejidos evaluados y en los estadios tumoral y normal adyacente. Si bien vtRNA1-1, vtRNA1-2 y vtRNA2-1/nc886 correlacionan con una peor sobrevida de los pacientes, vtRNA1-2 y vtRNA2-1/nc886 son los que presentan mayor cambio en el tejido tumoral, posicionándose como OG y TSG/OG respectivamente. Llamativamente, revelamos que vtRNA2-1/nc886 estaría co-regulado con genes asociados con la respuesta inmune nativa o la inmunomodulación y que vtRNA1-2 se encuentra asociado con la proliferación y el proceso de herida-cicatrización. De hecho, observamos asociación entre la accesibilidad de la cromatina de los vtRNAs con otros

genes que terminan por sugerir que, en conjunto, los vtRNAs podrían encontrarse relacionados globalmente con la respuesta inmune en cáncer.

Estos resultados contribuyen con la comprensión de la función de vtRNA2-1/nc886 en cáncer de próstata y de la posible participación de los 4 vtRNAs en el cáncer.

Abreviaturas:

3p	brazo del extremo 3' del microARN
3'-UTR	región al 3’ no traducida
5-aza-CdR	5-AZA-2'-deoxicitidina
5-aza-CR	5-Azacitidina
5p	brazo del extremo 5' del microARN
5'-UTR	región al 5’ no traducida
ADN	Ácido Desoxirribonucleico
AR	Receptores de Andrógenos
ARN	Ácido Ribonucleico
ARNm	ARN mensajero
ASOs	Oligos Antisentidos
ATAC-seq	The Assay for Transposase-Accessible Chromatin with sequencing
CCP	Firma de genes asociada con la progresión del ciclo celular
CHC	Líneas Celulares Humanas Tumorales
Chip-Seq	Chromatin immunoprecipitation followed by sequencing
CPM	Counts Per Million
DRE	Examinación Dígito-Rectal
DSE	Secuencia de Elemento Distal
EBV	Virus Epstein-Barr
EMT	Transición Epitelio-Mesenquimal
EVs	Vesículas Extracelulares
FC	Fold Change
FDR	False Discovery Rate
FISH	Fluorescence *in situ* hybridization
GEO	Gene Expression Omnibus
HITS-CLIP	High-throughput sequencing of RNA isolated by crosslinking immunoprecipitation
IAV	Virus Influenza A
lncARNs	ARNs largos no codificantes
LOH	Pérdida de Heterocigosidad
MDR	Resistente a Multidrogas
miCLIP	Customized version of the individual-nucleotide-resolution crosslinking and immunoprecipitation (iCLIP) method
nc886	ARN no codificante 886
ncARNs	ARNs no codificantes
NPC	Complejo del Poro Nuclear
nt	nucleótidos
OG	Oncogén
pb	pares de bases
PIN	Neoplasia Intraepitelial Prostática
PNHC	Líneas Celulares Humanas Primarias Normales
PRAD-TCGA	Prostate Adenocarcinoma - The Cancer Genome Atlas
PrCa	Cáncer de Próstata
pre-microARN	precursor de microARNs
pri-microARN	microARN primario
PSA	Antígeno Prostático Específico
PSE	Secuencia de Elemento Proximal
RISC	Complejo de Silenciamiento Inducido por ARN
RNA-seq	RNA-sequencing
RNP	Complejos Ribonucleoproteico
RT-qPCR	Quantitative reverse transcription PCR

SILAC	Stable Isotope Labeling by/with Amino acids in Cell culture
snc886s	microARNs derivados de vtRNA2-1/nc886
sncARNs	ARNs pequeños no codificantes
snoRNAs	Small nucleolar RNAs
snRNAs	Small nuclear RNAs
SRA	Sequence Read Archive
sRNA-seq	Secuenciación masiva de pequeños ARNs no codificantes
svRNA	Pequeños ARNs derivados de vtRNA1-1
TCGA	The Cancer Genome Atlas
TMM	Trimmed Mean of M values
TNM	Estadificación clínica Tumor, Nodo, Metástasis
TSG	Gen Supresor de Tumor
vtRNA	vault RNA

INTRODUCCIÓN

I. EL CÁNCER

Cáncer es un término general utilizado para identificar un amplio número de patologías, que pueden afectar a cualquier órgano o tejido del cuerpo. Específicamente, puede definirse como un grupo heterogéneo de trastornos, caracterizados por la presencia de células que no responden a los controles normales de la división celular (Pierce et al., 1978). El cáncer puede tener un componente hereditario producto de mutaciones presentes en las células germinales, pero es mayormente esporádico, es decir, es el producto de mutaciones espontáneas y de la acción de agentes carcinógenos ambientales en ausencia de un componente heredado. Una gran variedad de factores se encuentra involucrados en el origen del cáncer e influyen en el riesgo de padecerlo. Estos incluyen tanto factores intrínsecos de la célula como también factores ambientales (virus, radiaciones o sustancias químicas), constatándose tempranamente que aproximadamente el 80% de los cánceres esporádicos son promovidos por la exposición ambiental (Guerrero & Pellicer, 1987). Incluso, se determinó que ciertas infecciones también pueden estimular e inducir el desarrollo del cáncer (Devi & Hossain, 2000; De Marzo et al., 2006). A pesar del intenso esfuerzo internacional destinado al conocimiento acerca de los cambios moleculares y celulares involucrados en el inicio y desarrollo del cáncer, aún continúa siendo el principal azote a la salud humana. El cáncer es la primera causa de muerte a nivel mundial, según la Agencia Internacional de Investigación en Cáncer (IARC, GLOBOCAN 2018). En 2018 hubo 18,1 millones de nuevos casos y 9,5 millones de muertes (Ferlay et al., 2019). De hecho, se estima que para el 2040 esta cifra aumente hasta los 30 millones de afectados (Figura 1) (Ferlay et al., 2019). En Uruguay se registraron más de 15.000 nuevos casos de cáncer en 2018 y es la segunda causa de muerte (aproximadamente el 25% del total) (Garau et al., 2019).

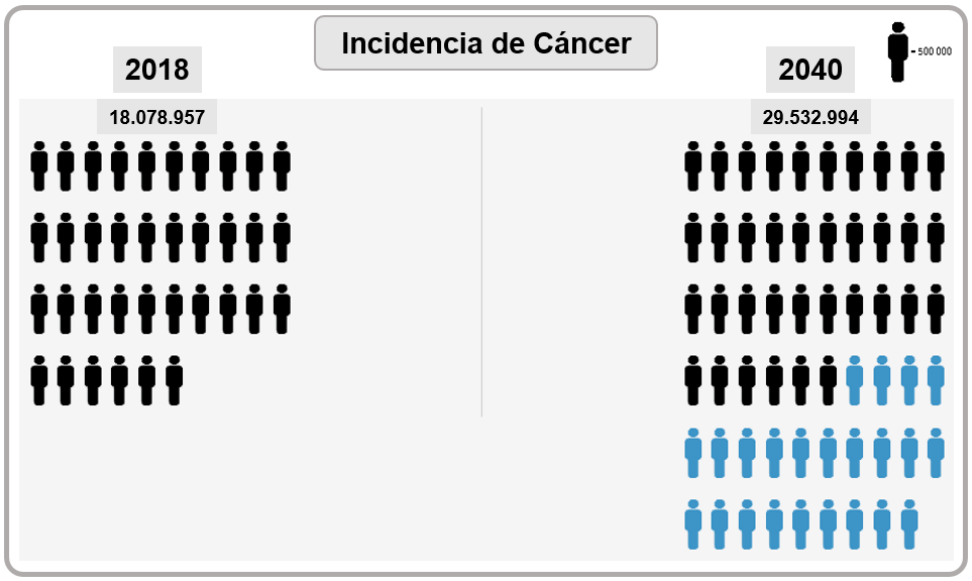

Figura 1. **Proyección de la incidencia del cáncer a nivel global.**

Esquema que expone el aumento de la proyección de la incidencia del cáncer a nivel global desde el 2018 al 2040, por la Agencia Internacional de Investigación en Cáncer (IARC, GLOBOCAN 2018). Imagen extraída y modificada de https://gco.iarc.fr/ Ferlay et al., 2019.

1. ASPECTOS BÁSICOS DEL DESARROLLO DEL CÁNCER.

La bibliografía acerca de la temática expone que, en el transcurso del proceso de carcinogénesis, existen una serie de cambios o alteraciones fenotípicas que resultan ineludibles o comunes en el proceso de transformación a células cancerosas. Estas alteraciones son revisadas en Hanahan & Weinberg, 2011 y se mencionan a continuación: capacidad de autosuficiencia en el desarrollo de señales de crecimiento y mantenimiento de señales de proliferación, evasión de las señales antiproliferativas, evasión del ataque inmune, promoción de la inflamación tumoral, activación y adquisición de capacidad invasiva (metástasis), inestabilidad genómica y mutaciones, energética celular desregulada, desarrollo de una capacidad proliferativa inmortal, inducción de la angiogénesis y resistencia a la muerte celular (Figura 2).

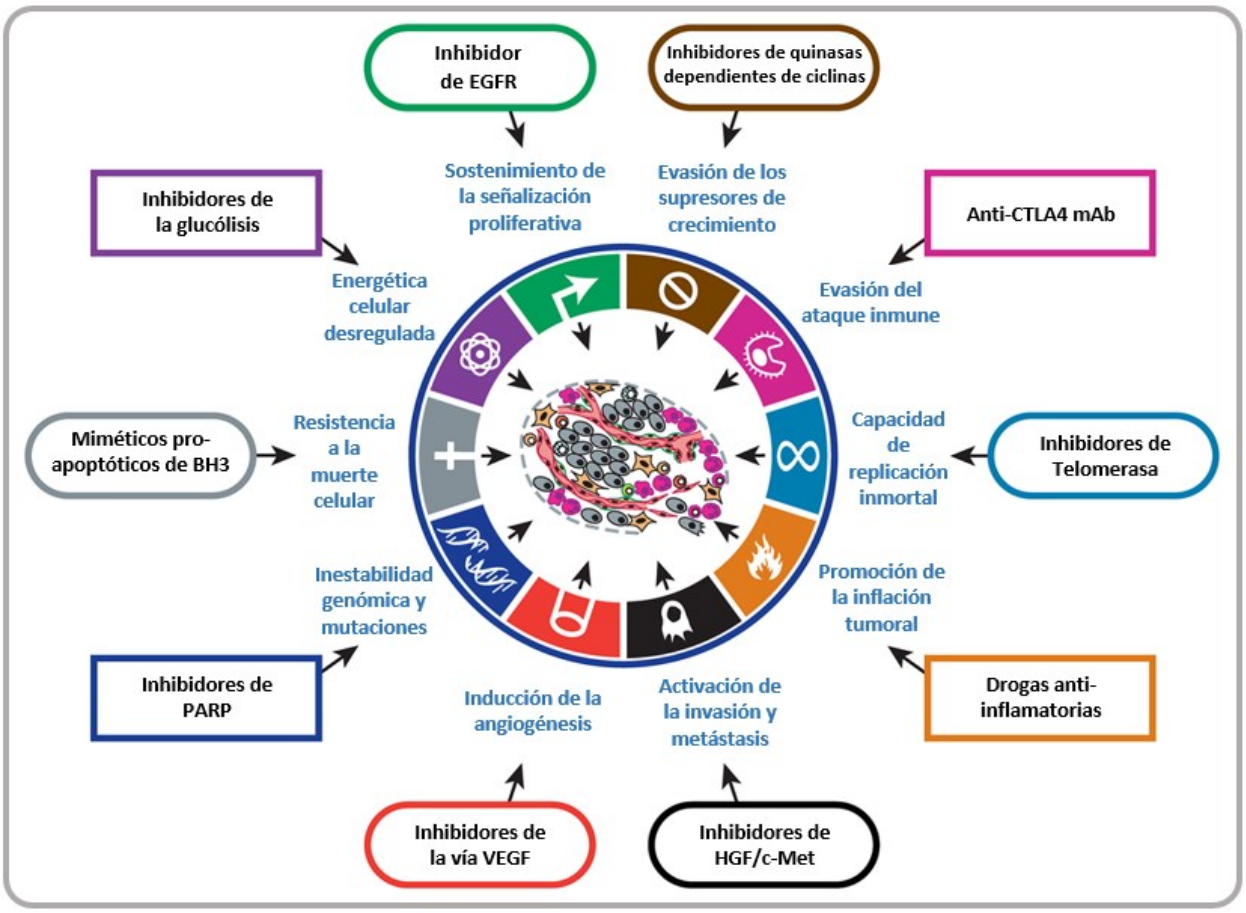

Figura 2. **Cambios o alteraciones fenotípicas comunes en el proceso de transformación a células cancerosas.**

Esquema que resume las diferentes capacidades o alteraciones que debe experimentar una célula normal en el desarrollo del cáncer (carcinogénesis) y sus potenciales drogas, inhibidores o puntos de control. Imagen extraída y modificada de Hanahan & Weinberg, 2011.

II. CÁNCER DE PRÓSTATA.

Dentro de los tumores sólidos, el cáncer de próstata (PrCa) es una de las enfermedades oncológicas de mayor incidencia en países occidentales. En nuestro país el PrCa tuvo una incidencia de 1510 casos en 2018 (19% de cáncer en hombres (Bray et al., 2018)) y es el tumor maligno más frecuente en hombres (Figura 3) (Barrios & Garau, 2017; Garau et al., 2019). De hecho, uno de cada seis hombres será diagnosticado con PrCa en su vida. El PrCa es actualmente reconocido como una enfermedad multifactorial. A pesar de que se reconoce un aporte ambiental al desarrollo del PrCa, se cree que la predisposición genética cumple un papel importante en el desarrollo de la enfermedad. De hecho, se estima que la predisposición genética al PrCa podría encontrarse entre un 10-20% (Brandão et al., 2020; Pritzlaff et al., 2020). Una gran variedad de factores influye en el riesgo de

padecer PrCa, incluyendo la edad, etnia, estilo de vida e historia familiar. Los hombres mayores de 65 años presentan el mayor riesgo de padecer PrCa (Zhang et al., 2019). Si consideramos las distintas etnias, los afroamericanos son quienes presentan la tasa más alta de riesgo de padecer PrCa, presentando un 50% más de probabilidades que los caucásicos de ser diagnosticados con PrCa (Farkas et al., 2000; Zhang et al., 2020). Los factores ambientales relacionados al PrCa son muy diversos, e involucran numerosos aspectos como la actividad sexual, la ingesta de grasa animal, la ingesta de alcohol, el tabaquismo, la obesidad, la ingesta de minerales (calcio, selenio, zinc) y vitaminas D y E (Kral et al., 2011).

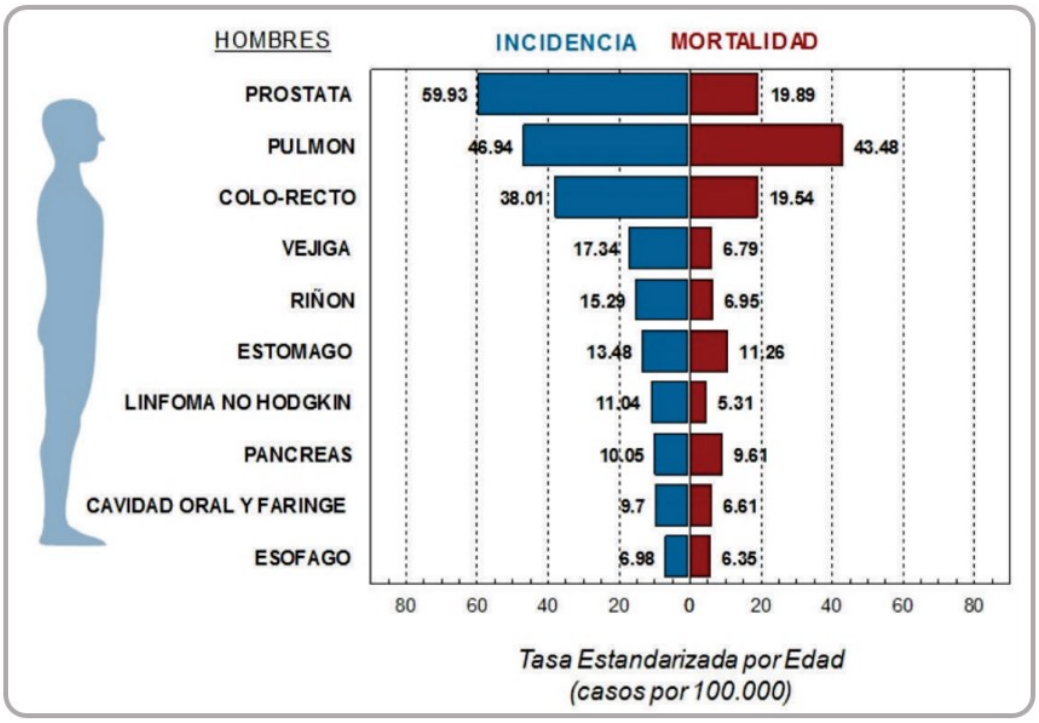

Figura 3. **Tasas de incidencia y mortalidad de los diferentes tipos de cáncer en hombres en Uruguay (2009 – 2013).**

Registro Nacional de Cáncer (RNC), Comisión Honoraria de la Lucha contra el Cáncer. Imagen extraída y modificada de Barrios & Garau, 2017.

1. Etiología del cáncer de próstata.

Una de las características que presenta el PrCa es la multifocalización, presentándose múltiples sitios de transformación neoplásica en la glándula prostática. Sin embargo, la mayoría de estos focos iniciales darán origen a la forma latente del PrCa, que no progresará a la enfermedad clínica agresiva (Abeshouse et al., 2015; Witte, 2009). La etapa precursora del PrCa es la denominada Neoplasia Intraepitelial Prostática (PIN) (De Marzo et al.,

2003, 2006). A nivel histológico en esta etapa se pueden observar algunas características distintivas, expansión del núcleo y nucléolo, aparición de hiperplasia epitelial luminal, estado hipercromático y atipia del núcleo. Asimismo, a nivel molecular se reportan aumentos en los niveles de los marcadores de proliferación celular (Shappell et al., 2004). En el desarrollo del PrCa, aquellas formas latentes que avancen a la forma clínica, en el 95% de los casos, serán clasificados como adenocarcinoma; siendo mayoritariamente adenocarcinomas acinares, que expresan los receptores de andrógenos (AR). Mientras que el tumor maligno no haya invadido el tejido circundante y se encuentre confinado en la cápsula prostática, se clasificará como carcinoma *in situ*. Si el tumor continúa progresando y comienza a invadir los tejidos circundantes, pasará a ser considerado invasivo. Sin embargo, si el desarrollo del mismo aún no ha alcanzado otros tejidos y órganos del cuerpo, se le denominará carcinoma primario. Para que sea clasificado como carcinoma secundario o metastásico, algunas células cancerosas deben trasladarse más allá del sitio original (primario), invadiendo otros órganos donde establecerán un nuevo foco. Las células tumorales invasivas (metastáticas) muestran la adquisición de inestabilidad genómica, que se refleja en los múltiples reordenamientos cromosómicos, observados típicamente en los estadios avanzados de la enfermedad (Holcomb et al., 2008, 2009). Los sitios más comunes de metástasis en el PrCa, suelen ser los ganglios linfáticos y el tejido óseo (caracterizado por las lesiones osteoblásticas) (Bubendorf et al., 2000; Fornetti et al., 2018; Gundem et al., 2015). Si bien el advenimiento de la era genómica dio lugar a grandes avances en la comprensión de las metástasis, sin embargo, la relación de las células tumorales y la formación de metástasis, sigue aún sin resolverse completamente. Asimismo, los factores moleculares que promueven y gobiernan la metástasis del PrCa al tejido óseo, se encuentran aún mal caracterizados (Sartor & De Bono, 2018).

2. DIAGNÓSTICO Y CLASIFICACIÓN CLÍNICA.

A pesar de que el PrCa es de alta incidencia, el curso indolente de la patología en conjunto con el potencial adverso del tratamiento, han generado controversias acerca de la detección temprana y el tratamiento de la enfermedad. La búsqueda de una definición del PrCa clínicamente significativo lleva décadas de investigación, aún hoy se continúa investigando la definición de los criterios clínicos y la interpretación de los métodos diagnósticos para diferenciar el PrCa que necesita intervención del que no la precisa (Matoso & Epstein, 2019). En este contexto, el examen físico es la primera aproximación al diagnóstico, la examinación dígito-rectal (DRE) en busca de masas o endurecimiento de la próstata son los primeros signos a evaluar. Complementariamente, la determinación de los niveles de PSA (antígeno prostático específico) en sangre es otro factor diagnóstico clave. Por tanto, niveles de PSA > 4ng/mL y un DRE sospechoso serán indicadores de posible PrCa (Castillejos-Molina & Gabilondo-Navarro, 2016). Sin embargo, a pesar de la alta sensibilidad del PSA, éste posee limitaciones debido a su baja especificidad que da lugar a falsos positivos. De hecho, existe variación en los niveles de PSA debido a variación entre individuos

o producto del trauma, inflamación e infecciones prostáticas que pueden elevar los niveles de PSA. Recientemente, el marcador PCA3 (un ARN no codificante específico de la próstata) que es cuantificado en el sedimento urinario, ha presentado ventajas frente al PSA debido a su mayor sensibilidad y especificidad, por no estar relacionado con el volumen de la próstata o la prostatitis. Sin embargo, su utilización en la clínica aún es limitada (Castillejos-Molina & Gabilondo-Navarro, 2016).

Actualmente, la biopsia de próstata es el método estándar para el diagnóstico del PrCa. Se basa en la evaluación al microscopio de biopsias extraídas mediante aguja, típicamente entre 10 y 12 muestras de tejido (5-6 por cada lóbulo de la próstata), guiadas por ultrasonido trans-rectal. Las muestras serán examinadas por un anatomopatólogo que realizará una categorización del tejido según la arquitectura y apariencia microscópica de las células. La categorización del grado de diferenciación histológica del tejido dará lugar una clasificación numérica, en una escala del 1 (diferenciado) al 5 (indiferenciado), llamado sistema de puntuación o categorización de Gleason (Litwin & Tan, 2017). El mismo consiste en la suma de los valores asignados a las categorizaciones del patrón histológico predominante primario y secundario del tejido prostático obtenido por las biopsias. Recientemente, se estableció una nueva reclasificación para los valores de puntuación de Gleason y la estratificación del cáncer de próstata. Se establecieron 5 grados, donde el grado 1 corresponde con un Gleason primario 3 + secundario 3; el grado 2 con 3 + 4; el grado 3 con 4 + 3; el grado 4 con 4 + 4, 3 + 5 y 5 + 3; el grado 5 con 4 + 5, 5 + 4 y 5 + 5 (ver Tabla 1 (Epstein et al., 2016; Litwin & Tan, 2017).

Tabla 1. **Estratificación del PrCa basado en la clasificación de Gleason.**

Grupos	Clasificación de Gleason	Descripción
Grado 1	3+3	Glándulas bien diferenciadas
Grado 2	3+4	Predominan glándulas bien diferenciadas, con un componente menor de tejido mas indiferenciado o cribiforme
Grado 3	4+3	Predominan glándulas poco diferenciadas o cribiformes, con un componente menor de tejido con glándulas bien diferenciadas
Grado 4	4+4, 3+5 y 5+3	Solo glándulas poco diferenciadas o cribiformes o tejido bien diferenciadas mas áreas con ausencia de glándulas
Grado 5	4+5, 5+4 y 5+5	Glándulas no diferenciadas o necróticas, con o sin zonas poco diferenciadas o cribiformes

Tabla extraída y modificada de Epstein et al., 2016.

Conjuntamente con las biopsias, la imagenología radiológica permitirá determinar la ubicación, extensión del tumor y la búsqueda de esparcimiento del tumor a nódulos linfáticos y a otros tejidos. En este sentido, la tomografía computada e imagenología de resonancia magnética han resultado muy útil para estos fines y para la determinación del estadio de la patología. La determinación de la estadificación del cáncer es importante para determinar el pronóstico y tratamiento. Generalmente, se utiliza la escala tumor, nodo, metástasis (TNM) para clasificar clínica y patológicamente los estadios de la enfermedad (ver Tabla 2 (Litwin & Tan, 2017)). Entonces, los médicos clínicos en base a la suma de la categorización de Gleason, los niveles de PSA (el antígeno específico prostático) y el estadio clínico podrán realizar una estadificación de la enfermedad y ponderar el riesgo de la misma. De hecho, la clasificación D'Amico (Hernandez et al., 2007) se basa en los parámetros antes mencionados para el establecimiento de 3 grupos de pacientes con diferente proporción de sobrevida a 10 años: 83% para bajo riesgo (Gleason 6, PSA < 10 ng/mL y estadio de T1-T2a), 46% para riesgo intermedio (Gleason 7, PSA 10-20 ng/mL y T2b) y 29% para alto riesgo (Gleason 8-10, PSA > 20 ng/mL y estadio mayor de T2c) (Castillejos-Molina & Gabilondo-Navarro, 2016; Hernandez et al., 2007; Litwin & Tan, 2017).

Tabla 2. **Clasificación del PrCa según el sistema TNM.**

Categorías TNM	Definición
T - tumor primario	
TX	El tumor primario no pudo ser juzgado
T0	No hay evidencia del tumor primario
T1x	El tumor no puede identificarse durante el DRE y no se observa durante las pruebas por imágenes. El tumor invade el tejido conectivo subepitelial, es subcategorizado: **a** 5 % o menos del tejido removido, **b** más del 5 % del tejido removido y **c** el paciente tenía un nivel elevado de PSA.
T2x	El tumor invade alguno de los siguientes: el estroma prostático, el cuerpo esponjoso o el músculo peritelial. Es subcategorizado: **a** cuando el tumor compromete la mitad de un lado de la próstata, **b** el tumor compromete más de la mitad de un lado de la próstata, pero no ambos lados, **c** el tumor ha crecido a ambos lados de la próstata.
T3x	El tumor invade alguno de los siguientes: el cuerpo cavernoso, fuera de la cápsula prostática, el cuello de la vejiga. Es subcategorizado: **a** el tumor ha crecido a través de la próstata (extensión extraprostática), **b** el tumor invadió la(s) vesícula(s) seminal(es), el (los) conducto(s) seminales.
T4	El tumor invade otros organos adyacentes: invade la vejiga o el recto
N - nódulos linfáticos regionales (Ganglio)	
NX	Los nódulos linfáticos no pudieron ser juzgados
N0	No hay metastasis en nódulos linfáticos regionales
N1	Metastasis en un nódulo linfático
N2	Metastasis en múltiples nódulos linfáticos
M - metastasis distantes	
M0	No hay metastasis distantes
M1	Metastasis distantes

Tabla extraída y modificada de Litwin & Tan, 2017.

3. UNA VISIÓN MOLECULAR DEL CÁNCER DE PRÓSTATA.

La literatura de la temática expuso una serie de genes que se encuentran asociados a las distintas etapas de la carcinogénesis del PrCa. Según su función, estos genes se clasifican como, genes supresores de tumor (TSG), oncogenes (OG) y genes cuidadores o "caretakers" (Tabla 3) (De Marzo et al., 2007; Tomlins et al., 2007). Estudios a nivel molecular, han revelado la presencia de una serie de eventos genéticos que se relacionan diferencialmente con el origen y etapas tempranas del PrCa, o con las etapas avanzadas y metastáticas de la patología. Los cambios implicados con el origen y las etapas tempranas, comprenden tanto cambios generales, que involucran mutaciones puntuales y alteraciones epigenéticas; o cambios específicos, como la pérdida del gen glutatión-S-transferasa P1, pérdida de heterocigosidad (LOH) del cromosoma 8 y cambios en el número de repetidos CAG en el gen del receptor de andrógenos. Los cambios implicados con las etapas avanzadas y metastáticas, comprenden la pérdida del brazo q del cromosoma 16, la pérdida del gen supresor de tumor RB, la inactivación del gen supresor de tumor p53 y la alteración en la expresión del gen de E-cadherina, entre otros. También existen mutaciones de genes que no se asocian directamente a una etapa particular, pero que son frecuentemente observados en los tumores de próstata; por ejemplo, este es el caso del gen PTEN (Phosphatase and tensin homolog) (De Marzo et al., 2007; Tomlins et al., 2007). Por otro lado, las mutaciones asociadas a los genes de AR están directamente relacionadas con la adquisición de un fenotipo independiente de andrógenos, que resulta fundamental en la clínica puesto que definirá si la terapia de privación de andrógenos será efectiva o no.

Tabla 3. Genes directamente asociados al desarrollo del PrCa.

Gen	Localización	Descripción General
Genes Supresores de Tumor		
CDKN1B	12p13.1	Codifica el inhibidor de quinasas dependiente de ciclinas p27. Uno de los alelos es deletado frecuentemente en los tumores primarios.
NKX3.1	8p21.2	Codifica la proteína homeobox restringida a próstata. Suprime el crecimiento de las células prostáticas. Uno de los alelos es deletado frecuentemente en los tumores primarios.
PTEN	10q23.31	Codifica el homólogo de la tensina y fosfatasa, suprime el crecimiento e incrementa la apoptosis. Uno de los alelos es perdido frecuentemente en los tumores primarios.
TP53	17p13.1	Posee muchas funciones supresoras de tumor, induce el arresto del ciclo celular en respuesta a daño en el ADN e induce la apoptosis. Frecuentemente mutado en estados avanzados del cáncer de próstata.
Oncogenes		
MYC	8q24	Factor de transcripción que regula muchos genes blancos involucrados en la proliferación celular, senescencia, apoptosis y metabolismo. Su sobreexpresión conduce directamente a la transformación celular.
ERG	21q22.3	Propuesto como nuevo oncogén del cáncer de próstata. Transcriptos fusionados con la porción 5' del gen regulado por andrógenos TMPRSS22, es comúnmente encontrado en todas las fases del cáncer de próstata.
ETV1-4	7p21.3, 19q13.12, 1q21, 17q21.31	Codifica para los factores de transcripción de tipo ETS 1-4. Transcriptos fusionados con la porción 5' del gen regulado por andrógenos TMPRSS22, es comúnmente encontrado en todas las fases del cáncer de próstata.
AR	Xq11-12	Codifica para el receptor de andrógenos. Se observa su expresión la mayoría de los cánceres de próstata. Generalmente, su locus se encuentra amplificado o mutado en estados avanzados del cáncer.
Activación de la enzima Telomerasa		Mantiene la función telomérica y contribuye con el estado de inmortalización. Generalmente, se encuentra activada en el cáncer de próstata.
Genes "Caretakers"		
GSTP1	11q13	Codifica la enzima que cataliza la conjugación del glutatión reducido a sustratos electrofílicos. Cumple función detoxificante de carcinógenos. Es epigenéticamente inactivado en más del 90% de PIN.
Disfunción Telomérica	Extremos cromosómicos	Contribuye a la inestabilidad cromosómica. El acortamiento de los telómeros es encontrado en más del 90% de PIN.
Anormalidades centrosómicas		Contribuye a la inestabilidad cromosómica.
Otros cambios somáticos		
PTGS2, APC, MDR1, EDNRB, RASSF1α, RARβ2	Varios	Alteraciones epigenética son frecuentemente encontradas en las regiones reguladoras.

Tabla extraída y modificada de De Marzo et al., 2007.

III. PEQUEÑOS ARNS NO CODIFICANTES.

El dogma central de la biología molecular fue desafiado cuando se identificó un subgrupo de pequeños fragmentos de ARNs no codificantes que poseían la capacidad de regular negativamente genes codificantes de proteínas (Lee et al., 1993). El estudio de los pequeños ARNs no codificantes (sncARNs) ha ganado particular atención desde el descubrimiento de los microARNs (Lee et al., 1993) y, más recientemente, desde el advenimiento de las técnicas

de secuenciación masiva. Esto se marca muy notoriamente en el crecimiento del número de microARNs anotados en miRBase (Griffiths-Jones, 2006). Si bien existen múltiples estrategias para el estudio de microARNs, la secuenciación masiva de pequeños ARNs no codificantes (sRNA-seq) ha sido la técnica más utilizada (Vickers et al., 2015). El sRNA-seq implica básicamente generar librerías de sncARNs mediante la ligación de adaptadores en los extremos de los pequeños ARNs no codificantes seleccionados por tamaño, la transcripción reversa y su posterior secuenciación en alguna de las plataformas disponibles en el mercado. Si bien los microARNs son una de las múltiples clases de sncARNs presentes en un set de datos obtenidos por sRNA-seq, hoy en día siguen siendo los más reportados. En gran medida, esto es debido al mayor conocimiento de sus características generales así como su mecanismo de acción (Bartel, 2009, 2018; Vickers et al., 2015). Sin embargo, actualmente conocemos muchas otras clases de sncARNs presentes en el transcriptoma celular (Figura 4), los cuales demandan más investigación. Se reconoce que los ARNs no codificantes (ncARNs) son actores clave en la iniciación y la progresión del cáncer (Bolton et al., 2014; Doldi et al., 2016; Mouraviev et al., 2016). Su identificación en fluidos corporales y su fácil cuantificación estimuló su intensa investigación (Wang et al., 2016; Yuan et al., 2016). Los ncARNs se clasifican según su tamaño y función, aquellos de longitud <200 nt son denominados "ARNs pequeños no codificantes" (sncARNs (microARNs, piwiARNs, snoARNs)), mientras que aquellos >200nt son denominados "ARNs largos no codificantes" (lncARNs) (Figura 4) (Romano et al., 2017; Wilusz et al., 2009).

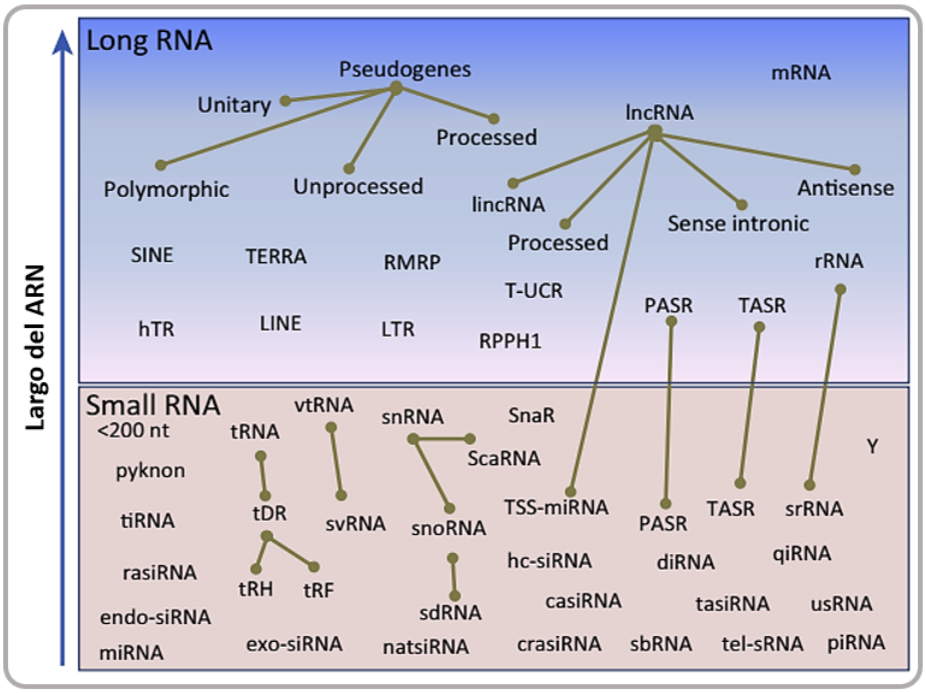

Figura 4. **Ilustración esquemática de la diversidad de ARNs no codificantes pequeños y largos.**

Las conexiones en color *mostaza* establecen los sncARNs que derivan de un precursor de mayor tamaño. Los pequeños ARNs no codificantes (*Small RNAs*) son menores de 200 nt, mientras que los ARNs no codificantes largos son mayores en longitud (*Long RNAs*).

lncARNs (en inglés, Long RNAs): ***hTR****, human telomerase RNA;* ***lincRNA****, large intergenic non-coding RNA;* ***LINE****, long interspersed element;* ***lncRNA****, long non-coding RNA;* ***LTR****, long terminal repeat;* ***mRNA****;* ***PASR****, promoter-associated long RNA;* ***RMPR****, RNA component of mitochondrial RNA processing endoribonuclease RPPH1, ribonuclease P RNA component H1;* ***rRNA****, ribosomal RNA;* ***SINE****, short interspersed element;* ***TASR****, termini-associated sRNA;* ***TERRA****, telomeric repeat-containing RNA;* ***T-UCR****, transcribed ultraconserved region.* **sncARNs (en inglés, Small RNAs):** ***casiRNA****, cis-acting siRNA;* ***crasiRNA****, centromere repeat-associated sRNA;* ***diRNA****, double-strand breakinduced sRNA;* ***endo-siRNA****, endogenous small interfering RNA;* ***exo-siRNA****, exogeneous small interfering RNA;* ***hc-siRNA****, heterochromatic small interfering RNA;* ***miRNA****, microRNA;* ***natsiRNA****, natural antisense siRNA;* ***piRNA****, Piwiinteracting RNA;* ***qiRNA****, QDE-2-interacting sRNA;* ***rasiRNA****, repeat-associated siRNA;* ***ScaRNA****, small Cajal-body RNA;* ***sbRNA****, stem-bulge RNA;* ***sdRNA****, snoRNA-derived small RNA;* ***SNAR****, small NF90-associated RNA;* ***snoRNA****, small nucleolar RNA;* ***snRNA****, small nuclear RNA;* ***srRNA****, sRNAs-derived from rRNA;* ***svRNA****, small vault RNA;* ***tasiRNA****, trans-acting siRNA;* ***tDR****, tRNA-derived sRNA;* ***tel-sRNA****, telomere-specific sRNA;* ***tiRNA****, transcription initiation sRNA;* ***tRH****, tRNAderived halves;* ***tRF****, tRNA-derived fragments;* ***TSS-miRNA****, transcriptional startsite-microRNA;* ***usRNA****, unusually small RNA;* **vtRNA**, vault RNA; **Y**, Y RNA. Imagen extraída y modificada de Vickers et al., 2015.

La gran mayoría de estos sncARNs no son meros productos de degradación, debido a que poseen extremos claramente definidos en múltiples tejidos y especies, y generalmente son señales de un producto del clivaje específico de ARNasas de tipo III (Berezikov et al., 2011; Langenberger et al., 2013; Park et al., 2011). Incluso, la

gran mayoría cuentan con un gran soporte de lecturas y características propias de secuencia (Miñones-Moyano et al., 2013; Starega-Roslan et al., 2011). Si bien conocemos poco sobre muchas de estas categorías de sncARNs, esto no impide que posean un gran potencial para participar de importantes funciones biológicas y regular la expresión génica como se determinó para los microARNs (Bartel, 2009, 2018; Martens-Uzunova et al., 2012).

IV. MICROARNS.

Los microARNs son pequeñas moléculas de ARN simple hebra de aproximadamente 22 nt de longitud, codificados en el genoma de una diversidad de organismos como plantas, animales, hongos y virus. Es ampliamente aceptado, que los microARNs son moléculas centrales en la regulación post-transcripcional, desempeñando su función como represores de la expresión génica (Bartel, 2004, 2009, 2018; Friedman et al., 2008; Romano et al., 2017). Específicamente, suprimen la expresión génica a través de una interacción por complementariedad de bases imperfecta, principalmente con el 3'-UTR de sus respectivos ARN mensajeros blancos. Producto de esta compleja interacción pueden disparar mecanismos generales de represión de la expresión génica. Se estima que más del 60% de los genes humanos se encuentran bajo el control de microARNs (Friedman et al., 2008; Seok et al., 2016). Los genes de microARNs pueden estar presentes tanto en secuencias intergénicas, con sus propios elementos reguladores, o en regiones intrónicas y en este último caso se pueden transcribir de forma independiente o dependiente del huésped, pudiendo llegar a escindirse mediante los eventos de "splicing" alternativo (miRtrons) (Bartel, 2018; Berezikov, 2011).

1. BIOGÉNESIS.

A pesar de que el proceso individual en cada especie puede llegar a diferir en algunos detalles específicos, el proceso básico de generación de los microARNs es compartido en animales, plantas y hongos. El mecanismo evolutivamente conservado que da lugar al microARN maduro, implica dos procesos consecutivos de corte endonucleotídicos precisos, realizados por las enzimas tipo RNasa III DROSHA y DICER (Figura 5) (Bartel, 2004; Kim et al., 2009, 2016; Winter et al., 2009). Una vez, generado el transcrito primario por la ARN polimerasa II (principal ARN polimerasa de transcripción de microARNs), los microARNs primarios (pri-microARN) poseen las propiedades estructurales características de los genes de clase II (caperuza en el 5', así como cola poli(A) al 3'). En el siguiente paso en la biogénesis, el complejo microprocesador nuclear enzimático compuesto por DROSHA y DGCR8 (proteína de unión a ARN doble hebra (Pasha)), procesa el transcrito primario, generando una estructura en forma de horquilla de aproximadamente 60-100 nt de longitud. Esta estructura es el llamado microARN precursor (pre-microARN) (Bartel, 2004; Kim et al., 2009, 2016; Winter et al., 2009). En el próximo paso, la interacción del pre-

microARN con el factor de exportación nuclear XPO5 (exportin 5) y Ran-GTP, promoverá que el microARN sea transportado al citoplasma donde sufrirá una segunda ronda de clivaje específico catalizado por la enzima DICER en complejo con TRBP (proteína de unión a ARN de doble cadena). Este evento de escisión dará a lugar a un nuevo fragmento de ARN doble hebra de aproximadamente unos 22nt, que estará compuesto por dos hebras de microARN maduro, una correspondiente al 5' (5p) y la otra al 3' (3p) de los extremos del precursor de microARN (Bartel, 2004; Kim et al., 2009, 2016; Winter et al., 2009). Inmediatamente, el microARN maduro será incorporado al gran complejo proteico denominado complejo de silenciamiento inducido por ARN (RISC). El microARN maduro funcionará como guía del complejo RISC para el reconocimiento específico de un grupo de ARN mensajeros blancos. El complejo RISC podrá inhibir la traducción de aquellos ARN mensajeros blancos que presenten complementariedad parcial con el microARN en el 3'-UTR.

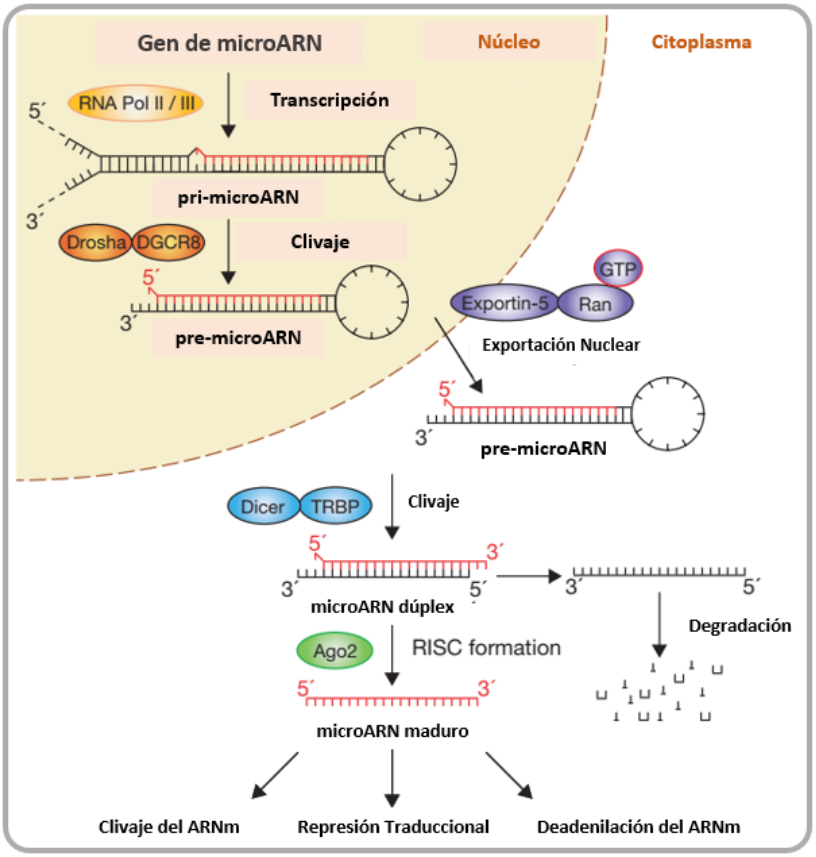

Figura 5. **Esquema de la biogénesis de los microARNs.**

El proceso consiste básicamente en la transcripción de moléculas de ARN bicatenario que posteriormente serán procesadas en moléculas de ARN simple hebra más pequeñas. Estas a su vez mediarán el reconocimiento de una secuencia específica en el ARN mensajero blanco por unión directa por complementariedad de bases, conllevando a la represión de la expresión de dicho ARN mensajero. Se pueden apreciar los tres mecanismos básicos de represión. Imagen extraída y modificada de Winter et al., 2009.

2. REPRESIÓN GÉNICA.

Principalmente los microARNs regulan la expresión génica de sus ARN mensajeros (ARNm) blancos mediante la interacción de 6 nucleótidos ubicados en el extremo 5' del microARN (2-7nt denominados región semilla) con secuencias fundamentalmente localizadas en la región 3'-UTR del ARNm blanco (Figura 6), produciendo la inhibición de la traducción o la desestabilización del ARNm (Bartel, 2009, 2018; Guo et al., 2010; Quévillon Huberdeau & Simard, 2019). Típicamente la represión efectuada por los microARNs afecta 20-50% de la expresión. Múltiples sitios de regulación en el mismo ARN mensajero puede contribuir con un efecto más pronunciado, principalmente aquellos cercanos (8-40nt), pueden contribuir con un efecto cooperativo (Bartel, 2018). Los mecanismos utilizados por los microARNs para regular la expresión génica más ampliamente aceptados son cuatro: degradación co-traduccional de la proteína, inhibición de la elongación de la traducción, terminación prematura de la traducción e inhibición del inicio de la traducción (Bartel, 2018; Eulalio et al., 2008). El modelo más aceptado en la actualidad es que el microARN produce la inhibición de la traducción del ARNm, contribuyendo de esta manera con la desprotección y consecuentemente con la degradación del mismo (Wilczynska & Bushell, 2015). De hecho, mediante el uso de la técnica de "ribosome profiling" se identificó que en mamíferos la disminución de los niveles de ARNm contribuye en gran medida (aproximadamente 84%) con el descenso de los niveles de proteína (Guo et al., 2010). Los microARNs son usualmente considerados escultores del transcriptoma celular, debido a que realizan un ajuste fino de la expresión génica y, en gran medida, eliminan el "ruido" o variación intrínseca en la expresión génica celular (Schmiedel et al., 2015). Es importante destacar que el efecto represor de un microARN sobre uno/varios ARNm blanco puede variar en diferentes tejidos, contextos celulares y etapas del desarrollo, pudiendo contribuir con un efecto moderado de ajuste de la expresión o un efecto agudo que termine por gatillar una transición o cambio celular (Bartel, 2018).

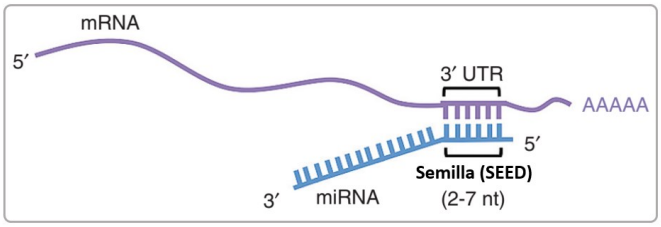

Figura 6. **Esquema de reconocimiento del microARN al ARN mensajero blanco.**

Complementariedad parcial del microARN (miRNA) a través de su región semilla "seed" (nucleótidos (nt) del 2-7 del extremo 5´ del microARN) con el ARN mensajero blanco (mRNA) en su región al 3' no traducida (3' UTR). Imagen extraída y modificada de Lam et al., 2015.

3. MICROARNS Y CÁNCER.

El hecho de que un único microARN presente numerosos ARNm blancos pertenecientes a una o múltiples vías celulares, sugiere que la expresión desregulada del mismo afectará a los procesos en los que participan los productos proteicos de sus ARN mensajeros blancos. Hoy es conocido, que la desregulación de los microARNs afecta múltiples procesos biológicos celulares que desembocan en eventos patológicos complejos, como las enfermedades cardiovasculares, neurodegenerativas, envejecimiento, desordenes metabólicos, así como el inicio y progresión del cáncer (Acunzo et al., 2015; Bouyssou et al., 2014; Esteller, 2011; Romano et al., 2017). Tal es así, que los microARNs al igual que los genes asociados al cáncer se clasifican según funcionen como OG o como TSG. Los microARNs TSG, se encontrarán subexpresados en el tejido tumoral, y tendrán por blanco el ARNm de OGs (Figura 7). Lo opuesto sucede con los microARNs OGs (oncomir), que se encontrarán sobreexpresados en las células tumorales y tendrán por blanco ARNm de genes con funciones de TSG (Figura 7) (Acunzo et al., 2015; Fuziwara & Kimura, 2014; Romano et al., 2017; Wang et al., 2010). Múltiples reportes científicos evidencian la participación y modulación de los microARNs en procesos como el desarrollo, proliferación celular, diferenciación, apoptosis, adhesión celular, migración e invasión, angiogénesis, metástasis en otros procesos biológicos (Acunzo et al., 2015; Aghdam et al., 2019; Hesse & Taipaleenmäki, 2019; Rupaimoole & Slack, 2017; Subramaniam et al., 2019; Weidle et al., 2019). Estudios de asociación han encontrado un gran número de microARNs que se ubican cercanos o directamente inmersos en regiones genómicas estrechamente asociadas al cáncer (Calin et al., 2002). Evidencia biológica experimental en modelos animales, muestra la asociación de niveles anormales de expresión de microARNs asociados con el desarrollo y progresión de cánceres humanos (Takamizawa et al., 2004). Particularmente, se ha comprobado que el mal funcionamiento de un único microARN resulta suficiente para causar cáncer en ratones (Costinean et al., 2006). Las nuevas tecnologías genómicas, han facilitado el estudio de perfiles de expresión de microARNs, demostrando una desregulación general de los microARNs en los tumores humanos (Abeshouse et al., 2015; Chu et al., 2016). Ha existido un progreso significativo en estos últimos años en relación con la asociación entre los microARNs y el cáncer, gracias al gran avance y la disminución de los costos de las tecnologías genómicas. Estudios a gran escala de perfiles genómicos de expresión de microARNs en diversos tipos de tumores, muestran una estrecha asociación entre el perfil de expresión de microARNs y el tumor estudiado (Abeshouse et al., 2015; Devor et al., 2014). Esto motiva a que algunos autores lleguen a plantearse la posibilidad de que cada tipo específico de tejido y de cáncer pueda ser identificado por un perfil o una firma determinada de microARNs desregulados. Incluso, la posible clasificación y estratificación de los distintos tipos de cáncer, basándose en los perfiles de expresión particular de microARNs de cada tumor (Volinia & Croce, 2013).

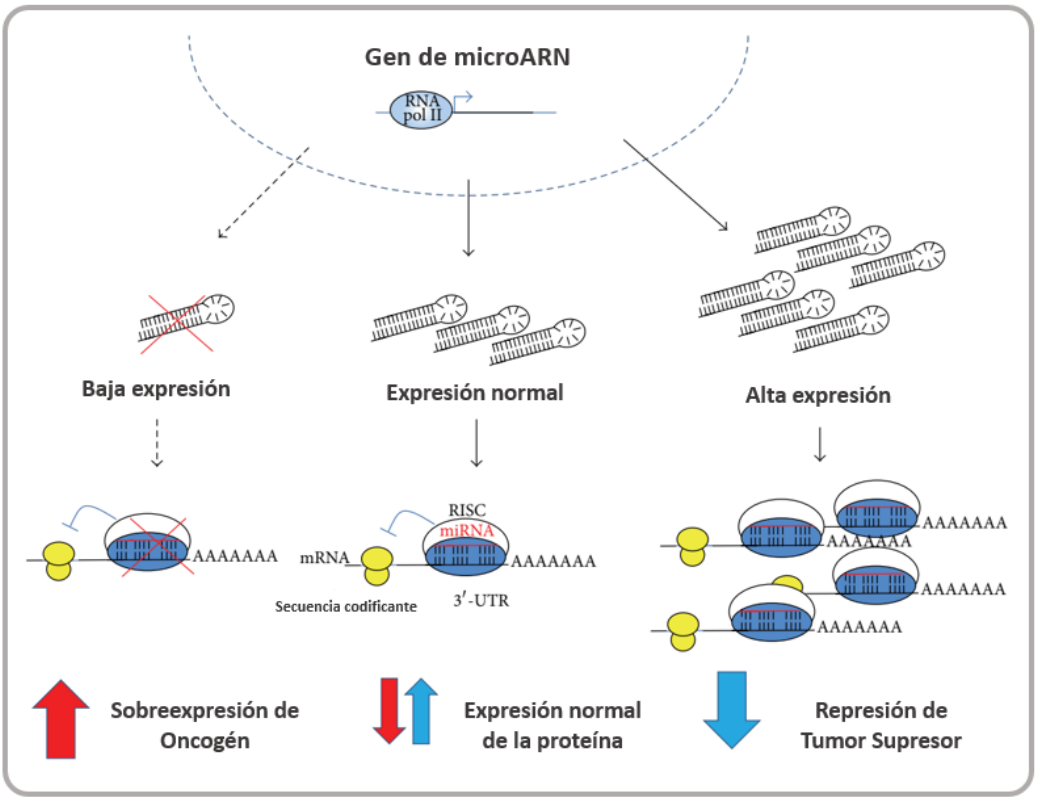

Figura 7. **Función de los microARNs como supresores tumorales y como oncogenes**.

La desregulación de los microARNs conlleva al desbalance de la expresión de sus ARNs mensajeros blancos. Los microARNs son denominados oncogén (oncomiR) cuando se encuentran sobreexpresados en el tumor y reprimen la expresión de un gen supresor de tumor. Los microARNs son denominados supresores de tumor cuando se encuentran reprimidos en el tumor y reprimen la expresión de un ARN mensajero oncogénico. Las dos situaciones suceden concomitantemente en el desarrollo del cáncer. Imagen extraída y modificada de Fuziwara & Kimura, 2014.

4. MicroARNs y cáncer de próstata.

Inicialmente, se observó que los perfiles de expresión de microARNs en tumores de próstata poseen una extensa desregulación global de los mismos (Gandellini et al., 2009). Además, se demostró que los patrones de expresión diferencial de los microARNs en el PrCa, pueden correlacionarse robustamente con la clínica, postulando su uso como indicadores de diagnóstico y pronóstico (Schaefer et al., 2009, 2010). Por ejemplo, se determinó que los tumores con elevada expresión de hsa-miR-21, presentan 2,5 veces más riesgo de padecer recurrencia bioquímica, posicionándolo como un posible biomarcador de la enfermedad (Leite et al., 2015). Existe un gran número de microARNs que se expresan anormalmente en PrCa, asociados directamente al desarrollo del mismo (Figura 8) (Aghdam et al., 2019). Muchos microARNs (oncomirs) se encuentran sobreexpresados en el PrCa regulando

negativamente muchos TSG, conduciendo al crecimiento tumoral y a la metástasis. Por ejemplo, dos microARNs que presentan una altísima homología de secuencia entre ellos, el hsa-mir-221 y hsa-mir-222, han sido reportados sobreexpresados en PrCa. Estos microARNs se encontraron directamente relacionados con la metástasis y el crecimiento tumoral a través de la represión del gen blanco p27kip1 (Mercatelli et al., 2008). Por otro lado, el rol tumor supresor de los microARNs en el PrCa se encuentra asociado con la habilidad de interferir con la migración celular y la invasión, así como mediar o promover la apoptosis celular. De hecho, la pérdida de microARNs supresores de tumor es un mecanismo bastante común asociado al PrCa. Por ejemplo, la pérdida del locus del hsa-mir-101 asociado a la sobreexpresión del gen EZH2, se encontró en un 37.5% de muestras clínicas de PrCa localizado y en un 66.7% de muestras de PrCa metastásico. Asimismo, la sobreexpresión del hsa-mir-101 se encuentra asociada con bajos niveles de EZH2, así como con la supresión del crecimiento y de la invasividad en células de PrCa (Varambally et al., 2008). Se observó también que los sncARNs (incluidos los microARNs) originados de células tumorales de próstata pueden ser cuantificados en la sangre, lo que impulsó la posibilidad de su seguimiento en el suero de pacientes con cáncer (Pardini et al., 2019). En la actualidad, múltiples trabajos se centran en encontrar firmas de expresión o paneles de microARNs presentes en fluidos corporales que puedan correlacionarse con la clínica, para su uso como indicadores de diagnóstico, pronóstico y terapéutica del PrCa (Konoshenko et al., 2020). De hecho, varios microARNs presentes en el suero (por ejemplo: Let-7c, let-7e, let-7i, hsa-miR-26a-5p, hsa-miR-26b-5p, hsa-miR-18b-5p y hsa-miR-25-3p), han sido confirmados como biomarcadores capaces de discriminar estadios benignos y avanzados de la enfermedad (Cochetti et al., 2016).

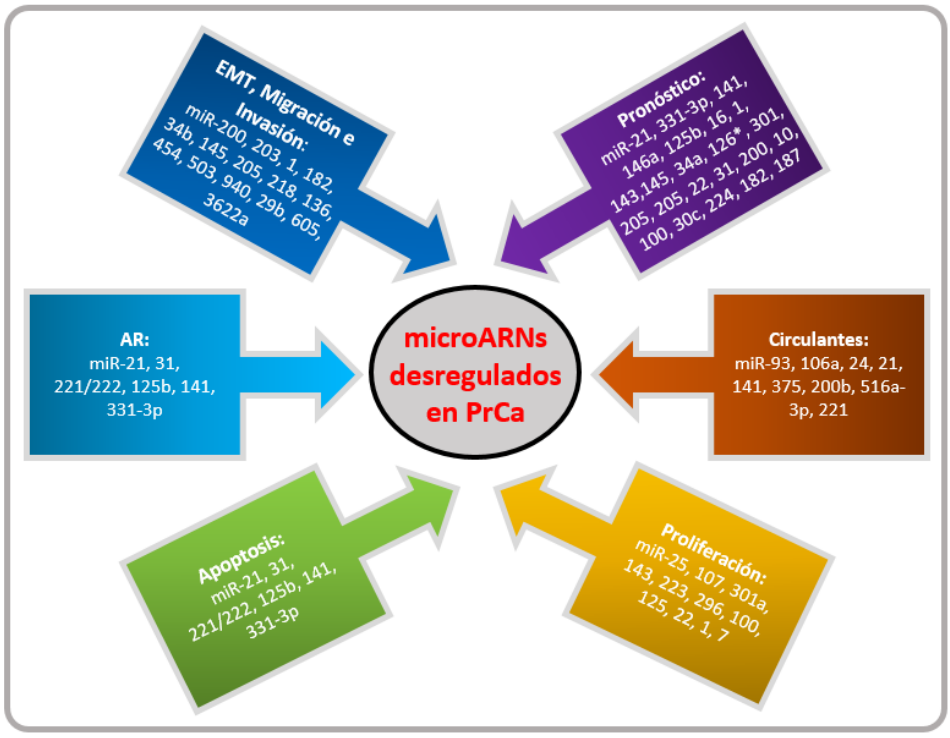

Figura 8. **MicroARNs expresados anormalmente en el PrCa asociados con diferentes etapas y procesos celulares de la enfermedad.**

AR: Receptor de Andrógenos; **EMT**: Transición Epitelial-Mesenquimal; **PrCa**: PrCa. Imagen extraída y modificada de Aghdam et al., 2019.

V. LA PARTÍCULA VAULT.

1. BREVE DESCRIPCIÓN DE LA PARTÍCULA VAULT Y SUS COMPONENTES.

En 1986 Kedersha y Rome (Kedersha & Rome, 1986), describieron a la partícula bóveda, en inglés "vault", como la partícula ribonucleoproteica más grande descrita hasta hoy en día (tres veces más grandes que los ribosomas). La partícula vault está formada por componentes proteicos y un pequeño ARN no codificante, denominado como ARN bóveda, vault ARN en inglés (vtRNA). El nombre de la partícula refiere a su compleja estructura tridimensional que se asemeja a las bóvedas (en inglés: vault) de las catedrales góticas (Kedersha & Rome, 1986). Los primeros estudios acerca de la partícula vault estuvieron enfocados en su composición proteica y estructural, hallando que estas características se encuentran altamente conservadas en mamíferos (*Rattus norvegicus* y *Oryctolagus cuniculus*), anfibios (*Rana catesbeiana* y *Xenopus laevis*) y eucariotas inferiores como el *Dictyostelium discoideum* (Kedersha et al., 1990). Estos primeros hallazgos revelaron una alta conservación y sugirieron que la morfología de la partícula vault (estructura, composición y tamaño) es probablemente muy importante para su función. Cada

partícula vault se conforma por dos mitades huecas con forma de barril (Figura 9) (Kedersha et al., 1991) y posee una masa total de aproximadamente 13MDa, de la cual el 70% de la misma corresponde a la proteína principal o mayor denominada en inglés *major vault protein* (MVP), que se encuentra en 96 copias por partícula. Sin embargo, se describió que alrededor de un 5% de la proteína MVP no se encuentra asociada a la partícula, despertando preguntas acerca de una posible función independiente de la partícula. Conjuntamente con la proteína MVP, la partícula vault está compuesta por otras dos proteínas: TEP1 (telomerase-associated protein 1) y PARP4 (the vault poly(ADP-ribose) polymerase), que son componentes menores de la misma, 2 copias y 8 copias por partícula, respectivamente (Kedersha et al., 1991; Van Zon et al., 2003). Estudios de crio-microscopía electrónica revelaron que las partículas vault poseen la capacidad de abrirse en estructuras similares a "flores". De hecho, se observó que estas estructuras tipo flores, se encuentran de a pares lo que, sugiere que una partícula vault está organizada por dos de estas estructuras, cada una compuesta por 8 pétalos que rodean un anillo central (Figura 9) (Kedersha et al., 1991). En cada célula se encuentran alrededor de 10,000–100,000 partículas vault y las mismas poseen una distribución citoplasmática (Kedersha et al., 1991; Kickhoefer et al., 1998). Estudios de expresión en la ameba *D. discoideum* revelaron que la proteína MVP se expresa en todas las fases del ciclo de vida, incluyendo las fases mitóticas y no mitóticas, la fase de agregación e incluso durante las fases finales de fructificación (una fase de alto catabolismo producto de la inanición). Llamativamente, MVP se mantiene en altos niveles de expresión en las fases de alto catabolismo cuando la actina y miosina prácticamente desaparecen, lo que sugiere una posible función en las fases no mitóticas y autofagocíticas (Kedersha et al., 1990). Basándose en la simetría y geometría de las partículas vault y en la marcada similitud estructural con los complejos de poros nucleares (NPCs), se propuso que podrían poseer un origen y función común (Van Zon et al., 2003). Sin embargo, aún se desconoce la función principal de la partícula vault.

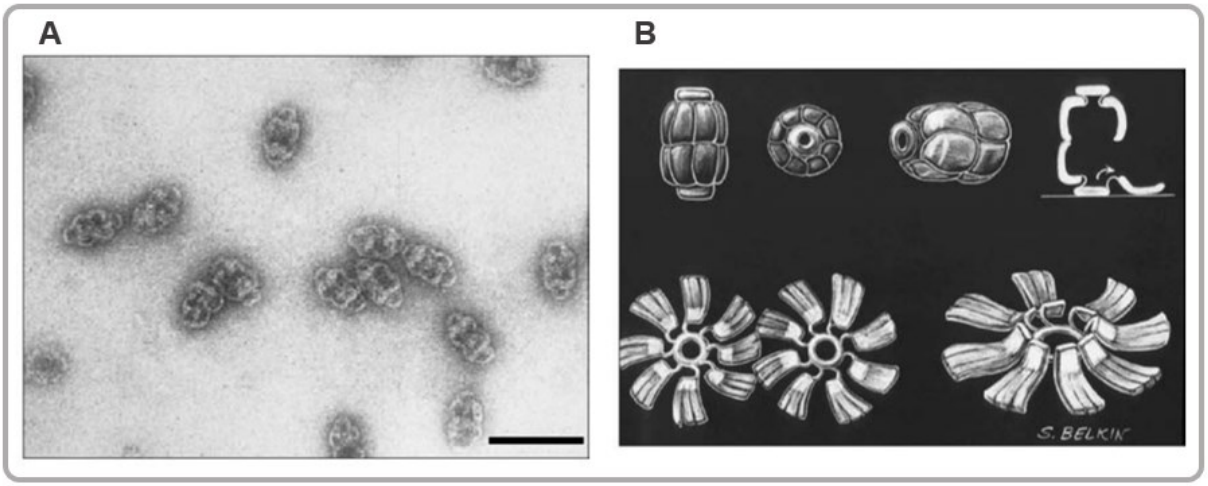

Figura 9. **Micrografía electrónica de las partículas vault y su modelado.**

A. Micrografía electrónica de partículas vault purificadas de hígado de rata, teñidas negativamente con acetato de uranilo (*barra negra* corresponde a 100nm). **B.** Modelado de la partícula vault evidenciando su estructura similar a un medio barril formada por 8 estructuras similares a pétalos. La estequiometría indica que cada pétalo está formado por 6 monómeros de la proteína MVP. Imagen extraída y modificada de Van Zon et al., 2003.

VI. LOS VAULT ARNS (VTRNAS)

1. ASPECTOS GENERALES DE LOS VTRNAS.

Los vault ARNs, son los ARNs no codificantes que forman parte de la partícula vault y comprenden como máximo un 5% de la masa total de la partícula. De hecho, no parecen cumplir un papel estructural en la misma, debido a que el tratamiento con ARNasas no reveló diferencias estructurales en la partícula (Kedersha & Rome, 1986; Kedersha et al., 1991). No obstante, el hecho de que la estructura secundaria de los vault ARNs se encuentre muy conservada sugiere que los mismos son un componente esencial de las partículas (Kickhoefer et al., 1993). De hecho, los vault ARNs de mamíferos poseen una similitud de secuencia de aproximadamente 80% (Stadler et al., 2009). Aunque la mayoría de los mamíferos poseen un único vtRNA en su genoma (ejemplos: ratón y rata), inicialmente en el humano se identificaron por homología 3 copias. Los primeros tres vault ARNs humanos definidos fueron el vtRNA1-1 de 98pb, vtRNA1-2 y vtRNA1-3 de 88-89pb (Figura 10). Los primeros tres vault ARNs humanos fueron denominado el clúster del locus vtRNA1. Estudios evolutivos determinaron que los vtRNA1-2 y vtRNA1-3 son duplicaciones que ocurrieron recientemente en el linaje de los primates (Stadler et al., 2009). El clúster locus vtRNA1, se ubica en el cromosoma 5 brazo q región 33.1 (5q33.1) y consiste en tres copias génicas espaciadas por aproximadamente 7500pb. Asimismo, el clúster del locus vtRNA1 se posiciona entre los genes ZMAT2 (Zinc Finger Matrin-Type 2) y PCDHA (protocadherin-α) (van Zon et al., 2001). Adicionalmente, se identificó

un pseudogen de los vtRNAs que no se expresa, el vtRNA3-1P, ubicado en el cromosoma X (van Zon et al., 2001). Más recientemente, se identificó un nuevo transcrito de vault ARN, que inicialmente fue anotado como un precursor de microARNs (precursor miR-886 (Landgraf et al., 2007)). El pre-miR-886 fue re-clasificado como un homólogo de los vault ARNs y consecuentemente renombrado como vtRNA2-1/nc886 (Stadler et al., 2009). El vtRNA2-1/nc886 (locus vtRNA2) se localiza en el cromosoma 5 a una distancia de aproximadamente 0.5Mb de la ubicación del clúster locus vtRNA1 y se encuentra en dirección antisentido entre los genes SMAD5 (SMAD Family Member 5) y TGFB1 (Transforming growth factor beta 1) (Stadler et al., 2009). Mientras que las copias del clúster locus vtRNA1 poseen una gran similitud de secuencia en primates, el locus vtRNA2 presenta diferencias de secuencia sustanciales en primates (Stadler et al., 2009). Llamativamente, existe sintenia evolutiva respecto a la ubicación del clúster locus vtRNA1 y vtRNA2 con sus genes vecinos, sin embargo, aún no se conoce la razón de la misma (Stadler et al., 2009). Los vault ARNs son transcriptos de la ARN polimerasa III. Los promotores de la ARN polimerasa III se clasifican en tres categorías: tipo-1, tipo-2 y tipo-3, basándose en las diferencias de la arquitectura de los elementos que los componen (Park et al., 2017). Específicamente, los vault ARNs poseen promotores de tipo-2, dado que poseen las cajas A y B internamente en el transcrito (Figura 10) y un tracto de 4 Ts que es la señal de terminación al final del transcrito (Kickhoefer et al., 1993). El pseudogen vtRNA3-1P, posee múltiples mutaciones en sitios clave de la caja B que explican su inactivación (van Zon et al., 2001). Si bien los vtRNAs humanos poseen alrededor de un 84% de similitud de secuencia entre ellos, la región de secuencia interna entre las cajas A y B es más divergente. Abordajes de ChIP-seq (Inmunoprecipitación de cromatina y posterior secuenciación) permitieron confirmar la ocupación de las regiones previamente predichas de unión en el promotor de los vault ARNs humanos por los complejos del promotor de tipo-2. Específicamente, se verificó el posicionamiento del complejo TFIIIB que se ubica al inicio transcripcional (TSS) conformado por: BDP1 (B double prime 1), TBP (TATA-box binding protein), BRF1 (B-related factor 1) y POLR3D (RNA Polymerase III Subunit D) (Canella et al., 2010). Complementariamente, en la región río arriba de los vtRNAs se identificó varias regiones de unión a factores característicos de promotores de tipo-3. Concretamente, se identificó la caja TATA posicionada a unos ≥ 20pb, una secuencia de elemento proximal (PSE) a unos ≥ 70pb y dos elementos de secuencia distales (DSE) a unos ≥ 340pb y ≥ 440pb (van Zon et al., 2001). El conjunto de los elementos internos de secuencia de los vault ARNs y los factores Staf/Oct-1 (PSE) y SNAPc (DSE) que se unen a los elementos externos, contribuyen a la regulación de la expresión de los vtRNAs (Nikitina et al., 2011; Vilalta et al., 1994). Más recientemente, se evidenció que la regulación epigenética de los promotores de los vtRNAs, es en gran medida el factor primario de su regulación transcripcional (Helbo et al., 2017). De hecho, se definió que el posicionamiento de los nucleosomas, las marcas de histonas y la metilación del ADN, resultan elementos decisivos que permiten o no el acceso de los factores en trans, que promoverán su posterior transcripción (Helbo et al., 2017; Park et al., 2017).

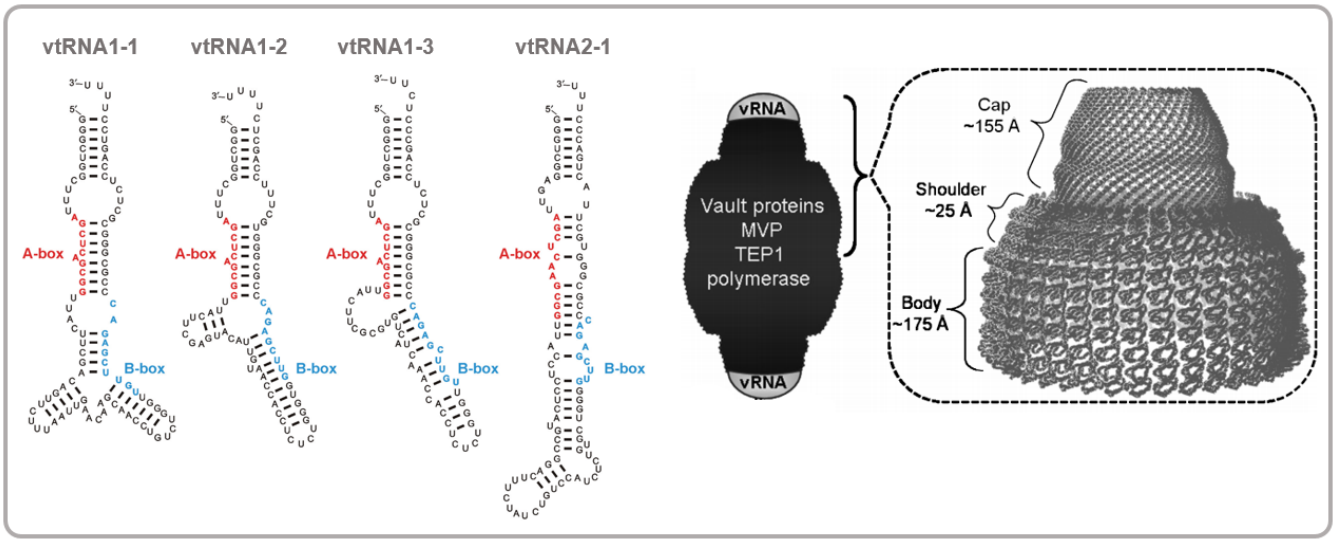

Figura 10. **Los vault ARNs y la partícula vault.**

Izquierda: Estructura secundaria predictiva de los vault ARNs humanos donde se indica las bases correspondientes a los elementos A y B (promotor interno de la ARN polimerasa III). Imagen extraída y modificada de Mrazek et al., 2007. **Derecha**: La estructura de la partícula vault con una masa de aproximadamente de 13MDa (dimensiones: 400 x 400 x 700 Å), se indica en color gris los extremos de la partícula vault donde se unen los vtRNAs (*vRNA*). La estructura cristalizada corresponde a la mitad de una partícula vault de rata a una resolución de 3,5 Å. Imagen extraída y modificada de Gopinath et al., 2010.

2. El locus vtRNA1: vtRNA1-1, vtRNA1-2 y vtRNA1-3.

En promedio entre el 5-20% del total de los vault ARNs se encuentra asociado a la partícula vault. Incluso, no existe una correlación directa entre el nivel de expresión de los vtRNAs y su grado de asociación a la partícula vault, siendo el vtRNA1-1 el que se encuentra principalmente asociado a la misma (Nandy et al., 2009; van Zon et al., 2001). Debido a que se determinó que el restante 85-90% de los niveles de vtRNAs no se asocia a la partícula vault y se encuentran en forma soluble en la fracción citoplasmática, surge la pregunta acerca de la función que podrían cumplir independientemente de la partícula. El estudio de la expresión de los vtRNAs en líneas celulares humanas (5 líneas celulares tumorales y 2 no tumorales) reveló que éstos varían en las diferentes líneas celulares y que el vtRNA2-1/nc886 es el que más variación presenta respecto al resto (Stadler et al., 2009). Debido a que los primeros hallazgos en torno a la partícula vault revelaron que sus componentes proteicos se encuentran incrementados en líneas celulares de cáncer resistentes a multidrogas (MDR), se precipitó la búsqueda de una asociación de los vtRNAs con este fenómeno. Incluso, esto se vió potenciado por la observación de que la sobreexpresión de los componentes proteicos de la partícula, no fue suficiente para el desarrollo del fenotipo de resistencia a drogas (Scheffer et al., 1995). Sin embargo, se observó que el vtRNA1-1 y el vtRNA1-2 (no el vtRNA1-

3) interactúan directamente con la mitoxantrona (Gopinath et al., 2005). Posteriormente, se confirmó esta interacción e incluso se describió nuevas interacciones directas para vtRNA1-2 con la doxorubicina y el etopósido (Mashima et al., 2008). Complementariamente, se evidenció que la sobreexpresión y la inhibición de vtRNA1-1 contribuyen con el incremento y la disminución de la resistencia a mitoxantrona, respectivamente (Gopinath et al., 2010). La búsqueda de proteínas que interactúan con los vault ARNs reveló que los mismos co-localizan con la proteína TEP1 en la partícula. De hecho, se reportó que TEP1 es necesario para que los vtRNAs se asocien con la partícula vault (Kickhoefer et al., 2001). Otro reporte evidenció que los vtRNAs interactúan con la proteína La de 50kDa (actualmente llamada: SSB) (Kickhoefer et al., 2002). La fosfoproteína proteína La (SSB) es capaz de asociarse con ARNs no codificantes durante su incorporación y procesamiento a grandes complejos ribonucleoproteicos (RNPs). La asociación de la proteína SSB con sus ARNs no codificantes blanco es dirigida por secuencias de poli-uridinas, comunes en las regiones 3' de los transcritos de la ARN polimerasa III (Kickhoefer et al., 2002). Más recientemente, se evidenció que el vtRNA1-1 se asocia con el factor de corte y empalme PSF/SFPQ (PTB-associated Splicing Factor/Splicing Factor Proline-Glutamine rich), una proteína del "spliceosome" que ha sido vinculada con procesos de replicación viral, recombinación y cáncer (Chen et al., 2018a). Asimismo, ensayos de EMSA e inmunoprecipitación evidenciaron que el vtRNA1-1 se asocia a PSF/SFPQ para formar un complejo con la región promotora de GAGE6 y así modular la expresión transcripcional del gen (Chen et al., 2018a). Igualmente, revelaron que el aumento y la represión de vtRNA1-1 en la línea celular MCF-7 (células de tumor de mama) provocan la activación y represión de GAGE6, respectivamente. Incluso, la expresión ectópica de vtRNA1-1 provocó un aumento de la proliferación y la formación de colonias, dependiente de la modulación por PSF/SFPQ (Chen et al., 2018a). Otro reporte reveló que vtRNA1-1, vtRNA1-2 y vtRNA1-3 son sustratos de la exonucleasa DIS3L2 (una exoribonucleasa humana de sentido 3´->5´) (Łabno et al., 2016). La uridilación de ARNs constituye una señal potenciadora de decaimiento mediado por DIS3L2 y las TUTasas son las proteínas encargadas de uridilar diferentes ARNs, entre los cuales se encuentran los vtRNAs. Concordantemente, se expuso que la sobreexpresión de TUT7 provoca el decaimiento de los niveles de vtRNA1-2. Incluso, se demostró que la presencia de las TUTs, conlleva a que DIS3L2 degrade más rápidamente a vtRNA1-2 en comparación a la degradación en ausencia de TUTs (Łabno et al., 2016). Más recientemente, se encontró que la proteína p62 es capaz de interaccionar con múltiples ARNs (165 ARNs) siendo los vtRNAs la categoría de ARNs más enriquecida. Ensayos *in vitro* e *in vivo* revelaron que el vtRNA1-1 es capaz de unirse a p62 e inhibir la autofagia (revisado en Büscher et al., 2020). Incluso, se expuso que la dependencia de la modulación de la autofagia y la concomitante modulación de los niveles de p62, está mediada por los niveles de vtRNA1-1. Asimismo, se logró identificar que es mediante un dominio de dedos de zinc que la proteína p62 se une a vtRNA1-1 y que esta interacción modula su posterior interacción con las proteínas tipo Atg8 (LC3B y GABARAP) (Horos et al., 2019). En este escenario, los investigadores proponen que

vtRNA1-1 no sería un sustrato canónico de p62 y por tanto, su unión interfiere con la formación del complejo multimérico de p62, lo cual evita la interacción del complejo con otras proteínas (Horos et al., 2019; Johansen, 2019). En el mismo sentido, se expuso el papel de vtRNA1-1 en la regulación de la apoptosis en múltiples líneas celulares, y se evidenció su capacidad para reprimir la vía intrínseca y extrínseca de la apoptosis. Los autores comprobaron que la capacidad de la modulación de la apoptosis por vtRNA1-1 se encontraría asociada a la vía ERK1/2 MAPK (Bracher et al., 2020).

Respecto a la regulación epigenética del clúster vtRNA1, se determinó que el tratamiento con 5-aza-CdR en la línea celular de cáncer mieloide HL60 conlleva a la sobreexpresión de vtRNA1-2 y vtRNA1-3 (Helbo et al., 2015). Incluso, se expuso que luego del tratamiento con 5-aza-CdR los promotores de vtRNA1-2 y vtRNA1-3 se encontraban desmetilados y presentaban una mayor marcación de histonas H3K4me (señal de cromatina activa). Por otro lado, se determinó que el promotor de vtRNA1-1 se encuentra desmetilado en las líneas celulares tumorales y normales hematopoyéticas. El promotor de vtRNA1-2 se encontró altamente metilado en niveles similares en las líneas celulares tumorales y normales hematopoyéticas (Helbo et al., 2015). Sin embargo, el promotor de vtRNA1-3, mostró un perfil tumor supresor, por encontrarse mayormente metilado en las líneas tumorales hematopoyéticas y asociarse con un peor pronóstico de sobrevida en los pacientes con síndrome mielodisplásico (Helbo et al., 2015). Otro reporte que estudió la expresión y asociación del estado de la cromatina para los vtRNAs humanos en las líneas celulares HL60, IMR90 (fibroblastos de pulmón), RKO (carcinoma de colon) y K562 (leucemia mielógena) reveló que el vtRNA1-1 se expresa a mayor nivel que vtRNA1-3 (Helbo et al., 2017). Incluso se evidenció que vtRNA1-1 se expresa en las 4 líneas celulares evaluadas y que en ellas el promotor se encuentra mayormente depletado de nucleosomas. Sin bien los grandes cambios de expresión de los vtRNAs podrían explicarse por la accesibilidad a la cromatina de los promotores, los cambios finos de expresión entre las líneas celulares no se explican únicamente por la ocupancia de nucleosomas en el promotor, esto implicaría la regulación por la actividad de factores de transcripción (Helbo et al., 2017).

3. LOS VAULT ARNS EN EL CONTEXTO DE LA INFECCIÓN VIRAL Y RESPUESTA INMUNE.

Los vault ARNs fueron vinculados con la respuesta inmune e infección viral en múltiples reportes que evidenciaron su sobreexpresión durante la infección viral. De hecho, se encontró que el vtRNA1-1 experimenta una gran inducción (un incremento de aproximadamente 1200 veces), conjuntamente con los ARNs virales EBER1 y EBER2 durante la infección de γ-herpesviridae (Nandy et al., 2009). Si bien el vtRNA2-1/nc886 también experimentó una gran inducción producto de la infección viral, este no mostró correlación con los ARNs virales EBER1 y EBER2. En este sentido, otro grupo reportó la inducción de los 4 vtRNAs humanos durante la infección con virus influenza A

(IAV) que sería dependiente de la dosis de viral (Li et al., 2015). Concretamente, la proteína viral NS1 sería la que promueve el aumento de los niveles de expresión de los vtRNAs durante la infección de IAV (Li et al., 2015). Adicionalmente, mostraron que la inhibición de los vtRNAs con oligos antisentidos (ASOs), promueve la inhibición de la replicación viral, siendo la inhibición de vtRNA2-1/nc886 la que provocó la mayor represión de la replicación viral (Li et al., 2015). Concordantemente, la represión de la expresión del vtRNA en ratones infectados con IAV, conduce a una menor pérdida de peso, menor severidad de los edemas pulmonares y una reducción de la infiltración de células inflamatorias. La inhibición con ASOs de vtRNA1-1 y vtRNA2-1/nc886 provocó un aumento de la activación de PKR (fosforilación del residuo Thr446) durante la infección viral en células A549 (carcinoma pulmonar), lo que sugiere que los vtRNAs modularían la activación de PKR. Globalmente estos resultados sugieren que la infección viral provoca el aumento de los vtRNAs, con el fin de evitar o atenuar la respuesta antiviral celular provocada por la transcripción de los ARNs virales que activan a PKR (Li et al., 2015). En este mismo sentido, Amort et. al. (2015) reportó que la infección del virus Epstein-Barr (EBV) en células BL2 (linfoma), conduce a un aumento significativo de vtRNA1-1 inducido por la proteína LMP1 (latency phase III protein) (Amort et al., 2015). Adicionalmente, se observó que los inhibidores de NFkB reprimen la activación de la expresión de vtRNA1-1 inducida por LPM1. Concordantemente, la sobreexpresión de vtRNA1-1 en células BL41 (linfoma) evidenció un mejor establecimiento viral de la infección de EBV y una disminución de la muerte celular respecto a la sobreexpresión de los parálogos vtRNA1-2 o vtRNA1-3 (Amort et al., 2015). Llamativamente, fuera del contexto de infección viral, la represión de vtRNA1-1 provocó un aumento de la muerte celular espontánea en células HeLa (carcinoma cervical) y HS578T (cáncer de mama). En este sentido, la modulación de vtRNA1-1 alteró los niveles de genes vinculados a las vías de apoptosis intrínseca y extrínsecas (NOL3, BCL2-like 1 y TNF/TNFR). Finalmente, los autores comprobaron que si bien la expresión estable de vtRNA1-1 provoca un aumento de la proteína MVP, la represión de MVP no altera los niveles de vtRNA1-1 ni los efectos funcionales asociados, lo que sugiere que el efecto de vtRNA1-1 es independiente de la partícula vault (Amort et al., 2015).

4. LOS VAULT ARNS Y LA VÍA DE LOS PEQUEÑOS ARNS NO CODIFICANTES.

El hecho de que los vtRNAs posean estructuras secundarias tipo horquillas y que se encontraran pequeños ARNs derivados de ellos, condujo a la posibilidad de que puedan participar en la vía de los microARNs. El primer reporte que exploró esta posibilidad expuso que los vtRNAs producen pequeños ARNs derivados (svARNs) y que éstos poseen una función tipo microARN (Persson et al., 2009). De hecho, Persson et. al. 2009 demostró que los pequeños ARNs derivados de vtRNA1-1 (svRNAa y svRNAb) se generan de manera independiente de DROSHA pero dependientes de DICER. Incluso reportó que svRNAa y svRNAb, muestran asociación y enriquecimiento en las proteínas argonautas AGO2 y AGO3 del complejo (RISC) (Persson et al., 2009). Adicionalmente, demostraron que

svRNAb es capaz de modular la expresión de CYP3A4 (cytochrome P450 family 3 subfamily A member 4) de manera directa. Recientemente un reporte independiente, confirmó la represión directa de la expresión de CYP3A4 por svRNAb en la línea celular HepG2 (carcinoma hepático) (Meng et al., 2016). En este sentido, mediante ensayos de HITS-CLIP (High-throughput sequencing of RNA isolated by crosslinking immunoprecipitation) se confirmó la asociación de fragmentos derivados de los vtRNAs a las proteínas de la biogénesis de los microARNs, incluso a las argonautas (AGO2 y AGO3) (Wang et al., 2020). Por otra parte, ensayos de miCLIP (versión customizada del método individual-nucleotide-resolution crosslinking and immunoprecipitation (iCLIP)) revelaron que la proteína NSUN2 (NOP2/Sun RNA methyltransferase 2), una metiltransferasa de ARN m^5C de eucariotas superiores, es capaz de metilar a vtRNA1-1, vtRNA1-2 y vtRNA1-3 (Hussain et al., 2013). Concretamente, NSUN2 metila la citosina 69 en el vtRNA1-1 y las citosinas 27 y 59 en los vtRNA1-2 y vtRNA1-3, lo que provoca un aumento del procesamiento del vtRNA1-1 a pequeños ARNs, concretamente, la formación del pequeño ARN derivado del extremo 3´ (svRNA4) (Hussain et al., 2013). Incluso, evidenciaron que svRNA4 es capaz de asociarse con las proteínas AGO2 y AGO3, y que su sobreexpresión regula negativamente a CACNG7 y CACNG8 (calcium voltage-gated channel auxiliary subunit gamma 7/8) (Hussain et al., 2013). Recientemente, el mismo grupo confirmó la producción de svRNA4 en fibroblastos de dermis y que su aumento es debido a la metilación de la citosina 69 de vtRNA1-1 por NSUN2 (Sajini et al., 2019). Asimismo, ensayos de cuantificación de proteínas por SILAC (Stable Isotope Labeling by/with Amino acids in Cell culture) donde se comparó a vtRNA1-1 metilado y no metilado, revelaron que SRSF2 (serine and arginine rich splicing factor 2), una proteína vinculada en el corte y empalme de ARNs mensajeros, se une diferencialmente (Sajini et al., 2019). Incluso, reportaron que la unión de SRSF2 a vtRNA1-1 prevenía la formación de svRNA4, mientras que la metilación de vtRNA1-1 mediada por NSUN2 evita la unión e induce la concomitante formación de svRNA4. Adicionalmente, demostraron que este proceso es clave en el proceso de diferenciación de queratinocitos (McElhinney et al., 2020; Sajini et al., 2019).

VII. EL LOCUS VTRNA2: PRE-MIR-886/VTRNA2-1/NC886.

Inicialmente, pre-miR-886 fue anotado como un precursor de microARNs (hsa-mir-886) en la versión 10 de miRBase (08/2007) (Griffiths-Jones, 2006), debido a la identificación de microARNs derivados (Landgraf et al., 2007). Posteriormente, su homología de secuencia con los vtRNAs humanos del clúster vtRNA1 condujo a su reclasificación como vault ARN (vtRNA2-1) (Stadler et al., 2009) y a su eliminación de miRBase v16 (11/2011). En 2011, el grupo de Y. S. Lee determinó la disminución de la expresión de hsa-miR-886-3p y hsa-miR-886-5p en células de cáncer de pulmón (H1299) respecto a células epiteliales de pulmón (CRL2741) utilizando microarreglos de expresión de microARNs. Sin embargo, mediante ensayos de *Northern blot* demostraron que el precursor

(vtRNA2-1/nc886) se encontraba más ampliamente expresado en relación con sus microARNs derivados (hsa-miR-886-3p y hsa-miR-886-5p) en células de pulmón (Lee et al., 2011). De hecho, revelaron que los niveles de expresión de vtRNA2-1/nc886 se encuentran en el orden de otros ARN no codificantes de alta expresión como, snoRNAs y snRNAs (aproximadamente $1x10^5$ copias por célula) en las líneas celulares HeLa, WI-38 (fibroblastos de pulmón) y CRL2741 (Lee et al., 2011). Incluso, reportaron la expresión elevada de vtRNA2-1/nc886 en tejidos y líneas celulares normales respecto a tumorales de mama, melanoma, cérvix, pulmón, oral y próstata, sugiriendo un papel TSG en estos tejidos (Lee et al., 2011). Llamativamente, aunque los vtRNAs fueron descubiertos y definidos debido a su asociación con la partícula vault (Kedersha & Rome, 1986), ensayos de centrifugación diferencial revelaron que vtRNA2-1/nc886 no se asocia a la partícula vault, lo que despertó preguntas acerca de su posible función (Lee et al., 2011). Igualmente, se determinó que vtRNA2-1/nc886 se encuentra mayormente en el citoplasma celular en *foci* discretos indicando una localización no aleatoria. Incluso, se observó que vtRNA2-1/nc886 no es procesado por DROSHA y que es poco eficientemente procesado por DICER (aproximadamente 5% de producción de sus derivados 3p y 5p) (Lee et al., 2011), observaciones que fueron confirmadas posteriormente por otros reportes (Miñones-Moyano et al., 2013; Treppendahl et al., 2012). En este sentido, evaluaron el potencial funcional de los microARNs derivados de vtRNA2-1/nc886 utilizando ensayos de luciferasa pero no se observó modulación de la expresión de los reporteros con sitios complementarios a hsa-miR-886-3p y hsa-miR-886-5p (Lee et al., 2011). El conjunto de estas evidencias condujo a que el grupo de Y. S. Lee postulara a vtRNA2-1/nc886 como un ncARN ubicuo y conservado, cuya función no estaría relacionada a la partícula vault o como precursor de microARNs, renombrándolo como "non-coding RNA 886" (nc886) (Lee et al., 2011). Ensayos funcionales reprimiendo la expresión de vtRNA2-1/nc886 con ASOs en líneas celulares tumorales (mama, cérvix, colon y pulmón), evidenciaron una disminución de la proliferación (Lee et al., 2011). La búsqueda de interactores de vtRNA2-1/nc886 mediante ensayos de captura con vtRNA2-1/nc886 biotinilado como presa identificó a PKR (Protein kinase R) como una de las proteínas capaces de asociarse al mismo. PKR es una quinasa centinela celular que es capaz de activarse (autofosforilarse) al entrar en contacto con ARNs doble cadena u horquillas mayores de 30pb (revisado en Lee et al., 2019b). El papel de PKR en la célula está muy bien establecido en el contexto de una infección viral, donde se generaran múltiples ARNs doble cadena que inducirán la activación de PKR y conducirán a la subsecuente muerte celular, debido al paro traduccional provocado por la fosforilación de eIF2α (Eukaryotic translation initiation factor 2 subunit 1), que previene la expansión del virus (Li et al., 2015). Si bien la activación de PKR provoca la fosforilación del factor de traducción eIF2α que conduce al paro traduccional por inhibir la traducción global de ARNm (señal anti-proliferativa), en simultáneo PKR activada también conduce a la activación de la vía NF-kB mediante la fosforilación de su subunidad inhibidora IkB (señal pro-proliferativa) (Lee et al., 2011). NF-kB activado regula al alza la expresión de las citoquinas del interferón, que funcionan para propagar la señal

antiviral de manera local. La interacción directa entre PKR y vtRNA2-1/nc886 fue caracterizada y se definió que PKR une a vtRNA2-1/nc886 utilizando sus dos dominios de unión al ARN doble cadena (dsRBM1 y dsRBM2), con una afinidad similar a la que posee para el ARN PolyI:C sintético (un activador conocido de PKR) (Calderon & Conn, 2017; Jeon et al., 2012a). Ensayos de protección con RNAsa I mostraron que la asociación de vtRNA2-1/nc886 con PKR es a través de la región central de vtRNA2-1/nc886 (región apical de la horquilla en estructura secundaria), y que ésta no depende de los extremos de la secuencia. De hecho, la mutación de bases en la región comprendida entre las bases 46-56nts de vtRNA2-1/nc886 provoca un descenso en la afinidad por PKR (Jeon et al., 2012a). Sin embargo, vtRNA2-1/nc886 en lugar de activar a PKR, atenúa su activación frente a otros ARNs doble cadena (Calderon & Conn, 2017; Golec et al., 2019; Jeon et al., 2012b; Kunkeaw et al., 2019; Lee et al., 2011; Li et al., 2015). El conjunto de estas evidencias condujeron a que se propusiera tempranamente el modelo de "supervisión tumoral" (*tumor surveillance model* (Jeon et al., 2012b; Lee, 2015)), que explicará el papel de vtRNA2-1/nc886 y PKR en el contexto tumoral. El grupo de Y.S. Lee propone que en células normales con altos niveles de vtRNA2-1/nc886, PKR se encontraría atenuada, sin embargo, durante la carcinogénesis el silenciamiento de la expresión de vtRNA2-1/nc886, provocaría la activación de PKR y consecuentemente, la muerte celular debido al paro traduccional (fosforilación de eIF2α) (Figura 11) (Jeon et al., 2012b; Lee, 2015). Este sería un mecanismo normal de control tumoral o supervisión tumoral (en inglés, *tumor surveillance model*) de las células (Jeon et al., 2012b; Lee, 2015). No obstante, sabemos que la activación de PKR también induce la activación de la vía de NF-kB que posee un efecto prosupervivencia y protumorigénico que contribuiría con la progresión tumoral. Entonces, este modelo también supone que aquellas células tumorales que lograron franquear el paso de control de PKR, contarán con la contribución protumorigénica de la vía NF-kB (Jeon et al., 2012b; Lee, 2015). En este sentido, la restauración de la expresión de vtRNA2-1/nc886 en aquellas células tumorales que lograron franquear el paso de control, conllevaría a una atenuación de la activación de PKR y por tanto, a una reducción de la contribución de la vía NF-kB; que consecuentemente disminuiría los atributos malignos asociados (Jeon et al., 2012b; Lee, 2015). De todos modos, se deben considerar las diferencias naturales observadas en las células normales y tumorales, por origen de tejido, antecedentes genéticos, epigenéticos y ambientales que podrían contribuir a las diferencias en la respuesta a la activación de PKR.

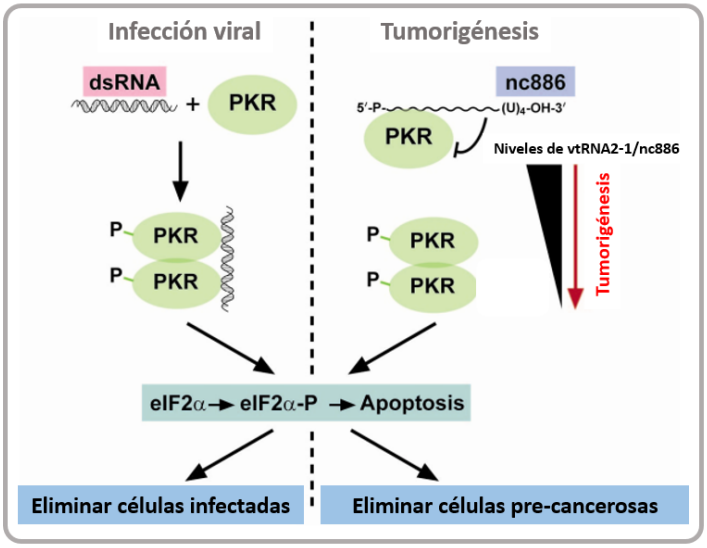

Figura 11. **Modelo de "supervisión tumoral".**

Similitud entre el modelo de supervisión tumoral y de respuesta a una infección viral. PKR (en inglés *protein kinase R)*; eIF2α (en inglés *eukaryotic initiation factor 2α subunit*). Imagen extraída y modificada de Lee, 2015.

Posteriormente, se identificó a OAS1 (2'-5'-oligoadenylate synthetase 1) como otra proteína que es capaz de ser modulada por vtRNA2-1/nc886 (Calderon & Conn, 2018; Vachon et al., 2015). Análogamente a PKR, OAS1 participa de la respuesta inmune activándose en respuesta a la unión de ARN doble cadena, principalmente, durante la respuesta a infecciones virales provocando el paro de la maquinaria traduccional y replicación viral (Calderon & Conn, 2018). De hecho, se reportó que vtRNA2-1/nc886 provoca la inducción de OAS1, similar a la activación que provocan otros ARNs virales como EBER1. En este sentido, la transfección de vtRNA2-1/nc886 provocó la activación de OAS1 y la consecuente activación de la vía de RNAsa L de degradación del ARN ribosomal (Calderon & Conn, 2018). Análogamente a lo observado para PKR, se determinó que la región central de la secuencia de vtRNA2-1/nc886 (37-67nt) es clave para la interacción y activación de OAS1 (Calderon & Conn, 2018). Llamativamente, vtRNA2-1/nc886 conduce a la activación de OAS1, pero a la atenuación de PKR. Más recientemente, otro reporte confirmó la asociación de vtRNA2-1/nc886 a PKR en las células HUT78 (linfocitos T) donde exploraron la implicancia de vtRNA2-1/nc886 en la modulación y respuesta del sistema inmune, evidenciando que vtRNA2-1/nc886 se encuentra inducido en células T $CD4^+$ activadas. En este sentido, revelaron que vtRNA2-1/nc886 es altamente inducido en células T CD28 y CD46 co-estimuladas, en aquellas con alta expresión CD46 y en células Th1 que secretan IFN-gamma y/o IL10 (Golec et al., 2019). Por último, revelaron que la modulación de la expresión de vtRNA2-1/nc886 en las líneas celulares Jurkat y PM1 (linfocitos T) es necesaria para la expresión de IFN-gamma en células T activadas (Golec et al., 2019).

1. vtRNA2-1/nc886 SU PERFIL DE EXPRESIÓN Y FUNCIÓN EN CÁNCER.

El descubrimiento de la acción de vtRNA2-1/nc886 como modulador de PKR (Lee et al., 2011) y el modelo de supervisión tumoral propuesto por el grupo de Y.S. Lee (Jeon et al., 2012b; Lee, 2015) contribuyó al desarrollo de múltiples reportes que evidenciaron funciones de tipo TSG y OG para vtRNA2-1/nc886 en diferentes tejidos.

Un aspecto muy importante de vtRNA2-1/nc886 en el cáncer es su regulación epigenética, debido a que se encuentra inmerso en una isla CpG. El primer reporte que reveló la vinculación entre la expresión de vtRNA2-1/nc886 y la metilación de su promotor fue Treppendahl et al. (2012), evidenciando que el promotor de vtRNA2-1/nc886 se encuentra hemimetilado en el 75% y completamente metilado en el 25% de las células sanguíneas de donantes sanos (Treppendahl et al., 2012). Incluso evidenciaron que el tratamiento de la línea celular HL60 con 5-azacitidina (5-aza-CR) o 5-aza-2′-desoxicitidina (5-aza-CdR), conducía a un incremento de la expresión de vtRNA2-1/nc886 acompañada con la disminución de la metilación del promotor (Treppendahl et al., 2012). En este mismo sentido, mostraron que el aumento de la expresión de vtRNA2-1/nc886 producto del tratamiento con agentes desmetilantes se asociaba con la atenuación de PKR. Finalmente, al evaluar la asociación de la metilación del promotor de vtRNA2-1/nc886 en pacientes con leucemia mieloide aguda (AML), encontraron que la hipermetilación del promotor de vtRNA2-1/nc886 se asociaba con una peor sobrevida de los pacientes (Treppendahl et al., 2012). Otro reporte donde analizaron el perfil de metilación del promotor de vtRNA2-1/nc886 en diferentes cánceres, reveló que el mismo se encuentra hipermetilado en un 25%, 36%, 16.5% y 29% en tumores de vejiga, mama, colon y pulmón respectivamente (Romanelli et al., 2014). Múltiples reportes evidenciaron un perfil de expresión TSG de vtRNA2-1/nc886 asociado a un incremento de la metilación de su promotor en el tejido tumoral respecto al tejido normal en cáncer de mama, pulmón, colon, vejiga, hígado, esófago y estómago (Cao et al., 2013; Joo et al., 2018; Lee et al., 2014a, 2014b; Romanelli et al., 2014; Treppendahl et al., 2012; Yu et al., 2020). Incluso se expuso la asociación de la metilación de vtRNA2-1/nc886 con el pronóstico/supervivencia del paciente en cáncer de pulmón, esófago, estómago, hígado y AML (Cao et al., 2013; Joo et al., 2018; Lee et al., 2014b; Treppendahl et al., 2012; Yu et al., 2020).

El estudio funcional de vtRNA2-1/nc886 en cáncer evidenció una función TSG en colangiocarcinoma, esófago, estómago y próstata (Im et al., 2020; Kunkeaw et al., 2012; Lee et al., 2014a, 2014b; Ma et al., 2020), y sugiere una función TSG en cáncer de piel y colorectal (Lee et al., 2019a; Ortega-García et al., 2020). Concretamente, se evidenció que el aumento de vtRNA2-1/nc886 conduce a la inhibición de la proliferación acompañada de una inducción de la apoptosis en colangiocarcinoma, esófago y estómago (Im et al., 2020; Lee et al., 2014a, 2014b). En esófago incluso se observó una asociación con alteraciones en la transición G1/S (Im et al., 2020). Particularmente en cáncer gástrico, se observó que la transfección específica de la región central de vtRNA2-

1/nc886 (sin las regiones 5’ y 3’ de vtRNA2-1/nc886) es suficiente para mantener el efecto funcional antiproliferativo (Lee et al., 2014b). En este sentido, los autores también exploraron el posible efecto funcional asociado a los pequeños ARNs derivados de vtRNA2-1/nc886 y no encontraron una modulación de la proliferación, pese a que fueron capaces de modular la expresión de reporteros de luciferasa con sitios complementarios en su 3’-UTR (Lee et al., 2014b). En un reporte reciente donde evaluaron la respuesta inmunitaria al establecimiento de metástasis de células de próstata en ratones, determinaron que la línea celular tumoral de próstata PC3M-1E8 (altamente invasiva) al sobreexpresar vtRNA2-1/nc886 presenta una menor capacidad de establecimiento del tumor respecto a las células control (Ma et al., 2020). En este contexto, observaron que vtRNA2-1/nc886 es capaz de reprimir directamente la expresión de TAP1 (Transporter associated with Antigen Processing 1) y MHC-I (Major Histocompatibility Complex Class I), por lo que alteraría la presentación de antígenos tumorales. En este sentido, evidenciaron un aumento de células T citotóxicas CD8+ en las lesiones óseas de las inyecciones de células de PC3M-1E8 que sobreexpresan vtRNA2-1/nc886 respecto a las células control. Esto sugiere que las células que sobreexpresan vtRNA2-1/nc886 serían más fácilmente reconocidas en etapas tempranas por las células T citotóxicas CD8+ del sistema inmune respecto a las células control (Ma et al., 2020). Finalmente, evidenciaron que la sobreexpresión de vtRNA2-1/nc886 reprime la expresión de TGFB1 respecto a las células control, contribuyendo a la polarización de macrófagos tipo M1 proinflamatorios, mientras que la alta expresión de TFGB1 en las células control induciría la polarización de macrófagos tipo M2 contribuyendo con la inmunosupresión (Ma et al., 2020).

Es importante destacar que en colangiocitos se estableció uno de los posibles mecanismos de evasión de las células tumorales a la actividad supervisora de tumor de PKR. Concretamente, proponen que aquellas líneas celulares tumorales que poseían PKR activada (línea celular M214) y consecuentemente eIF2α fosforilado, presentan una sobreexpresión de eIF2B, lo que permitía contrarrestar el efecto de detención traduccional normalmente provocado por la fosforilación de eIF2α (Kunkeaw et al., 2012). Los autores propusieron que ésta puede ser una de las alteraciones que permitiría a las células tumorales escapar del efecto de eIF2α, y por ende que predomine el efecto pro-tumoral de NF-kB. En acuerdo con esta hipótesis, determinaron el aumento de genes blancos de la activación de la vía NF-kB en las células tumorales que presentaban PKR activada (Kunkeaw et al., 2012). En este contexto, la supresión de vtRNA2-1/nc886 con ASOs provocó la activación de PKR en las células no malignizadas MMNK1 e indujo el clivaje de la caspasa-3 y PARP (Poli(ADP-ribosa) polimerasa), mientras que la sobreexpresión atenuó la activación de PKR en las células tumorales (Kunkeaw et al., 2012). En carcinoma de esófago, el análisis de genes modulados por la inhibición de vtRNA2-1/nc886 en tres líneas celulares diferentes, identificó 33 genes inducidos y 6 reprimidos en común, relacionados con cáncer, blancos de NF-kB, inflamación y apoptosis (Lee et al., 2014a). Más recientemente, el mismo grupo profundizó en su mecanismo de acción en

cáncer de esófago, revelando que el silenciamiento de vtRNA2-1/nc886 conlleva a la activación de la vía AKT. Incluso lograron definir una firma de genes asociadas al silenciamiento de vtRNA2-1/nc886 que se asocia al pronóstico de los pacientes (Im et al., 2020). En células de cáncer gástrico, la represión con ASOs de vtRNA2-1/nc886 respecto a las células control reveló la inducción de genes de la familia de FOS (FOS, FOSB y FOSL1), MYC, MAP quinasas y blancos de la vía de NF-kB cuantificados mediante ensayos de microarreglos de expresión génica (Lee et al., 2014b).

Como mencionamos, otros reportes recientes sugieren una función TSG para vtRNA2-1/nc886 en cáncer de piel y cáncer colorectal. En células de la piel se reportó que los niveles de expresión de vtRNA2-1/nc886 disminuyen con la radiación UV. De hecho, se observó que la radiación UVB en queratinocitos (HaCat) conduce a la represión de vtRNA2-1/nc886 respecto a las células no irradiadas. Incluso, observaron que la represión e incremento de vtRNA2-1/nc886 se da concomitantemente con el aumento y disminución de MMP9 (matrix metallopeptidase 9) y PTGS2 (Prostaglandin-Endoperoxide Synthase 2) respectivamente (Lee et al., 2019a). Asimismo, el *knockdown* de PKR contribuyó a disminuir la inducción de MMP9 y PTGS2, provocada por la irradiación con UVB lo que sugiere un posible rol TSG de vtRNA2-1/nc886 en queratinocitos (Lee et al., 2019a). Por otro lado, un estudio reciente ambispectivo con 197 pacientes con cáncer colorectal metastásico, evaluó el nivel de expresión de vtRNA2-1/nc886 y determinó que niveles de expresión altos de vtRNA2-1/nc886 se relacionan con una buena respuesta a la terapia con la droga 5-fluorouracilo (Ortega-García et al., 2020).

Paralelamente, también existen reportes que demostraron una función OG para vtRNA2-1/nc886 en cáncer de tiroides, ovario, endometrio, cérvix y riñón (Ahn et al., 2018; Hu et al., 2017; Lee et al., 2016; Lei et al., 2017; Li et al., 2017). En cáncer de tiroides se reportó que vtRNA2-1/nc886 experimenta un incremento de la expresión en el tejido tumoral respecto al tejido normal, e incluso que su expresión correlaciona con mayor agresividad del tumor y metástasis en nódulos linfáticos (Lee et al., 2016). Además, la represión de vtRNA2-1/nc886 con ASOs condujo a un incremento de la activación de PKR y la concomitante represión de la proliferación. Asimismo, observaron la disminución de la viabilidad celular, la formación de colonias, migración e invasión en aquellas líneas celulares con *knockout* de vtRNA2-1/nc886 (PKRwt/vtRNA2-1^{ko}; PKR^{ko}/vtRNA2-1^{ko}), respecto a líneas celulares con vtRNA2-1/nc886 silvestre (PKR^{wt}/vtRNA2-1^{wt}) (Lee et al., 2016). Llamativamente, las células que presentan el *knockout* de PKR y vtRNA2-1/nc886 (PKR^{ko}/vtRNA2-1^{ko}) o PKR silvestre y vtRNA2-1/nc886 *knockout* (PKR^{wt}/vtRNA2-1^{ko}), no mostraron diferencias significativas de crecimiento entre ellas. Esto revela que el efecto constatado para la modulación de vtRNA2-1/nc886 en este tejido podría ser independiente de su modulación de PKR (Lee et al., 2016). Posteriormente, evaluaron la expresión génica de las tres líneas celulares ensayadas (PKR^{wt}/vtRNA2-1^{wt}; PKR^{wt}/vtRNA2-1^{ko} y PKR^{ko}/vtRNA2-1^{ko}) mediante microarreglos, evidenciando la alteración de 13 procesos

ontológicos vinculados con el ciclo celular, crecimiento, apoptosis y organización del citoesqueleto (Lee et al., 2016).

En cáncer de endometrio, mediante FISH (fluorescence *in situ* hybridization) evidenciaron un aumento de la expresión de vtRNA2-1/nc886 en el tejido tumoral respecto al tejido normal. Incluso evidenciaron que el silenciamiento de vtRNA2-1/nc886 en las células HEC-1A (adenocarcinoma endometrial) conducía a un aumento de PKR y de caspasa-3, pero a una disminución de NF-kB y VEGF (vascular endothelial growth factor) (Hu et al., 2017). Congruentemente, el silenciamiento de vtRNA2-1/nc886 fue acompañado por una disminución de la proliferación y un aumento de la apoptosis (Hu et al., 2017). En cáncer de riñón, observaron un aumento de vtRNA2-1/nc886 en el tejido tumoral respecto al tejido normal e incluso mostró mayor expresión en los estadios más avanzado III-V respecto los estadios más tempranos I-II de la carcinogénesis de riñón (Lei et al., 2017). El incremento de vtRNA2-1/nc886 reveló una disminución de la apoptosis y un aumento de la proliferación e invasión, mientras que la represión de vtRNA2-1/nc886 mostró los efectos opuestos (Lei et al., 2017). Estos resultados fueron relacionados con la activación de la vía JAK2/STAT3 asociada al aumento de la expresión de vtRNA2-1/nc886 en las células de carcinoma renal A-498 (Lei et al., 2017). En cáncer cervical, se identificó un aumento de la expresión dosis dependiente de vtRNA2-1/nc886 con las drogas paclitaxel y etopósido (Li et al., 2017). Incluso, revelaron la expresión aumentada y coordinada de vtRNA2-1/nc886, MVP y E2F1 en el tejido tumoral respecto al normal de cérvix. Adicionalmente, mediante ensayos funcionales en células SiHa observaron que la inhibición de vtRNA2-1/nc886 provoca un aumento de la sensibilidad al paclitaxel asociada a un aumento de la apoptosis. Finalmente, identificaron a E2F1 como un regulador de vtRNA2-1/nc886 y demostraron que su sobreexpresión conduce a un aumento de los niveles de vtRNA2-1/nc886 (Li et al., 2017).

Un reporte reciente, reveló un nuevo aspecto de la biología de vtRNA2-1/nc886 en cáncer de ovario. El reporte de Ahn et. al. 2018 evidenció que vtRNA2-1/nc886 es capaz de emular la acción de TGFB1, desde el punto de vista molecular y fenotípico en cáncer de ovario metastásico (Ahn et al., 2018). En primer lugar, observaron que vtRNA2-1/nc886 y TGFB1 correlacionan positivamente en 25 tejidos tumorales de pacientes con cáncer de ovario. Incluso evidenciaron que TGFB1 promueve la inducción de vtRNA2-1/nc886 a nivel de la regulación de la cromatina, fundamentalmente modulando la metilación del promotor de vtRNA2-1/nc886 (Ahn et al., 2018). Utilizando líneas celulares tumorales que expresan establemente vtRNA2-1/nc886 (SKOV3 y A2780), observaron la inducción de la migración e invasión *in vitro*, conjuntamente con un aumento de la invasión y metástasis *in vivo*, emulando el fenotipo observado por las células tratadas con TGFB1 (Ahn et al., 2018). De igual manera, la expresión de vtRNA2-1/nc886 o el tratamiento con TGFB1 evidenció una disminución de la sensibilidad a la citotoxicidad provocada por el paclitaxel en células de cáncer de ovario. Asimismo, el análisis de expresión génica

mediante microarreglos expuso que vtRNA2-1/nc886 emula el perfil de expresión génica del tratamiento con TGFB1 en las líneas celulares tumorales (OSE80PC, SKOV3 y A2780). De hecho, definieron una firma de 118 genes asociada a la alta expresión de vtRNA2-1/nc886, que permitió estratificar pacientes con peor pronóstico, alta recurrencia y baja sobrevida. Llamativamente, observaron que la modulación de vtRNA2-1/nc886 y TGFB1 coincidían en la modulación global de genes modulados por microARNs, concretamente, la actividad de microARNs supresores de tumor (Ahn et al., 2018). Confirmaron que tres microARNs (miR-124-3p, -200c-3p, y -203a-3p) aumentan cuando vtRNA2-1/nc886 es eliminado, pero se ven reprimidos cuando vtRNA2-1/nc886 es incrementado o frente al tratamiento con TGFB1. Ensayos de *pull-down* con vtRNA2-1/nc886 biotinilado mostraron que vtRNA2-1/nc886 se asocia a DICER. Globalmente, los autores proponen que vtRNA2-1/nc886 funcionaría como un *pseudo* sustrato de DICER y por ende terminaría bloqueando el procesamiento de precursores de microARNs. Esto conllevaría a la disminución global de los microARNs maduros y por ende, a una disminución de la actividad de esos microARNs en el tejido tumoral (Ahn et al., 2018).

El conjunto de estos reportes evidencia que vtRNA2-1/nc886 posee efectos TSG y OG en diferentes tejidos, con efectos que difieren en los tejidos normales y tumorales dependiendo del contexto celular. Estos reportes también exponen que vtRNA2-1/nc886 podría alterar o interactuar con diferentes proteínas que afectan diferentes vías dependiendo el contexto y origen celular (Figura 12) (revisado en Yeganeh & Hernandez, 2020.

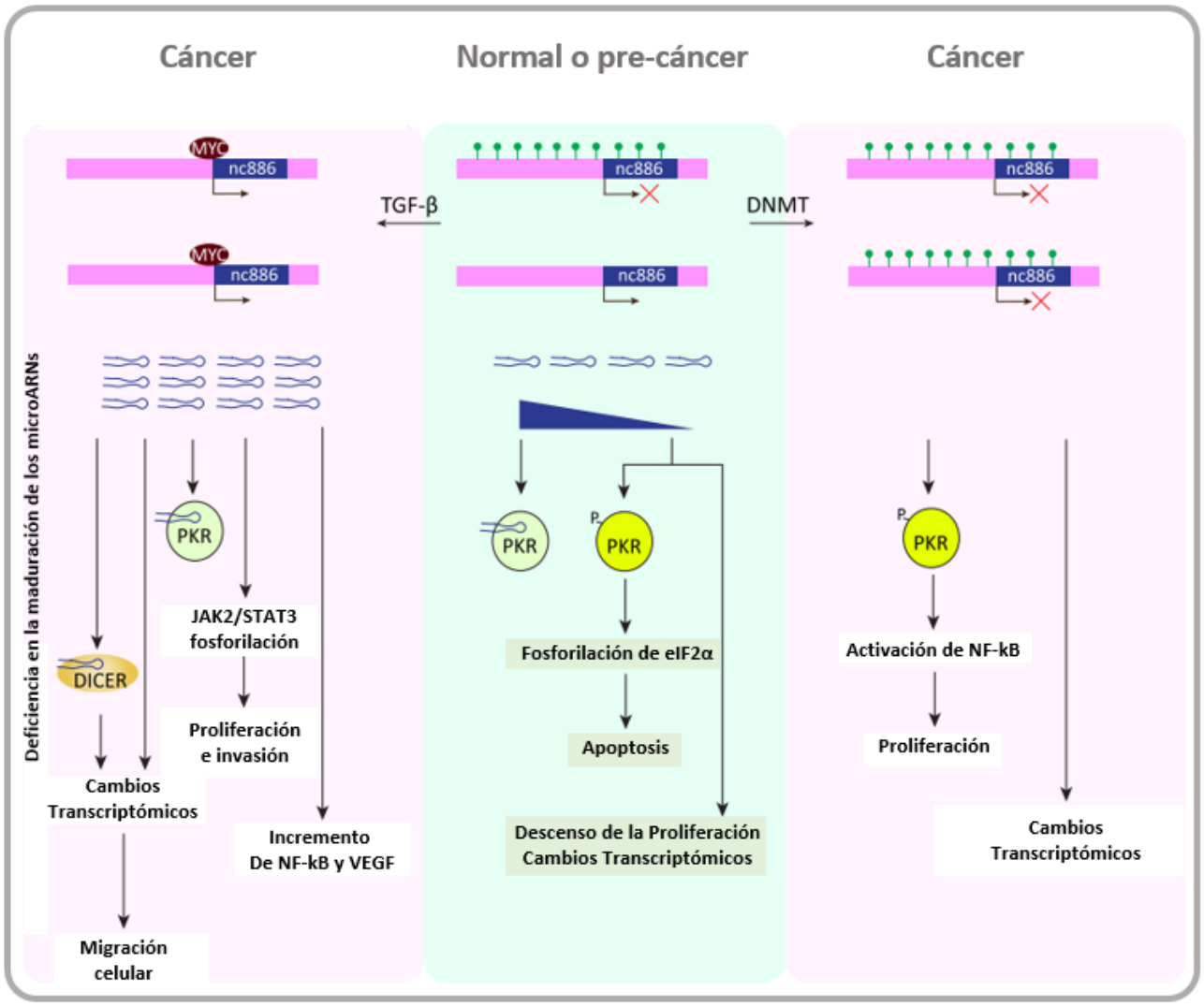

Figura 12. **VtRNA2-1/nc886 en cáncer.**

En células normales el locus de vtRNA2-1/nc886 está metilado de manera alelo específica y los niveles de expresión de vtRNA2-1/nc886 son suficientes para atenuar la activación de PKR mediante asociación directa. Una de los modelos aceptados en células normales, es que la disminución de los niveles de vtRNA2-1/nc886 conduce a la activación de PKR y al consecuente paro traduccional, disminución de la proliferación e inducción de la apoptosis. También se reportó que los efectos funcionales de vtRNA2-1/nc886 pueden ser independientes de PKR. Se describió que en algunos tipos de cáncer la expresión de vtRNA2-1/nc886 disminuye debido al aumento de la metilación del locus dependiente de las DNMTs. Alternativamente, se determinó que los niveles de vtRNA2-1/nc886 aumentan debido al aumento de la expresión de MYC y/o TGFB1, lo que conlleva a la desmetilación del locus de vtRNA2-1/nc886. El global de la literatura evidencia que los cambios en los niveles de expresión de vtRNA2-1/nc886 pueden conducir a cambios a nivel transcriptómico, la modulación de la actividad de DICER, modulación de PKR, modulación de la vía de JAK2/STAT3 y/o NF-kB y/o VEGF. Imagen extraída y modificada de Yeganeh & Hernandez, 2020.

2. LOS PEQUEÑOS ARNS DERIVADOS DE VTRNA2-1/NC886.

Como comentamos anteriormente, la capacidad precursora de pequeños ARNs derivados de vtRNA2-1/nc886 y su actividad tipo microARNs fue previamente descrita. Existen varios reportes que demostraron que los pequeños ARNs derivados de vtRNA2-1/nc886 se generan de manera no canónica, independiente de DROSHA y dependiente de DICER (Figura 13) (Cloonan et al., 2011; Miñones-Moyano et al., 2013; Pillai et al., 2010; Treppendahl et al., 2012).

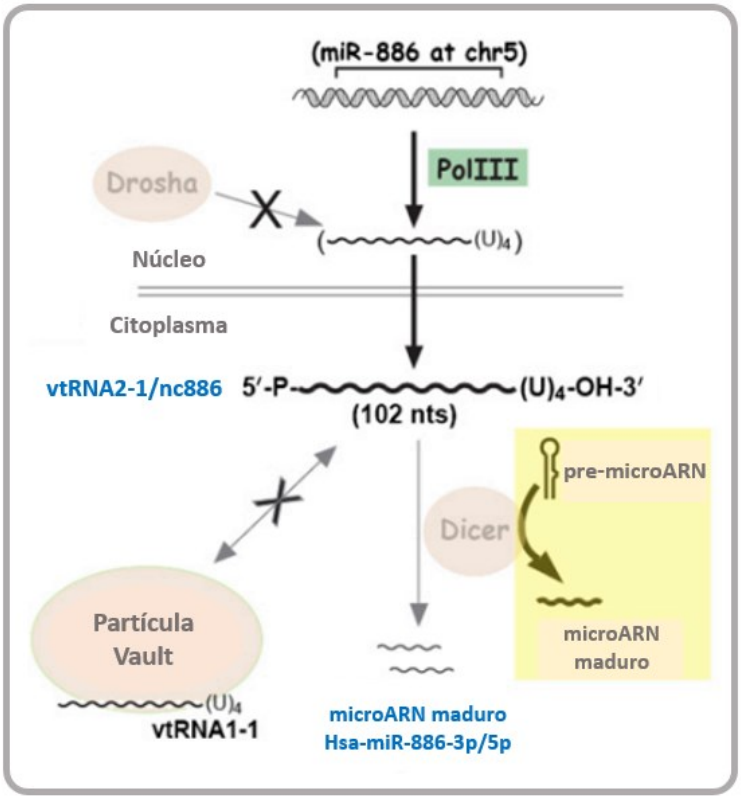

Figura 13. **Biogénesis de vtRNA2-1/nc886 y formación de pequeños ARNs.**

El locus de vtRNA2-1/nc886 es transcripto por la ARN polimerasa III, el transcrito de vtRNA2-1/nc886 no es procesado por DROSHA, es exportado del núcleo y al llegar al citoplasma no se asocia con la partícula vault. Su asociación a DICER y la formación de pequeños ARNs derivados (hsa-miR-886-5p y hsa-miR-886-3p) ha sido evidenciada en algunos reportes. Imagen extraída y modificada de Lee et al., 2011.

Adicionalmente, el advenimiento de las tecnologías de transcriptómica de pequeños ARNs no codificantes condujo a la aparición de varios reportes que también revelaron la presencia de fragmentos derivados de los vtRNAs en plasma y vesículas extracelulares (EVs) (Arroyo et al., 2011; van Balkom et al., 2015; Li et al., 2013; Lunavat et al., 2015; McDonald et al., 2019; Nolte'T Hoen et al., 2012; Perfetti et al., 2014; Tosar et al., 2015; Xiang et al., 2019),

incluso para los pequeños ARNs derivados específicamente de vtRNA2-1/nc886 en plasma o EVs (Arroyo et al., 2011; McDonald et al., 2019; Perfetti et al., 2014; Xiang et al., 2019). Se ha mencionado el posible potencial biomarcador de hsa-miR-886-5p/snc886-5p en mieloma y distrofia miotónica (Perfetti et al., 2014; Xiang et al., 2019). Es por esto que a pesar de que los microARNs (hsa-miR-886-3p/snc886-3p y hsa-miR-886-5p/snc886-5p) fueron eliminados de la base datos miRBase a partir de la actualización v16 (11/2011), igual existen reportes en cáncer sobre los pequeños ARNs derivados de vtRNA2-1/nc886.

En particular, hsa-miR-886-3p/snc886-3p el fragmento derivado del extremo 3' de vtRNA2-1/nc886 ha sido reportado como TSG en cáncer: próstata (Aakula et al., 2015; Fendler et al., 2011), vejiga (Nordentoft et al., 2012), mama (Tahiri et al., 2014), colon (Yu et al., 2011), pulmón (Bi et al., 2014; Cao et al., 2013; Gao et al., 2011; Shen et al., 2018) y tiroides (Dettmer et al., 2014; Xiong et al., 2011). Múltiples reportes de evidenciaron efectos funcionales de tipo TSG al modular la expresión de hsa-miR-886-3p/snc886-3p, concretamente su expresión disminuye la proliferación en próstata (Aakula et al., 2015), vejiga (Nordentoft et al., 2012), mama (Tahiri et al., 2014), pulmón (Cao et al., 2013; Shen et al., 2018) y tiroides (Xiong et al., 2011); disminuye la migración y/o invasión *in vitro* en pulmón (Cao et al., 2013; Shen et al., 2018) y tiroides (Xiong et al., 2011); la capacidad de crecimiento de esferoides en tiroides (Xiong et al., 2011) y disminuye la invasión y el crecimiento tumoral *in vivo* en pulmón (Cao et al., 2013; Shen et al., 2018). No obstante, pocos reportes demostraron un perfil de expresión OG para hsa-miR-886-3p/snc886-3p en cáncer: renal (Yu et al., 2014), colorrectal (Schou et al., 2014) y esófago (Okumura et al., 2016). De hecho, sólo encontramos un reporte en cáncer renal que evidencia una función OG asociada a hsa-miR-886-3p/snc886-3p, donde aumentó la proliferación, migración y redujo la apoptosis (Yu et al., 2014).

En la literatura encontramos múltiples genes blanco de acción directa reportados para hsa-miR-886-3p/snc886-3p: PLK1 (polo like kinase 1), TGFB1, CDC6 (cell division cycle 6), CXCL12 (C-X-C motif chemokine ligand 12), PITX1 (paired like homeodomain 1) y FXN (frataxin) (Cao et al., 2013; Mahishi et al., 2012; Pillai et al., 2010; Xiong et al., 2011; Yu et al., 2014).

Globalmente, de los 6 reportes en cáncer donde realizaron ensayos funcionales con hsa-miR-886-3p/snc886-3p en 5 de ellos evidencian su función TSG mientras que en uno su función OG.

En paralelo, existen reportes sobre la actividad en cáncer de hsa-miR-886-5p/snc886-5p, el sncARN derivado del extremo 5' de vtRNA2-1/nc886. Llamativamente, la mayoría de los reportes sobre hsa-miR-886-5p/snc886-5p lo postulan como OG en cáncer: cervical (Kong et al., 2015; Li et al., 2011), oral (Xiao et al., 2012), linfoma (Liu et al., 2013), mama (Zhang et al., 2014), tiroides (Dettmer et al., 2014), vejiga (Khoshnevisan et al., 2015) y mieloma

múltiple (Xiang et al., 2019). No obstante, sólo dos reportes mostraron un perfil TSG para hsa-miR-886-5p/snc886-5p: pulmón (Gao et al., 2011) y carcinoma hepatocelular (Han et al., 2012). Los reportes que realizaron ensayos funcionales modulando la expresión de hsa-miR-886-5p/snc886-5p en cáncer, evidencian un efecto OG. Resumidamente, estos reportes exponen que hsa-miR-886-5p/snc886-5p contribuye: aumentando la proliferación y disminuyendo la apoptosis en cáncer cervical (Kong et al., 2015; Li et al., 2011), mama (Zhang et al., 2014) y mieloma múltiple (Xiang et al., 2019); regulando positivamente la transición de G1/S del ciclo celular en mieloma múltiple (Xiang et al., 2019); disminuyendo la sensibilidad al cisplatino en cáncer cervical (Kong et al., 2015); aumentando la capacidad de migración e invasión en cáncer cervical (Kong et al., 2015), mama (Zhang et al., 2014) y mieloma múltiple (Xiang et al., 2019); y aumentando el crecimiento tumoral *in vivo* en cáncer cervical (Kong et al., 2015).

También se reportaron posibles genes blancos de acción de hsa-miR-886-5p/snc886-5p: BAX (BCL2 associated X, apoptosis regulator) y p53 en cáncer cervical (Kong et al., 2015; Li et al., 2011) y mieloma múltiple (Xiang et al., 2019). Sin embargo, el único gen blanco de acción directa de hsa-miR-886-5p/snc886-5p validado en cáncer es p53 (Kong et al., 2015).

Complementariamente a las funciones descritas en cáncer para los fragmentos derivados de vtRNA2-1/nc886 existen reportes que los mencionan participando en otras patologías. En este sentido, hsa-miR-886-3p/snc886-3p fue descrito como un microARN involucrado en enfermedades hematológicas (Pillai et al., 2010) y en la ataxia de Friedrich (Mahishi et al., 2012). Por otro lado, hsa-miR-886-5p/snc886-5p fue vinculado con la enfermedad de Parkinson (Miñones-Moyano et al., 2013).

3. OTROS ASPECTOS DE LA REGULACIÓN EPIGENÉTICA DE VTRNA2-1/NC886.

Como se mencionó anteriormente la regulación epigenética de vtRNA2-1/nc886 ha sido objeto de múltiples reportes en la literatura de cáncer y ha revelado aspectos poco convencionales en su regulación epigenética. El estudio del perfil de metilación de vtRNA2-1/nc886 en tejidos normales (leucocitos, hígado, cerebro y placenta), mediante ensayos de secuenciación de bisulfito y microarreglos de metilación (Infinium HumanMethylation450 BeadChip array) reveló que el 76% de las muestras presentan un alelo metilado, siendo mayoritariamente el alelo materno y que la metilación de vtRNA2-1/nc886 es un evento post-fertilización (Romanelli et al., 2014). Más recientemente, se evidenció que vtRNA2-1/nc886 es uno de los epialelos metastables que más responde al ambiente (van Dijk et al., 2018; Richmond et al., 2018; Silver et al., 2015). De hecho, un reporte evaluó la influencia del momento de la concepción, diferentes estaciones climáticas, sobre la metilación global del genoma en individuos de Gambia rural. Llamativamente, reportaron que vtRNA2-1/nc886 presenta una distribución bi-modal

de la metilación en los individuos, que no sería mediada genéticamente (Silver et al., 2015). Incluso, se evidenció que los niños concebidos en la estación seca exhiben hipometilación del promotor vtRNA2-1/nc886 (<40%) comparado con aquellos niños que fueron concebidos en la estación lluviosa. Conjuntamente, se determinó que la metilación fue establecida en las etapas iniciales del embrión y que esta es mantenida durante el desarrollo y la diferenciación (Silver et al., 2015). Asimismo, se logró establecer un vínculo entre el estado nutricional de las madres y el establecimiento de la metilación en los niños, concretamente, vinculado a los biomarcadores del metabolismo del carbono. Se encontró que aquellas madres con baja vitamina B2 (riboflavina) y metionina en el momento de la concepción, se asociaban con un estado hipometilado de vtRNA2-1/nc886. Contrariamente, los bajos niveles de dimetilglicina resultaron protectivos del estado de hipometilación de vtRNA2-1/nc886 (Silver et al., 2015). Finalmente, evidenciaron que el estado de metilación de vtRNA2-1/nc886 una vez establecido en el individuo es preservado durante al menos 10 años (Silver et al., 2015). Incluso se observó que el vtRNA2-1/nc886 presenta variabilidad inter-individuos, mostrando un patrón de metilación atípico denominado impronta polimórfica (Joo et al., 2018; Lei et al., 2017; Park et al., 2017; Romanelli et al., 2014).

HIPÓTESIS

VtRNA2-1/nc886 es un ARN no codificante transcripto por la ARN polimerasa III que posee la capacidad de modular la activación de proteínas como PKR y/o OAS1, que consecuentemente alteran funciones celulares como la traducción global, proliferación y apoptosis. Asimismo, el vtRNA2-1/nc886 se encuentra diferencialmente regulado en algunos tipos de cáncer, pudiendo actuar como supresor de tumor u oncogén de manera tejido específico. Sumado a esto existen evidencias que permiten suponer que vtRNA2-1/nc886 puede ser procesado a pequeños ARNs no codificantes, y que los mismos poseen la capacidad de regular la expresión génica mediante la vía de microARNs. En este contexto, entendemos que la represión de la expresión de vtRNA2-1/nc886, así como la de los pequeños ARNs no codificantes con función tipo microARNs derivados (hsa-miR-886-3p/snc886-3p), contribuyen al desarrollo y/o mantenimiento del fenotipo maligno en el cáncer de próstata.

OBJETIVOS

1. OBJETIVO GENERAL

Descubrir las implicancias de la desregulación de vtRNA2-1/nc886 y su pequeño ARN derivado (hsa-miR-886-3p/snc886-3p) en el fenotipo tumoral de adenocarcinoma de próstata.

2. OBJETIVOS ESPECÍFICOS

2.1. Determinar las implicancias de la desregulación de vtRNA2-1/nc886 en el origen y el mantenimiento del fenotipo tumoral de adenocarcinoma de próstata.

2.1.1. Determinar el nivel de expresión y la posible desregulación de vtRNA2-1/nc886 en muestras de tejido normal y tumoral.

2.1.2. Identificar el origen molecular de la desregulación de vtRNA2-1/nc886.

2.1.3. Determinar el efecto de la desregulación de vtRNA2-1/nc886 en el fenotipo neoplásico.

2.1.4. Descubrir posibles mecanismos moleculares regulados por vtRNA2-1/nc886.

2.1.5. Valorar la relevancia clínica de la desregulación de vtRNA2-1/nc886.

2.2. Determinar si vtRNA2-1/nc886 funciona como precursor para la formación de pequeños ARNs no codificantes y evaluar las implicancias de su desregulación en el origen y el mantenimiento del fenotipo tumoral de adenocarcinoma de próstata.

2.2.1. Validar la expresión y desregulación de hsa-miR-886-3p/snc886-3p en muestras de tejido normal y tumoral.

2.2.2. Determinar si los fragmentos derivados de vtRNA2-1/nc886 funcionan como microARNs.

2.2.3. Determinar el efecto de la desregulación de hsa-miR-886-3p/snc886-3p en el fenotipo neoplásico.

2.2.4. Descubrir mecanismos moleculares regulados por hsa-miR-886-3p/snc886-3p.

2.2.5. Determinar la expresión de hsa-miR-886-5p/snc886-5p en la carcinogénesis prostática y su asociación con la enfermedad.

2.3. Determinar el perfil de expresión global de vtRNA2-1/nc886 y su posible asociación con los vtRNAs canónicos en el cáncer de diferente origen tisular.

2.3.1. Determinar la expresión global de los cuatro vtRNAs humanos en cáncer.

2.3.2. Determinar si existe co-regulación y asociación funcional de los cuatro vtRNAs.

2.3.3. Determinar si la expresión de los vtRNAs se asocia a diferencias en la sobrevida de los pacientes.

2.3.4. Identificar transcritos co-regulados junto con los vtRNAs y las vías celulares sobrerepresentadas en estos genes.

RESULTADOS Y DISCUSIÓN

I. IMPLICANCIAS DE LA DESREGULACIÓN DE VTRNA2-1/NC886 EN EL ORIGEN Y EL MANTENIMIENTO DEL FENOTIPO TUMORAL DE ADENOCARCINOMA DE PRÓSTATA

***Objetivo específico 2.1*: Determinar las implicancias de la desregulación de vtRNA2-1/nc886 en el origen y el mantenimiento del fenotipo tumoral de adenocarcinoma de próstata.**

Los resultados obtenidos respecto al desarrollo del ***objetivo específico 2.1*** en el marco de la hipótesis de la tesis fueron incluidos en una publicación científica (Fort et al., 2018) adjunta a continuación.

En este manuscrito abordamos el estudio de la expresión del transcrito completo de vtRNA2-1/nc886 en tejido tumoral y normal adyacente de prostatectomías radicales incluidas en parafina, de una cohorte pequeña del Hospital Policial de Montevideo que seleccionamos con Anatomopatólogos de la Institución (*objetivo específico 2.1.1*). A continuación, para abordar el *objetivo específico 2.1.2*, extendimos el análisis de expresión de vtRNA2-1/nc886 a líneas celulares modelo de la enfermedad y evaluamos su asociación con el estado de metilación de su promotor. Complementariamente, valoramos en líneas celulares de PrCa el impacto del tratamiento con agentes desmetilantes en la expresión de vtRNA2-1/nc886 y el estado de metilación de su promotor. Incluso evaluamos la posible asociación entre el estado de metilación del promotor de vtRNA2-1/nc886 y las enzimas DNMTs (ADN metiltransferasas) en la transición tumoral de la próstata. Asimismo, examinamos los niveles de metilación del promotor de vtRNA2-1/nc886 en muestras de tejido tumoral y normal adyacente de próstata, y su asociación con parámetros de la clínica de la enfermedad, disponibles en los grandes repositorios de datos públicos (*The Cancer Genome Atlas* (PRAD-TCGA) y *Gene Expression Omnibus* (GEO)) (*objetivo específico 2.1.5*). Para explorar el *objetivo específico 2.1.3* generamos líneas celulares modelo de PrCa (DU145 y LNCaP) con la transducción estable de vtRNA2-1/nc886 y un ARN control con estructura de horquilla correspondiente. Utilizamos estas líneas celulares para evaluar el efecto de su sobreexpresión (restitución) *in vitro* sobre la viabilidad celular, la alteración del ciclo celular y la capacidad invasiva *in vitro*. El crecimiento tumoral fue también evaluado *in vivo* mediante ensayos de xenotransplante en ratones inmunocomprometidos. Finalmente, como parte del *objetivo específico 2.1.4* exploramos la asociación entre los niveles de metilación del promotor de vtRNA2-1/nc886 y una firma de genes

asociada con la progresión del ciclo celular (CCP, (Cuzick et al., 2011) en muestras de PrCa (PRAD-TCGA), encontrando una correlación invertida con los transcritos de esta firma que apoya su efecto anti-proliferativo en los tejidos de los pacientes.

El conjunto de las aproximaciones realizadas y expuestas en el manuscrito (Fort et al., 2018) nos permitió ponderar la hipótesis acerca de la presencia y desregulación de vtRNA2-1/nc886 en el PrCa y determinar que es un transcrito de expresión relativamente alta cuyos niveles disminuyen cuando el tejido maligniza, lo que está de acuerdo con una función de TSG. Determinamos la asociación del estado de metilación de su promotor con la desregulación de su expresión en la carcinogénesis prostática, así como su relación con los parámetros clínicos de la enfermedad. Esto nos llevó a establecer que la etiología de la desregulación consiste en alteraciones epigenéticas del promotor del gen, las cuales se asocian a la evolución. Finalmente, evaluamos la contribución de vtRNA2-1/nc886 en la alteración de fenotipos tumorales en el PrCa a través de su sobreexpresión, y encontramos que afecta diversos atributos tumorales como un TSG.

Artículo científico 1: Fort, R.S., Mathó, C., Geraldo, M.V., Ottati, M.C., Yamashita, A.S., Saito, K.C., Leite, K.R.M., Méndez, M., Maedo, N., Méndez, L., et al. (2018). Nc886 is epigenetically repressed in prostate cancer and acts as a tumor suppressor through the inhibition of cell growth. BMC Cancer 18, 127. doi: 10.1186/s12885-018-4049-7

Las contribuciones y actividades en las que participó cada autor están discriminadas en el manuscrito.

Fort et al. BMC Cancer (2018) 18:127
DOI 10.1186/s12885-018-4049-7

BMC Cancer

RESEARCH ARTICLE Open Access

Nc886 is epigenetically repressed in prostate cancer and acts as a tumor suppressor through the inhibition of cell growth

Rafael Sebastián Fort[1,2], Cecilia Mathó[1,2], Murilo Vieira Geraldo[3,9], María Carolina Ottati[1,2,8], Alex Shimura Yamashita[3], Kelly Cristina Saito[3], Katia Ramos Moreira Leite[4], Manuel Méndez[5], Noemí Maedo[5], Laura Méndez[5], Beatriz Garat[1], Edna Teruko Kimura[3], José Roberto Sotelo-Silveira[6,7] and María Ana Duhagon[1,2*]

Abstract

Background: Nc886 is a 102 bp non-coding RNA transcript initially classified as a microRNA precursor (Pre-miR-886) , later as a divergent homologue of the vault RNAs (vtRNA 2–1) and more recently as a novel type of RNA (nc886). Although nc886/vtRNA2–1/Pre-miR-886 identity is still controversial, it was shown to be epigenetically controlled, presenting both tumor suppressor and oncogenic function in different cancers. Here, we study for the first time the role of nc886 in prostate cancer.

Methods: Nc886 promoter methylation status and its correlation with patient clinical parameters or DNMTs levels were evaluated in TCGA and specific GEO prostate tissue datasets. Nc886 level was measured by RT-qPCR to compare normal/neoplastic prostate cells from radical prostatectomies and cell lines, and to assess nc886 response to demethylating agents. The effect of nc886 recovery in cell proliferation (in vitro and in vivo) and invasion (in vitro) was evaluated using lentiviral transduced DU145 and LNCaP cell lines. The association between the expression of nc886 and selected genes was analyzed in the TCGA-PRAD cohort.

Results: Nc886 promoter methylation increases in tumor vs. normal prostate tissue, as well as in metastatic vs. normal prostate tissue. Additionally, nc886 promoter methylation correlates with prostate cancer clinical staging, including biochemical recurrence, Clinical T-value and Gleason score. Nc886 transcript is downregulated in tumor vs. normal tissue -in agreement with its promoter methylation status- and increases upon demethylating treatment. In functional studies, the overexpression of nc886 in the LNCaP and DU145 cell line leads to a decreased in vitro cell proliferation and invasion, as well as a reduced in vivo cell growth in NUDE-mice tumor xenografts. Finally, nc886 expression associates with the prostate cancer cell cycle progression gene signature in TCGA-PRAD.

Conclusions: Our data suggest a tumor suppressor role for nc886 in the prostate, whose expression is epigenetically silenced in cancer leading to an increase in cell proliferation and invasion. Nc886 might hold clinical value in prostate cancer due to its association with clinical parameters and with a clinically validated gene signature.

Keywords: Cancer, Prostate, Metastasis, Vault RNA, nc886, vtrna2-1, miR-886, DNA methylation, Tumor suppressor, TCGA

* Correspondence: mduhagon@fcien.edu.uy; http://www.fcien.edu.uy/
[1]Laboratorio de Interacciones Moleculares, Facultad de Ciencias, Universidad de la República, Montevideo, Uruguay
[2]Departamento de Genética, Facultad de Medicina, Universidad de la República, Montevideo, Uruguay
Full list of author information is available at the end of the article

Background

Prostate cancer (PrCa) is the solid tumor with the highest incidence in men in Western countries, representing the second leading cause of male cancer death [1, 2]. Worldwide, one sixth of men will be diagnosed with prostate cancer in their lifetime. Although most patients can be treated successfully, a minor proportion develop an aggressive form of the disease that is currently incurable. It is fundamental to develop biomarkers that allow the precise prognosis at early stages, as well as new therapeutic tools to treat these patients in advanced stages. Non-coding RNAs have recently emerged as key players in cancer initiation and progression [3, 4], therefore their clinical value is under intense investigation [5–7].

The large collection of non-coding RNAs (ncRNAs) of the human genome is broadly grouped per size and function in two main types: a group of < 40 nt long RNAs known as "small RNAs" (including microRNAs, piwiRNAs, snoRNAs) and a group of > 200 nt long RNA named "long non-coding RNAs" [8]. The "vault" RNAs (vtRNAs) are a class of 84-141 nt long eukaryotic RNAs, that are transcribed by RNA polymerase III. They associate with conserved vault proteins forming the vault particle, a complex whose function and relevance in cancer remains scarcely understood [9]. Whereas the three human vtRNA1–1-3 are integral components of the vault particle, vtRNA 2–1 is a more divergent homologue, whose transcript is neither associated to the vault particle or co-regulated with the vtRNA1–1-3 [10, 11]. Before miRBase version 16, vtRNA2–1 was classified as a microRNA precursor, thus annotated as "precursor of hsa-miR-886-3p" (pre-miR-886); however, the recognition of its sequence homology with the three vtRNA-1 RNAs [11] led to its re-classification as vtRNA2–1 and the elimination of its derived microRNAs from miRBase. However, vtRNA2–1/pre-miR-886, was more recently proposed to be a new type of non-coding RNA (referred there as "nc886"), that acts as a tumor suppressor, inhibiting the activation of Protein Kinase RNA-activated (PKR) by direct interaction [12–14]. Consistent with these findings, Treppendahl et al. showed that nc886 functions as an epigenetically regulated tumor suppressor gene in acute myeloid leukemia, and that genome demethylating treatment inhibits PKR phosphorylation [15]. However, in the same work, the authors detected mature miRNAs derived from nc886, and showed they are products of the processing of pre-miR-886 by a non-canonical pathway independent of DROSHA. In addition, other groups have identified the mature microRNAs derived from pre-miR-886 in lung small cell carcinoma [16] and prostate cancer [17], presenting evidence of its association with disease progression.

Different lines of evidence have revealed that the epigenetic control of nc886 is complex and may own clinical relevance. Independent reports in breast, lung, colon, bladder, esophagus and stomach cancer showed that its promoter is differentially methylated in tumor vs. normal tissue [18, 19]. In fact, in lung cancer, chronic myeloid leukemia and gastric cancer, its differential methylation correlates with patient prognosis and survival [15, 16, 20]. Although these findings support a tumor suppressor role for nc886, a recent communication proposed its action as an oncogene in thyroid cancer [21]. Intriguing aspects of the epigenetic regulation of this locus, include its dependence on the parental origin of the allele [22], and its sensitivity to the periconceptional environment [23].

The aim of this study was to investigate the possible involvement of nc886 in PrCa etiology and behavior. Analyzing clinical samples, we found that the full transcript of nc886 is present in prostate tissue and diminishes its abundance in tumor compared to normal tissue, thus showing a gene expression pattern of a tumor suppressor gene. The increased methylation of nc886 promoter in transformed vs. non-transformed tissue, as well as demethylating agent treated vs. untreated cell lines, indicate that the molecular etiology of nc886 downregulation is the methylation of its promoter. Indeed, nc886 promoter methylation level correlates with clinical parameters of PrCa (Gleason Score, clinical T value and biochemical relapse). Forced restitution of nc886 in DU145 and LNCaP cell lines produces an inhibition of cell invasion and proliferation in vitro and a reduction of DU145 tumor growth in vivo. These results are consistent with a tumor suppressor role, suggesting a nc886 antiproliferative function in normal prostate tissue. Finally, the interrogation of the Prostate Adenocarcinoma of The Cancer Genome Atlas (TCGA-PRAD) cohort, uncovered a negative association between the expression of nc886 and the expression of genes belonging to the PrCa cell cycle progression gene signature (CCP), providing a molecular support for the phenotype experimentally observed after nc886 recovery.

Methods

Human specimens

Tissue sections were obtained from paraffin fixed blocks stained with hematoxylin and eosin (H&E) of 6 archived radical prostatectomies and were evaluated by three pathologists at the Department of Anatomic-pathology of the Police Hospital. This study was approved by the Hospital Policial, D.N.AA.SS., Montevideo, Uruguay (2010).

Matched normal and tumor regions, showing similar parenchyma-stroma ratio and similar cytological findings at the stroma were selected. Unstained section of 10-μm thickness, contiguous to the sections selected by the pathologist, were then freshly obtained to extract small RNAs using the RNeasy FFPE (Qiagen) Kit, with the

following modifications: two extra washes with xylene and absolute ethanol were added. The RNA was resuspended in RNAse free water and stored at − 20 °C for further analysis.

Cell lines

RWPE-1, LNCaP (ATCC CRL-1740), PC-3 and DU145 human prostate cancer cell lines were obtained from ATCC (Manassas, VA, USA). LNCaP, DU145 and PC-3 were maintained in RPMI 1640 (R7755) supplemented with 10% FBS (PAA™) and penicillin/streptomycin. RWPE-1 cell line was cultured in Keratinocyte Serum Free Medium (Gibco by LifeTechnologies™) supplemented with 0.03 mg/mL bovine pituitary extract (BPE) and 0.5 ng/mL EGF human recombinant epidermal growth factor (EGF) and penicillin/streptomycin. All cell lines were maintained in a 5% carbon dioxide atmosphere at 37 °C.

A lentiviral vector bearing the precursor nc886 or a scrambled sequence of the same length, both cloned downstream of the CMV promoter (miExpress precursor expression clones, pEZX-MR02, GeneCopoeia) were transduced in DU145 and LNCaP. Transduced cells were then selected by growth in the presence of puromycin.

5-Azacytidine treatment

DU145, RWPE-1, PC-3 and LNCaP cells were treated for 72 h with 1.5 μmol/L 5-Azacytidine (ab142744, Abcam) and DMSO as control, replacing the medium with freshly added drug every 24 h following manufacturer's instructions.

RNA extraction, reverse transcription and quantitative real time PCR

Total RNA was extracted using the Qiagen™ miRNAeasy kit. Reverse transcription was performed using the Qiagen PCR miScript II System. Quantitative real time PCR (qPCR) was performed with the miScript SYBR Green PCR Kit using specific oligonucleotides. For nc886: 5′CGGGTCGGAGTTAGCTCAAGCGG3′ forward primer and 5′AAGGGTCAGTAAGCACCCGCG3′ reverse primer, as in Lee K et al. [12]. U6 RNA was amplified using the primer assay purchased from Qiagen (Hs_RNU6-2_11 miScript Primer Assay (MS00033740)) and the miScript Universal Primer (Qiagen). The relative quantification was attained using the ΔΔCT method, in a Rotor-Gene 6000 equipment (Corbett Life Science), employing U6 as the internal control of RNA load.

MTT assay

Five thousand DU145 and LNCaP cells per well were seeded in 96 culture plates. Twenty μL of 3-(4,5-dimethylthiazol-2-yl)-2,5-diphenyl-2H-tetrazolium bromide (MTT) 5 mg/mL solution dissolved in 1X PBS was added to the wells and cultures were incubated for 4 h at 37 °C in a 5% CO_2 controlled atmosphere. The medium was then aspirated and 100 μL of DMSO was added to each well and incubated at room temperature in the dark for 15 min with moderate orbital shaking. Optical density (OD) was read in a plate spectrophotometer (Thermo Scientific Varioskan® Flash Multimode) at 570 nm and 690 nm wavelengths.

Flow cytometry for DNA content

DU145 cells transfected with lentiviral vectors producing nc886 or a scrambled RNA control were seeded in triplicate in 6-well plates. Upon reaching 60% confluence, cells were harvested by trypsinization, washed twice with 1X PBS and resuspended in 1X PBS by gentle vortexing. Cells were then fixed by adding 1 mL of ice cold 70% ethanol dropwise in 1X PBS and incubated at − 20 °C for 30 min. Next, cells were washed with 1X PBS and centrifugated at 1200 rpm at 4 °C for 5 min and the resuspended cell pellets were incubated with 0.1 mg/mL of RNase and 50 μg/mL propidium iodide for 15 min at room temperature in the dark. Flow cytometry measurement of nuclear DNA content was performed in a Accuri™ C6 flow cytometer (BD Bioscience), counting 10.000 total events per sample (BD Accuri C6 software).

Matrigel invasion assays

24-well transwell inserts of 8 μM pore size (Corning #3422) were coated with Matrigel (Corning) for in vitro invasion assays. Fifteen thousand (DU145) or 20,000 (LNCaP) cells were seeded in serum-free RPMI 1640 and migrated towards the bottom chamber containing RPMI 1640 supplemented with 10% FBS. After 48 h the cells were fixed with 100% methanol and stained with hematoxylin and eosin (H&E). Non-invading cells were scrubbed with a cotton swab. Five microscopic fields were photographed and counted for each sample. Values were averaged from at least 3 independent experiments.

Mice xenograft

Six 4-week-old male athymic NUDE BALB/C mice were maintained according to the protocols and ethical regulations of the animal facility of the Institute of Biomedical Science, at the University of Sao Paulo, Brazil (protocol 134/10, approved by the Ethics Committee for Animal Use). In order to grow tumors, these mice were subcutaneously injected on both flanks using 3×10^6 DU145 cells resuspended in 50 μl of Matrigel matrix (Corning Inc.) per inoculation. The tumor growth was measured weekly with calipers and the corresponding volumes were calculated as: length x width x height x π/2. When tumors reached 2 cm, the animals were euthanized, and tumors were extracted and properly stored for further analysis.

Analysis of mice tumors

The study of histological sections of the tumors extracted from the mouse xenotransplantation assays, was conducted at the Laboratory of Medical Research – LIM55, Urology Department, of the University of Sao Paulo, Brazil. Specifically, the percentage of necrosis and mitotic indexes in the histological sections of the tumors stained with H&E were quantified.

Dataset analysis

The TCGA-PRAD data was downloaded from the TCGA portal (https://tcga-data.nci.nih.gov/docs/publications/tcga/?) [24] and the Methhc database (http://methhc.mbc.nctu.edu.tw/php/index.php) [25]. This dataset includes the RNA-Seq expression values of 50 matched normal and tumor tissue and additional unmatched normal and tumor samples, generated using Illumina sequencing technology. The methylation data of the TCGA-PRAD cohort, was extracted from the Illumina Infinium Human Methylation 450 BeadChip array data of the 49-paired normal and prostate tumor samples and additionally unmatched normal and tumor tissues (336 in total). Several public methylomes available at the Gene Expression Omnibus (GEO) repository [26] were also analyzed: matched normal and tissue PrCa GSE76938 [27], PrCa metastasis GSE38240 [28], PrCa cell lines GSE34340, GSE62053 and GSE54758 [29, 30] and HCT166 cell lines GSE51810 [31]. The average of the normalized beta-values for the 6 CpGs sites located at the nc886 TSS200 promoter (cg18678645, cg06536614, cg26328633, cg25340688, cg26896946, cg00124993) were calculated. Hierarchical clusterization obtained through Euclidean algorithm was performed using the Gene-E (http://www.broadinstitute.org/cancer/software/GENE-E/) for the methylation beta-values and Morpheus (https://software.broadinstitute.org/morpheus/) for gene expression values.

Statistical analysis

All experiments were performed at least in triplicate, and the corresponding variables are expressed as average value ± standard deviation or standard error. Statistical analyses were done using single and two-tailed t-test, and the statistical significance of the observed differences were expressed using the p-value (* $p < 0.05$, ** $p < 0.01$, *** $p < 0.001$). D'Agostino-Pearson was conducted as the normality test and nonparametric Spearman was used to test correlation.

Results

Nc886 promoter methylation is increased in neoplasic relative to normal prostatic tissue and correlates with biochemical recurrence and tumor grade

In view of the existing background about the role of nc886 promoter methylation in other types of cancer [15, 16, 18, 19], we analyzed the methylation levels of its proximal promoter in PrCa. For that, we selected the region of 200 nt located upstream of the transcription start site (TSS200) of nc886 in the genome wide methylation microarray data available at TCGA-PRAD. The analysis of the available 50 paired tissue samples showed a statistically significant increase of the methylation average in tumor (0.6615 ± 0.08215) relative to normal tissue (0.5734 ± 0.08049) (p-value < 0.001) (Fig. 1a). An identical analysis was performed using a recently published PrCa cohort [27] comprising 52 matched cancer and benign-adjacent tissue of radical prostatectomies from Stanford University Medical Center, yielding very similar results (0.5437 ± 0.06445 normal vs 0.6092 ± 0.06278 tumor) (Fig. 1a). It is worth to note that nc886 TSS200 methylation is quite variable among the samples. Nevertheless, regardless of the initial methylation status, the tumor tissue consistently shows a higher methylation relative to the adjacent normal tissue, as depicted in the TSS200 methylation clustering of patient samples presented in Additional file 1: Figure S1.

Seeking to investigate the relevance of nc886 promoter methylation in the metastatic stage of PrCa, we analyzed its status in 4 normal prostates from organ donors and 8 PrCa metastases in a rapid autopsy cohort of lethal metastatic PrCa available at the GEO [28]. We observed that the metastases have a significant higher average nc886 promoter methylation (0.7456 ± 0.0771) than the normal tissue (0.4331 ± 0.1283) (p-value < 0.001) (Fig. 1b) of the same study. Interestingly, the metastatic tumors present similar levels of nc886 promoter methylation (0.7456 ± 0.0771) than the highest methylated group of samples among the primary tumors (0.7239 ± 0.0478) and normal tissues (0.6945 ± 0.0386) defined in Additional file 2: Figure S2. To assess the clinical relevance of nc886 promoter methylation, we studied its association with the clinical data of the patients of the TCGA- PRAD cohort. We found that nc886 TSS200 average methylation is significantly associated with Gleason score (p-value < 0.05), clinical T-value (p-value < 0.05) and biochemical relapse (p-value < 0.01) (Fig. 1c-e). We also found that the nc886 methylation status in the normal prostatic tissue dissected from prostatectomies [19], calculated with the 10 selected CpG sites (Additional file 2: Figure S2), is associated with the clinical T-value of the matched patient tissue (Additional file 2: Figure S2D) (p-value < 0.05).

Increased promoter methylation of nc886 causes a reduction of the transcript level in prostate cancer

Although growing evidence is demonstrating a tumor suppressor role for nc886 in several types of cancer, there is fewer assessment of the molecular etiology of its downregulation by promoter methylation during

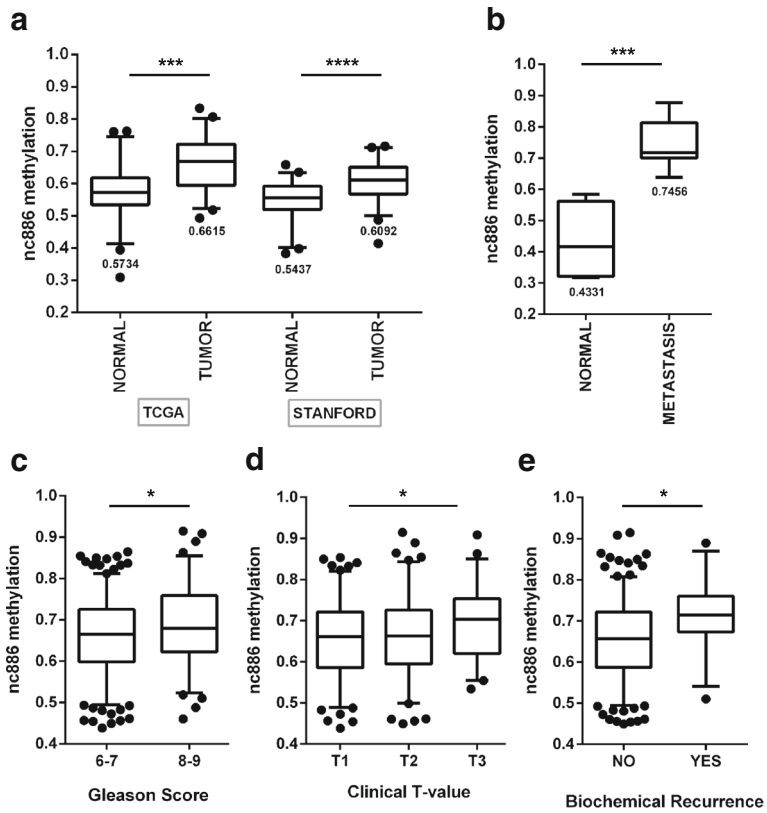

Fig. 1 Nc886 TSS200 methylation status and its correlation with clinical parameters of PrCa in patients of the TCGA-PRAD cohort. **a** Average TSS200 methylation of nc886 in matched normal and tumor prostate tissue of 50 patients from TCGA cohort and 52 patients from STANFORD cohort data available in GSE76938 GEO dataset. **b** Average TSS200 methylation of nc886 for normal and metastatic prostate tissue data available in GSE38240 GEO dataset. In A and B the numbers below the boxes indicate the mean value of each distribution. **c** Average TSS200 methylation of nc886 in association with Gleason Score of tumor tissue of 329 patients. **d** Association between average TSS200 methylation of nc886 and clinical T values of tumor tissue of 272 patients. **e** Association between average TSS200 methylation of nc886 and biochemical recurrence in 276 patients. Clinical data analyses incorporate TCGA-PRAD DNA methylation data of the tissues with available associated Gleason score data (**c**), Clinical T-value data (**d**) and Biochemical recurrence data (**e**). Two-tailed T test was performed for all categories, and only significant differences are depicted: * *P* value < 0.05; ** *P*-value < 0.01; *** *P* -value < 0.001; **** *P*-value < 0.0001

carcinogenesis. Thus, we sought to find a direct association between nc886 transcripts levels and the methylation of its promoter in PrCa clinical samples. We first investigated the presence and deregulation of the full nc886 transcript in PrCa. Consequently, we isolated RNA from six paired normal and tumor samples from paraffin blocks obtained from radical prostatectomies, and we performed RT-qPCR with oligonucleotides specific for the nc886 transcript. We found that nc886 transcript is significantly suppressed in tumor relative to normal tissue, with an average fold change in expression of – 0.56 ± 0.14 (Fig. 2a). Furthermore, the interrogation of several datasets available at GEO showed that the average methylation value of nc886 promoter in prostate cell lines (PrEC, DU145, RPWE-1, LNCaP and PC-3) inversely correlates with the levels of its transcript (rs = – 0.80) (Fig. 2b). In addition, the treatment of DU145, LNCaP, RWPE-1 and PC-3 cell lines with the DNA demethylating agent 5-Aza-cytidine increases nc886 levels (Fig. 2c). As seen in the clinical specimens, the level of nc886 expression/nc886 methylation in the PrCa cell lines is variable (Fig. 2b). Although we know the nc886 status in the matched normal/tumor tissue of the clinical specimens (Fig. 1a), we unfortunately do not know the nc886 status in the normal prostate cells of the cell line donor patients. However, based on the clinical data, nc886 expression is expected to be higher in the non-transformed cells of the donor. In this context, what is relevant for the hypothesis is the decrease in nc886 expression during malignant transformation independently of the initial status of the gene. Interestingly, nc886 status separates the cell lines in two groups, one comprising PrEc and DU145 and another comprising RWPE-1, LNCaP and PC3. These two groups of cell lines are representative of the variable nc886 status in the prostate tissues. Therefore, DU145 and LNCaP/PC-3 PrCa cell lines represent suitable models for the spectrum of nc886 variability observed in the clinical set.

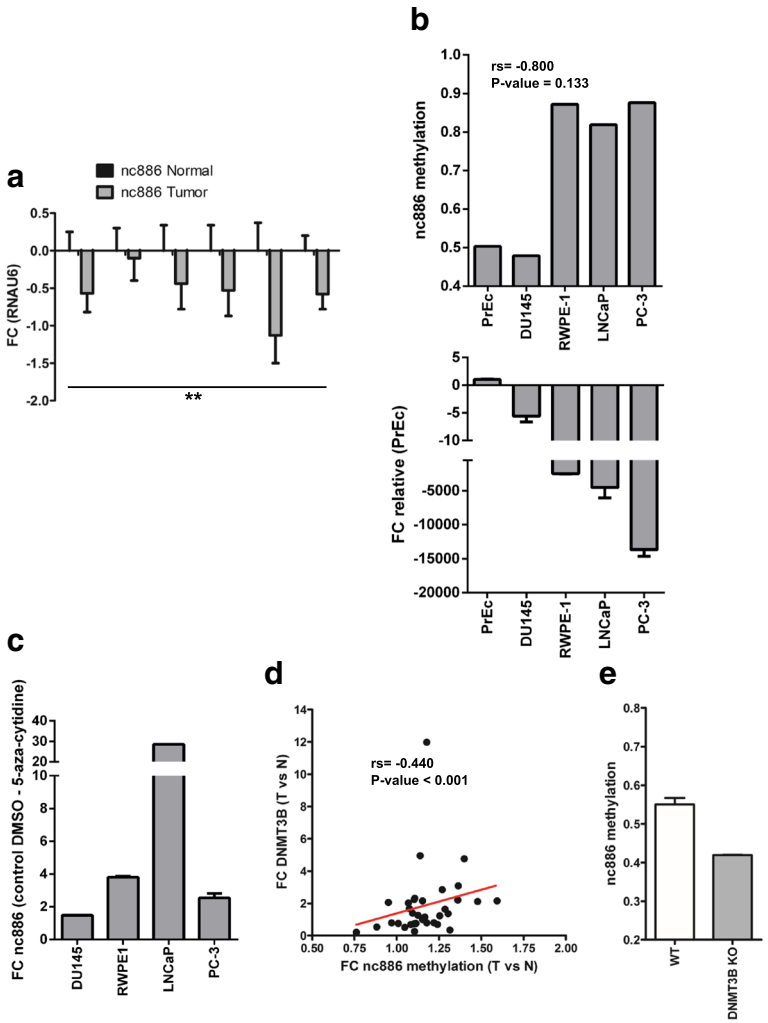

Fig. 2 Nc886 expression and its correlation with promoter methylation in prostate cells. Expression levels of nc886 were determined using RT and qPCR with specific primers (see Materials and Methods) and RNAU6 was used as and endogenous control of RNA amount (A, B and C). **a** Expression of nc886 in 6 matched normal and tumor human prostate tissue relative to RNAU6. **b** Expression of nc886 relative to PrEC are presented (upper plot) and average methylation of nc886 promoter (lower plot) in prostate cancer cell lines. Methylation data was extracted from publicly available GEO datasets GSE34340, GSE62053 and GSE54758. **c** Expression of nc886 in prostate cancer cell lines treated with 5-Azacytidine relative to untreated cell lines (control DMSO). **d** Correlation between the fold change in average nc886 TSS200 methylation and DNMT3B expression in tumor vs. normal tissue, assessed in 50 matched samples of the TCGA-PRAD dataset. **e** Average methylation of nc886 promoter 10 CpG sites of wt HCT116 and DNMT3B KO HCT116 cell line (GEO dataset GSE51810). P-value < 0.05 t-test two-tailed. * P-value < 0.05; ** P-value < 0.01; *** P-value < 0.001; two tailed t-test. The correlation was conducted by D'Agostino-Pearson normality and nonparametric Spearman tests

Patterns of DNA methylation during development and carcinogenesis are established by DNA methyl transferases, comprising maintenance DNMT1 and de novo DNMT3A and DNMT3B. To investigate which of these enzymes would be responsible for the increase in nc886 TSS200 methylation in prostate carcinogenesis, we compared the expression of the DNMTs with the level of nc886 TSS200 methylation in TCGA-PRAD tumor samples. Of the 3 DNMTs both DNMT3A and DNMT3B increase their transcript level in tumor compared to matched normal samples of this cohort (Additional file 3: Table S1), as calculated from the RNA-seq data. Interestingly, nc886 TSS200 average methylation positively correlates with the expression of DNMT3B, and DNMT3A, but not DNMT1 (Additional file 3: Table S1). More interestingly, a correlation between the fold change of expression of DNMT3B and the fold change in nc886 methylation in the 34-paired normal vs. tumor tissues is observed ($rs = 0.4402$, p-value < 0.001, Fig. 2d and Additional file 3: Table S1). Further support for the specific role of DNMT3B in nc886 promoter methylation is provided by the analysis of a GEO dataset [31], which uncovered a drastic reduction in its methylation upon the deletion of DNMT3B in the HCT116 cell line (Fig. 2e).

Overexpression of nc886 causes a decrease in tumor growth in vitro and in vivo

Since the pattern of expression and promoter methylation of nc886 in PrCa suggested that nc886 could function as tumor suppressor gene in the prostate, we decided to investigate the phenotypic consequence of nc886 transcript recovery. The overexpression of nc886 was forced into the cell line DU145 and LNCaP by stable transfection of a lentiviral vector encoding nc886 under CMV promoter regulation. A control vector, overexpressing a random RNA sequence, which has no complementarity with human genomic sequences, was used as a control in all the experiments. The overexpression of nc886 was confirmed by RT-qPCR, demonstrating an increase of nc886 of 4.9 ± 0.2 in DU145 and 43.87 ± 0.01 in LNCaP (Fig. 3a). The fold change in expression in DU145 transfectant mimics the difference observed between the expression of nc886 in the malignant DU145 vs. the normal PrEC cell line (Fig. 2b); it is also comparable with the fold change in nc886 expression observed in the tumor vs. normal tissue of the clinical samples (Fig. 2a). Since one of the essential hallmarks of malignant transformation is the increased cell proliferation, we evaluated this phenotype using the cell viability MTT assay. We found that DU145 and LNCaP cell lines overexpressing nc886 have a lower rate of proliferation

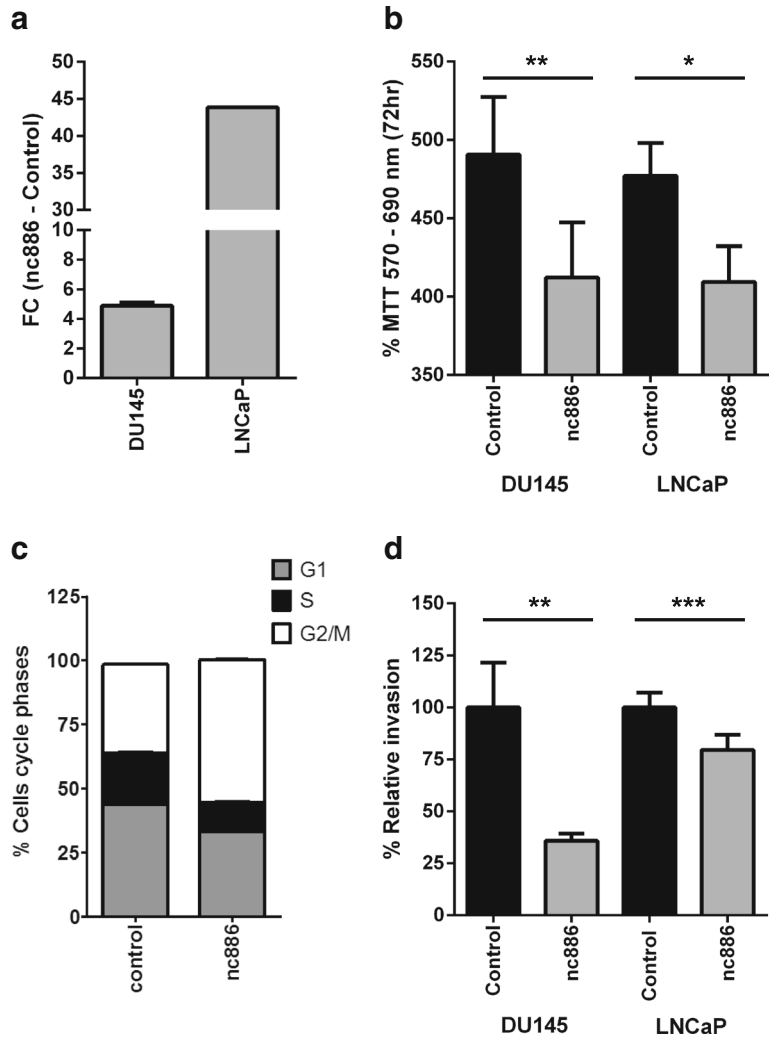

Fig. 3 In vitro effect of the overexpression of nc886 in tumor cell proliferation and invasion. **a** Expression of nc886 in DU145 and LNCaP nc886 overexpressing relative to control cell line. Expression levels of nc886 were determined using RT and qPCR with specific primers (see Methods) and RNAU6 was used as and endogenous control of RNA amount. **b** Cell viability assay by MTT for DU145 and LNCaP cell lines overexpressing nc886 and control hairpin RNA. The absorbance at 72hs (570-690 nm) is shown as percentage. **c** Flow cytometric cell cycle assay based on DNA content measured with propidium iodide. The cumulative percentage of cells at the different cell cycle phases are shown for DU145 cell line overexpressing nc886 and control hairpin RNA. **d** Matrigel invasion assay of DU145 (3 replicates) and LNCaP (4 replicates) overexpressing nc886 and control hairpin RNA. Percentage invasion for nc886 overexpressing cell lines was calculated relative to control cell lines. * P value < 0.05; ** P-value < 0.01; *** P-value < 0.0001 two tailed t-test

relative to the corresponding control cell lines (Fig. 3b). To study this phenotype in greater depth, we performed an analysis of DNA content by flow cytometry in DU145, whose results revealed an enrichment of cells in G2/M phase in the nc886 overexpressing transfectant compared to the control (Fig. 3c).

To investigate whether this anti-proliferative effect also took place in vivo, we performed a xenograft assay in NUDE BALB-C mice. Specifically, 6 male mice were subcutaneously inoculated in opposite flanks with DU145 cell line overexpressing nc886 or the control vector. As shown in Fig. 4a and b, the tumors resulting from the DU145 control cell line had a significantly higher growth relative to the tumors of the DU145 cell line overexpressing nc886. This growth difference is also reflected in the mass of the tumors (Fig. 4b and c). Additionally, the histology of the tumors was analyzed by optical microscopy of paraffin derived tumor sections stained with hematoxylin and eosin. This showed a trend towards a higher mitotic index and a lower percentage of necrosis in tumors of the control cell line compared to the tumors overexpressing nc886 (Fig. 4d and e). Thus, the results obtained in vivo reinforce those previously observed in vitro.

Overexpression of nc886 causes a decrease in tumor cell invasion in vitro

The ability of the tumor cells to cross the extracellular matrix (which in epithelia is represented by the basement membrane) and invade surrounding and distant tissues is a fundamental hallmark of malignancy. Taking in consideration the increment in nc886 promoter methylation in metastatic relative to normal tissue observed in the cohort of Aryee et al. (Fig. 1b), we sought to investigate the effect of its overexpression in cell invasion. We then performed Matrigel in vitro invasion assays with the overexpressing cell lines (Fig. 3a). A significant decrease in the invasion capacity was observed

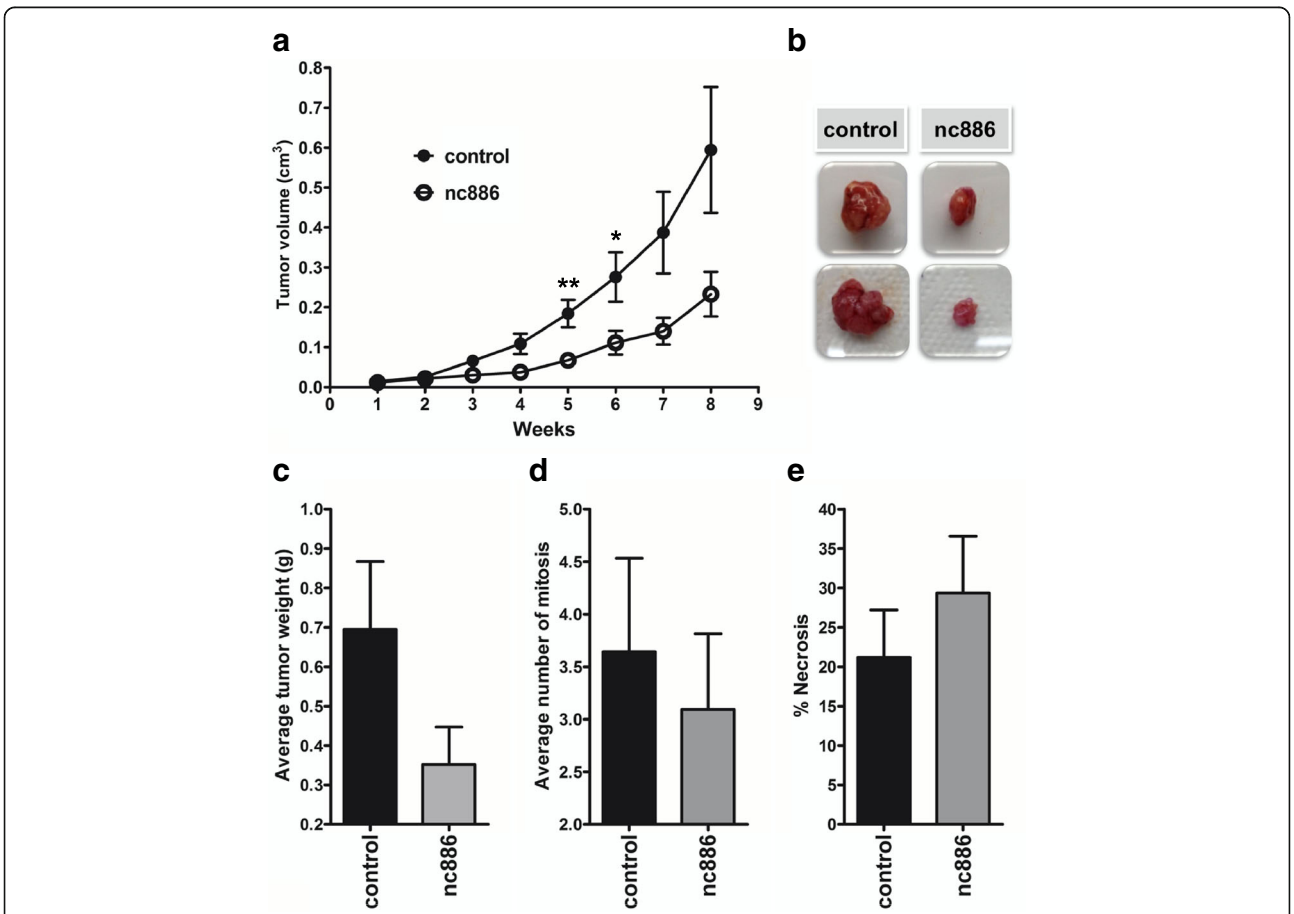

Fig. 4 In vivo effect of nc886 overexpression in tumor phenotype. **a** Tumor xenograft assay in NUDE BALB-C mice of DU145 cell lines overexpressing nc886 and control hairpin RNA. Tumor growth curves of 6 mice expressed as the average tumor volume (cm^3). **b** Macroscopic images of selected tumors grown in NUDE BALB-C mice inoculated in with DU145 cell lines overexpressing nc886 and corresponding control cell line. The average mass(g) (**c**), average number of mitosis (**d**) and average percentage of tumor necrosis (**e**) of the 6 tumors assayed at the end time of the assay are shown. * *P* value < 0.05; ** *P*-value < 0.001; two-tailed t-test

for both DU145 and LNCaP cell lines overexpressing nc886 relative to their corresponding controls (Fig. 3d).

The expression of nc886 correlates with the expression of genes linked to tumor proliferation in PrCa

In order to study the molecular basis of the effect of nc886 in cell proliferation, we analyzed the putative association between the expression of nc886 and selected gene sets using the TCGA-PRAD cohort. Initially, we studied the expression of differentially expressed genes identified in a knock down of nc886 in esophageal, gastric and thyroid cell lines [18, 20, 21]. We did not find the predicted association between nc886 and these gene signatures in prostate samples (Additional file 4: Table S2). Indeed, none of the analyzed genes correlate with nc886 expression as described in the former reports and 18 out of 38 showed significantly negative correlation with TSS200 nc886 average methylation in the TCGA--PRAD cohort (p-value < 0.0001). In addition, based on our in vitro and in vivo phenotypic data, we looked at the expression of the genes belonging to the PrCa CCP proposed by Cuzick et al., a 31-gene subset of 126 previously identified cell-cycle-related genes [32]. The score derived from the CCP has been later shown to possess clinical value by several independent studies, and is commercialized as the Prolaris test (Myriad Genetics, Salt Lake City,Utah, USA). When we analyzed all the tumors of the TCGA-PRAD dataset, 6 out of 28 genes of the signature show a concordant significantly positive correlation with the TSS200 nc886 methylation (p-value < 0.0001) and none of them show a negative correlation with TSS 200 nc886 methylation (Additional file 5: Table S3). Additionally, we defined two group of samples (25 tumors each one) showing low and high nc886 promoter methylation (Fig. 5a); tumors at the 10th percentile (average beta-value 0.542 ± 0.003) were classified as low TSS200 methylation and consequently high nc886 expression, while tumors at the 90th percentile (average beta-value 0.780 ± 0.003) were classified as high TSS200 methylation and consequently low nc886 expression. As depicted in the Fig. 5b, low and high TSS200 nc886 methylation tumors tend to cluster based on the expression of the CCP signature. Furthermore, the transcripts belonging to the CCP signature showed increased expression in the high TSS200 methylation compared to the low TSS200 methylation group.

Discussion

Nc886 has been recently shown to act as a tumor suppressor ncRNA in cholangiocarcinoma, esophageal carcinoma, gastric cancer and leukemia [15, 18, 20, 33]. The etiology of its downregulation in cancer has been linked to the methylation of its promoter in leukemia, colon, lung, gastric, bladder, breast and esophageal tumors [15, 16, 18–20]. Furthermore, nc886 has been proposed both as a tumor suppressor and as an oncogene, depending of the context and the tissue involved, as was recently showed in thyroid cancer [21]. Thus, a more comprehensive picture of nc886 action in cancer, including tissue specific differences and potentially specific molecular mechanisms is still required.

Here we present the first study of the role of nc886 in PrCa. We found an increased methylation of nc886 gene promoter in prostatic tumor tissue vs. its matched normal counterpart, analyzing the samples available at the TCGA-PRAD dataset and in the cohort of Kirby et al. A similar observation was made in leukemia, colon, lung, gastric, bladder, breast and esophageal tumors [15, 16, 18–20], supporting the hypothesis of increased nc886 promoter methylation as a recurrent event in the initiation step of solid tumors. Indeed, we found that the level of nc886 promoter methylation correlates with PrCa patient clinical evolution, reinforcing previous findings in gastric, lung, leukemia and esophageal cancer [15, 16, 18, 20]. Furthermore, the predominant medium and high nc886 methylation groups tissues, in both normal and tumor TCGA-PRAD samples, positively correlate with the clinical outcome of the disease. It is worth to note, that the so-called “normal adjacent” prostatic tissue from PrCa patients (Fig. 1a), may be in fact abnormally modified by tumor induced changes at the organ level [28], thus conclusions derived exclusively from this type of tissue should be taken with caution. Indeed, the study of Aryee et al. (Fig. 1b) reports lower levels of average nc886 promoter methylation in bona fide prostate normal tissue obtained from organ donors, suggesting that “normal tissue” adjacent to tumor tissue may had already undergone an increase in nc886 promoter methylation. Alternatively, methodological differences between the two studies may explain the divergence in the average methylation. The fact that another recent study using normal adjacent tissue reports nc886 promoter methylation comparable to TCGA-PRAD, favors the former interpretation. In addition, we found significantly lower levels of average nc886 promoter methylation in bona fide normal tissue obtained from organ donors in comparison with metastatic tissues. The finding of similar levels of TSS200 methylation in high methylated samples from normal and primary tumors in comparison with metastatic tissue, suggests that nc886 promoter methylation is a pre-requisite for tumor metastasis. Altogether, our results favor a tumor suppressor role for nc886 in several steps of PrCa tumorigenesis. It also indicates that nc886 silencing is a driver epi-mutation in PrCa. Finally, our findings point out to a potential use of nc886 for disease stratification in PrCa.

Our study also proves that the level of expression of nc886 in PrCa tissue is significant lower than in the

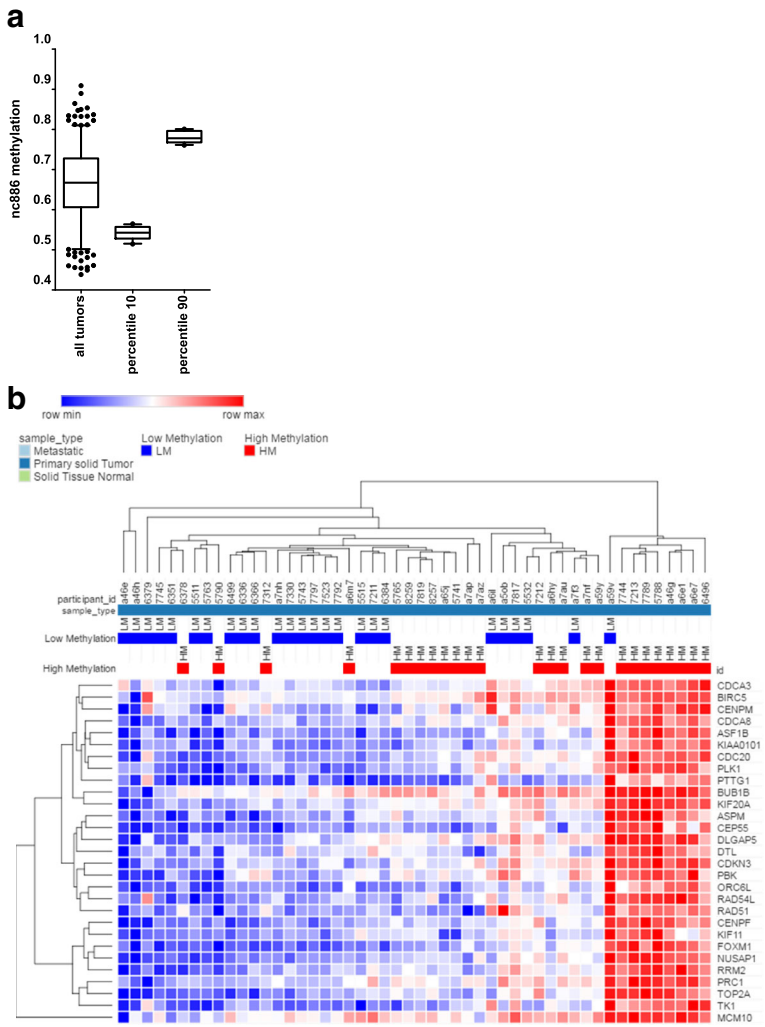

Fig. 5 Association between TSS200 nc886 methylation status and the prostate cancer cell cycle progression (CCP) gene expression signature in the TCGA- PRAD cohort. **a** Box plot of the distribution of nc886 average promoter methylation in the total TCGA-PRAD dataset and the edge 10-percentile samples selected for the clusterization. **b** Heat map of the expression of the genes belonging to the prostate cancer cell cycle progression (CCP) gene expression signature [32] in 10th percentile low and 90th high nc886 promoter methylated samples of TCGA-PRAD. The heatmap was generated using the Euclidean algorithm clusterization with the Morpheus software

normal counterpart. This goes in agreement with findings in other tissues, in which nc886 was proposed as a tumor suppressor gene [12, 15, 18, 20, 33]. In addition, we show that nc886 promoter methylation negatively regulates its transcript abundance in PrCa cell lines, as was shown previously in leukemia, gastric and esophageal tumors [15, 18, 20].

Although aberrant DNA hypermethylation in PrCa is a fundamental driver of tumor progression and overexpression of the DNMTs is a signature of disease origin and evolution, the mechanism responsible for the epigenetic silencing of nc886 in cancer has not been addressed so far. Among the three DNMTs, DNMT3B has been consistently shown to increase its levels in transformed vs. normal prostate tissue, both in patient tumors and in cell lines [34–37] and its expression increase along with adverse clinical parameters [36, 37]. Functional studies in siRNA cell lines, cadmium-transformed prostate epithelial cells and TRAMP mouse models [35, 38, 39], together with the association between PrCa risk and a polymorphism in DNMT3B leading to increased enzyme expression [40], have provided further support to this hypothesis. Thus, DNMT3B seems to be the most important DNMT driver in PrCa. Concordantly, we found a positive correlation between the fold change in expression of DNMT3B and nc886 promoter methylation in matched normal to tumor tissue in the TCGA-PRAD cohort, which favors DNMT3B involvement in nc886 promoter methylation during neoplastic transformation in the

prostate. Nevertheless, further experiments in PrCa models are needed to prove the hypothesis.

Seeking the effect of nc886 deregulation in prostate tissue, we analyzed several PrCa cell lines finding support for the correlation between nc886 expression and methylation seen in the clinical samples. In addition, the cell lines show quite variable expression of nc886 in agreement with the patient data. Accordingly, an important heterogeneity in nc886 promoter methylation has been reported in several studies. The natural variation in the methylation of the locus in humans might be explained by imprinting and methylation in response to the peri-conceptional environment [19, 22, 23]. Nevertheless, the increase in the methylation of nc886 promoter in tumor vs. matched normal tissue regardless of the initial level of expression in the normal tissue, has strong support in the cancer literature [15, 16, 18–20]. In this context, we chose two cell lines with different levels of nc886 methylation and concomitant expression to cover the spectrum of nc886 variation in prostate tissue. In addition, these cells lines model the androgen sensitive (LNCaP) and androgen insensitive (DU145) forms of PrCa disease. We found that nc886 overexpression produces a significant decrease of the in vitro proliferation, possibly by a retention of the cells in the G2/M stage of the cell cycle. Additionally, when we assessed the effect of overexpression of nc886 in vivo we found a significant decrease in tumor growth. The decreased growth of nc886 overexpressing tumors was accompanied by a high percentage of necrosis, low number of mitosis and low tumor weight trends. Forced overexpression of nc886 causes a reduction in in vitro invasion through Matrigel. The concordant pattern of methylation and expression of nc886 observed together with the phenotype of the overexpressing cells strongly contributes to the idea that nc886 functions as a tumor suppressor gene in the prostate.

Then we looked for possible transcriptomic changes responsible for the proliferative effect of nc886 in PrCa. We observed that most of the expression of genes previously shown to be upregulated upon nc886 knock-down in cell lines models of esophageal, gastric and thyroid cancer, do not correlate with nc886 expression in prostate tumor tissues. This finding suggests that the molecular changes induced by nc886 deregulation in esophageal, gastric and thyroid cancer are different that those in the prostate, thus favoring a tissue specific model of nc886 action in cancer. Remarkably, we found that the CCP, a validated clinically useful PrCa proliferation gene signature, positively associates with nc886 expression in the TCGA-PRAD cohort. This goes in agreement with the negative effect of nc886 in cell proliferation observed both in vitro and in vivo using a gain-of-function of nc886 in PrCa cell lines and poses candidate genes that might be co-regulated with, responsive to or regulators of nc886. While different molecular mechanisms of nc886 action in cancer have been proposed, including the modulation of the PKR/NFkB pathway [12, 41] and the generation of microRNAs [16, 17], the relative contribution of nc886 and derived microRNAs in cancer has been hardly addressed in the literature. They could either modulate the same or completely independent cellular processes through diverse molecular pathways. Interestingly, some of the genes belonging to the CCP signature have mRNA motifs complementary to the seed region of the microRNAs potentially derived from nc886. Indeed, one of these has already been validated as a target gene in another tissue [16]. Although more work is necessary to elucidate the precise molecular mechanism of action of nc886 in the prostate cells, its association with the CCP at the level of gene expression in the clinical set reinforces its clinical relevance in PrCa disease.

Conclusions

This investigation validates the presence of nc886 transcript in the prostate, and its downregulation during the progression of PrCa. The correlation between nc886 promoter methylation and several PrCa clinical parameters suggest its clinical importance in PrCa progression and is consistent with data previously reported for other cancers. The analysis of cell lines provided direct prove of nc886 regulation by DNA methylation and identifies DNMT3B as potentially responsible for the increase in nc886 methylation during malignant transformation in the prostate. Functional studies using a gain-of function of nc886 in PrCa cell lines exposed its negative influence on cell proliferation and invasion. The relevance of the proliferative effect in the clinical set is supported by the positive correlation between TSS200 nc886 methylation and the PrCa proliferation gene signature (CCP) in the TCGA-PRAD. These data point out to a tumor suppressor role nc886 in PrCa, whose expression is epigenetically silenced in cancer resulting in an increased cell proliferation and invasion through tissue specific molecular mechanisms.

Additional files

Additional file 1: Figure S1. Hierarchical cluster based on nc886 methylation status of paired normal and tumor tissue of PrCa patients from TCGA-PRAD and Stanford datasets. Clusterization was performed by MEV [42] using Euclidean algorithm with default parameters. The beta-values of methylation of the 6 CpG sites comprise the TSS200 in the normal and tumor tissue considered as a unit. Each row corresponds to one patient whose identity is indicated at the right of the heatmap using the ID provided by the original study. Upper rulers indicate the amplitude of gene expression represented by the colors of the heatmap. (PDF 147 kb)

Additional file 2: Figure S2. Hierarchical cluster of 50 paired normal and tumor tissue of PrCa patients from TCGA-PRAD dataset. A. 50 normal prostate tissue B. 50 prostate tumor tissues. Clusterization was performed by Gene-E Euclidean algorithm using default parameters. The two major clusters, indicated as "high" and "medium" methylation, were selected for further clinical association studies shown in D and F. The average methylation of 10 CpG sites of nc886 promoter (including the 6 sites of the TSS200, 1 located at the gene body and 3 located 200-350pb upstream of the TSS200) is shown for normal (C) and tumor tissue (E). The clinical variables reported at the TCGA-PRAD were analyzed for correlations with the methylation status of nc886 promoter, and only the statistically significant associations found are shown. D. Average clinical T value is associated with the methylation status of the normal tissue (normal) of the patient. F. Average pathological T value is associated with the methylation status of the tumor tissue (tumor) of the patient. *P-value < 0.05; ** P-value < 0.01; *** P-value < 0.001 two-tailed t-test. (PDF 419 kb)

Additional file 3: Table S1. Correlation of the expression of the DNMTs with nc886 TSS200 methylation level in TCGA-PRAD tumor samples. (XLSX 9 kb)

Additional file 4: Table S2. Correlation of the differentially expressed genes identified in a knock down of nc886 in esophageal, gastric and thyroid cell lines and nc886 TSS200 methylation level in TCGA-PRAD tumor samples. (XLSX 11 kb)

Additional file 5: Table S3. Correlation of the expression of PrCa cell-cycle progression gene signature (CCP) and nc886 TSS200 methylation level in TCGA-PRAD tumor samples. (XLSX 10 kb)

Abbreviations

CCP: Prostate Cancer Cell Cycle Progression Gene Signature; DMSO: Dimethyl Sulfoxide; GEO: Gene Expression Omnibus; H&E: Hematoxylin and Eosin; MTT: 3-(4,5-dimethylthiazol-2-yl)-2,5-diphenyl-2H-tetrazolium bromide; ncRNA: Non-Coding RNA; nt: Nucleotide; OD: Optical Density; PBS: Phosphate Buffer Solution; PRAD: Prostate Adenocarcinoma; PrCa: Prostate Cancer; pre-miR-886: Precursor of hsa-miR-886; qPCR: Quantitative Polymerase Chain Reaction; RT: Reverse transcription; TCGA: The Cancer Genome Atlas; TSS200: Region of 200 nt located upstream of the transcription start site; vtRNA: Vault RNA

Acknowledgements

We are very grateful to Dr. Mercedes Rodríguez-Teja (Departamento de Genética, Facultad de Medicina, UdelaR), Dr. José Badano (Laboratorio de Genética Molecular Humana, Institut Pasteur de Montevideo) and MSc. Ximena Camacho (Radiofarmacia, Centro de Investigaciones Nucleares, Facultad de Ciencias, UdelaR) for kindly providing reagents.

Funding

This study was funded by Comisión Honoraria de Lucha contra el Cáncer (CHLC), Agencia Nacional de Investigación e Innovación (ANII), Comisión Sectorial de Investigación Científica (CSIC) and Programa de Desarrollo de las Ciencias Básicas (PEDECIBA) from Uruguay.

Availability of data and materials

All data generated or analysed during this study are included in this published article [and its supplementary information files].

Authors' contributions

Study conception: MAD, ETK, JRSS. **Study design:** MAD. **Acquisition of the clinical data:** MCO, RSF, MAD, CM, MM, NM, LM. **Acquisition of the experimental data:** RSF, CM, MAD, MCO, MVG, ASY, KCS, KRML. **Analysis of the data:** RSF, MAD, MVG, CM, ASY. **Interpretation of data:** MAD, RSF, BG, JRSS. **Drafting of manuscript:** MAD, RSF. **Critical revision:** MAD, RSF, CM, ETK, MVG, MCO, ASY, KRML, BG, JRSS.
All authors read and approved the final manuscript.

Ethics approval and consent to participate

The human specimens study was approved by the Hospital Policial, D.N.AA.SS., Ministerio del Interior, Montevideo, Uruguay (2010). As it involved only the study of existing archived human pathological specimens, and did not require subject identification, a written informed consent from the patients was exempt. The animal xenograft study was approved by the Ethics Committee for Animal Use Institute of Biomedical Science, at the University of Sao Paulo, Brazil (protocol 134/10).

Consent for publication

Not applicable.

Competing interests

The authors declare that they have no competing interests.

Publisher's Note

Author details

[1]Laboratorio de Interacciones Moleculares, Facultad de Ciencias, Universidad de la República, Montevideo, Uruguay. [2]Departamento de Genética, Facultad de Medicina, Universidad de la República, Montevideo, Uruguay. [3]Departamento de Biologia Celular e do Desenvolvimento, Instituto de Ciências Biomédicas, USP, São Paulo, Brazil. [4]Laboratório de Investigação Médica en Urologia, LIM55, Departamento de Urología, Faculdade de Medicina, USP, São Paulo, Brazil. [5]Departamento de Anatomía Patológica, Hospital Policial, Montevideo, Uruguay. [6]Departamento de Genómica, Instituto de Investigaciones Biológicas Clemente Estable, Montevideo, Uruguay. [7]Departamento de Biología Celular y Molecular, Facultad de Ciencias, Universidad de la República, Montevideo, Uruguay. [8]Present Address: Departamento de Diagnóstico y Tratamientos Especiales, Dirección Nacional de Sanidad de las Fuerzas Armadas, Hospital Central de las Fuerzas Armadas, Montevideo, Uruguay. [9]Present Address: Department of Structural and Functional Biology, Institute of Biology, Universidade Estadual de Campinas (UNICAMP), Campinas, Sao Paulo, Brazil.

Received: 14 March 2017 Accepted: 24 January 2018
Published online: 02 February 2018

References

1. Ferlay J, Shin HR, Bray F, Forman D, Mathers C, Parkin DM. Estimates of worldwide burden of cancer in 2008: GLOBOCAN 2008. Int J Cancer. 2010; 127:2893–917.
2. Ferlay J, Soerjomataram I, Dikshit R, Eser S, Mathers C, Rebelo M, et al. Cancer incidence and mortality worldwide: sources, methods and major patterns in GLOBOCAN 2012. Int J Cancer. 2015;136:E359–86.
3. Bolton EM, Tuzova AV, Walsh AL, Lynch T, Perry AS. Noncoding RNAs in prostate cancer: the long and the short of it. Clin Cancer Res. 2014;20:35–43. https://doi.org/10.1158/1078-0432.CCR-13-1989.
4. Croce CM. Causes and consequences of microRNA dysregulation in cancer. Nat Rev Genet. 2009;10:704–14. https://doi.org/10.1038/nrg2634.
5. Mouraviev V, Lee B, Patel V, Albala D, Johansen TEB, Partin A, et al. Clinical prospects of long noncoding RNAs as novel biomarkers and therapeutic targets in prostate cancer. Prostate Cancer Prostatic Dis. 2016;19:14–20. https://doi.org/10.1038/pcan.2015.48.
6. Doldi V, Pennati M, Forte B, Gandellini P, Zaffaroni N. Dissecting the role of microRNAs in prostate cancer metastasis: implications for the design of novel therapeutic approaches. Cell Mol Life Sci. 2016;73:2531–42. https://doi.org/10.1007/s00018-016-2176-3.
7. Saini S. PSA and beyond: alternative prostate cancer biomarkers. Cell Oncol (Dordr). 2016;39:97–106. https://doi.org/10.1007/s13402-016-0268-6.
8. Wilusz JE, Sunwoo H, Spector DL. Long noncoding RNAs: functional surprises from the RNA world. Genes Dev. 2009;23:1494–504. https://doi.org/10.1101/gad.1800909.
9. Amort M, Nachbauer B, Tuzlak S, Kieser A, Schepers A, Villunger A, et al. Expression of the vault RNA protects cells from undergoing apoptosis. Nat Commun. 2015;6:7030. https://doi.org/10.1038/ncomms8030.
10. Nandy C, Mrázek J, Stoiber H, Grässer FA, Hüttenhofer A, Polacek N. Epstein-Barr virus-induced expression of a novel human vault RNA. J Mol Biol. 2009; 388:776–84. https://doi.org/10.1016/j.jmb.2009.03.031.
11. Stadler PF, Chen JJL, Hackermüller J, Hoffmann S, Horn F, Khaitovich P, et al. Evolution of vault RNAs. Mol Biol Evol. 2009;26:1975–91.
12. Lee K, Kunkeaw N, Jeon SH, Lee I, Johnson BH, Kang G-Y, et al. Precursor miR-886, a novel noncoding RNA repressed in cancer, associates with PKR

and modulates its activity. RNA. 2011;17:1076–89. https://doi.org/10.1261/rna.2701111.
13. Jeon SH, Lee K, Lee KS, Kunkeaw N, Johnson BH, Holthauzen LMF, et al. Characterization of the direct physical interaction of nc886, a cellular non-coding RNA, and PKR. FEBS Lett. 2012;586:3477–84. https://doi.org/10.1016/j.febslet.2012.07.076.
14. Jeon SH, Johnson BH, Lee YS. A tumor surveillance model: a non-coding RNA senses neoplastic cells and its protein partner signals cell death. Int J Mol Sci. 2012;13:13134–9.
15. Treppendahl MB, Qiu X, Søgaard A, Yang X, Nandrup-Bus C, Hother C, et al. Allelic methylation levels of the noncoding VTRNA2-1 located on chromosome 5q31.1 predict outcome in AML. Blood. 2012;119:206–16.
16. Cao J, Song Y, Bi N, Shen J, Liu W, Fan J, et al. DNA methylation-mediated repression of miR-886-3p predicts poor outcome of human small cell lung cancer. Cancer Res. 2013;73:3326–35.
17. Fendler A, Jung M, Stephan C, Honey RJ, Stewart RJ, Pace KT, et al. miRNAs can predict prostate cancer biochemical relapse and are involved in tumor progression. Int J Oncol. 2011;39:1183–92.
18. Lee H-S, Lee K, Jang H-J, Lee GK, Park J-L, Kim S-Y, et al. Epigenetic silencing of the non-coding RNA nc886 provokes oncogenes during human esophageal tumorigenesis. Oncotarget. 2014;5:3472–81. https://doi.org/10.18632/oncotarget.1927.
19. Romanelli V, Nakabayashi K, Vizoso M, Moran S, Iglesias-Platas I, Sugahara N, et al. Variable maternal methylation overlapping the nc886/vtRNA2-1 locus is locked between hypermethylated repeats and is frequently altered in cancer. Epigenetics. 2014;9:783–90.
20. Lee K-S, Park J-L, Lee K, Richardson LE, Johnson BH, Lee H-S, et al. nc886, a non-coding RNA of anti-proliferative role, is suppressed by CpG DNA methylation in human gastric cancer. Oncotarget. 2014;5:3944–55. http://www.impactjournals.com/oncotarget/index.php?journal=oncotarget&page=article&op=view&path%5B%5D=2047&path%5B%5D=3069
21. Lee EK, Hong S-H, Shin S, Lee H-S, Lee J-S, Park EJ, et al. nc886, a non-coding RNA and suppressor of PKR, exerts an oncogenic function in thyroid cancer. Oncotarget. 2016;7:75000–12. https://doi.org/10.18632/oncotarget.11852.
22. Paliwal A, Temkin AM, Kerkel K, Yale A, Yotova I, Drost N, et al. Comparative anatomy of chromosomal domains with imprinted and non-imprinted allele-specific DNA methylation. PLoS Genet. 2013;9:e1003622.
23. Silver MJ, Kessler NJ, Hennig BJ, Dominguez-Salas P, Laritsky E, Baker MS, et al. Independent genomewide screens identify the tumor suppressor VTRNA2-1 as a human epiallele responsive to periconceptional environment. Genome Biol. 2015;16:118. https://doi.org/10.1186/s13059-015-0660-y.
24. Goldman M, Craft B, Swatloski T, Ellrott K, Cline M, Diekhans M, et al. The UCSC cancer genomics browser: update 2013. Nucleic Acids Res. 2013;41:D949–54. https://doi.org/10.1093/nar/gks1008.
25. Huang W-Y, Hsu S-D, Huang H-Y, Sun Y-M, Chou C-H, Weng S-L, et al. MethHC: a database of DNA methylation and gene expression in human cancer. Nucleic Acids Res. 2015;43(Database issue):D856–61. https://doi.org/10.1093/nar/gku1151.
26. Barrett T, Wilhite SE, Ledoux P, Evangelista C, Kim IF, Tomashevsky M, et al. NCBI GEO: archive for functional genomics data sets–update. Nucleic Acids Res. 2013;41(Database issue):D991–5. https://doi.org/10.1093/nar/gks1193.
27. Kirby MK, Ramaker RC, Roberts BS, Lasseigne BN, Gunther DS, Burwell TC, et al. Genome-wide DNA methylation measurements in prostate tissues uncovers novel prostate cancer diagnostic biomarkers and transcription factor binding patterns. BMC Cancer. 2017;17:273. https://doi.org/10.1186/s12885-017-3252-2.
28. Aryee MJ, Liu W, Engelmann JC, Nuhn P, Gurel M, Haffner MC, et al. DNA methylation alterations exhibit intraindividual stability and interindividual heterogeneity in prostate cancer metastases. Sci Transl Med. 2013;5:169ra10. https://doi.org/10.1126/scitranslmed.3005211.
29. Statham AL, Robinson MD, Song JZ, Coolen MW, Stirzaker C, Clark SJ. Bisulfite sequencing of chromatin immunoprecipitated DNA (BisChIP-seq) directly informs methylation status of histone-modified DNA. Genome Res. 2012;22:1120–7. https://doi.org/10.1101/gr.132076.111.
30. Shukeir N, Stefanska B, Parashar S, Chik F, Arakelian A, Szyf M, et al. Pharmacological methyl group donors block skeletal metastasis *in vitro* and *in vivo*. Br J Pharmacol. 2015;172:2769–81. https://doi.org/10.1111/bph.13102.
31. Yang X, Han H, De Carvalho DD, Lay FD, Jones PA, Liang G. Gene body methylation can alter gene expression and is a therapeutic target in cancer. Cancer Cell. 2014;26:577–90. https://doi.org/10.1016/j.ccr.2014.07.028.
32. Cuzick J, Swanson GP, Fisher G, Brothman AR, Berney DM, Reid JE, et al. Prognostic value of an RNA expression signature derived from cell cycle proliferation genes in patients with prostate cancer: a retrospective study. Lancet Oncol. 2011;12:245–55. https://doi.org/10.1016/S1470-2045(10)70295-3.
33. Kunkeaw N, Jeon SH, Lee K, Johnson BH, Tanasanvimon S, Javle M, et al. Cell death/proliferation roles for nc886, a non-coding RNA, in the protein kinase R pathway in cholangiocarcinoma. Oncogene. 2012;32:3722–31. https://doi.org/10.1038/onc.2012.382.
34. Patra SK, Patra A, Zhao H, Dahiya R. DNA methyltransferase and demethylase in human prostate cancer. Mol Carcinog. 2002;33:163–71. http://www.ncbi.nlm.nih.gov/pubmed/11870882. Accessed 22 Dec 2016
35. Du Y-F, Liang L, Shi Y, Long Q-Z, Zeng J, Wang X-Y, et al. Multi-target siRNA based on DNMT3A/B homologous conserved region influences cell cycle and apoptosis of human prostate cancer cell line TSU-PR1. Genet Mol Biol. 2012;35:164–71. http://www.ncbi.nlm.nih.gov/pubmed/22481891. Accessed 22 Dec 2016
36. Gravina GL, Ranieri G, Muzi P, Marampon F, Mancini A, Di Pasquale B, et al. Increased levels of DNA methyltransferases are associated with the tumorigenic capacity of prostate cancer cells. Oncol Rep. 2013;29:1189–95.
37. Hoffmann MJ, Engers R, Florl AR, Otte AP, Muller M, Schulz WA. Expression changes in EZH2, but not in BMI-1, SIRT1, DNMT1 or DNMT3B are associated with DNA methylation changes in prostate cancer. Cancer Biol Ther. 2007;6:1403–12. http://www.ncbi.nlm.nih.gov/pubmed/18637271. Accessed 29 Dec 2016
38. Morey Kinney SR, Smiraglia DJ, James SR, Moser MT, Foster BA, Karpf AR. Stage-specific alterations of DNA methyltransferase expression, DNA hypermethylation, and DNA hypomethylation during prostate cancer progression in the transgenic adenocarcinoma of mouse prostate model. Mol Cancer Res. 2008;6:1365–74. https://doi.org/10.1158/1541-7786.MCR-08-0040.
39. Benbrahim-Tallaa L, Waterland RA, Dill AL, Webber MM, Waalkes MP. Tumor suppressor gene inactivation during cadmium-induced malignant transformation of human prostate cells correlates with overexpression of *de Novo* DNA methyltransferase. Environ Health Perspect. 2007;115:1454–9. https://doi.org/10.1289/ehp.10207.
40. Singal R, Das PM, Manoharan M, Reis IM, Schlesselman JJ. Polymorphisms in the DNA methyltransferase 3b gene and prostate cancer risk. Oncol Rep. 2005;14:569–73. http://www.ncbi.nlm.nih.gov/pubmed/16012746. Accessed 22 Dec 2016
41. Lee YS. A novel type of non-coding RNA, nc886, implicated in tumor sensing and suppression. Genomics Inform. 2015;13:26–30. https://doi.org/10.5808/GI.2015.13.2.26.
42. Saeed AI, Sharov V, White J, Li J, Liang W, Bhagabati N, et al. TM4: a free, open-source system for microarray data management and analysis. BioTechniques. 2003;34:374–8. http://www.ncbi.nlm.nih.gov/pubmed/12613259. Accessed 24 Nov 2017

Figure S1

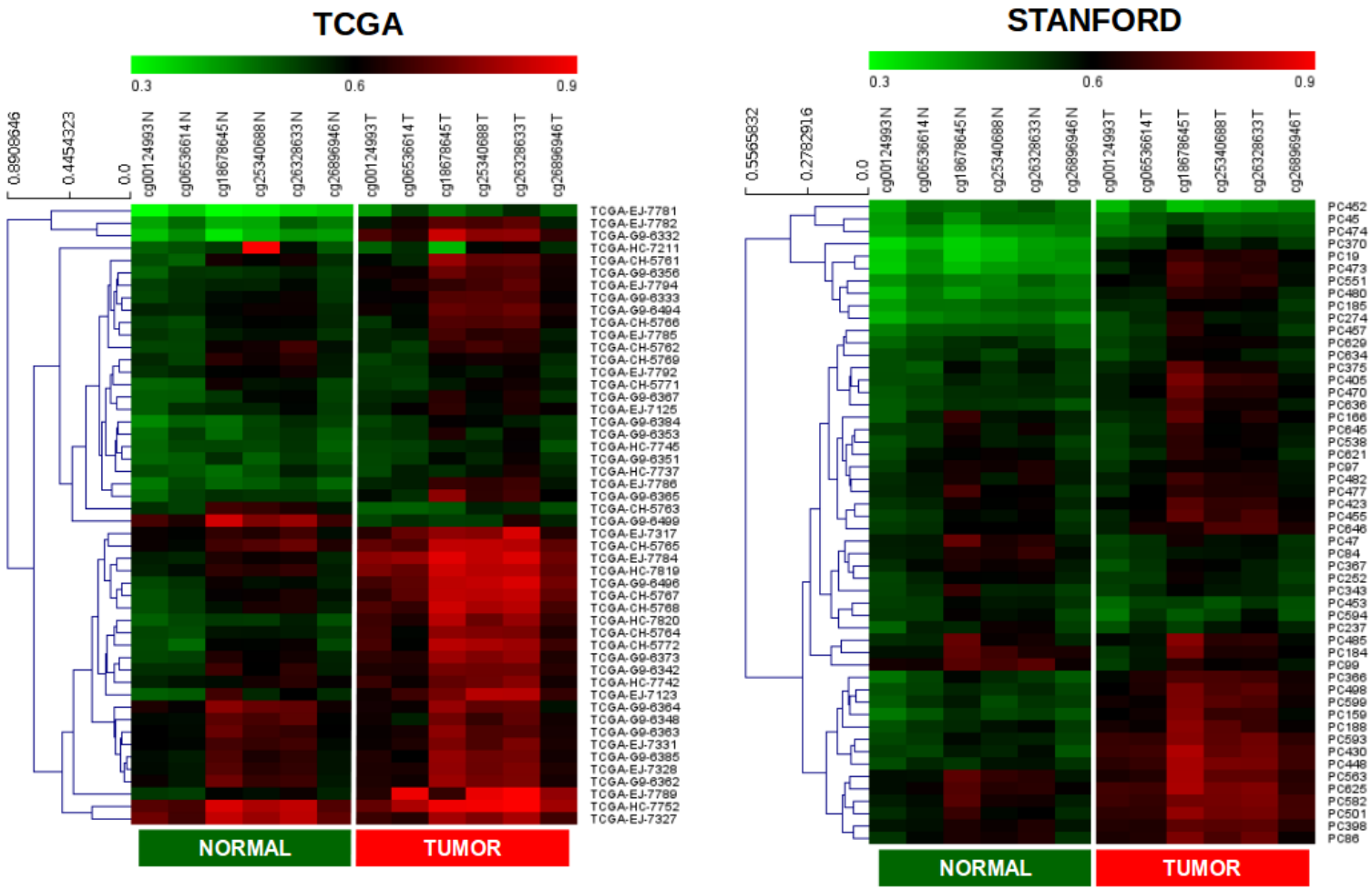
TCGA
0.3
0.6
0.9
0.8906646
0.4454323
0.0
cg00124993N
cg06536614N
cg18678645N
cg25340688N
cg26328633N
cg26896946N
cg00124993T
cg06536614T
cg18678645T
cg25340688T
cg26328633T
cg26896946T
TCGA-EJ-7781
TCGA-EJ-7782
TCGA-G9-6332
TCGA-HC-7211
TCGA-CH-5761
TCGA-G9-6356
TCGA-EJ-7794
TCGA-G9-6333
TCGA-G9-6494
TCGA-CH-5766
TCGA-EJ-7785
TCGA-CH-5762
TCGA-CH-5769
TCGA-EJ-7792
TCGA-CH-5771
TCGA-G9-6367
TCGA-EJ-7125
TCGA-G9-6384
TCGA-G9-6353
TCGA-HC-7745
TCGA-G9-6351
TCGA-HC-7737
TCGA-EJ-7786
TCGA-G9-6365
TCGA-CH-5763
TCGA-G9-6499
TCGA-EJ-7317
TCGA-CH-5765
TCGA-EJ-7784
TCGA-HC-7819
TCGA-G9-6496
TCGA-CH-5767
TCGA-CH-5768
TCGA-HC-7820
TCGA-CH-5764
TCGA-CH-5772
TCGA-G9-6373
TCGA-G9-6342
TCGA-HC-7742
TCGA-EJ-7123
TCGA-G9-6364
TCGA-G9-6348
TCGA-G9-6363
TCGA-EJ-7331
TCGA-G9-6385
TCGA-EJ-7328
TCGA-G9-6362
TCGA-EJ-7789
TCGA-HC-7752
TCGA-EJ-7327
NORMAL
TUMOR
STANFORD
0.3
0.6
0.9
0.5565832
0.2782916
0.0
cg00124993N
cg06536614N
cg18678645N
cg25340688N
cg26328633N
cg26896946N
cg00124993T
cg06536614T
cg18678645T
cg25340688T
cg26328633T
cg26896946T
PC452
PC46
PC474
PC370
PC19
PC473
PC551
PC480
PC185
PC274
PC457
PC629
PC634
PC375
PC405
PC470
PC636
PC166
PC645
PC538
PC621
PC97
PC482
PC477
PC423
PC455
PC646
PC47
PC84
PC367
PC252
PC343
PC453
PC594
PC237
PC485
PC184
PC99
PC366
PC498
PC599
PC159
PC188
PC593
PC430
PC448
PC563
PC625
PC582
PC501
PC398
PC86
NORMAL
TUMOR

Figure S2

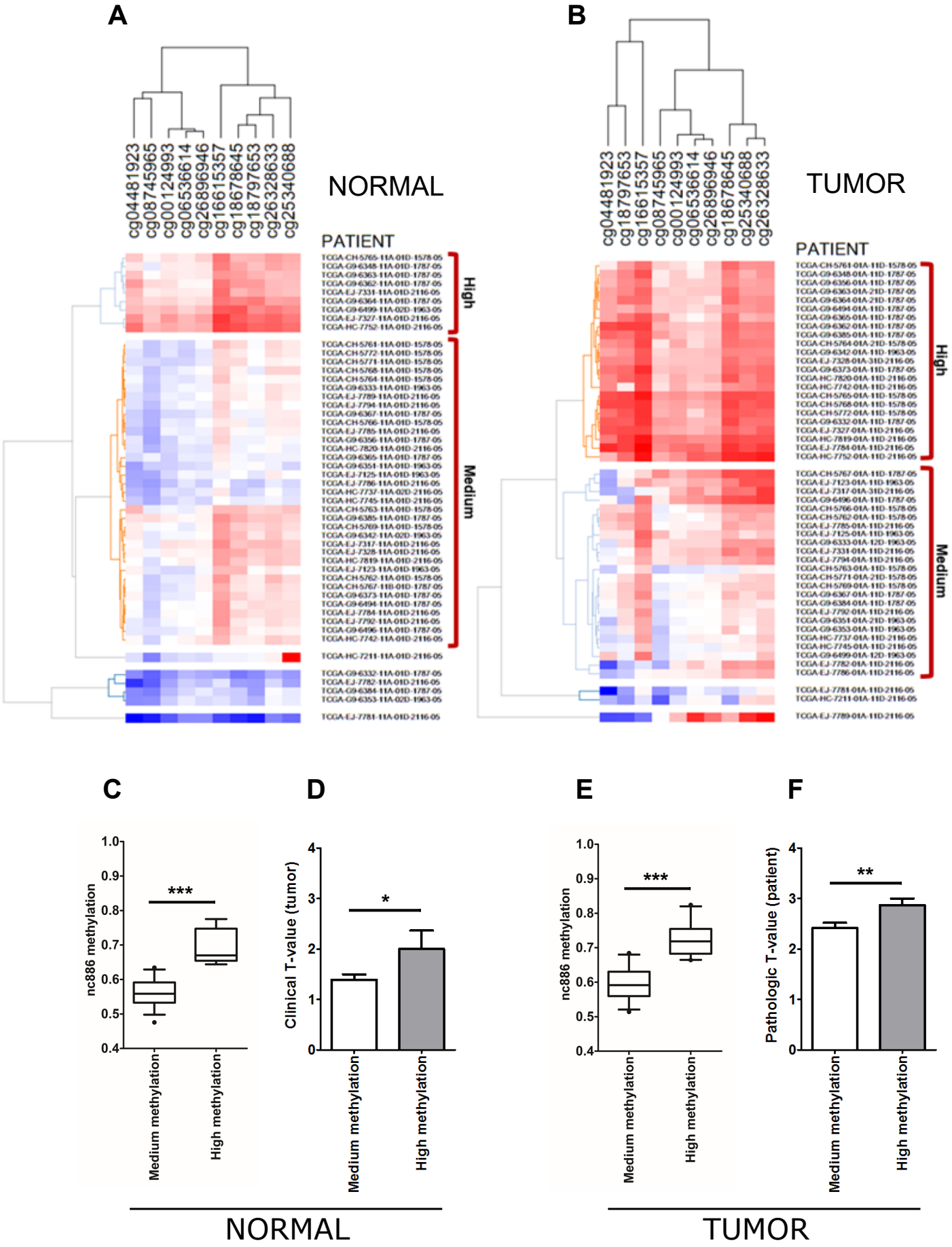
A
cg04481923
cg08745965
cg00124993
cg06536614
cg26896946
cg16615357
cg18678645
cg18797653
cg26328633
cg25340688
NORMAL
PATIENT
High
Medium
B
cg04481923
cg18797653
cg16615357
cg08745965
cg00124993
cg06536614
cg26896946
cg18678645
cg25340688
cg26328633
TUMOR
PATIENT
High
Medium
C
nc886 methylation
***
Medium methylation
High methylation
D
Clinical T-value (tumor)
*
Medium methylation
High methylation
NORMAL
E
nc886 methylation
***
Medium methylation
High methylation
F
Pathologic T-value (patient)
**
Medium methylation
High methylation
TUMOR

II. SNC886-3P EL PEQUEÑO ARN NO CODIFICANTE DERIVADO DEL EXTREMO 3' DE VTRNA2-1/NC886 Y SU IMPLICANCIA EN EL ORIGEN Y EL MANTENIMIENTO DEL FENOTIPO TUMORAL DE ADENOCARCINOMA DE PRÓSTATA.

***Objetivo específico 2.2*: Determinar si vtRNA2-1/nc886 funciona como precursor para la formación de pequeños ARNs no codificantes y evaluar las implicancias de su desregulación en el origen y el mantenimiento del fenotipo tumoral de adenocarcinoma de próstata.**

Objetivo específico 2.2.1 al 2.2.4

Partiendo de los antecedentes previamente mencionados en ***Resultados y discusión I***, abordamos el ***objetivo específico 2.2.*** Los resultados obtenidos fueron incluidos en una publicación científica (Fort et al., 2020) adjunta a continuación.

En este manuscrito evaluamos la formación de pequeños ARNs derivados de vtRNA2-1/nc886 y su posible papel en la biología del PrCa. Comenzamos abordando el *objetivo específico 2.2.1,* realizando el re-análisis de datos de transcriptómica de pequeños ARNs no codificantes en células de próstata para determinar la presencia y desregulación de los pequeños ARNs derivados de vtRNA2-1/nc886 a nivel de RNA-seq. Asimismo, evaluamos el procesamiento de los pequeños ARNs derivados de vtRNA2-1/nc886 en la vía de biogénesis de microARNs, incluyendo el estudio de su asociación con las proteínas argonautas del complejo RISC mediante el re-análisis de datos de estudios de inmunoprecipitación de Argonauta y *knock-out* de las proteínas de procesamiento de microARNs publicados por otros autores (*objetivo específico 2.2.2*). Además, evaluamos la correlación de la expresión del sncARN derivado del extremo 3' de vtRNA2-1/nc886 (hsa-miR-886-3p/snc886-3p) con la expresión de su precursor vtRNA2-1/nc886 en una cohorte. Incluso estudiamos la expresión de hsa-miR-886-3p/snc886-3p en líneas celulares de próstata y en cohortes de datos pública de tejidos de PrCa (GEO, SRA y PRAD-TCGA). Con el fin de abordar el *objetivo específico 2.2.4* realizamos la transfección de mimics de hsa-miR-886-3p/snc886-3p en una línea celular modelo de PrCa (DU145) y evaluamos vías y procesos celulares alterados por hsa-miR-886-3p/snc886-3p mediante microarreglos de expresión génica. Con estos datos, elaboramos una lista de posibles genes blanco directo de represión por hsa-miR-886-3p/snc886-3p, buscando genes con regulación diferencial y presencia de sitios blanco de acción para hsa-miR-886-3p/snc886-3p en su 3'-UTR. Para evaluar los efectos

funcionales asociados a la desregulación de hsa-miR-886-3p/snc886-3p, realizamos la transfección con mimics de hsa-miR-886-3p/snc886-3p de líneas celulares modelo de PrCa (DU145, LNCaP y PC3) y exploramos el efecto de esta sobreexpresión *in vitro* sobre la viabilidad celular, el ciclo celular y la apoptosis temprana (*objetivo específico 2.2.3)*. Finalmente, relativo al *objetivo específico 2.2.4,* evaluamos la asociación de los niveles de expresión de los genes blanco de acción de hsa-miR-886-3p/snc886-3p seleccionados con la recurrencia de la enfermedad y otros parámetros clínicos.

El conjunto de estas aproximaciones nos permitió investigar si se forman pequeños ARNs derivados de vtRNA2-1/nc886, y si los mismos pueden actuar como microARNs en células de glándula prostática. También nos permitió evaluar su desregulación en la carcinogénesis y su asociación con la desregulación de su precursor. Finalmente, los experimentos permitieron evaluar la hipótesis de una acción de TSG para hsa-miR-886-3p/snc886-3p, al estudiar su contribución en la alteración de atributos tumorales en la biología de las líneas celulares derivadas de próstata.

Artículo científico 2: Fort, R.S., Garat, B., Sotelo-Silveira, J.R., and Duhagon, M.A. (2020). vtRNA2-1/nc886 Produces a Small RNA That Contributes to Its Tumor Suppression Action through the microRNA Pathway in Prostate Cancer. Non-Coding RNA 6, 7. doi:10.3390/ncrna6010007

Las contribuciones y actividades en las que participó cada autor están descritas en el manuscrito.

non-coding RNA

MDPI

Article

vtRNA2-1/nc886 Produces a Small RNA That Contributes to Its Tumor Suppression Action through the microRNA Pathway in Prostate Cancer

Rafael Sebastián Fort [1,2], Beatriz Garat [1], José Roberto Sotelo-Silveira [3,4] and María Ana Duhagon [1,2,*]

1 Laboratorio de Interacciones Moleculares, Facultad de Ciencias, Universidad de la República, Montevideo 11400, Uruguay; rfort@fcien.edu.uy (R.S.F.); bgarat@fcien.edu.uy (B.G.)
2 Departamento de Genética, Facultad de Medicina, Universidad de la República, Montevideo 11800, Uruguay
3 Departamento de Genómica, Instituto de Investigaciones Biológicas Clemente Estable, Montevideo 11600, Uruguay; sotelojos@gmail.com
4 Departamento de Biología Celular y Molecular, Facultad de Ciencias, Universidad de la República, Montevideo 11400, Uruguay
* Correspondence: mduhagon@fcien.edu.uy; Tel.: +598-2-525-8618 (ext. 7237)

Received: 23 December 2019; Accepted: 11 February 2020; Published: 20 February 2020

Abstract: vtRNA2-1 is a vault RNA initially classified as microRNA precursor hsa-mir-886 and recently proposed as "nc886", a new type of non-coding RNA involved in cancer progression acting as an oncogene and tumor suppressor gene in different tissues. We have shown that vtRNA2-1/nc886 is epigenetically repressed in neoplastic cells, increasing cell proliferation and invasion in prostate tissue. Here we investigate the ability of vtRNA2-1/nc886 to produce small-RNAs and their biological effect in prostate cells. The interrogation of public small-RNA transcriptomes of prostate and other tissues uncovered two small RNAs, snc886-3p and snc886-5p, derived from vtRNA2-1/nc886 (previously hsa-miR-886-3p and hsa-miR-886-5p). Re-analysis of PAR-CLIP and knockout of microRNA biogenesis enzymes data showed that these small RNAs are products of DICER, independent of DROSHA, and associate with Argonaute proteins, satisfying microRNA attributes. In addition, the overexpression of snc886-3p provokes the downregulation of mRNAs bearing sequences complementary to its "seed" in their 3'-UTRs. Microarray and in vitro functional assays in DU145, LNCaP and PC3 cell lines revealed that snc886-3p reduced cell cycle progression and increases apoptosis, like its precursor vtRNA2-1/nc886. Finally, we found a list of direct candidate targets genes of snc886-3p upregulated and associated with disease condition and progression in PRAD-TCGA data. Overall, our findings suggest that vtRNA2-1/nc886 and its processed product snc886-3p are synthesized in prostate cells, exerting a tumor suppressor action.

Keywords: vault RNA; vtRNA2-1; nc886; hsa-miR-886-3p; cancer; prostate; small RNA; microRNA; TCGA; PRAD

1. Introduction

Prostate cancer (PrCa) is a heterogeneous disease, the molecular mechanisms of which are still not fully elucidated [1]. It is currently the solid tumor with the highest incidence in men in Western countries, representing the second leading cause of male cancer death [2]. The incidence of PrCa is increasing mainly because of population ageing, increased awareness, and the widespread introduction of the prostate-specific antigen (PSA) test. Despite the fact that most patients can be successfully treated, a minor proportion develop an aggressive form of the disease that is currently incurable. Despite the remarkable progress in the development of molecular biomarker to aid disease diagnosis

and risk stratification [3], improved biomarkers for treatment prediction and patient surveillance are still needed. The current advance of genomic technologies has contributed to the identification of thousands of non-coding RNAs (ncRNAs) in the human genome; nonetheless, no function has been assigned for the majority of them [4]. NcRNAs have emerged as significant players in cancer initiation and progression [5], therefore their clinical value is under intense investigation [6]. Pre-miR-886 was annotated as a microRNA precursor in 2007 (hsa-mir-886) (release v10 of miRBase (08/2007)) [7] after the identification of microRNAs derived from it in small RNA libraries from different human cell types [8]. Due to the recognition of its sequence homology with the human vaults RNAs (vtRNAs) vtRNA1-1/2/3 [9], pre-miR-886 was later re-classified as a vault RNA (vtRNA2-1) and therefore removed from miRBase (release v16 (11/2011)). Although the vtRNAs were discovered for their association with the vault particle [10], there is a large cytoplasmic fraction of vtRNAs, including vtRNA2-1, not associated with it [11,12]. Recently, vtRNA2-1 was proposed as a new type of ncRNA functioning as a tumor suppressor that inhibits Protein Kinase RNA-activated (PKR), and was consequently renamed as "nc886" [12–15]. In agreement with the former result, we previously found that vtRNA2-1/nc886 (from here on referred as nc886) is a tumor suppressor in the prostate, the expression of which is epigenetically silenced in tumors and associated with a worse clinical behavior [16]. In addition, its overexpression leads to a decrease in in vitro cell proliferation and invasion and a decrease in in vivo tumor growth [16]. Nevertheless, the ability of nc886 to function as a small RNA precursor by a non-canonical pathway independent of DROSHA was recognized early [17–19]. Indeed, despite the removal of microRNAs derived from hsa-mir-886/vtRNA2-1/nc886 from miRBase (release v16 (11/2011)) several groups detected hsa-miR-886-3p and hsa-miR-886-5p in cells and tissues and assigned them a microRNA function in cancer. Hsa-miR-886-3p was proposed as a tumor suppressor microRNA in several types of cancer (prostate [20], bladder [21], breast [22], colon [23], lung [24–27] and thyroid [28,29]) and as a microRNA involved in other diseases (hematological [30] and Friedreich ataxia [31]). In the prostate, the loss of expression of hsa-miR-886-3p was associated with early biochemical relapse (<1 year after radical prostatectomy) [20], but a recent study shows an increased abundance of circulating hsa-miR-886-3p in high-grade compared to low-grade prostate cancer in plasma samples [32]. Notwithstanding, few reports showed an oncogenic action of hsa-miR-886-3p in renal cell carcinoma [33], colorectal carcinoma [34] and esophageal squamous cell carcinoma [35]. A recent finding proposing a nc886/PKR loss mediated doxorubicin cytotoxicity raised a novel view about its specific contribution to chemotherapy response [36]. Overall, despite of the various reports assigning a microRNA function to hsa-miR-886-3p, its production as a specific nc886 processed product, its dependence on DICER and its association to Argonaute proteins has not been consistently demonstrated.

The aim of this study was to investigate the production of small RNAs with microRNA-like function from nc886, and the biological effect and clinical significance of this small RNAs in prostate cancer. The analysis of small-RNA-seq data from prostate cell lines and tissues demonstrated the presence of small RNAs derived from nc886 (herein designated as snc886-3p and 5p). Snc886-3p shows DICER processing hallmarks and associates with Argonaute proteins. Snc886-3p level decreases in tumor compared to normal tissues, correlating with the methylation of its gene promoter and the expression of its precursor nc886 in prostate tissue. Furthermore, we found that snc886-3p functions as a tumor suppressor microRNA-like RNA in prostate tissue, affecting cell viability, cell cycle phases and early apoptosis in PrCa cell lines. Through global gene expression analysis of cancer cell lines overexpressing snc886-3p, we identified a group of transcripts that might be targets of direct repression by snc886-3p and could explain the observed phenotype. We finally built a snc886-3p direct candidate target gene set supported by in silico predictions of microRNA binding sites AGO-PAR-CLIP (photoactivatable ribonucleoside-enhanced crosslinking and immunoprecipitation) and gene expression analysis in PRAD-TCGA and cell line data. This approach led us to the identification of 106 direct snc886-3p candidate target genes the expression of which is associated with the methylation of the nc886 promoter and a poor prognosis of PrCa patients. Overall, these findings suggest that snc886-3p functions as a

non-canonical tumor suppressor microRNA derived from nc886 in prostate tissue that executes an antiproliferative effect per se, concordant with the effect of its precursor nc886.

2. Results

2.1. vtRNA2-1/nc886 Produces Small RNAs with microRNA-Like Features

To investigate the presence of small RNAs derived from nc886 in prostate tissue, we performed a re-analysis of publicly available small-RNA-seq data sets of prostate tissues and cell lines. We pooled the reads from normal and tumor cell lines transcriptomes (GSE26970, GSE66035 and SRP109305 [37–39]), available at Sequence Read Archive (SRA, [40]) and Gene Expression Omnibus (GEO, [41]). This analysis reveals that most of the reads mapping to nc886 gene piles up over the two sequences corresponding to the previously annotated microRNAs hsa-miR-886-3p (23 nt) and hsa-miR-886-5p (24-25 nt), both in normal (Figure 1A) and tumor (Figure 1B) cell lines. Considering the controversy of the function of hsa-mir-886/vtRNA2-1/nc886 we named the microRNA-like fragments derived from it as snc886-3p and snc886-5p. Genome BLAST analysis of the mature sequences of snc886-3p and snc886-5p shows that their only possible origin is the nc886 transcript (Table S1). Remarkably, while snc886-3p is more abundant than snc886-5p in the normal cell lines (Figure 1A), the opposite is observed in the cancer cell lines (Figure 1B), suggesting a strand preference switch of nc886 processing upon malignant transformation. Figure 1A,B also show that the precise distribution of reads over nc886 sequence is consistent with a specific nuclease processing of nc886 instead of its random degradation [42]. Moreover, the pattern of mapping recalls the distinctive processing of DICER, defined by a sharp 5′ end cut and a less precise 3′ end cut [42,43], which is seen at both snc886-3p and snc886-5p in prostate. Consistently, a similar stacking of reads over nc886 and the same strand preference is observed in cell lines derived from different human tissues (Figure S1A,B).

A predictive secondary structure of nc886 (101 nt) obtained using RNAstructure (MFE) essentially agrees with previous reports [45,46] (see Figure 1C, indicating the location of the two small RNAs identified in the small-RNA-seq data). The RNA folds into a hairpin (stem loop) with a 1-3 nt nucleotides overhangs in one end and an internal loop contiguous to the mature derived small RNAs, thus complying to the requirements of a DICER processing substrate [19,47].

A fundamental feature of a small non-coding RNA functioning as a microRNA is its association with Argonaute proteins [48,49]. To investigate if the snc886-3p/5p fragments satisfy this criterion, we re-analyzed Argonaute PAR-CLIP (AGO-PAR-CLIP) small-RNA-seq data and total small-RNA-seq of DU145 PrCa cell line (SRP075075 and SRP109305) [38,50]. We observed an enrichment of snc886-3p in the fraction associated with Argonaute proteins, similar to that observed for canonical microRNAs such as hsa-miR-301b, hsa-miR-130b and hsa-miR-320b (Figure 1D). Even though snc886-5p is more expressed than snc886-3p, it is not preferentially associated with the Argonaute fraction in DU145 cell line (Figure 1D). These findings are confirmed by a correlation analysis of AGO-PAR-CLIP versus total RNA reads of the same cell line, which shows a lower abundance but higher association with AGO-associate fraction of snc886-3p relative to snc886-5p, in the context of all the small RNAs detected in the study (Figure S1C). Indeed, the association to Argonaute of snc886-3p in DU145 is above the average of microRNAs (log2 RPM Average microRNAs AGO association = 5.56, log2 RPM snc886-3p AGO association = 6.44), suggesting an active association of snc886-3p to the RISC (RNA-induced silencing complex) machinery. It is worth mentioning that experiments in other PrCa cell lines analyzed by Hamilton et al. [50] do not detect snc886-3p, probably because of its low expression (see below and Figure 2B,C) due to the high DNA methylation of its promoter [16].

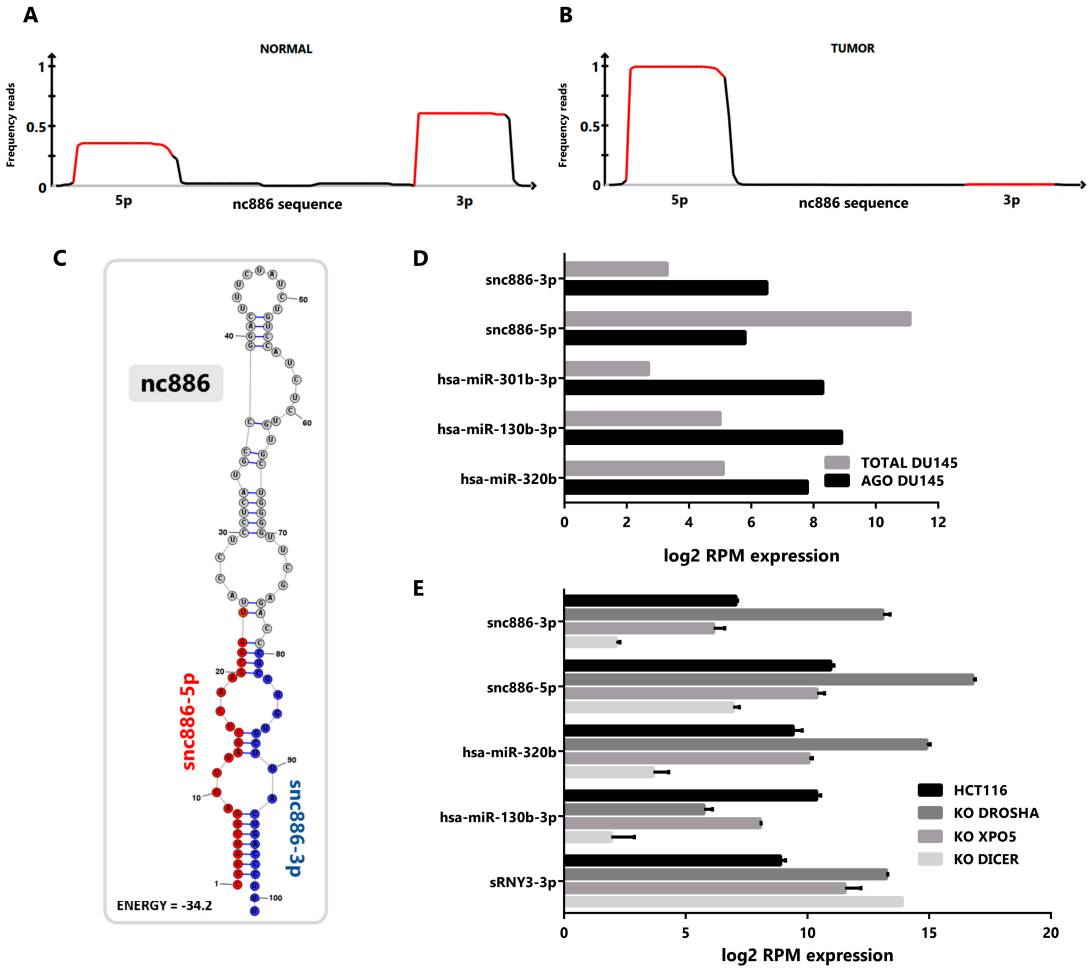

Figure 1. nc886 derived fragments are produced in prostate cell lines and exhibit microRNA features. (**A**,**B**) Mapping of prostate cell small RNA reads along the sequence of nc886. Reads obtained from small-RNA transcriptomes of non-transformed prostate PrEc and PrSC (GEO id: GSE26970) (**A**) and tumor DU145, PC-3 and LNCaP cell lines (SRA id: SRP109305 and GEO id: GSE66035) (**B**) were mapped to nc886. A diagram of nc886 (Refseq (NR_030583.2)), plus additional 10 nt at both ends, is depicted below the plots. Red lines in the plots represent the previously annotated hsa-miR-886-3p and -5p. (**C**) Predicted secondary structure of nc886 (Refseq (NR_030583.2)) based on maximum free energy (MFE) generated with the RNAstructure software [44]. (**D**) Association of small RNAs to Argonaute in transcriptomic analysis of DU145 cell line. The graph shows the normalized expression, reads per million (RPM), of small non-coding RNAs in total cellular RNA (TOTAL DU145) and in the Argonaute PAR-CLIP fraction (AGO DU145). Data set available at SRA id: SRP075075. (**E**) Transcriptomic analysis of small non-coding RNAs of the HCT116 cell line with knockouts for the microRNAs biogenesis proteins DROSHA, EXPORTIN 5 and DICER. Data set available at GEO id: GSE77989. Average value and standard error are shown.

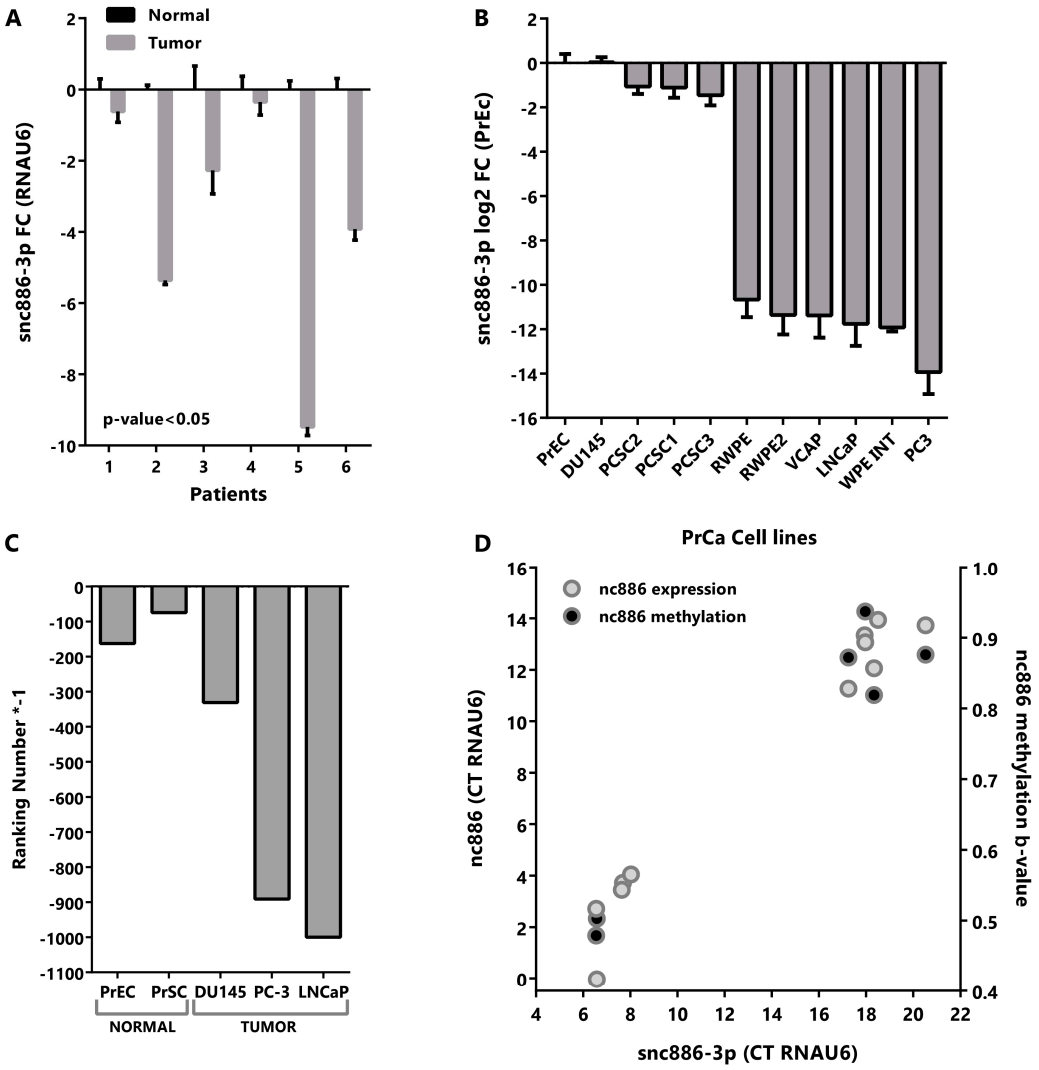

Figure 2. Snc886-3p is downregulated in tumor vs normal prostate tissue and cell lines. (**A**) Expression of snc886-3p in paired normal and tumor tissues from patient prostatectomies. Expression of snc886-3p in tumor relative to normal matched prostate tissue was determined by qRT-PCR (ΔΔCt) using RNAU6 as normalizer. Two-tailed paired T-test was performed. (**B**) Expression of snc886-3p in prostate cell lines. Expression of snc886-3p relative to normal prostate cell line PrEc, determined by qRT-PCR (ΔΔCt) using RNAU6 as normalizer. The order of the cell lines is only based on the expression of snc886-3p (**C**) Expression of snc886-3p in transcriptomic analysis of small non-coding RNAs from different prostate normal (GEO id: GSE26970) and tumor (SRA id: SRP109305 and GEO id: GSE66035) cell lines. For a better comparison of the different cell lines considering the differences in the depth sequencing among experiments, ranking number of appearances of snc886-3p is shown. (**D**) Correlation between nc886 and snc886-3p expression and average TSS200nt methylation on prostate cell lines (GSE68379: PrEc, RWPE-1, DU145, PC3, VCAP and LNCaP). Expression data is the same as in (**B**). Average values and standard deviation are shown.

Seeking additional evidence of the role of snc886-3p, we investigated its dependence on the canonical microRNA biogenesis pathway through the analysis of the changes in the small-RNA-seq transcriptome in knockouts (KO) of DROSHA, XPO5 and DICER generated in the HCT116 cell line [51]. We used a canonical microRNA (hsa-miR-130b), a Drosha-independent microRNA (hsa-miR-320b) [51] and a small RNA fragment derived from the three prime region of RNY3 RNA (sRNY3-3p) as controls. We reasoned that the global reduction in microRNA biogenesis would lead to the overrepresentation of DROSHA-independent small RNAs in the transcriptome. Thus, the observed reduction in hsa-miR-130b

and increase of snc886-3p/5p and hsa-miR-320b in the DROSHA-KO indicates that the processing of the last three small RNAs is DROSHA-independent (Figure 1E). In addition, XPO5-KO produces a significant reduction in hsa-miR-130b and a small decrease in snc886-3p and snc886-5p, indicating that the two latter may be substrates of this exportin. In concordance with previous reports [12,19], DICER-KO decreases the production of snc886-3p and snc886-5p by 96% and 93% respectively, as well as the production of the control microRNAs (Figure 1E). As expected, no reduction of the fragment derived from RNY3 (sRNY3-3p) was observed for all these knockouts [52].

Overall, our findings indicate that nc886 is a precursor of two small RNAs that meet key microRNA criteria in prostate tissue.

2.2. Snc886-3p Has the Expression Profile of a Tumor Suppressor in Prostate Cells

In order to assess the relevance of snc886-3p in prostate we evaluated available microRNA expression datasets of prostate tissues (microarray and qRT-PCR). The analysis reveals a decrease in the expression of snc886-3p in cancer vs normal prostate tissue but no association with stage/prognosis (Table 1).

Table 1. Analysis of snc886-3p abundance in PrCa microRNA datasets.

GEO ACC *	PUBMED ID	Platform	Total Samples	Benign	Cancer	Fold Change (N/B vs T)	*p*-Value	Analytical Tool
GSE45604	24518785	Affymetrix	60	10 Normal	50 Cancer	−1.4	0.05	GEO2R
GSE26964	21647377	Capitalbio	13	6 Primary PrCa	7 Metastasis Bone	−2.7	N.S.	GEO2R
GSE23022	21400514	Affymetrix	40	20 Normal	20 Cancer	−1.3	0.03	GEO2R
GSE55323	24967583	Agilent	40	20 Non-Recurrent	20 Recurrent	−1.2	N.S.	GEO2R
GSE62610	25416653	Taqman qPCR	36	14 Non-Recurrent	22 Recurrent	−1.7	N.S.	GEO2R
GSE21036	20579941	Agilent	140	28 Normal	112 Cancer	−2.0	0.001	GEO2R
GSE36802	23233736	Affymetrix	42	21 Benign	21 Cancer	−1.8	0.0002	GEO2R
TCGA data	26544944	Small-RNA-Seq	24 [a]	12 Normal	12 Cancer	−3.2	0.03	miRDeep2

* GEO accession number; [a] PRAD-TCGA paired normal/tumor samples (52) with at least 2 reads for sdnc886-3p in normal tissue (24), paired t-test; N.S. non-significant.

In addition, we analyzed the expression of snc886-3p in six paired normal and tumor samples obtained from paraffin fixed tissues derived from radical prostatectomies [16]. Quantitative RT-PCR confirmed a significant decrease of the expression of snc886-3p in tumor compared to normal tissues in this cohort (Figure 2A). Similarly, the qRT-PCR quantitation of various prostate cell lines shows a reduction in the expression of snc886-3p in tumor cell lines in comparison to the normal prostate cell line PrEc (Figure 2B). Further analysis of publicly available small-RNA-seq data of prostate cell lines (GSE26970, GSE66035 and SRP109305) reinforce this finding (Figure 2C). The reduced expression of snc886-3p in malignant vs benign cells, observed in both patient tumors and prostate cancer cell lines, is in agreement with a tumor suppressor function.

We have previously demonstrated an epigenetically driven reduction of nc886 in PrCa, thus we wonder whether the decrease in snc886-3p is due to it. As expected, there is a positive correlation between the expression of snc886-3p and nc886 in the cell lines (r Spearman = 0.95, Figure 2D). Likewise, the expression of snc886-3p correlates with the methylation status of the 200nt region upstream to the transcription start site (TSS200nt) of nc886 (r Spearman = 0.71, Figure 2D).

Altogether these findings suggest that the reduction of snc886-3p levels in prostate cancer is due to the decreased levels of its precursor nc886, which in turn is a consequence of the increased methylation of the nc886 promoter.

2.3. Snc886-3p Modulates Transcripts Affecting Cell Cycle and Apoptosis

Aiming to discover the snc886-3p effect on gene expression, we overexpressed the small RNA in DU145 cell line (Figure 3A) and performed a global gene expression analysis using Affymetrix gene microarrays 48 h after transfection. We used Sylamer algorithm [53] to estimate the enrichment of all 6-nt k-mers in the 3′ untranslated regions (3′-UTR) of transcripts of the differentially expressed genes. A landscape plot that tracks the occurrence biases of the different k-mers on all transcripts ranked by their differential expression is obtained. We observed that 5′ACCCGC3′, which is the complementary sequence to the snc886-3p seed (6-mer, 2-7-nt), is the most enriched 6-nt k-mer in the 3′-UTR of the repressed transcripts (adjusted p-value < 0.01) (Figure 3B). This finding favors a direct and sequence specific repressive interaction of snc886-3p with the mRNA targets. Furthermore, we identified 1358 DEGs (fold change ≥ 1.5) including 704 downregulated and 654 upregulated transcripts (Table S1). Microarray experiments were confirmed by qRT-PCR of selected transcripts (r = 0.97, p-value < 0.0003) (Figure S2A). Independent snc886-3p overexpression experiments in DU145, LNCaP and PC3 (Figure S2B) demonstrate a similar regulation of these genes in these cell lines (Figure S2C).

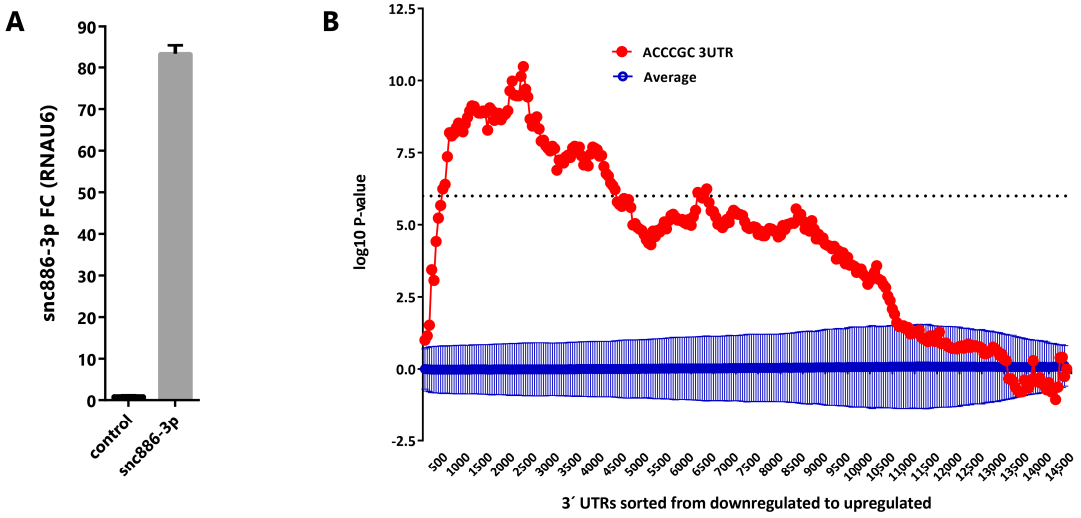

Figure 3. Snc886-3p downregulates transcripts bearing a 5′ACCCGC3′ sequence complementary to its putative seed in their 3′-UTR. (**A**) Expression of snc886-3p in DU145 cells transfected with 20nM of mimic snc886-3p and negative control (Dharmacon) after 48 h. Quantification by qRT-PCR using RNAU6 as a normalizer. (**B**) Sylamer enrichment landscape plot for 6-nt k-mer in all genes ranked by their change in abundance after snc886-3p overexpression compared to control determined by Affymetrix microarrays. The x-axis represents the sorted gene list (downregulated and upregulated genes are plotted in the left and right part of the axis respectively). The y-axis shows the hypergeometric significance for each 6-nt k-mer at each leading bin. Positive and negative values indicate enrichment or depletion of the 6-nt k-mer sequence at the 3′-UTR of the genes. The dotted horizontal line symbolizes an E-value threshold of 0.01 (Bonferroni corrected). The red line embodies the values obtained for the 6-nt k-mer (5′ACCCGC3′) complementary to the 6-nt seed (6-mer, 2-7-nt) of snc886-3p. The blue line shows the average profile of 6-nt k-mer unrelated to the seed region of snc886-3p (dark blue), with standard deviation as vertical bars.

Since canonical microRNAs are known to act mostly through complementary nucleotide pairing at the 3′-UTR of the target gene mRNAs, we analyzed if the repressive action of snc886-3p transfection was associated with the location of its binding site along the gene. We calculated the average fold change in expression of the transcripts bearing 6-8-mers sequence complementary to the snc886-3p seed in DU145 cell line transfected with snc886-3p (microarray experiments) (Figure S3A and Table S1). As expected, snc886-3p causes an average global repression of the genes bearing its complementary site. Most important, its action is significantly stronger when the site is located at the 3′-UTR of the

transcript (Figure S3A). Furthermore, we confirmed this finding using most stringent direct target genes narrowed down for their association to AGO [50]. Transcript with a snc886-3p 6-mer (2-7-nt) binding motif at their 3′-UTR show a higher proportion of repression (39%) than those having motifs differing in two-nucleotides (24% and 22%) (Fisher's exact test, p-value < 0.0001 and Odds ratio 2.0 to 5′AACCCC3′ and 2.2 to 5′AGCCAC3′ for the substituted sequences) (Figure S3B and Table S1). Overall, the evidence indicates that snc886-3p negative regulation of mRNA levels is dependent on the seed sequence and on the location of the complementary site in the 3′-UTR of the target genes.

In order to investigate the functional consequences of snc886-3p perturbation, we performed gene enrichment analysis of pathways and processes among the DEGs using GSEA curated gene sets [54]. The top 10 significant terms are shown in Table 2. In agreement with our previous study [16], cell cycle, apoptosis and mitogenic pathways are enriched. Particularly, three formerly validated direct targets of hsa-miR-886-3p, PLK1, TGFB1 and CDC6 [25,28], are downregulated upon snc886-3p overexpression. Additionally, candidate snc886-3p direct target CDT1, which is a partner of CDC6, has been associated with cell cycle impairment [55]. A more detailed picture of the snc886-3p responsive genes belonging to the KEGG cell cycle pathway highlights additional downregulated genes (Figure S2D).

Table 2. Gene enrichment analysis GSEA (curated gene sets).

Gene Set Name	Genes in Gene Set (K)	Genes in Overlap (k)	p-Value	FDR q-Value
KEGG_NEUROTROPHIN_SIGNALING_PATHWAY	126	21	1.26×10^{-9}	2.34×10^{-7}
KEGG_INSULIN_SIGNALING_PATHWAY	137	18	7.63×10^{-7}	6.13×10^{-5}
KEGG_APOPTOSIS	88	14	1.26×10^{-6}	6.13×10^{-5}
KEGG_CELL_CYCLE	128	17	1.32×10^{-6}	6.13×10^{-5}
KEGG_PATHWAYS_IN_CANCER	328	28	6.45×10^{-6}	2.40×10^{-4}
KEGG_VALINE_LEUCINE_AND_ISOLEUCINE_DEGRADATION	44	9	1.22×10^{-5}	3.79×10^{-4}
KEGG_TGF_BETA_SIGNALING_PATHWAY	86	12	2.81×10^{-5}	6.73×10^{-4}
KEGG_CHRONIC_MYELOID_LEUKEMIA	73	11	2.89×10^{-5}	6.73×10^{-4}
KEGG_MAPK_SIGNALING_PATHWAY	267	23	3.61×10^{-5}	7.46×10^{-4}
KEGG_MTOR_SIGNALING_PATHWAY	52	9	4.99×10^{-5}	9.28×10^{-4}

2.4. Snc886-3p Causes a Decrease in Cell Viability

We had previously shown that the forced recovery of nc886, the precursor of snc886-3p, reduced in vitro and in vivo cell viability of PrCa cells [16]. In view of the enrichment of cell cycle related pathways in the DEGs caused by snc886-3p overexpression (Table 2), we sought to determine if snc886-3p affects cell viability. We found that the overexpression of snc886-3p in the prostate cell lines DU145, LNCaP and PC3 produces a significant decrease in cell viability relative to the control (Figure 4A). In addition, we performed cell cycle analysis with propidium iodide to determine cells distribution in the different cell cycle phases (Figure 4B). We found an accumulation of cells in the S and G2/M phase of the cell cycle in DU145 cell line, that could be associated with the decreased expression of PLK1 evidenced previously (Figure S2A,C). Indeed, PLK1 was reported as a target of hsa-miR-886-3p, the downregulation of which leads to an arrest in the anaphase stage of mitosis [25,56]. Additionally, LNCaP and PC3 showed an accumulation of cells in G1 phase of the cell cycle (Figure 4B). These results lead us to propose an effect of snc886-3p on apoptosis. Annexin V, a marker of early apoptosis, significantly increases in DU145 (14% of early apoptosis equivalent to an increase of 69% relative to control) and LNCaP (24% of early apoptosis equivalent to an increase of 366% relative to control) when snc886-3p is overexpressed (Figure 4C). On the contrary, we found no changes of early apoptosis in PC3 cells between conditions, though we cannot completely discard earlier apoptotic events completed at 72 h (Figure 4C). Despite the significant overall decrease in cell viability caused by snc886-3p overexpression in the three prostate cell lines tested, the distinct contribution of proliferation

and apoptosis may be due to the intrinsic differences of these cell lines. Globally, these analyses show that snc886-3p decreases cell viability, due to a modulation of cell proliferation and early apoptosis.

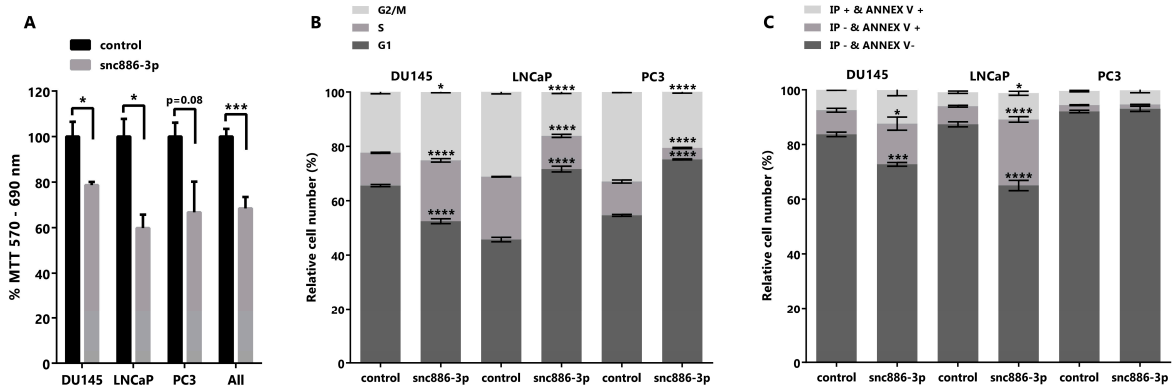

Figure 4. Cytotoxicity, cell cycle and early apoptosis assay in prostate tumor cell lines overexpressing snc886-3p. DU145, PC-3 and LNCaP cells transfected with 20 nM of mimic snc886-3p and negative control (Dharmacon) were evaluated 72 h after transfection. All analyses were performed in triplicates to determine average values and standard error. * p-value < 0.05; *** p-value < 0.001; **** p-value < 0.0001. (**A**) MTT assay to determine cell viability. p-values of T-test of the individual cell lines and the three cell lines considered as replicates (all) are indicated over the horizontal brackets. (**B**) DNA content analysis to determine the distribution of cell cycle stages. 10,000 cells/experiment were stained with Propidium Iodide and evaluated by flow cytometry. (**C**) Early apoptosis assay. 10,000 cells/experiment were stained with Annexin V (Annex V) and Propidium Iodide (IP) and evaluated by flow cytometry. Viable cells are negative for Annexin V and Propidium Iodide, cells positive for Annexin V and negative for Propidium Iodide are in early apoptosis and cells positive for Annexin V and Propidium Iodide are necrotic cells. Two-way ANOVA Test for the cell cycle and early apoptosis assays was used to estimate statistical significance of the observed differences.

2.5. Direct Candidate Target Genes of snc886-3p Are Associated with Clinical Worse Prognosis in Prostate Cancer Patients

We had previously found that nc886 [16] and snc886-3p expression (Table 1) are associated to worse clinical outcome in PrCa. We now sought to investigate if snc886-3p direct candidate target genes are also associated with the disease. A list of 253 snc886-3p possible direct target genes was built based on two criteria: the association to Argonaute determined by AGO-PAR-CLIP experiments using DU145 (reads with a sequence complementary to the 6-mer (2-7-nt) snc886-3p seed sequence) identified in Hamilton et al. [50] and the downregulation of at least 1.25 FC in DU145 after snc886-3p overexpression (Table S1). A hierarchical clustering of the PRAD-TCGA samples in association with clinical status (pathological, clinical, Gleason score, residual tumor, biochemical recurrence) is shown in Figure 5. The expression of the 253 genes segregates the samples of patients with worse (red/violet) from those with better (non-red) clinical presentation as well as the normal tissues (green). Additionally, two major gene groups are clustered. Remarkably, the positive association of the 106 genes cluster with worse clinical parameters suggests that they may be the relevant direct candidate targets of snc886-3p repression in vivo (individual genes are listed in Table S1). We also found that men harboring tumors with low expression of the 253 snc886-3p direct candidate target genes (percentile 25th) have a longer disease-free survival compared with the high expressing ones (percentile 75th) (HR=2, p-value 0.031) (Figure 6A). Disease-Free Survival analysis based on the expression of the 106-gene list showed a greater statistical difference in patient survival probability (HR=3.2, p-value 0.00018) compared with the 253-gene list (Figure 6A,B). Furthermore, the expression of the 106-genes associates with higher methylation of nc886 TSS200nt (thus of snc886-3p) (r 0.29, $p < 0.0001$) (Figure S4A,B). These results provide in vitro and in vivo support of a tumor suppressor microRNA-like role of snc886-3p in prostate, acting through the direct repression of transcripts bearing complementary sequences at their 3′-UTR.

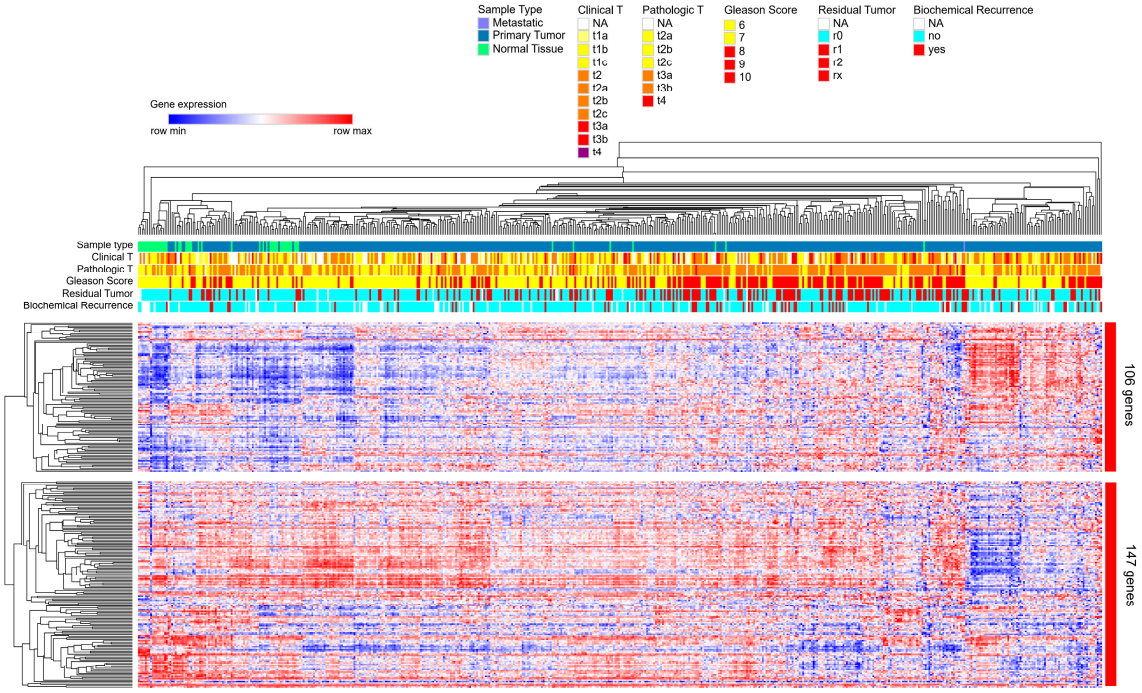

Figure 5. Hierarchical clustering based on the expression of 253-snc886-3p direct candidate target genes in prostate tissue of PRAD-TCGA. Heatmap of the expression of the 253 genes obtained by a two-way hierarchical clustering using the Spearman rank correlation algorithm with the Morpheus software and PRAD-TCGA data. The principal two gene clusters formed are shown (cluster of 106 genes and cluster of 147 genes). Color scale indicates the relative expression level of the genes across the samples (red and blue represent higher and lower expression relative to the mean). Clinical status for different parameters (Clinical T value, Pathological T value, Gleason Score, Residual Tumor and Biochemical Recurrence) are represented by horizonal marks on the top of the heatmap. The values for each parameter are indicated by colors in the top right legends.

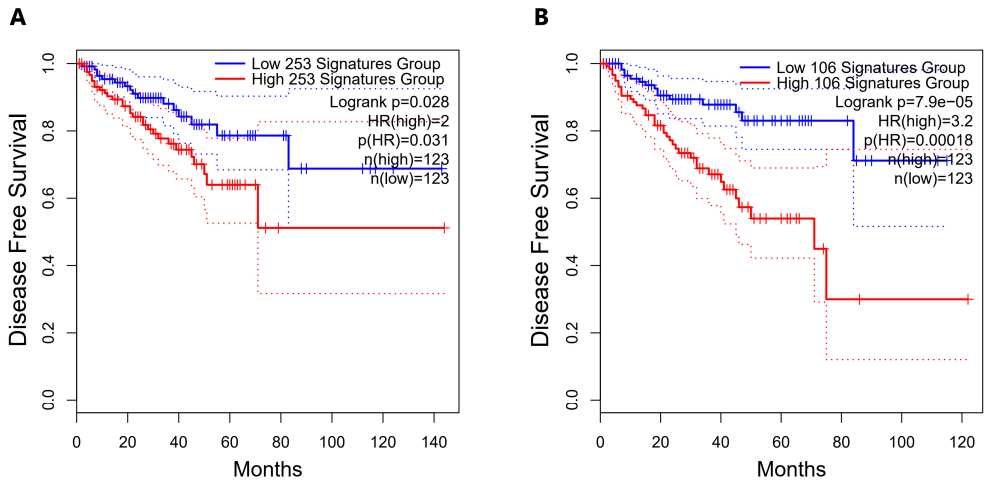

Figure 6. Disease-Free Survival analysis for PRAD-TCGA patients according to the expression of the snc886-3p direct candidate target genes. Disease-Free Survival Kaplan–Meier curve for the expression status of candidate target genes of snc886-3p in PRAD-TCGA was generated using GEPIA2 software [57]. (**A**) 253-snc886-3p direct candidate target gene list. (**B**) 106-snc886-3p direct candidate target gene list. Two groups of patient tumors are compared: percentile 25th expression of the candidate target genes (low expression: blue line) and percentile 75th expression of the candidate target genes (high expression: red line). Hazard Ratio (HR), *p*(HR) and number of patients in each group are indicated. The dotted lines represent the confidence interval of each group.

3. Discussion

Hsa-miR-886-3p (snc886-3p) was initially classified as a microRNA derived from pre-miR-886 [8], which was later removed from miRBase microRNA precursors (Release v16) due to its homology with vtRNA1-1/2/3 and renamed as vtRNA2-1 [9]. Although several studies reported the dysregulation of hsa-miR-886-3p in different pathological conditions [20–22,24–28,33,58], the specific synthesis of fragments with microRNA-like function from nc886 has been poorly addressed.

We previously found that nc886 acts as a tumor suppressor in prostate cancer and the vector-driven overexpression of this RNA inhibited cell proliferation and invasion [16]. Due to existing reports about the production of small RNA with microRNA function derived from vtRNAs [59–61], we wonder if there is a specific processing of nc886 into small RNAs in prostate cells and if it could possibly contribute to the described nc886 induced phenotype in prostate cancer cells [16].

To assess the synthesis of vtRNA2-1/nc886 small fragments, we interrogated published small-RNA-seq prostate datasets, revealing a pattern of small RNA read stacking over nc886 sequence that resemble the cleavage of DICER which generates complementary 5p and 3p fragments (Figure 1A, Figure S1A,B). Additionally, the analysis of Kim et al. dataset showed that DICER knockout impaired the production of snc886-3p/5p in the HCT116 cell line [51]. Interestingly, although the secondary structure of nc886 resembles a microRNA hairpin precursor, it is not fully optimized as a canonical microRNA precursor [47,62–64]. Indeed, the 101 nt nc886 sequence of is longer than the median 83 nt of human microRNA precursors (range 41-180 nt), generating mature small RNA fragments that are also longer (23 nt of snc886-3p and 24-25 nt of snc886-5p) than the 22 nt median human mature microRNAs (range 16-27 nt); this pattern was described for other DICER substrates of similar length [63,64]. Moreover, the presence of asymmetrical mismatches and bulges in the predictive nc886 secondary structure is associated with longer mature sequences [63]. Overall, its structural divergence with the optimized human microRNA hairpin precursor might lead to a low efficient DICER processing and consequently a small amount of microRNAs observed in our and former studies [12,18]. Evolutionary hypothesis of new microRNA precursor proposes their birth as non-efficiently processed precursor RNAs, until specific target genes are evolutionary selected; this avoids the non-specific repression of genes allowing the optimization of the hairpin structure for DICER processing [65]. The identification of the presence of a large fraction of nc886 and a less abundant fraction of derived small RNA may be the result of its recent evolutionary origin in eutherians [9].

To further investigate the putative microRNA-like function of snc886s we analyzed their association with Argonaute proteins. Previously, other groups reported small RNA fragments derived from vtRNA1 associated to Argonaute, holding microRNA function in breast and lymphoid tissue [59,60]. Here, we show that snc886-3p is also associated with Argonaute in lung cell line WI-38 (Figure S1D), which is in agreement with the proposed microRNA identity of hsa-miR-886-3p (here snc886-3p) acting through direct repression of PLK1 and TGFB1 in lung cancer [25,27]. Concordantly, we found proof for the association of snc886-3p with Argonaute protein in prostate by analysis of AGO-PAR-CLIP available small-RNA-seq data from prostate cell line DU145 [50]. Indeed, snc886-3p enrichment is above the average of the microRNAs in these experiments, indicating a specialized microRNA-like function for this small RNA product in comparison to the 5p. Although our study shows a low association of snc886-5p to AGO it does not rule out the function of snc886-5p as a microRNA, which has been shown previously in other tissues (brain [19], cervical [66,67], breast [68]). Alternatively, snc886-5p might be involved in another pathway or be a non-functional secondary product of nc886 processing.

In view of the possible microRNA-like identity of snc886-3p, we then investigated its association with PrCa in existing small RNA studies obtained using various techniques (qRT-PCR, microarray and small-RNA-seq). We found that hsa-miR-886-3p/snc886-3p is globally downregulated in worsened disease conditions in the published datasets (Table 1), as well as in our patient cohort (Figure 2A) and laboratory stablished cell lines (Figure 2B,C). These datasets show that snc886-3p has the expression pattern of a tumor suppressor gene the level of which in prostate cells is in the low-medium microRNAs expression range. In addition, we found that snc886-3p expression positively correlates with nc886

expression and negatively correlates with the methylation of nc886 TSS200nt. Furthermore, snc886-3p has a bimodal expression in prostate cell lines (Figure 2B,D), similar to what we reported for nc886 promoter methylation in prostate cell lines and tissues. This distribution could be explained by zygotic differences in the promoter methylation status of the gene [16]. Despite this pre-existing variation in the methylation status of nc886 TSS200nt, both patient groups present an increased promoter methylation in tumor compared with the normal matched tissue [16].

Different direct targets of microRNA regulation by hsa-miR-886-3p have been proposed in the literature mostly after its removal from miRBase (PLK1, TGFB1, CDC6, CXCL12 and FXN) [25,28,30,31]. If snc886-3p functions as a microRNA in PrCa it is expected to sequence-specifically bind to target mRNAs to repress their expression. In order to test this hypothesis, we performed a global gene expression study of DU145 cell line overexpressing snc886-3p vs a control small RNA. Sylamer analysis of the differentially expressed transcripts demonstrated that the sequence complementary to snc886-3p seed is the most overrepresented 6-nt k-mer in the 3'-UTR of the downregulated transcripts by snc886-3p overexpression, which strongly favors a microRNA mechanism of action. Furthermore, the identification of previously validated targets PLK1, CDC6 and TGFB1, among the downregulated transcripts of this experiment, reinforces the assumption.

To obtain an insight of the biological effect of snc886-3p, we studied the pathways enriched in the DEGs identified by the microarray experiment, finding an enrichment in cell cycle and apoptosis processes which predicts a proliferative inhibition. This inference was confirmed by in vitro cell viability and cell cycle distribution determination in DU145, LNCaP and PC3 PrCa cell lines. Snc886-3p overexpression reduces proliferation of the three cell lines and provokes a distinctive phase specific cell cycle arrest in DU145 (G2/M) compared to LNCaP and PC3 (G1). An increase in early apoptosis after snc886-3p transfection was validated through Annexin V determination in DU145 and LNCaP, while no change was observed in PC3 cell line. Cell line specific effects may be due to differences in cell cycle control. A similar effect of snc886-3p in cell viability was previously reported in thyroid, lung and breast tissues in vitro and in vivo [22,25,27,28]. Additionally, a high-throughput analysis of seed 6-nt k-mers RNAs exposed that the snc886-3p 6-nt seed k-mer causes a significant decrease in cell viability in several non-prostate cancer cell lines [69]. In agreement with these findings, the overexpression of nc886 produces a similar phenotype in tissues where is described as a tumor suppressor (prostate [16,70], thyroid [28], gastric [71] and esophageal [72]), whereas its silencing produces the same effect in non-malignant cells in agreement with the tumor surveillance model proposed by Kunkeaw et al. (cholangiocarcinoma [73]). Accordingly, hsa-miR-886-3p and nc886 act as pro-proliferative and anti-apoptotic RNAs in tissues where it is proposed as an oncogenic RNA (renal [33], ovarian [74], thyroid [75] and endometrial [76]). Our current results together with our previous study indicate that both snc886-3p and nc886 have an antiproliferative effect and a tumor suppressor function in prostate cells. Nonetheless, given their different size, structure, and abundance, they are expected to participate in different effectors pathways. The specific production of small RNAs from nc886 is controversial in the literature, probably because of the differences in the tissue types and methods employed for its detection (RNA-seq, northern blot, microarray, qRT-PCR). In addition, the effect of both molecules has been studied using exclusively the nc886 or the snc886-3p, thus their interdependence has been mostly ignored. Indeed, the overexpression and inhibition of nc886 is expected to produce an increase/decrease of hsa-miR-886-3p/snc886-3p respectively. Meanwhile, the inhibition of snc886-3p using anti-miRs could modify the abundance, folding or endogenous interactors of the precursor molecule. As an example, a study in bladder cancer, where hsa-miR-886-3p expression is associated with short patient survival, found that both hsa-miR-886-3p knock down and nc886 overexpression lead to a decrease of cell viability in half of the cell lines tested [21]. For that reason, the effects assigned to only one of the molecules could be in fact the result of the modulation of both nc886 and its snc886 products. Indeed, the study of snc886 mimics circumvents most of these problems, allowing the discrimination of the sole effect of hsa-miR-886-3p/snc886-3p. Nevertheless, it is worth recalling that in vivo both molecules are synthesized and functional in the cells. To our knowledge,

five previous reports analyzed functional effects and direct target genes of hsa-miR-886-3p/snc886-3p using mimic molecules (lung cancer) [25,27], human marrow stromal cells [30], breast cancer [22] and gastric cancer [71] and their findings are consistent to ours in prostate cancer cells. Remarkably, the only study that examined the function of both nc886 (transfection) and snc886-3p (mimic) using gastric cancer cells, found that only the transfection of nc886 (but not snc886-3p) affects cell proliferation and viability, although they showed its ability to function as a microRNA in a reporter gene assay harboring a complementary binding site at the 3′-UTR [71].

We and others have shown that the expression of nc886 and snc886s is associated with patient clinical outcome [20,25,71,72,74,75]. The group of Lee also showed the clinical association of the gene signature of nc886 knockout [71,72,74,75]. To our knowledge, there is no clinical association study of the snc886-3p direct candidate target genes in the literature. We built 253- and 106-gene sets composed of transcripts bearing a sequences complementary to snc886-3p seed (6-mer, 2-7-nt) protected in AGO-PAR-CLIP experiments and downregulated in our microarray experiments, the expression of which turned out to be significantly associated with a lower disease-free survival in PRAD-TCGA and unfavorable clinical parameters. Furthermore, the negative association of the 106-gene set with nc886 promoter methylation strengthens the specificity of these in vitro defined gene set. Overall, these results are strong indicators of the validity of the snc886-3p DEGs identified in vitro in DU145 cell line and reinforce the tumor suppressor function of snc886-3p in PrCa in the clinical set.

Although RNA biomarkers are increasingly established in prostate cancer management [77], snc886-3p does not fulfill relevant biomarker attributes, such us tissue specificity and upregulation in the disease condition. However, small non-coding RNAs derived from nc886 have been repeatedly detected in body fluids [78–85] and, contrary to our findings in the tumor tissue, a recent study of circulating microRNAs in the plasma of prostate cancer patients reported an increase expression of snc886-3p in high-grade compared to low-grade tumor biopsy [32]. In this context, the value of snc886-3p as a cancer biomarker is still unclear. Notwithstanding, previous reports suggested that the methylation of the nc886 promoter may be worthy of further investigation in the prostate cancer biomarker field [16,86]. Finally, the expression of snc886-3p candidate direct target genes that associate with prostate cancer prognosis may be valuable for future biomarker research.

4. Materials and Methods

4.1. Human Specimens

Tissue sections were obtained from paraffin fixed blocks stained with hematoxylin and eosin (H&E) of 6 archived radical prostatectomies and were evaluated by three pathologists at the Department of Anatomic-pathology of the Police Hospital. This study was approved by the Hospital Policial, D.N.AA.SS., Montevideo, Uruguay (2010).

Matched normal and tumor regions, showing similar parenchyma-stroma ratio and similar cytological findings at the stroma were selected. Unstained section of 10-micron thickness, contiguous to the sections selected by the pathologist, were then freshly obtained to extract small RNAs using the RNeasy FFPE (Qiagen) Kit, with the following modifications: two extra washes with xylene and absolute ethanol were added. The RNA was resuspended in RNAse free water and stored at −20 °C for further analysis.

4.2. Cell Lines

LNCaP and DU145 cell lines derive from a supraclavicular lymph node and a brain metastasis respectively, while PC3 and VCaP derive from vertebral bone metastatic sites. In addition, LNCaP and VCaP are androgen sensitive, whereas DU145 and PC3 are androgen independent. Cell lines PCSC-1, PCSC-2 and PCSC-3 are highly metastatic androgen independent primary prostate cancer cell lines enriched in CD133+ stem cells. RWPE-1/2 are non-malignant cells derived from normal adult prostate epithelium and WPE-int is a less differentiated derivative of RWPE1.

LNCaP, PC-3 and DU145 human prostate cancer cell lines were obtained from ATCC (Manassas, VA, USA). LNCaP, DU145 and PC-3 were maintained in RPMI 1640 (R7755) supplemented with 10% FBS (PAA™) and penicillin/streptomycin. Cell lines PCSC-1, PCSC-2 and PCSC-3 prostate cancer stem cells (PCSCs) were purchased from Celprogen®; RWPE-1/2, VCaP and WPE were obtained from ATCC (Manassas, VA, USA) and maintained following the recommendations of the vendor's specifications. All cell lines were maintained in a 5% carbon dioxide atmosphere at 37 °C.

4.3. Cell Transfection

The snc886-3p mimic (5'CGCGGGUGCUUACUGACCCUU3') and negative controls (5'UCACAACCUCCUAGAAAGAGUAGA3') (NC, CN-001000-01-05) were synthesized Dharmacon (Miridian). According to the manufacturers' instructions, the mimic and control mimic 20nM, were transfected into cells in 12 and 96 well plates using Lipofectamine™ 3000 (Invitrogen, Carlsbad, CA, USA). After 24 h of transfection the medium was removed and fresh medium was added and 48 h (Affymetrix microarray and qRT-PCR analyses) or 72 h (Cytotoxicity assay, Flow Cytometry for DNA content analysis, Annexin V Alexa Fluor 488/PI apoptosis detection assay) after transfection cells were collected for further analysis.

4.4. RNA Extraction Reverse Transcription and Quantitative Real Time PCR

Total RNA was extracted using the Qiagen™ miRNAeasy kit. Quantification by reverse transcription and quantitative real time PCR (qRT-PCR) was performed using the Qiagen PCR miScript II System with oligonucleotides specific for snc886-3p (hsa-miR-886-3p (MS00010675, Qiagen)), RNAU6 (MS00033740, Qiagen) as the internal control of RNA load and the following specific gene primers pairs:

nc886: 5'CGGGTCGGAGTTAGCTCAAGCGG3' forward primer and 5'AAGGGTCAGTAA GCACCCGCG3' reverse primer, as in Lee K et al. [12], PLK1: 5'CCTTGTTAGTGGGCAAACCACC3' forward primer and 5'CGGGGTTGATGTGCTTGGGAA3' reverse primer; TGFB1: 5'CCGTGGAGG GGAAATTGAGGG3' forward primer and 5'GCCGGTAGTGAACCCGTTGAT3' reverse primer; CDT1: 5'CGGAGCGTCTTTGTGTCCGAA3' forward primer and 5'GGTGCTTCTCCATTTCCCC AGG3' reverse primer; CDC6: 5'ATCAGGTTCTGGACAATGCTGC3' forward primer and 5'CAATAGCTCTCCTGCAAACATCCA3' reverse primer; C8orf82: 5'CGCGAGTATTTCTACT ACGTGGACC3' forward primer and 5'CTGCGGGTCTTTGAAGCAGGT3' reverse primer; NLPR13: 5'CATTGCACACACTTGGGTTGGC3' forward primer and 5'CCAGGCTCTTAC TGCTGCTGAG3' reverse primer; MMD: 5'CACACGCATTCCTCATTGTTCCG3' forward primer and 5'TGAAGAGGGCACAGAGTCCCA3' reverse primer; TBP: 5'GATCAAACCCAGAATTGTTCTCC3' forward primer and 5'ATGTGGTCTTCCTGAATCCCTTT3' reverse primer. The relative quantification was attained using the $2^{-\Delta\Delta CT}$ method [87], in a Rotor-Gene 6000 equipment (Corbett Life Science).

4.5. Microarray Experiments

Total RNA from 3 replicates of snc886-3p (hsa-miR-886-3p) mimic and negative controls (NC, CN-001000-01-05) was extracted after 48 h of transfection using the Qiagen™ miRNAeasy kit according to the manufacturer's protocol. The total RNA of the three replicates was pooled and labeled according to Affymetrix (Affymetrix, Santa Clara, CA, USA). Hybridization, staining and washing of the Affymetrix® HG-U133 Plus 2.0 Arrays were performed with the Affymetrix Fluidics Station 450 and Hybridization Oven 640 under standard conditions (Affymetrix, Santa Clara, CA, USA). Quality control analysis and Pre-processing of the CEL-files microarray expression data was done using a graphical user interface, Chipster (v1.4.3, CSC, Finland, http://chipster.csc.fi/) following the manufacturer's guidelines [88]. Normalization was performed using RMA algorithm [89] and annotation using the specific Affymetrix® HG-U133 Plus 2.0 Arrays probe set library in Chipster. Normalized log2 expression values were used to determine the fold change expression of the snc886-3p (hsa-miR-886-3p) mimic and negative controls (NC, CN-001000-01-05) (Table S1).

4.6. Cytotoxicity Assay

At 72 h after of transfection with snc886-3p or control RNA (60-80% cell culture confluence), 20 µL of 3-(4,5-dimethylthiazol-2-yl)-2,5-diphenyl-2H-tetrazolium bromide (MTT) 5 mg/mL in 1X PBS was added to the wells and cultures were incubated for 4 h at 37 °C in a 5% CO_2 controlled atmosphere. The medium was then aspirated and 200 µL of DMSO was added to each well and incubated at room temperature in the dark for 15 min with moderate orbital shaking. Optical density (OD) was read on a plate spectrophotometer (Varioskan® Flash Multimode, Thermo Scientific, Waltham, MA, USA) at 570 nm (for formazan absorbance measurement) and 690 nm (for background measurement).

4.7. Flow Cytometry for DNA Content Analysis

At 72 h after transfection with snc886-3p or control RNA (60–80% confluence) cells were harvested by trypsinization followed by two washes and resuspension in 1X PBS with gentle vortexing. Cells were then fixed by adding 1 mL of ice cold 70% ethanol dropwise and incubated at -20 °C for 30 min. Next, cells were washed with 1X PBS, centrifuged at 1200 rpm at 4 °C for 5 min and the resuspended cell pellets were incubated with 0.1 mg/mL of RNAse and 50 µg/mL propidium iodide for 15 min at room temperature in the dark. Flow cytometry measurement of nuclear DNA content was performed in an Accuri™ C6 flow cytometer (BD Bioscience), counting 10,000 total events per sample (BD Accuri C6 software).

4.8. Annexin V Alexa Fluor 488/PI Apoptosis Detection Assay

Apoptosis was detected by initially staining the cells with 0.1% (*v*/*v*) Annexin V and 100 µg/mL of propidium iodide solution, according to the Annexin V Alexa Fluor 488/PI apoptosis detection assay kit (catalog n° V13241, Invitrogen, USA), followed by flow cytometry analysis in an Accuri™ C6 flow cytometer (BD Bioscience), counting 10,000 total events per sample (BD Accuri C6 software).

4.9. Dataset Analysis

4.9.1. Analysis of microRNA Microarray Datasets

Depending on the type of study and the availability of the data, we followed different strategies. Data deposited at GEO was analyzed using the GEO2R tool using default settings [90], selecting the samples by clinical status definition. For all the microarray data of PrCa studies analyzed, relevant features used in the analyses are listed in Table 1.

4.9.2. Analysis of Small RNA Transcriptomic Datasets

Data on microRNA expression from tumor and matched normal prostate patient samples generated by the project The Cancer Genome Atlas (TCGA) were retrieved from dbGaP, miRNAseq data Level_2 Data (file names: *.bam) of 544 samples (project approved n° 7307). Additionally, several public small-RNA sequencing expression data available at the repository Gene Expression Omnibus (GEO) [41] or Sequence Read Archive (SRA) [40] were also analyzed: microRNA expression of several human cancer cell lines (GSE16579, [91]), microRNA expression from the evaluation of the roles of DROSHA, XPO5, and DICER in microRNA biogenesis (GSE77989, [51]), AGO-immunoprecipitation of microRNAs in human senescent fibroblast WI-38 (GSE34494, [92]), microRNA transcriptome (normal prostate and prostate cells, Figure S5 (GSE29904, [37])), microRNA transcriptome of DU145, LNCaP and PC3 cell lines (Figure S6 (SRP109305, [38] and GSE66035, [39])), Human Prostate Cancer cell lines AGO-PAR-CLIP (SRP075075, [50]). Data was downloaded with SRA Toolkit (https://www.ncbi.nlm.nih.gov/sra/docs/toolkitsoft/) and then trimmed, mapped, annotated, counted, and normalized using miRDeep2 package software [93]. We used the mapper module (mapper.pl) with the following parameters: -e -h -l 18 -m -k "adapter-sequence" and quantifier module (quantifier.pl) with default parameters and miRBase fasta files of precursor and mature sequences from Release v21 plus manually addition of RefSeq human

vtRNAs (vtRNA1-1/2/3 and 2-1) and human RNYs (RNY1/3/4/5). Normalized (Reads Per Million Reads (RPM)) log2 values were used in all cases for analysis. For the elaboration of the snc886-3p direct target candidate gene list, we used DU145 AGO-PAR-CLIP (SRP075075, [50]). Total sequencing reads were trimmed with cutadapt software [94] with the following parameters: -m 18 -q 20 and those with the sequence: 5′ ACCCGC 3′ (complementary to snc886-3p seed (6-mer, 2-7-nt)) were aligned to human genome (GRCh38/hg38) using Bowtie2 [95] with the following parameters: –L 6 -N 1. Total read counts for each gene transcript were obtained with HTSeq [96] using the Ensembl GTF file, from the reference genome sequence (GRCh38.97).

4.9.3. Analysis of Methylation Microarray Datasets

The methylation data of the PRAD-TCGA cohort, was extracted from the Illumina Infinium Human Methylation 450 BeadChip array data of the 49-paired normal and prostate tumor samples and additionally unmatched normal and tumor tissues (336 in total). Additionally, public methylomes available at the repository Gene Expression Omnibus (GEO) [41] obtained using Illumina Infinium Human Methylation 450 BeadChip arrays were also analyzed prostate cell lines PrEc, RWPE1, VCAP, LNCaP, DU145 and PC-3 gene dataset GSE68379 [97]. The average of the normalized beta-values for the 6 CpGs sites located at the nc886 TSS200nt promoter (cg18678645, cg06536614, cg26328633, cg25340688, cg26896946, cg00124993) were calculated.

4.9.4. Heatmap of Hierarchical Clusterization of 253 snc886-3p Candidate Direct Target Genes

Heatmap was performed by two-way hierarchical clustering using the Spearman rank correlation algorithm using Morpheus (https://software.broadinstitute.org/morpheus/) and gene expression values and clinical status for different parameters (Clinical T value, Pathological T value, Gleason Score, Residual Tumor and Biochemical Recurrence) of PRAD-TCGA dataset.

4.10. Statistical Analysis

All experiments were performed at least in triplicate and the corresponding variables are expressed as average value ± standard deviation or standard error (referred in the figure). Statistical analyses were done using single, two-tailed t-test, one-way and two-way ANOVA for multiple comparison tests, including Tukey's Honest Significant Difference test as a post-hoc tests (referred in the figure). D'Agostino–Pearson was conducted as normality test and Pearson or nonparametric Spearman was used to test correlation. Two-tailed Fisher exact test for difference in the proportions of genes was used. All the analyses were done in GraphPad Prism 6. The observed differences were expressed using the p-value (* $p < 0.05$, ** $p < 0.01$, *** $p < 0.001$, **** p-value < 0.0001). Results with a p-value of < 0.05 were considered significant.

5. Conclusions

Our study demonstrates the presence of hsa-miR-886-3p/snc886-3p in prostate tissue derived from the DICER mediated processing of vtRNA2-1/nc886, which associates to argonautes repressing transcripts bearing complementary seed sequences, thus functioning as a microRNA. We also found a DNA methylation dependent downregulation of snc886-3p and a concomitant upregulation of direct candidate targets of repression, both associated with PrCa disease condition and progression. Snc886-3p effects on global gene expression support the modulation of cell cycle progression and apoptosis observed in prostate cancer cell lines. Altogether, our results indicate that both nc886 and snc886-3p are simultaneously expressed in prostate cells at different levels, exerting a tumor suppressor action through probably different effector pathways.

Supplementary Materials: The following are available online at http://www.mdpi.com/2311-553X/6/1/7/s1, Figure S1: nc886 derived fragments are produced in non-prostate cell lines and exhibit microRNA features, Figure S2: Candidate target gene expression of snc886-3p in DU145, LNCaP and DU145, Figure S3: High expression of 106-snc886-3p direct targets correlates with nc886 promoter methylation in prostate tissue, Figure S4: High

expression of 106-snc886-3p direct targets correlates with nc886 promoter methylation in prostate tissue, Figure S5: Sequencing reads alignment to nc886 precursor of small-RNA-seq data of non-transformed prostate cell lines (PrEc and PrSc), Figure S6: Sequencing reads alignment to nc886 precursor of small-RNA-seq data of tumor prostate cell lines (DU145, LNCaP and PC3), Table S1: snc886-3p and 5p human transcriptome BLAST results, snc886-3p microarray expression data, snc886-3p microRNA target activity in DU145 based on seed and AGO-association and snc886-3p candidate target gene list for clinical associations.

Author Contributions: Conceptualization, M.A.D.; methodology, R.S.F. and M.A.D.; software, R.S.F.; validation, R.S.F.; formal analysis, R.S.F.; investigation, R.S.F. and M.A.D.; resources, M.A.D., B.G. and J.R.S.-S; data curation, M.A.D and R.S.F.; writing—original draft preparation, R.S.F.; writing—review and editing, M.A.D.; visualization, R.S.F.; supervision, M.A.D. and J.R.S.-S.; project administration, M.A.D.; funding acquisition, M.A.D. and J.R.S.-S. All authors have read and agreed to the published version of the manuscript.

Funding: This study was funded by Comisión Honoraria de Lucha contra el Cáncer (CHLC), Agencia Nacional de Investigación e Innovación (ANII), Comisión Sectorial de Investigación Científica (CSIC) and Programa de Desarrollo de las Ciencias Básicas (PEDECIBA) from Uruguay.

Acknowledgments: We thanks to Pablo Smircich for computing server technical support and Magister Santiago Chavez for assistance with microarray experiments.

Conflicts of Interest: The authors declare no conflict of interest.

Abbreviations

ncRNA	non-coding RNA
vtRNA	vault RNA
3′-UTR	three prime untranslated region
PrCa	Prostate Cancer
PSA	Prostate-Specific Antigen
nc886	non-coding RNA 886 (vtRNA2-1)
Pre-miR-886	hsa-mir-886 precursor of microRNAs hsa-miR-886-3p and 5p
snc886s	small non-coding RNA derived from nc886
snc886-3p	small non-coding RNA derived from nc886 at 3′ region
snc886-5p	small non-coding RNA derived from nc886 at 5′ region
svtRNA2-1	small non-coding RNA derived from vtRNA2-1/nc886
PAR-CLIP	photoactivatable ribonucleoside-enhanced crosslinking and immunoprecipitation
PRAD-TCGA	Prostate Adenocarcinoma—The Cancer Genome Atlas
SRA	Sequence Read Archive
GEO	Gene Expression Omnibus
DEG	Differentially Expressed Gene
MFE	Maximum Free Energy
RISC	RNA-induced silencing complex
qRT-PCR	quantitative Reverse Transcription Polymerase Chain Reaction
TSS200nt	200nt region upstream to the transcription start site
GSEA	Gene Set Enrichment Analysis
MTT	3-(4,5-dimethylthiazol-2-yl)-2,5-diphenyl-2H-tetrazolium bromide

References

1. Ceder, Y. Non-coding RNAs in prostate cancer: From discovery to clinical applications. In *Advances in Experimental Medicine and Biology*; Springer: New York, NY, USA, 2016; Volume 886, pp. 155–170.
2. Ferlay, J.; Soerjomataram, I.; Dikshit, R.; Eser, S.; Mathers, C.; Rebelo, M.; Parkin, D.M.; Forman, D.; Bray, F. Cancer incidence and mortality worldwide: Sources, methods and major patterns in GLOBOCAN 2012. *Int. J. Cancer* **2015**, *136*, E359–E386. [CrossRef]
3. Kohaar, I.; Petrovics, G.; Srivastava, S. A Rich Array of Prostate Cancer Molecular Biomarkers: Opportunities and Challenges. *Int. J. Mol. Sci.* **2019**, *20*, 1813. [CrossRef] [PubMed]
4. Bijnsdorp, I.V.; Van Royen, M.E.; Verhaegh, G.W.; Martens-Uzunova, E.S. The Non-Coding Transcriptome of Prostate Cancer: Implications for Clinical Practice. *Mol. Diagn. Ther.* **2017**, *21*, 385–400. [CrossRef] [PubMed]

5. Bolton, E.M.; Tuzova, A.V.; Walsh, A.L.; Lynch, T.; Perry, A.S. Noncoding RNAs in prostate cancer: The long and the short of it. *Clin. Cancer Res.* **2014**, *20*, 35–43. [CrossRef] [PubMed]
6. Mouraviev, V.; Lee, B.; Patel, V.; Albala, D.; Johansen, T.E.B.; Partin, A.; Ross, A.; Perera, R.J. Clinical prospects of long noncoding RNAs as novel biomarkers and therapeutic targets in prostate cancer. *Prostate Cancer Prostatic Dis.* **2016**, *19*, 14–20. [CrossRef]
7. Griffiths-Jones, S. miRBase: MicroRNA sequences, targets and gene nomenclature. *Nucleic Acids Res.* **2006**, *34*, D140–D144. [CrossRef]
8. Landgraf, P.; Rusu, M.; Sheridan, R.; Sewer, A.; Iovino, N.; Aravin, A.; Pfeffer, S.; Rice, A.; Kamphorst, A.O.; Landthaler, M.; et al. A Mammalian microRNA Expression Atlas Based on Small RNA Library Sequencing. *Cell* **2007**, *129*, 1401–1414. [CrossRef]
9. Stadler, P.F.; Chen, J.J.-L.; Hackermüller, J.; Hoffmann, S.; Horn, F.; Khaitovich, P.; Kretzschmar, A.K.; Mosig, A.; Prohaska, S.J.; Qi, X.; et al. Evolution of Vault RNAs. *Mol. Boil. Evol.* **2009**, *26*, 1975–1991. [CrossRef]
10. Kedersha, N.L.; Rome, L.H.; Krotoski, D.M.; Domingo, C.; Bronner-Fraser, M. Isolation and characterization of a novel ribonucleoprotein particle: Large structures contain a single species of small RNA. *J. Cell Boil.* **1986**, *103*, 699–709. [CrossRef]
11. Van Zon, A.; Mossink, M.H.; Scheper, R.J.; Sonneveld, P.; Wiemer, E.A.C. The vault complex. *Cell. Mol. Life Sci.* **2003**, *60*, 1828–1837. [CrossRef]
12. Lee, K.; Kunkeaw, N.; Jeon, S.H.; Lee, I.; Johnson, B.H.; Kang, G.-Y.; Bang, J.Y.; Park, H.S.; Leelayuwat, C.; Lee, Y.S. Precursor miR-886, a novel noncoding RNA repressed in cancer, associates with PKR and modulates its activity. *RNA* **2011**, *17*, 1076–1089. [CrossRef]
13. Jeon, S.H.; Johnson, B.H.; Lee, Y.S. A Tumor Surveillance Model: A Non-Coding RNA Senses Neoplastic Cells and Its Protein Partner Signals Cell Death. *Int. J. Mol. Sci.* **2012**, *13*, 13134–13139. [CrossRef]
14. Jeon, S.H.; Lee, K.; Lee, K.S.; Kunkeaw, N.; Johnson, B.H.; Holthauzen, L.M.F.; Gong, B.; Leelayuwat, C.; Lee, Y.S. Characterization of the direct physical interaction of nc886, a cellular non-coding RNA, and PKR. *FEBS Lett.* **2012**, *586*, 3477–3484. [CrossRef]
15. Golec, E.; Lind, L.; Qayyum, M.; Blom, A.M.; King, B.C. The Noncoding RNA nc886 Regulates PKR Signaling and Cytokine Production in Human Cells. *J. Immunol.* **2019**, *202*, 131–141. [CrossRef]
16. Fort, R.S.; Mathó, C.; Geraldo, M.V.; Ottati, M.C.; Yamashita, A.S.; Saito, K.C.; Leite, K.R.M.; Méndez, M.; Maedo, N.; Méndez, L.; et al. Nc886 is epigenetically repressed in prostate cancer and acts as a tumor suppressor through the inhibition of cell growth. *BMC Cancer* **2018**, *18*, 127. [CrossRef]
17. Cloonan, N.; Wani, S.; Xu, Q.; Gu, J.; Lea, K.; Heater, S.; Barbacioru, C.; Steptoe, A.L.; Martin, H.C.; Nourbakhsh, E.; et al. MicroRNAs and their isomiRs function cooperatively to target common biological pathways. *Genome Boil.* **2011**, *12*, R126. [CrossRef]
18. Treppendahl, M.B.; Qiu, X.; Søgaard, A.; Yang, X.; Nandrup-Bus, C.; Hother, C.; Andersen, M.K.; Kjeldsen, L.; Möllgaard, L.; Hellström-Lindberg, E.; et al. Allelic methylation levels of the noncoding VTRNA2-1 located on chromosome 5q31.1 predict outcome in AML. *Blood* **2012**, *119*, 206–216. [CrossRef]
19. Miñones-Moyano, E.; Friedländer, M.R.; Pallares, J.; Kagerbauer, B.; Porta, S.; Escaramís, G.; Ferrer, I.; Estivill, X.; Marti, E. Upregulation of a small vault RNA (svtRNA2-1a) is an early event in Parkinson disease and induces neuronal dysfunction. *RNA Boil.* **2013**, *10*, 1093–1106. [CrossRef]
20. Jung, K.; Fendler, A.; Stephan, C.; Honey, R.J.; Stewart, R.J.; Pace, K.T.; Erbersdobler, A.; Samaan, S.; Yousef, G.M. miRNAs can predict prostate cancer biochemical relapse and are involved in tumor progression. *Int. J. Oncol.* **2011**, *39*, 1183–1192. [CrossRef]
21. Nordentoft, I.K.; Birkenkamp-Demtroder, K.; Agerbæk, M.; Theodorescu, D.; Ostenfeld, M.S.; Hartmann, A.; Borre, M.; Ørntoft, T.F.; Dyrskjøt, L. miRNAs associated with chemo-sensitivity in cell lines and in advanced bladder cancer. *BMC Med. Genom.* **2012**, *5*, 40. [CrossRef]
22. Tahiri, A.; Leivonen, S.K.; Lüders, T.; Steinfeld, I.; Aure, M.R.; Geisler, J.; Mäkelä, R.; Nord, S.; Riis, M.L.H.; Yakhini, Z.; et al. Deregulation of cancer-related miRNAs is a common event in both benign and malignant human breast tumors. *Carcinogenesis* **2014**, *35*, 76–85. [CrossRef] [PubMed]
23. Yu, X.-F.; Zou, J.; Bao, Z.-J.; Dong, J. miR-93 suppresses proliferation and colony formation of human colon cancer stem cells. *World J. Gastroenterol.* **2011**, *17*, 4711–4717. [CrossRef]
24. Gao, W.; Shen, H.; Liu, L.; Xu, J.; Xu, J.; Shu, Y. MiR-21 overexpression in human primary squamous cell lung carcinoma is associated with poor patient prognosis. *J. Cancer Res. Clin. Oncol.* **2011**, *137*, 557–566. [CrossRef]

25. Cao, J.; Song, Y.; Bi, N.; Shen, J.; Liu, W.; Fan, J.; Sun, G.; Tong, T.; He, J.; Shi, Y.; et al. DNA Methylation-Mediated Repression of miR-886-3p Predicts Poor Outcome of Human Small Cell Lung Cancer. *Cancer Res.* **2013**, *73*, 3326–3335. [CrossRef]
26. Bi, N.; Cao, J.; Song, Y.; Shen, J.; Liu, W.; Fan, J.; He, J.; Shi, Y.; Zhang, X.; Lu, N.; et al. A MicroRNA Signature Predicts Survival in Early Stage Small-Cell Lung Cancer Treated with Surgery and Adjuvant Chemotherapy. *PLoS ONE* **2014**, *9*, e91388. [CrossRef]
27. Shen, J.; Zhou, W.; Bi, N.; Song, Y.-M.; Zhang, F.-Q.; Zhan, Q.-M.; Wang, L.-H. MicroRNA-886-3P functions as a tumor suppressor in small cell lung cancer. *Cancer Boil. Ther.* **2018**, *19*, 1185–1192. [CrossRef]
28. Xiong, Y.; Zhang, L.; Holloway, A.K.; Wu, X.; Su, L.; Kebebew, E. MiR-886-3p Regulates Cell Proliferation and Migration, and Is Dysregulated in Familial Non-Medullary Thyroid Cancer. *PLoS ONE* **2011**, *6*, e24717. [CrossRef]
29. Dettmer, M.S.; Perren, A.; Moch, H.; Komminoth, P.; Nikiforov, Y.E.; Nikiforova, M.N. MicroRNA profile of poorly differentiated thyroid carcinomas: New diagnostic and prognostic insights. *J. Mol. Endocrinol.* **2014**, *52*, 181–189. [CrossRef]
30. Pillai, M.M.; Yang, X.; Balakrishnan, I.; Bemis, L.; Torok-Storb, B. MiR-886-3p Down Regulates CXCL12 (SDF1) Expression in Human Marrow Stromal Cells. *PLoS ONE* **2010**, *5*, e14304. [CrossRef]
31. Mahishi, L.H.; Hart, R.P.; Lynch, D.R.; Ratan, R.R. miR-886-3p levels are elevated in Friedreich ataxia. *J. Neurosci.* **2012**, *32*, 9369–9373. [CrossRef]
32. McDonald, A.C.; Vira, M.; Walter, V.; Shen, J.; Raman, J.D.; Sanda, M.G.; Patil, D.; Taioli, E. Circulating microRNAs in plasma among men with low-grade and high-grade prostate cancer at prostate biopsy. *Prostate* **2019**, *79*, 961–968. [CrossRef] [PubMed]
33. Yu, Z.; Chen, D.; Su, Z.; Li, Y.; Yu, W.; Zhang, Q.; Yang, L.; Li, C.; Yang, S.; Ni, L.; et al. miR-886-3p upregulation in clear cell renal cell carcinoma regulates cell migration, proliferation and apoptosis by targeting PITX1. *Int. J. Mol. Med.* **2014**, *34*, 1409–1416. [CrossRef] [PubMed]
34. Schou, J.V.; Rossi, S.; Jensen, B.V.; Nielsen, D.L.; Pfeiffer, P.; Høgdall, E.; Yilmaz, M.; Tejpar, S.; Delorenzi, M.; Kruhøffer, M.; et al. miR-345 in Metastatic Colorectal Cancer: A Non-Invasive Biomarker for Clinical Outcome in Non-KRAS Mutant Patients Treated with 3rd Line Cetuximab and Irinotecan. *PLoS ONE* **2014**, *9*, e99886. [CrossRef]
35. Okumura, T.; Kojima, H.; Miwa, T.; Sekine, S.; Hashimoto, I.; Hojo, S.; Nagata, T.; Shimada, Y. The expression of microRNA 574-3p as a predictor of postoperative outcome in patients with esophageal squamous cell carcinoma. *World J. Surg. Oncol.* **2016**, *14*, 228. [CrossRef]
36. Kunkeaw, N.; Lee, Y.-S.; Im, W.R.; Jang, J.J.; Song, M.-J.; Yang, B.; Park, J.-L.; Kim, S.-Y.; Ku, Y.; Kim, Y.; et al. Mechanism mediated by a noncoding RNA, nc886, in the cytotoxicity of a DNA-reactive compound. *Proc. Natl. Acad. Sci. USA* **2019**, *116*, 8289–8294. [CrossRef]
37. Wyman, S.K.; Knouf, E.C.; Parkin, R.K.; Fritz, B.R.; Lin, D.W.; Dennis, L.M.; Krouse, M.A.; Webster, P.J.; Tewari, M. Post-transcriptional generation of miRNA variants by multiple nucleotidyl transferases contributes to miRNA transcriptome complexity. *Genome Res.* **2011**, *21*, 1450–1461. [CrossRef]
38. Marshall, E.A.; Sage, A.P.; Ng, K.W.; Martinez, V.D.; Firmino, N.S.; Bennewith, K.L.; Lam, W.L. Small non-coding RNA transcriptome of the NCI-60 cell line panel. *Sci. Data* **2017**, *4*, 170157. [CrossRef]
39. Takayama, K.-I.; Misawa, A.; Suzuki, T.; Takagi, K.; Hayashizaki, Y.; Fujimura, T.; Homma, Y.; Takahashi, S.; Urano, T.; Inoue, S. TET2 repression by androgen hormone regulates global hydroxymethylation status and prostate cancer progression. *Nat. Commun.* **2015**, *6*, 8219. [CrossRef]
40. Kodama, Y.; Shumway, M.; Leinonen, R. International Nucleotide Sequence Database Collaboration The Sequence Read Archive: Explosive growth of sequencing data. *Nucleic Acids Res.* **2011**, *40*, D54–D56. [CrossRef]
41. Clough, E.; Barrett, T. The Gene Expression Omnibus Database. In *Breast Cancer*; Springer Science and Business Media LLC: New York, NY, USA, 2016; Volume 1418, pp. 93–110.
42. Berezikov, E.; Robine, N.; Samsonova, A.; Westholm, J.O.; Naqvi, A.; Hung, J.H.; Okamura, K.; Dai, Q.; Bortolamiol-Becet, D.; Martin, R.; et al. Deep annotation of Drosophila melanogaster microRNAs yields insights into their processing, modification, and emergence. *Genome Res.* **2011**, *21*, 203–215. [CrossRef]
43. Park, J.-E.; Heo, I.; Tian, Y.; Simanshu, D.K.; Chang, H.; Jee, D.; Patel, D.J.; Kim, V.N. Dicer recognizes the 5′ end of RNA for efficient and accurate processing. *Nature* **2011**, *475*, 201–205. [CrossRef] [PubMed]

44. Bellaousov, S.; Reuter, J.S.; Seetin, M.G.; Mathews, D.H. RNAstructure: Web servers for RNA secondary structure prediction and analysis. *Nucleic Acids Res.* **2013**, *41*, W471–W474. [CrossRef] [PubMed]
45. Calderon, B.M.; Conn, G.L. Human noncoding RNA 886 (nc886) adopts two structurally distinct conformers that are functionally opposing regulators of PKR. *RNA* **2017**, *23*, 557–566. [PubMed]
46. Calderon, B.M.; Conn, G.L. A human cellular noncoding RNA activates the antiviral protein 2′–5′-oligoadenylate synthetase 1. *J. Boil. Chem.* **2018**, *293*, 16115–16124. [CrossRef]
47. Starega-Roslan, J.; Koscianska, E.; Kozlowski, P.; Krzyzosiak, W.J. The role of the precursor structure in the biogenesis of microRNA. *Cell. Mol. Life Sci.* **2011**, *68*, 2859–2871. [CrossRef] [PubMed]
48. Finnegan, E.F.; Pasquinelli, A.E. MicroRNA biogenesis: Regulating the regulators. *Crit. Rev. Biochem. Mol. Biol.* **2013**, *48*, 51–68. [CrossRef]
49. Kim, V.N.; Han, J.; Siomi, M.C. Biogenesis of small RNAs in animals. *Nat. Rev. Mol. Cell Boil.* **2009**, *10*, 126–139. [CrossRef]
50. Hamilton, M.P.; Rajapakshe, K.I.; Bader, D.A.; Cerne, J.Z.; Smith, E.A.; Coarfa, C.; Hartig, S.M.; McGuire, S.E. The Landscape of microRNA Targeting in Prostate Cancer Defined by AGO-PAR-CLIP. *Neoplasia* **2016**, *18*, 356–370. [CrossRef]
51. Kim, Y.-K.; Kim, B.; Kim, V.N. Re-evaluation of the roles of DROSHA, Export in 5, and DICER in microRNA biogenesis. *Proc. Natl. Acad. Sci. USA* **2016**, *113*, E1881–E1889. [CrossRef]
52. Chen, C.-J.; Heard, E. Small RNAs derived from structural non-coding RNAs. *Methods* **2013**, *63*, 76–84. [CrossRef]
53. Van Dongen, S.; Abreu-Goodger, C.; Enright, A.J. Detecting microRNA binding and siRNA off-target effects from expression data. *Nat. Methods* **2008**, *5*, 1023–1025. [CrossRef] [PubMed]
54. Subramanian, A.; Tamayo, P.; Mootha, V.K.; Mukherjee, S.; Ebert, B.L.; Gillette, M.A.; Paulovich, A.; Pomeroy, S.L.; Golub, T.R.; Lander, E.S.; et al. Gene set enrichment analysis: A knowledge-based approach for interpreting genome-wide expression profiles. *Proc. Natl. Acad. Sci. USA* **2005**, *102*, 15545–15550. [CrossRef]
55. Mahadevappa, R.; Neves, H.; Yuen, S.M.; Bai, Y.; McCrudden, C.M.; Yuen, H.F.; Wen, Q.; Zhang, S.D.; Kwok, H.F. The prognostic significance of Cdc6 and Cdt1 in breast cancer. *Sci. Rep.* **2017**, *7*, 985. [CrossRef]
56. Li, C.; Zhou, X.; Wang, Y.; Jing, S.; Yang, C.; Sun, G.; Liu, Q.; Cheng, Y.; Wang, L. miR-210 regulates esophageal cancer cell proliferation by inducing G2/M phase cell cycle arrest through targeting PLK1. *Mol. Med. Rep.* **2014**, *10*, 2099–2104. [CrossRef] [PubMed]
57. Tang, Z.; Kang, B.; Li, C.; Chen, T.; Zhang, Z. GEPIA2: An enhanced web server for large-scale expression profiling and interactive analysis. *Nucleic Acids Res.* **2019**, *47*, W556–W560. [CrossRef] [PubMed]
58. Shaoqing, Y.; Ruxin, Z.; Guojun, L.; Zhiqiang, Y.; Hua, H.; Shudong, Y.; Jie, Z. Microarray Analysis of Differentially Expressed microRNAs in Allergic Rhinitis. *Am. J. Rhinol. Allergy* **2011**, *25*, e242–e246. [CrossRef] [PubMed]
59. Amort, M.; Nachbauer, B.; Tuzlak, S.; Kieser, A.; Schepers, A.; Villunger, A.; Polacek, N. Expression of the vault RNA protects cells from undergoing apoptosis. *Nat. Commun.* **2015**, *6*, 7030. [CrossRef]
60. Persson, H.; Kvist, A.; Vallon-Christersson, J.; Medstrand, P.; Borg, A.; Rovira, C. The non-coding RNA of the multidrug resistance-linked vault particle encodes multiple regulatory small RNAs. *Nature* **2009**, *11*, 1268–1271. [CrossRef]
61. Hussain, S.; Sajini, A.A.; Blanco, S.; Dietmann, S.; Lombard, P.; Sugimoto, Y.; Paramor, M.; Gleeson, J.G.; Odom, D.T.; Ule, J.; et al. NSun2-Mediated Cytosine-5 Methylation of Vault Noncoding RNA Determines Its Processing into Regulatory Small RNAs. *Cell Rep.* **2013**, *4*, 255–261. [CrossRef]
62. Vermeulen, A.; Behlen, L.; Reynolds, A.; Wolfson, A.; Marshall, W.S.; Karpilow, J.; Khvorova, A. The contributions of dsRNA structure to Dicer specificity and efficiency. *RNA* **2005**, *11*, 674–682. [CrossRef]
63. Starega-Roslan, J.; Krol, J.; Koscianska, E.; Kozlowski, P.; Szlachcic, W.J.; Sobczak, K.; Krzyzosiak, W.J. Structural basis of microRNA length variety. *Nucleic Acids Res.* **2011**, *39*, 257–268. [CrossRef] [PubMed]
64. Fang, Z.; Du, R.; Edwards, A.; Flemington, E.K.; Zhang, K. The Sequence Structures of Human MicroRNA Molecules and Their Implications. *PLoS ONE* **2013**, *8*, e54215. [CrossRef] [PubMed]
65. Berezikov, E. Evolution of microRNA diversity and regulation in animals. *Nat. Rev. Genet.* **2011**, *12*, 846–860. [CrossRef] [PubMed]
66. Kong, L.; Hao, Q.; Wang, Y.; Zhou, P.; Zou, B.; Zhang, Y.-X. Regulation of p53 expression and apoptosis by vault RNA2-1-5p in cervical cancer cells. *Oncotarget* **2015**, *6*, 28371–28388. [CrossRef] [PubMed]

67. Li, J.-H.; Xiao, X.; Zhang, Y.-N.; Wang, Y.-M.; Feng, L.-M.; Wu, Y.-M.; Zhang, Y.-X. MicroRNA miR-886-5p inhibits apoptosis by down-regulating Bax expression in human cervical carcinoma cells. *Gynecol. Oncol.* **2011**, *120*, 145–151. [CrossRef] [PubMed]
68. Zhang, L.-L.; Wu, J.; Liu, Q.; Zhang, Y.; Sun, Z.-L.; Jing, H. MiR-886-5p inhibition inhibits growth and induces apoptosis of MCF7 cells. *Asian Pac. J. Cancer Prev.* **2014**, *15*, 1511–1515. [CrossRef]
69. Gao, Q.Q.; Putzbach, W.E.; Murmann, A.E.; Chen, S.; Sarshad, A.A.; Peter, J.M.; Bartom, E.T.; Hafner, M.; Peter, M.E. 6mer seed toxicity in tumor suppressive microRNAs. *Nat. Commun.* **2018**, *9*, 4504. [CrossRef]
70. Aakula, A.; Kohonen, P.; Leivonen, S.K.; Mäkelä, R.; Hintsanen, P.; Mpindi, J.P.; Martens-Uzunova, E.; Aittokallio, T.; Jenster, G.; Perälä, M.; et al. Systematic Identification of MicroRNAs That Impact on Proliferation of Prostate Cancer Cells and Display Changed Expression in Tumor Tissue. *Eur. Urol.* **2015**, *69*, 1120–1128. [CrossRef]
71. Lee, K.-S.; Park, J.-L.; Lee, K.; Richardson, L.E.; Johnson, B.H.; Lee, H.-S.; Lee, J.-S.; Kim, S.-B.; Kwon, O.-H.; Song, K.S.; et al. nc886, a non-coding RNA of anti-proliferative role, is suppressed by CpG DNA methylation in human gastric cancer. *Oncotarget* **2014**, *5*, 3944–3955. [CrossRef]
72. Lee, H.-S.; Lee, K.; Jang, H.-J.; Lee, G.K.; Park, J.-L.; Kim, S.-Y.; Kim, S.-B.; Johnson, B.H.; Zo, J.I.; Lee, J.-S.; et al. Epigenetic silencing of the non-coding RNA nc886 provokes oncogenes during human esophageal tumorigenesis. *Oncotarget* **2014**, *5*, 3472–3481. [CrossRef]
73. Kunkeaw, N.; Jeon, S.H.; Lee, K.; Johnson, B.H.; Tanasanvimon, S.; Javle, M.; Pairojkul, C.; Chamgramol, Y.; Wongfieng, W.; Gong, B.; et al. Cell death/proliferation roles for nc886, a non-coding RNA, in the protein kinase R pathway in cholangiocarcinoma. *Oncogene* **2012**, *32*, 3722–3731. [CrossRef] [PubMed]
74. Ahn, J.-H.; Lee, H.-S.; Lee, J.-S.; Lee, Y.-S.; Park, J.-L.; Kim, S.-Y.; Hwang, J.-A.; Kunkeaw, N.; Jung, S.Y.; Kim, T.J.; et al. nc886 is induced by TGF-β and suppresses the microRNA pathway in ovarian cancer. *Nat. Commun.* **2018**, *9*, 1166. [CrossRef] [PubMed]
75. Lee, E.K.; Hong, S.-H.; Shin, S.; Lee, H.-S.; Lee, J.-S.; Park, E.J.; Choi, S.S.; Min, J.W.; Park, D.; Hwang, J.-A.; et al. nc886, a non-coding RNA and suppressor of PKR, exerts an oncogenic function in thyroid cancer. *Oncotarget* **2016**, *7*, 75000–75012. [CrossRef] [PubMed]
76. Hu, Z.; Zhang, H.; Tang, L.; Lou, M.; Geng, Y. Silencing nc886, a Non-Coding RNA, Induces Apoptosis of Human Endometrial Cancer Cells-1A In Vitro. *Med. Sci. Monit.* **2017**, *23*, 1317–1324. [CrossRef]
77. Xi, X.; Li, T.; Huang, Y.; Sun, J.; Zhu, Y.; Yang, Y.; Lu, Z.J. RNA Biomarkers: Frontier of Precision Medicine for Cancer. *Non-Coding RNA* **2017**, *3*, 9. [CrossRef]
78. Xiang, P.; Liu, Y.; Liu, L.; Lin, Q.; Liu, X.; Zhang, H.; Xu, J.; Fang, B. The Biological Function and Clinical Significance of miR-886-5p in Multiple Myeloma. *Acta Haematol.* **2019**, *142*, 208–216. [CrossRef]
79. Perfetti, A.; Greco, S.; Bugiardini, E.; Cardani, R.; Gaia, P.; Gaetano, C.; Meola, G.; Martelli, F. Plasma microRNAs as biomarkers for myotonic dystrophy type 1. *Neuromuscul. Disord.* **2014**, *24*, 509–515. [CrossRef]
80. Arroyo, J.D.; Chevillet, J.R.; Kroh, E.M.; Ruf, I.K.; Pritchard, C.C.; Gibson, D.F.; Mitchell, P.S.; Bennett, C.F.; Pogosova-Agadjanyan, E.L.; Stirewalt, D.L.; et al. Argonaute2 complexes carry a population of circulating microRNAs independent of vesicles in human plasma. *Proc. Natl. Acad. Sci. USA* **2011**, *108*, 5003–5008. [CrossRef]
81. Tosar, J.P.; Gámbaro, F.; Sanguinetti, J.; Bonilla, B.; Witwer, K.W.; Cayota, A. Assessment of small RNA sorting into different extracellular fractions revealed by high-throughput sequencing of breast cell lines. *Nucleic Acids Res.* **2015**, *43*, 5601–5616. [CrossRef]
82. Van Balkom, B.W.M.; Eisele, A.S.; Pegtel, D.M.; Bervoets, S.; Verhaar, M.C. Quantitative and qualitative analysis of small RNAs in human endothelial cells and exosomes provides insights into localized RNA processing, degradation and sorting. *J. Extracell. Vesicles* **2015**, *4*, 26760. [CrossRef]
83. Nolte'T Hoen, E.N.M.; Buermans, H.P.J.; Waasdorp, M.; Stoorvogel, W.; Wauben, M.H.M.; Hoen, P.A.C. 'T Deep sequencing of RNA from immune cell-derived vesicles uncovers the selective incorporation of small non-coding RNA biotypes with potential regulatory functions. *Nucleic Acids Res.* **2012**, *40*, 9272–9285. [CrossRef] [PubMed]
84. Lunavat, T.R.; Cheng, L.; Kim, D.-K.; Bhadury, J.; Jang, S.C.; Lässer, C.; Sharples, R.A.; López, M.D.; Nilsson, J.; Gho, Y.S.; et al. Small RNA deep sequencing discriminates subsets of extracellular vesicles released by melanoma cells—Evidence of unique microRNA cargos. *RNA Boil.* **2015**, *12*, 810–823. [CrossRef] [PubMed]

85. Li, C.C.Y.; Eaton, S.A.; Young, P.E.; Lee, M.; Shuttleworth, R.; Humphreys, D.T.; Grau, G.E.; Combes, V.; Bebawy, M.; Gong, J.; et al. Glioma microvesicles carry selectively packaged coding and non-coding RNAs which alter gene expression in recipient cells. *RNA Boil.* **2013**, *10*, 1333–1344. [CrossRef]
86. Dugué, P.-A.; Dowty, J.G.; Joo, J.E.; Wong, E.M.; Makalic, E.; Schmidt, D.F.; English, D.R.; Hopper, J.L.; Pedersen, J.; Severi, G.; et al. Heritable methylation marks associated with breast and prostate cancer risk. *Prostate* **2018**, *78*, 962–969. [CrossRef] [PubMed]
87. Livak, K.J.; Schmittgen, T.D. Analysis of relative gene expression data using real-time quantitative PCR and the 2−ΔΔC*T* method. *Methods* **2001**, *25*, 402–408. [CrossRef] [PubMed]
88. Kallio, M.A.; Tuimala, J.T.; Hupponen, T.; Klemelä, P.; Gentile, M.; Scheinin, I.; Koski, M.; Käki, J.; Korpelainen, E.I. Chipster: User-friendly analysis software for microarray and other high-throughput data. *BMC Genom.* **2011**, *12*, 507. [CrossRef]
89. Irizarry, R.A.; Hobbs, B.; Collin, F.; Beazer-Barclay, Y.D.; Antonellis, K.J.; Scherf, U.; Speed, T.P. Exploration, normalization, and summaries of high density oligonucleotide array probe level data. *Biostatistics* **2003**, *4*, 249–264. [CrossRef]
90. Davis, S.; Meltzer, P.S. GEOquery: A bridge between the Gene Expression Omnibus (GEO) and BioConductor. *Bioinformatics* **2007**, *23*, 1846–1847. [CrossRef]
91. Mayr, C.; Bartel, D.P. Widespread Shortening of 3'UTRs by Alternative Cleavage and Polyadenylation Activates Oncogenes in Cancer Cells. *Cell* **2009**, *138*, 673–684. [CrossRef]
92. Benhamed, M.; Herbig, U.; Ye, T.; Dejean, A.; Bischof, O. Senescence is an endogenous trigger for microRNA-directed transcriptional gene silencing in human cells. *Nature* **2012**, *14*, 266–275. [CrossRef]
93. Friedländer, M.R.; Mackowiak, S.D.; Li, N.; Chen, W.; Rajewsky, N. miRDeep2 accurately identifies known and hundreds of novel microRNA genes in seven animal clades. *Nucleic Acids Res.* **2012**, *40*, 37–52. [CrossRef] [PubMed]
94. Martin, M. Cutadapt removes adapter sequences from high-throughput sequencing reads. *EMBnet J.* **2011**, *17*, 10. [CrossRef]
95. Langmead, B.; Salzberg, S.L. Fast gapped-read alignment with Bowtie 2. *Nat. Methods* **2012**, *9*, 357–359. [CrossRef] [PubMed]
96. Anders, S.; Pyl, P.T.; Huber, W. HTSeq-A Python framework to work with high-throughput sequencing data. *Bioinformatics* **2015**, *31*, 166–169. [CrossRef]
97. Iorio, F.; Knijnenburg, T.A.; Vis, D.J.; Bignell, G.R.; Menden, M.P.; Schubert, M.; Aben, N.; Gonçalves, E.; Barthorpe, S.; Lightfoot, H.; et al. A Landscape of Pharmacogenomic Interactions in Cancer. *Cell* **2016**, *166*, 740–754. [CrossRef] [PubMed]

non-coding RNA

MDPI

Article

Supplementary Figures.

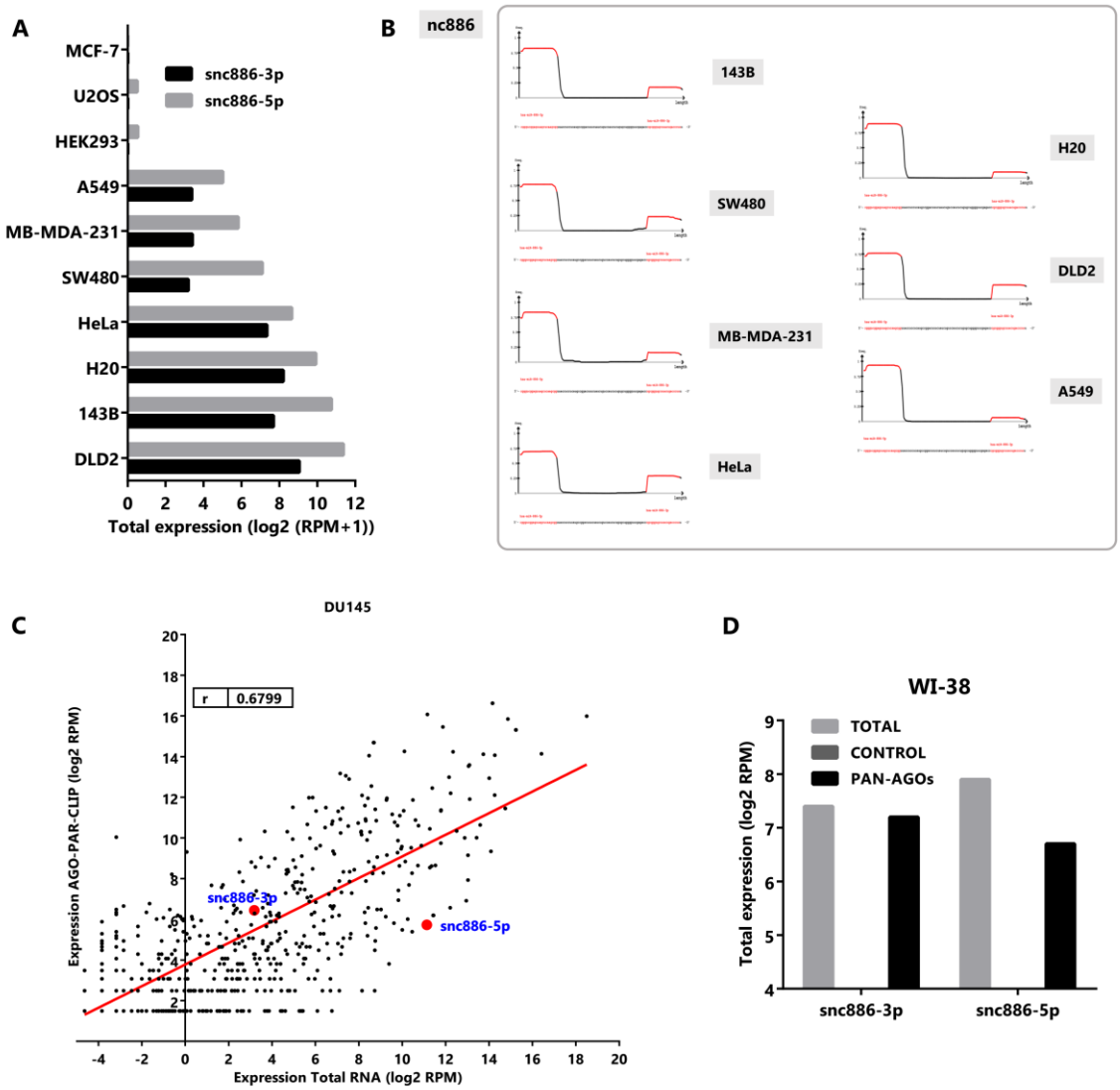

Figure S1. nc886 derived fragments are produced in non-prostate cell lines and exhibit microRNA features. (**a**). Normalized expression of snc886-3p (black) and 5p (gray) assessed in transcriptomic studies of small non-coding RNAs of different human cell lines. Dataset available at GEO id: GSE16579 (same used in part (**b**)). (**b**). Mapping profile of small non-coding RNAs along the nc886 sequence based on previous study. (**c**). Normalized expression of small non-coding RNAs in total cellular DU145 (TOTAL DU145) and in PAR-CLIP Argonaute RNA fraction (AGO DU145). The red dots highlight the snc886-3p and snc886-5p values in the scatterplot. Data set available at SRA id: SRP075075. (**d**). The normalized expression of snc886-3p (black) and snc886-5p (gray) in total and AGO-immunoprecipitate of WI-38 cell line. Data set available in GEO id: GSE34494.

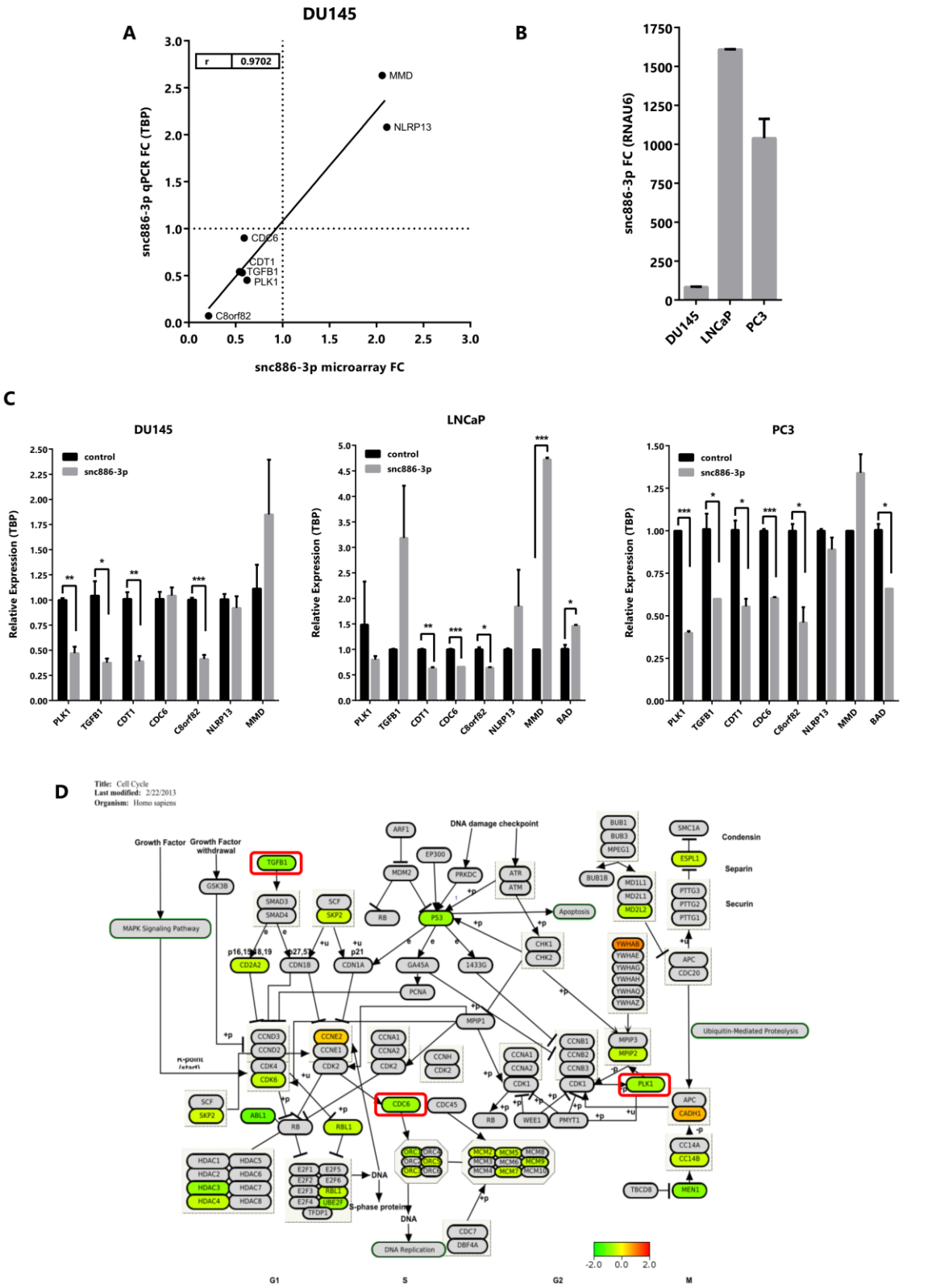

Figure S2. Candidate target gene expression of snc886-3p in DU145, LNCaP and DU145 (**a**). Correlation between the expression of the indicated genes caused by the overexpression of snc886-3p assessed by microarray (log2 of normalized fluorescence) and qRT-PCR (ΔCt using TBP expression as a control) in DU145 cell line. The fold change (FC) between snc886-3p mimic and control mimic is plotted. Pearson R correlation value is presented. (**b**). Expression of snc886-3p after transfection in DU145, LNCaP and PC3 with transfected with 20nM of mimic snc886-3p and negative control (Dharmacon), assessed by qRT-PCR (RNAU6 used as an internal control). (**c**). Effect of snc886-3p

overexpression on 5 selected candidate direct target genes (PLK1, TGFB1, CDT1, CDC6, C8orf82) and two control genes (NLRP13 and MMD lacking site for snc886-3p and identified as DEG in DU145 array). Expression was assessed by qRT-PCR and fold change between mimic (snc886-3p) and negative control (Dharmacon) transfection in DU145, LNCaP and PC3 cell lines using TBP as a normalizer is shown. Triplicated transfections and triplicated quantifications were analyzed for each cell line; T-Test was performed, * P-value <0.05, ** P-value <0.01, *** P-value <0.001. (**d**). The DEGs modulated after the overexpression of snc886-3p identified by microarrays (fold change > 1.25 and < -1.25) are colored in green (downregulated) or red (upregulated) over a KEGG cell cycle pathway flowchart.

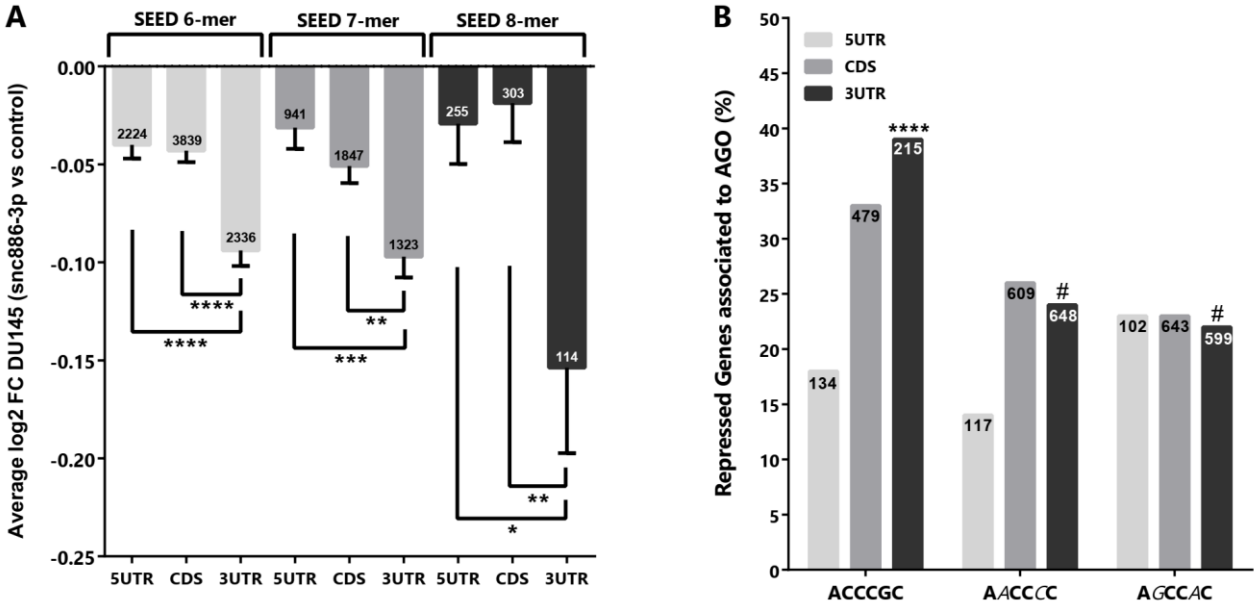

Figure S3. Analysis of snc886-3p microRNA-like target activity in DU145 cell line. DU145 cells were transfected with 20nM of mimic snc886-3p and negative control (Dharmacon) and cultured 48hrs. Total RNA was extracted for Affymetrix microarray global gene expression analysis. (a) Average change in the expression of all genes bearing a nucleotide motif complementary to the snc886-3p seed (5′ACCCGC3′) detected by the microarray. Seed binding site of 6-8-mer (2-7nt 5′ACCCGC3′, 2-8nt 5′cACCCGC3′, 1-8nt 5′cACCCGCg3′) were evaluated. One-way ANOVA test was used to estimate the statistical significance of the differences. (b) Percentage of genes bearing a motif complementary to the 6-mer snc886-3p seed that are downregulated in snc886-3p DU145 transfectants and present reads with this sequence motif in the AGO-bound fraction identified by PAR-CLIP experiments in DU145 cell line (Data set available at SRA id: SRP075075). The location of the motif at the 5′UTR, CDS or 3′UTR is discriminated and the number of genes in each group is shown inside the bars. Two motifs differing in 2 bases from the snc886-3p binding site were used as controls (5′A*A*CCCC3′ and 5′AGCC*A*C3′, differing in position 2 and 6 of the 6-mer scn886-3p 6-mer seed). They were verified to be not complementary to any known human microRNA binding site. Fisher's exact test for the category "3′UTR" of 5′ACCCGC3′ yield significant different proportions for the "3′UTR" marked with # (P-value <0.0001 and Odds Ratio of 2.0 and 2.2 for 5′A*A*CCCC3′ and 5′AGCC*A*C3′ respectively).

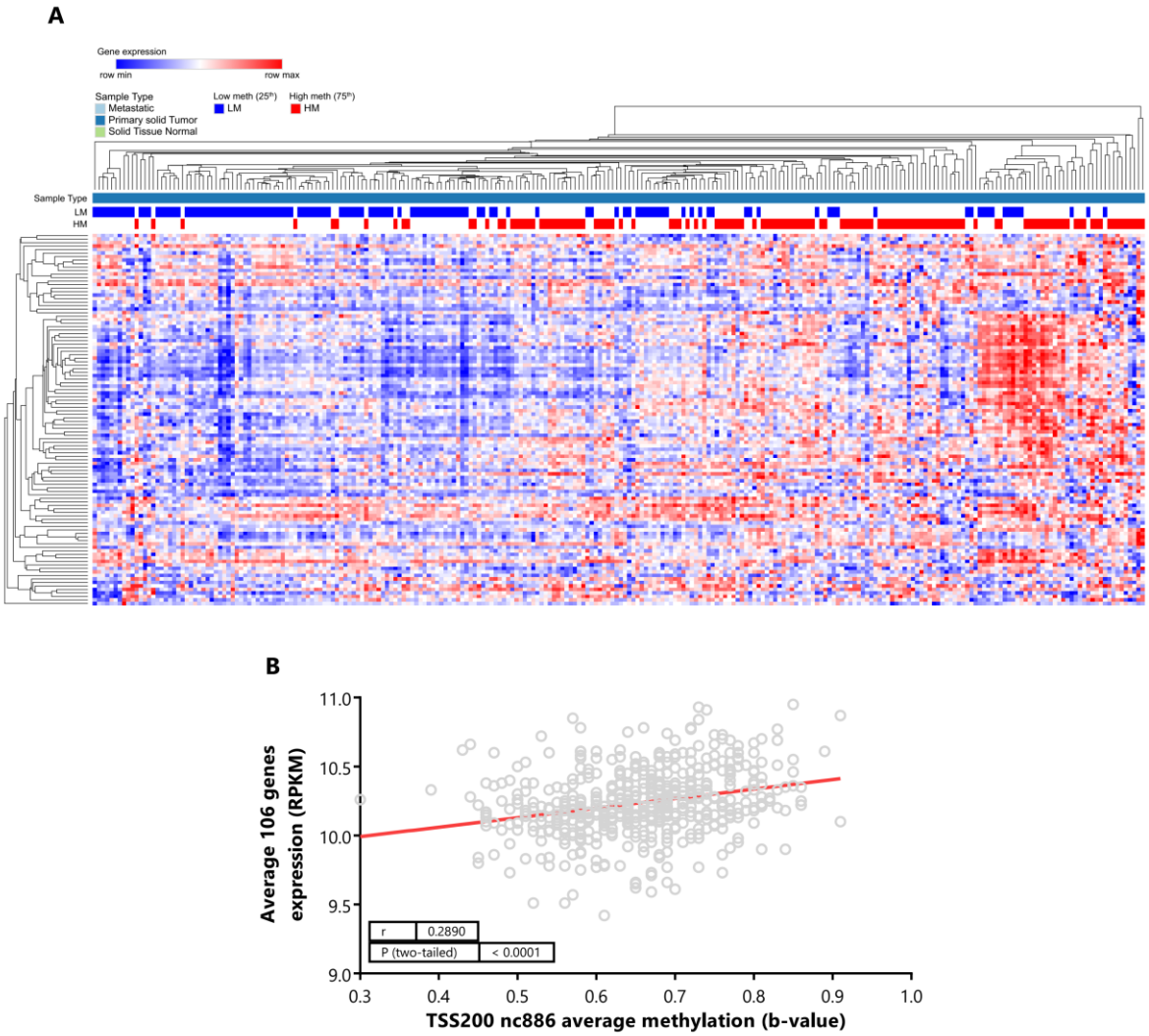

Figure S4. High expression of 106-snc886-3p direct targets correlates with nc886 promoter methylation in prostate tissue of PRAD-TCGA. (**a**). Heatmap of the expression of the genes of 106 direct candidate target genes of snc886-3p generated using the Spearman rank correlation algorithm clusterization with the Morpheus software and PRAD-TCGA data. The horizontal bars above the heatmap indicate the sample type and the methylation status of the nc886 TSS200nt: Percentile 25th (low methylation - high expression nc886: blue box LM) and 75th (high methylation - low expression nc886: red boxes HM). (**b**). Correlation between nc886 TSS200nt methylation and 106 snc886-3p direct candidate target gene expression in the TCGA-PRAD. Spearman R correlation and p-value are indicated.

III. SNC886-5P EL PEQUEÑO ARN NO CODIFICANTE DERIVADO DEL EXTREMO 5' DE VTRNA2-1/NC886 Y SU EXPRESIÓN EN ADENOCARCINOMA DE PRÓSTATA.

***Objetivo específico 2.2.5*:**

Para continuar profundizando en la comprensión del efecto de la desregulación de vtRNA2-1/nc886 en el PrCa y considerando los antecedentes presentados en ***Resultados y discusión I y II***, surge el *objetivo específico 2.2.5*. Los antecedentes de la literatura y nuestros resultados previos en células de próstata, exponen que vtRNA2-1/nc886 no solo es precursor de hsa-miR-886-3p/snc886-3p, sino que también origina un pequeño ARN no codificante del extremo 5', el hsa-miR-886-5p/snc886-5p. Más aún, nuestros análisis en líneas celulares mostraron que este último esta aumentado en el tumor, en contraste con la disminución de su análogo originado del extremo 3'. Por estos motivos, buscamos estudiar si el perfil de expresión de hsa-miR-886-5p/snc886-5p también se observaba en muestras de pacientes, para lo que realizamos el re-análisis de datos de transcriptómica de sncARNs en muestras de tejido tumoral y normal adyacente de próstata (PRAD-TCGA), así como su asociación con parámetros clínicos de la enfermedad (*objetivo específico 2.2.5*). Adicionalmente, evaluamos la expresión global de hsa-miR-886-3p/snc886-3p y hsa-miR-886-5p/snc886-5p en células normales y tumorales, en datos de transcriptómica de sncARNs disponibles en repositorios de datos públicos (SRA).

El conjunto de estos análisis nos permitió determinar la expresión de hsa-miR-886-5p/snc886-5p en el PrCa y su asociación con parámetros clínicos de la enfermedad. Asimismo, estudiamos la expresión de hsa-miR-886-3p/snc886-3p y hsa-miR-886-5p/snc886-5p en células tumorales y normales de diversos tejidos. Los resultados sugieren la posibilidad de que vtRNA2-1/nc886 sea blanco del fenómeno de procesamiento diferencial de brazos "arm switching" en la carcinogénesis. Dado que no hay muchos ejemplos descritos de un ARN que tenga un efecto como transcrito completo y origine productos más pequeños cuyos niveles cambien en forma opuesta y que provoquen efectos diferentes y opuestos en la carcinogénesis, nos pareció relevante dejar estas observaciones. Las mismas forjan la hipótesis de que hsa-miR-886-5p/snc886-5p podría actuar como oncogén, tal vez adicionando impacto a la supresión de vtRNA2-1/nc886 por metilación en la carcinogénesis y la disminución de hsa-miR-886-3p/snc886-3p, constituyendo así un antecedente interesante para una investigación futura.

Análisis de la expresión de hsa-miR-886-5p/snc886-5p en la carcinogénesis prostática y su asociación con la enfermedad.

INTRODUCCION

En nuestro trabajo previo, donde mostramos la formación de snc886-3p/hsa-miR-886-3p a partir de vtRNA2-1/nc886, también observamos la presencia de pequeños ARN con la secuencia específica de snc886-5p/hsa-miR-886-5p en tejido prostático, siendo los fragmentos predominantes derivados del precursor (Fort et al., 2020) Figura 1. Asimismo, notamos que en líneas celulares tumorales de próstata (DU145, PC-3 y LNCaP) aumentaba la expresión de snc886-5p en relación a la de líneas celulares no transformadas PrEc y PrSC, además de disminuir la de snc886-3p. Por otro lado, el estudio de la expresión de snc886-5p en células HCT116, mostró que los niveles de snc886-5p dependen de DICER pero son independientes DROSHA, al igual que ocurre para snc886-3p. Sin embargo, el análisis de inmunoprecipitaciones de la proteína argonauta en la línea celular DU145 expuso que snc886-5p no se asocia tanto a argonauta como snc886-3p, lo que sugiere que pueda actuar en forma diferente a la de los microARNs.

Estos hallazgos nos llevaron a preguntarnos si snc886-5p estaría también diferencialmente expresado en los tumores prostáticos humanos y si ocurriría un cambio en la preferencia de brazos en el procesamiento del precursor vtRNA2-1/nc886 durante la transformación neoplásica. Un incremento de la expresión en tejido tumoral posiciona a snc886-5p como un potencial ARN oncogénico. Si esto fuera cierto la contribución de vtRNA2-1/nc886 podría ocurrir a 3 niveles, en primer lugar, la acción supresora de tumor del vtRNA2-1/nc886, probablemente por la interacción directa con proteínas, en segundo lugar, la acción supresora de tumor de snc886-3p actuando como microARN y en tercer lugar, la acción oncogénica de snc886-5p, cuyo mecanismo podría ser otro, fenómeno que no ha sido descrito aún en la literatura para un vtRNA o un precursor de microARNs según nuestro conocimiento.

En este capítulo realizamos el análisis de la expresión de snc886-5p en la cohorte del PRAD-TCGA, que nos muestra que lo que observamos en forma preliminar en líneas celulares, efectivamente ocurre en los tumores prostáticos humanos y en múltiples líneas celulares de diversos orígenes tisulares. Es sugestivo además el hallazgo de que la expresión de snc886-5p se asocia con un mal pronóstico de la enfermedad, lo que nos lleva a preguntarnos si además funciona como un gen conductor de esta neoplasia y no sólo como un producto secundario del procesamiento de vtRNA2-1/nc886. Estos resultados apoyan la importancia de corroborar nuestra hipótesis en experimentos funcionales.

MATERIALES Y MÉTODOS.

Datos de transcriptómica de pequeños ARNs no codificantes.

Los re-análisis de expresión de microARNs de tejido tumoral y normal adyacente de próstata fueron realizados utilizando las muestras de pacientes del repositorio público "The Cancer Genome Atlas" (PRAD-TCGA), *miRNAseq data Level_2 Data* (archivos**.bam*), 546 muestras. Debido a que son datos de naturaleza restringida, porque contienen información de secuencia que puede permitir la identificación de los individuos, solicitamos el acceso a los datos al National Institute of Health de los Estados Unidos (NIH, National Cancer Institute (NCI-NIH), y al National Human Genome Institute (NHGRI-NIH), sometiendo un proyecto que fue aprobado oportunamente (Project #7307 : Study of cannonical and non-cannonical microRNAs expression and pathogenicity in Prostate Cancer, dbGAP 2015, PI: María Ana Duhagon, Institution: Facultad de Medicina). Adicionalmente, utilizamos sets de datos de transcriptómica de pequeños ARNs no codificantes disponibles en bases de datos públicas (Sequence Read Archive, SRA): líneas celulares humanas primarias normales (37 human normal primary cell lines, PRJNA358331 (McCall et al., 2017)) y celulares tumorales (59 NCI-60 human tumor cell lines, PRJNA390643 (Marshall et al., 2017)). Los datos de transcriptómica disponibles en SRA fueron descargados utilizando la herramienta *SRA toolkit* (https://github.com/ncbi/sra-tools).

Análisis de datos transcriptómicos de pequeños ARNs no codificantes.

Se realizó el recorte de adaptadores, el mapeo, la anotación y el conteo de los microARNs utilizando el programa miRDeep2 (algoritmos: mapper.pl y quantifier.pl), como se hizo previamente en Fort et al. (2020). Posteriormente, se realizó una normalización de los datos de las líneas celulares humanas primarias normales y tumorales, utilizando el método TMM (trimmed mean of M values (Robinson & Oshlack, 2010; Robinson et al., 2010)). Para el análisis de expresión diferencial, filtramos los microARNs de baja expresión, es decir, de bajo soporte estadístico, aplicando el algoritmo conducido por datos HTSFilter (Rau et al., 2013). Finalmente, para realizar el análisis de expresión diferencial de microARNs se utilizó el programa EdgeR (Robinson et al., 2010).

Análisis estadísticos.

Las variables se expresan como promedio y error estándar, o desvío estándar, y el test utilizado en cada caso se indica en los pies de las figuras. Aplicamos T-test de dos colas pareados (muestras pareadas tumor y normal adyacente) y no pareadas. Aplicamos Anova-test para ensayos de múltiples variables con la prueba de Tukey como *post-hoc*. Evaluamos la correlación entre dos variables mediante correlación de Spearman y aplicamos la regresión lineal de la curva para la evaluación de las pendientes de las curvas. Consideramos significativos aquellos

resultados con p-valor ≤ 0,05. Se utilizó el programa GraphPad Prism (https://www.graphpad.com/scientific-software/prism/) y paquetes estadísticos en R (https://www.r-project.org/about.html), EdgeR (Robinson et al., 2010) y HTSFilter (Rau et al., 2013).

RESULTADOS.

Buscando profundizar en el estudio del sncARN derivado del extremo 5' de vtRNA2-1/nc886 (hsa-miR-886-5p/snc886-5p), decidimos explorar su expresión en muestras de tejido de próstata. Para ello recurrimos a la mayor base de datos pública de transcriptómica de sncARNs de cáncer, que consiste en "The Cancer Genome Atlas" (TCGA). El set de datos de adenocarcinoma prostático (PRAD) presente en TCGA (PRAD-TCGA), cuenta con un total de 494 tumores prostáticos, de los cuales 52 tumores cuentan con muestras pareadas de tejido normal adyacente. Debido a que anteriormente hsa-mir-886 fue re-clasificado como vtRNA2-1, fue eliminado de miRBase (v16 (11/2011)), y por tanto hsa-miR-886-3p/snc886-3p y hsa-miR-886-5p/snc886-5p no son considerados desde ese entonces en los análisis de transcriptómica de sncARNs. Esto conlleva a que para determinar sus niveles de expresión debamos re-analizar los datos de transcriptómica de sncARNs (sRNA-seq) para estas muestras, tal como se hizo en Fort et al. 2020 (Fort et al., 2020). Comenzamos con los archivos *miRNAseq data Level_2 Data* (archivos**.bam*), que poseen las lecturas secuenciadas o "reads" filtradas por calidad y mapeadas al genoma humano según los criterios utilizados en el proyecto TCGA (Chu et al., 2015). Realizamos la anotación y conteo de todos los microARNs humanos utilizando la anotación de miRBase v22 e incluimos manualmente a snc886-5p (hsa-miR-886-5p), siguiendo la estrategia de análisis bioinformático realizada por Miñones-Moyano et al. 2013 (Miñones-Moyano et al., 2013), ya implementada para snc886-3p en Fort et al. (2020). El resultado de este re-análisis evidenció que snc886-5p se expresa en la glándula prostática, como evidenciamos anteriormente para líneas celulares de próstata (Fort et al., 2020). Sin embargo, observamos que snc886-5p muestra un incremento estadísticamente significativo de su expresión en el tejido tumoral respecto al tejido normal adyacente, correspondiente a un log2 $FC_{(TUMOR vs NORMAL)}$ = 0,76 ± 0,11 (Normal 52 y Tumor 494; Figura 1A) y pareado log2 $FC_{(TUMOR vs NORMAL)}$ = 0,43 ± 0,13 (Normal 52 *vs* Tumor 52; Figura 1B).

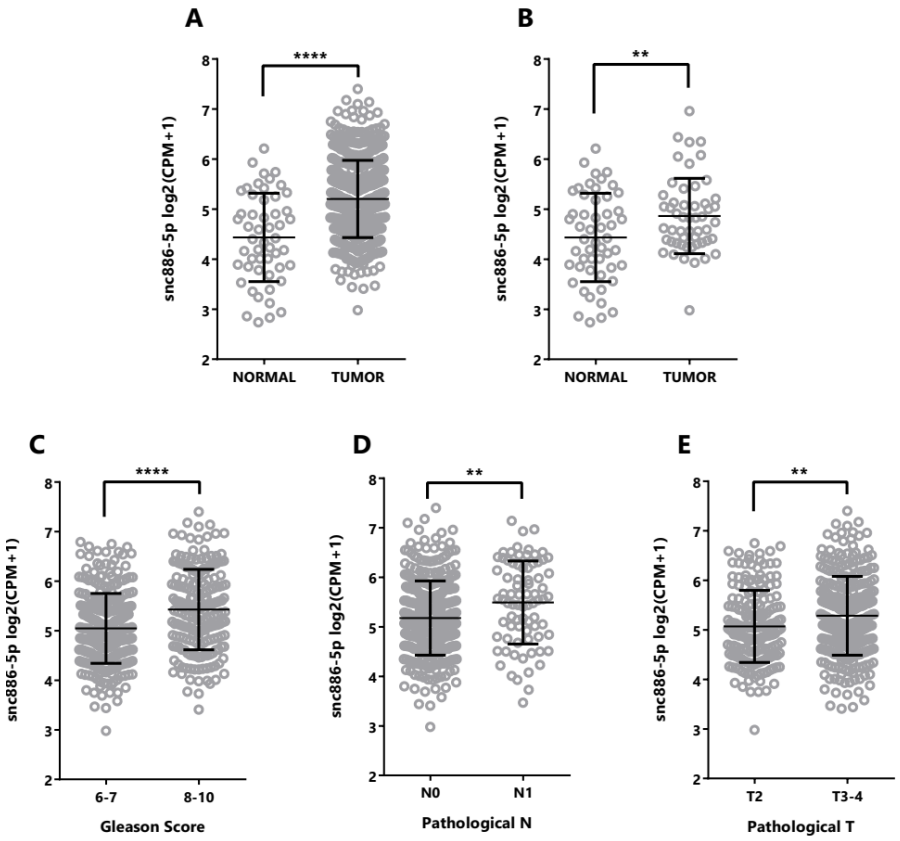

Figura 1. Expresión de snc886-5p en tumores primarios de adenocarcinomas de próstata y tejido normal adyacente de la cohorte PRAD-TCGA y su asociación con parámetros clínicos.

Se grafica la media y desvío estándar de la expresión normalizada de snc886-5p expresada en log2(CPM+1) (CPM: **C**ounts **P**er **M**illion) en el set de datos de transcriptoma de ARNs pequeños disponible analizados con el programa miRDeep2 (Friedländer et al., 2012) en los tejidos o en los agrupamientos clínicos indicados, para las muestras de PRAD-TCGA. **A.** Expresión de snc886-5p en muestras normales (52) comparada contra el total de las muestras tumorales (494). **B.** Expresión de snc886-5p en muestras normales (52) comparada contra las muestras del mismo paciente o pareadas de tejido normal y tumoral (52). Expresión de snc886-5p en muestras tumorales clasificadas en función de su valoración de Gleason (Gleason Score) (**C**), Pathological N (**D**) y Pathological T (**E**). T-test de dos colas pareado en **B** y no pareado en **A, C, D** y **E.** ** p-valor < 0,01; **** p-valor < 0,0001.

Los resultados evidencian que snc886-5p posee un perfil de expresión oncogénico debido a que se encuentra sobre-expresado en el tumor de próstata respecto al tejido normal adyacente. Esto resultó llamativo debido a que expone un perfil de expresión opuesto al de su precursor vtRNA2-1/nc886 y al de snc886-3p (fragmento que deriva del extremo 3´), en la transición carcinogénica prostática (Fort et al., 2018, 2020). Adicionalmente, evaluamos la posible asociación de la expresión de snc886-5p con los diferentes parámetros clínicos de la enfermedad disponibles en la cohorte PRAD-TCGA. Observamos que snc886-5p presenta una asociación positiva entre el

aumento de su expresión y los parámetros clínicos de la enfermedad que se indican en los gráficos (Figura 1C, 1D y 1E). Mostrando una asociación estadísticamente significativa con peores valores de puntación de Gleason, en inglés *Gleason Score* (Figura 1C), y los valores de estadificación del sistema TNM de tipo T (del tumor primario del inglés *Pathological T*) (Figura 1E) y N (de la propagación a nódulos linfáticos cercanos, del inglés *Pathological N* (Figura 1D). En suma, evidenciamos que snc886-5p aumenta su expresión en la transición de tejido normal a tumoral (Figura 1A y 1B, Tabla suplementaria 1) y que su expresión correlaciona con peores parámetros clínicos de la enfermedad (Figura 1C-E, Tabla suplementaria 1). Consecuentemente, estos resultados posicionan a snc886-5p como un posible oncogén en el PrCa, si bien también puede ser una alteración secundaria o pasajera sin efecto funcional. En cualquiera de los casos, este hallazgo supone que snc886-5p aumenta mientras que vtRNA2-1/nc886 y snc886-3p disminuye su expresión en el tejido tumoral respecto al tejido normal. Este fenómeno se conoce como cambio de preferencia de brazos y es llamado en inglés "arm switching", habiendo sido ya reportado en la literatura para algunos precursores de microARNs, incluso en la transición carcinogénica (Chen et al., 2018b; Griffiths-Jones et al., 2011; Guo et al., 2014; Kim et al., 2020; Kuo et al., 2016; Tsai et al., 2016).

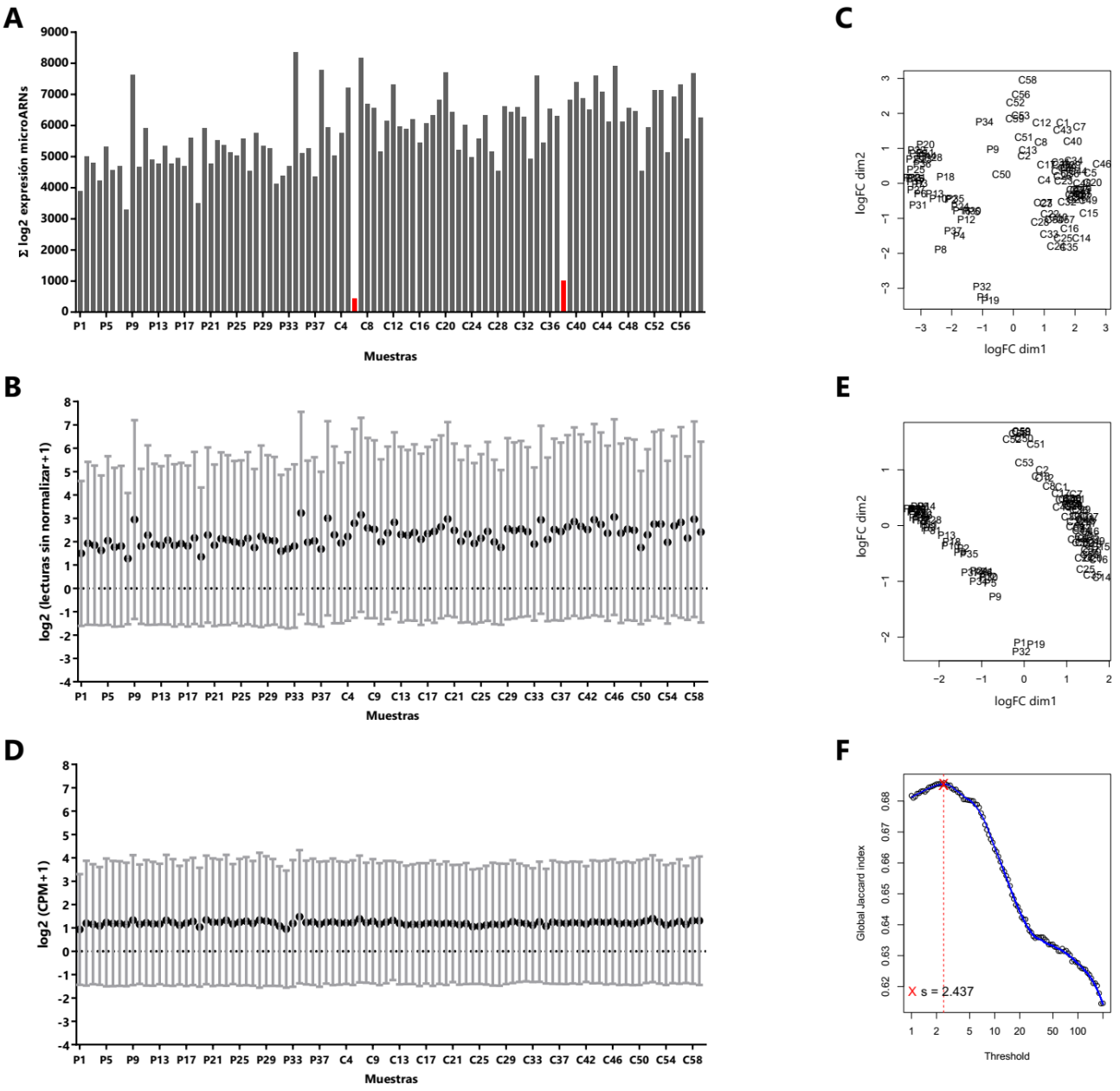

Figura 2. **Análisis transcriptómico de pequeños ARNs no codificantes en líneas celulares humanas primarias normales y tumorales.**

Estudio de 96 líneas celulares normales y tumorales. Para simplificar la representación del eje, se indican solo algunos números de muestra. **A.** Suma de los conteos de las lecturas mapeadas (log2) asignadas a microARNs para el total 96 muestras, en *rojo* se indican las 2 muestras que fueron identificadas como *outliers* utilizando el método estadístico ROUT. **B.** Promedio de cuentas totales y desvío estándar del total de microARNs anotados para cada muestra sin normalizar. En **C** se muestra el análisis de componentes principales de los datos en **B**, donde el *eje X* (logFC dim1) e *Y* (logFC dim2) muestran los componentes que representan la mayor varianza de las muestras. **D.** Promedio de cuentas totales y desvío estándar del total de microARNs anotados en cada muestra normalizados con TMM (*t*rimmed *m*ean of *M* values). Expresión normalizada expresada en log2(CPM+1) (CPM: **C**ounts **P**er **M**illion). En **E** se muestra el análisis de componentes principales de los datos en

D, donde se indican las líneas celulares primarias normales y tumorales. El *eje X* (logFC dim1) e *Y* (logFC dim2) muestran los componentes que representan la mayor varianza de las muestras. **F**. Gráfico de Jaccard index (*eje Y*) calculado para una serie de valores de *threshold* (*eje X*) de los datos normalizados, la *línea punteada roja* indica el valor de *threshold* **s** = 2,4 CPM seleccionado por el algoritmo (Rau et al., 2013).

Buscando extender la evidencia entorno al fenómeno de "arm switching" a datos de más profundidad que los del TCGA, así como a modelos *in vitro*, ampliamos el meta-análisis transcriptómico de sncARNs a sets de datos disponibles en repositorios públicos. Optamos por dos sets de datos de sRNA-seq de altísima calidad, disponibles en el repositorio *Sequence Read Archive* (SRA, (Leinonen et al., 2011)), que comprenden líneas celulares humanas primarias normales (37 human normal primary cell lines, PRJNA358331 (PNHC) (McCall et al., 2017)) y tumorales (59 NCI-60 human tumor cell lines, PRJNA390643 (CHC) (Marshall et al., 2017)). Efectuamos un nuevo análisis de los datos siguiendo la misma aproximación metodológica utilizada anteriormente (Figura 2A). Observamos que para la mayor parte de las muestras no hay diferencias notorias en las lecturas mapeadas totales a microARNs entre las líneas celulares normales y tumorales. Sin embargo, dos muestras tienen un total de lecturas bastante inferior al resto, nos preguntamos si se trataba de valores atípicos, en inglés *outliers*. Entonces, considerando las lecturas totales mapeadas a microARNs por librería, efectuamos la búsqueda de *outliers* utilizando el método estadístico ROUT (*False Discovery Rate*, Q = 1% (Motulsky & Brown, 2006)). Efectivamente, se identificaron como *outliers* las dos muestras antes mencionadas (líneas celulares UACC-257 y MALME-3M), quedando descartadas para los posteriores análisis (Figura 2A, Tabla suplementaria 2). Posteriormente, realizamos la normalización aplicando el método TMM (trimmed mean of M values (Robinson & Oshlack, 2010)); en las Figuras 2B-E se aprecia la distribución de las muestras previo (Figuras 2B y 2C) y posteriormente (Figuras 2D y 2E) a la aplicación de la normalización. A continuación, excluimos los microARNs de baja expresión (que portan bajo soporte estadístico para los análisis de expresión diferencial), aplicando el algoritmo HTSFilter (Rau et al., 2013), que selecciona el umbral o *threshold* basado en el cálculo de un índice de similitud "*s*" entre réplicas biológicas e identificó un umbral de 2,4 CPM (CPM: **C**ounts **P**er **M**illion) para estos datos (Figura 2F). Encontramos que luego de la normalización y filtrado de lecturas de baja expresión las muestras permanecen con datos para 1230 microARNs diferentes. Posteriormente, realizamos un ranking de expresión promedio de todos los microARNs y establecimos la posición de snc886-3p y snc886-5p en las líneas celulares (Figuras 3A y 3B, Tabla suplementaria 3). Este análisis reveló que snc886-3p baja mientras que snc886-5p sube su posición en el ranking en las líneas celulares tumorales (snc886-3p #489, snc886-5p #75) respecto a las primarias normales (snc886-3p #232, snc886-5p #147), mostrando perfiles de cambio opuestos. Incluso observamos que snc886-3p se ubica por debajo de la línea de expresión promedio de todos los microARNs en las líneas celulares tumorales (Figura 3B y Tabla suplementaria 3).

Alternativamente, realizamos la determinación de los sncARNs diferencialmente expresados entre las líneas celulares primarias normales y las líneas celulares tumorales, aplicando el algoritmo EdgeR (Robinson et al., 2010). Este análisis expuso la expresión diferencial estadísticamente significativa (FDR < 0,01) y opuesta de snc886-3p ($log2FC_{(TUMORvsNORMAL)}$ = -2,3) y snc886-5p ($log2FC_{(TUMORvsNORMAL)}$ = 4,2) (Figura 3C y 3D, Tabla suplementaria 4).

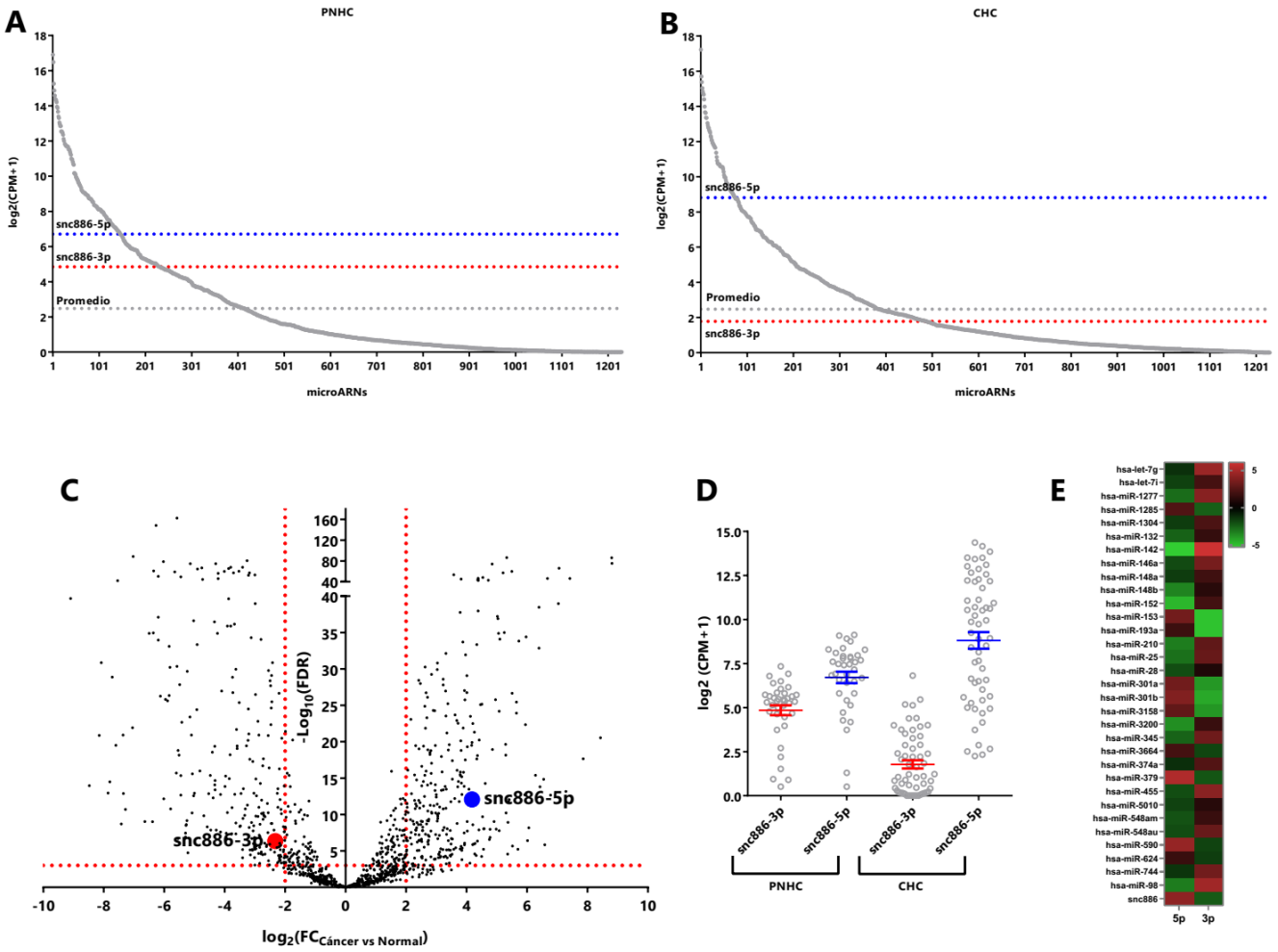

Figura 3. **Expresión diferencial de los microARNs entre las líneas celulares normales y tumorales.**

Expresión normalizada expresada en log2(CPM+1) (CPM: **C**ounts **P**er **M**illion). Ranking de los microARNs según su expresión promedio en las muestras de líneas celulares primarias normales **A** (PNHC) y tumorales **B** (CHC). Los valores para snc886-3p y snc886-5p se resaltan en rojo y azul, respectivamente. El gráfico muestra la expresión de cada uno de los microARNs, ordenados en el eje de las abscisas según su posición en el ranking, indicada por los números. Las líneas punteadas denotan la ubicación en el ranking de snc886-3p (PNHC # 232, promedio = 4.85; CHC # 489, promedio = 1.78), snc886-5p (PNHC # 147, promedio = 6.71; CHC # 75, promedio = 8.81) y el valor promedio del total de los microARNs (*en gris*) (PNHC promedio = 2.48; CHC promedio = 2.47). **C.** Gráfico de volcán de la expresión diferencial de los microARNs entre las líneas celulares tumorales (Cáncer) *vs* normales (Normal). En la abscisa se muestra los valores de cambio relativo expresado como $log_2(FC_{Cáncer\ vs\ Normal})$ y en la ordenada los valores de FDR (expresados como log_{10}(FDR (Benjamini-Hochberg). **D**. Distribución de los valores de expresión de snc886-3p y snc886-5p en el total de muestras evaluadas de las líneas celulares primarias normales y tumorales,

se indica el valor promedio y su error estándar. **E.** Mapa de calor "Heatmap" de la expresión diferencial de los 32 microARNs y snc886 que presentan "arm switching" en el set de datos de las líneas celulares primarias normales (PNHC) y tumorales (CHC), con diferencias de $FC_{(Cáncer\ vs\ Normal)} \geq |1|$ y FDR ≤ 0,05. Set de datos disponibles en SRA PRJNA358331 y PRJNA390643 analizados con el programa miRDeep2 y EdgeR (Friedländer et al., 2012; Robinson et al., 2010).

El cambio de expresión opuesta entre snc886-3p (disminuye en las líneas celulares tumorales) y snc886-5p (aumenta en las líneas celulares tumorales), constituye una nueva evidencia a favor de la hipótesis del fenómeno de "arm switching". Del mismo modo, contribuye a la hipótesis de una función TSG de snc886-3p y una función OG de snc886-5p en la tumorigénesis. Adicionalmente, es importante destacar que producto de este meta-análisis encontramos un 5,4% de microARNs (32 microARNs) que experimentan el fenómeno de "arm switching" con cambios 5p y 3p opuestos, es decir, FC(Cáncer *vs* Normal) ≥ |1| y FDR ≤ 0,05 (Figura 3E y Tabla suplementaria 4). El porcentaje de microARNs identificados que experimentan el fenómeno de "arm switching" es aproximado a lo reportado en la literatura (14%) (Kim et al., 2020). Incluso en la lista de 32 microARNs encontramos a los microARNs hsa-miR-193a, hsa-miR-146b y hsa-miR-744 (Figura 3E) que fueron anteriormente descritos como blanco de este fenómeno de procesamiento en el cáncer (Chen et al., 2018b; Tsai et al., 2016).

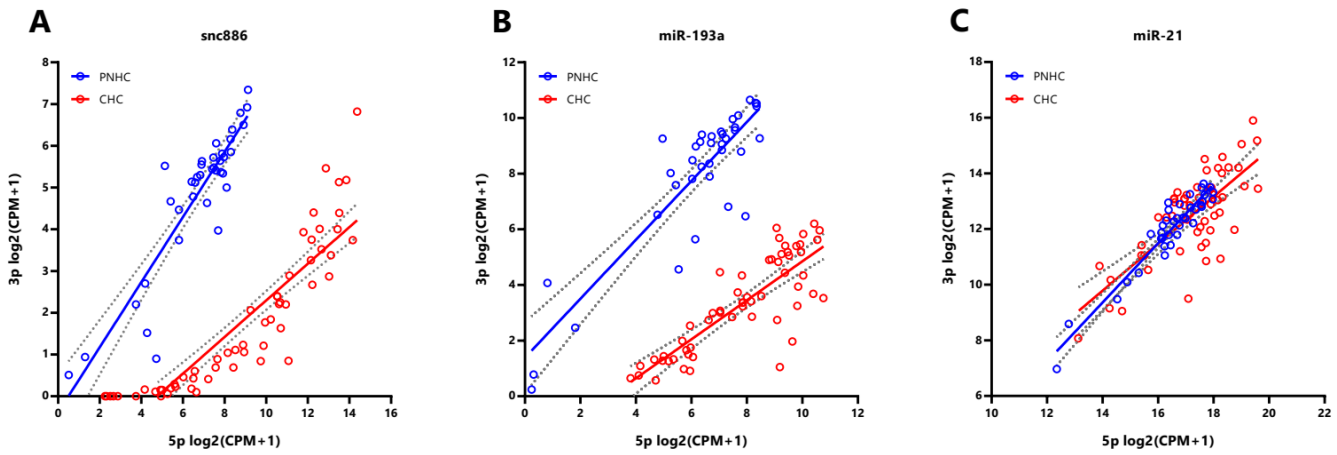

Figura 4. Correlación entre la expresión de los brazos 5p y 3p de microARNs entre las líneas celulares normales y tumorales.

Expresión normalizada expresada en log2(CPM+1) (CPM: **C**ounts **P**er **M**illion) de los brazos 5p (*eje x*) y 3p (*eje y*) de los microARNs. En **A** snc886s (snc886-5p y snc886-3p), en **B** miR-193a (miR-193a-5p y miR-193a-3p) y en **C** miR-21 (miR-21-5p y miR-21-3p). Los círculos de color azul corresponden a las muestras de líneas celulares normales (PNHC) y los círculos de color rojo a las tumorales (CHC). Las líneas continuas muestran la regresión lineal de la curva y las líneas punteadas denotan el intervalo de confianza al 95% de la curva.

Finalmente, para continuar examinando el procesamiento diferencial de vtRNA2-1/nc886, evaluamos la correlación de la expresión de los brazos 5p y 3p de vtRNA2-1/nc886 entre las líneas celulares no transformadas

(normales) (McCall et al., 2017) y las líneas celulares tumorales (Marshall et al., 2017), que comprenden en total 13 tipos diferentes de origen tisular, 12 diferentes en las células normales y 9 en las tumorales (Figura 4A). Producto de este análisis observamos una correlación global positiva (correlación Spearman = 0,44) entre snc886-5p y snc886-3p para todas las muestras, lo que es coherente con el origen de ambas moléculas de un precursor común. Sin embargo, identificamos dos curvas diferentes para la relación 5p y 3p en las líneas celulares normales (PNHC) y las tumorales (CHC) (Figura 4A). Entonces, si bien existe una correlación global positiva entre la expresión de los brazos 5p y 3p derivados de vtRNA2-1/nc886, la relación 5p/3p en las líneas celulares normales es diferente a la observada para las líneas celulares tumorales, esto se refleja en la diferencia significativa de las pendientes entre ambas curvas (p-valor < 0,0001) (Figura 4A). Particularmente, observamos que la relación de 5p/3p es mayor en las líneas celulares tumorales (pendiente = 0,43) respecto a las líneas celulares primarias normales (pendiente = 0,78) (Figura 4A). De igual manera, miR-193a que tiene antecedentes de "arm switching" en la literatura (Kim et al., 2020; Tsai et al., 2016), también experimenta un comportamiento similar (correlación Spearman = 0,30) pudiéndose también observar dos curvas con pendientes diferentes (p-valor = 0,0017; Figura 4B). Sin embargo, miR-21 (correlación Spearman = 0,71), que no evidencia "arm switching" en este set de datos, no presenta diferencia entre las pendientes de las curvas para las líneas celulares normales y las líneas celulares tumorales (p-valor = 0,12, Figura 4C). Estos resultados nos permiten suponer la existencia de un mecanismo que incide en el cambio de procesamiento y/o estabilidad diferencial de los brazos 5p y 3p entre las líneas celulares normales y tumorales para vtRNA2-1/nc886. Es importante mencionar que hubiera sido más informativo realizar este último análisis en las muestras de pacientes del PRAD-TCGA. Sin embargo, la menor profundidad de la secuenciación de estas muestras, sumada a la baja expresión de snc886-3p en el tejido tumoral, hace que la mayor parte de los transcriptomas no tengan lecturas confiables para este pequeño ARN.

DISCUSIÓN.

Hsa-miR-886-5p/snc886-5p fue inicialmente catalogado como uno de los microARNs maduros derivados de "hsa-mir-886" (vtRNA2-1/nc886) (Landgraf et al., 2007). Posteriormente, debido a su homología de secuencia con los vault ARNs, hsa-mir-886 fue re-catalogado como vtRNA2-1/nc886 (locus vtRNA2) (Stadler et al., 2009). Esta reclasificación condujo a su eliminación de la base de datos miRBase v16 (11/2011). A pesar de su pronta eliminación de miRBase y no ser considerado un precursor de microARNs canónico, posteriores reportes evidenciaron que vtRNA2-1/nc886 es procesado por DICER (independiente de DROSHA) generando pequeños sncARNs hsa-miR-886-5p/snc886-5p y hsa-miR-886-3p/snc886-3p (Cloonan et al., 2011; Fort et al., 2020; Miñones-Moyano et al., 2013; Pillai et al., 2010; Treppendahl et al., 2012). En la próstata nosotros evidenciamos que vtRNA2-1/nc886 también posee la capacidad de producir sncARNs específicos (snc886-5p y snc886-3p) y que

estos se asocian a las proteínas argonautas (Fort et al., 2020) y sus síntesis depende de DICER y no de DROSHA. En ese mismo trabajo nosotros mostramos un descenso de la expresión de snc886-3p concomitante con un incremento en la expresión de snc886-5p, siendo ambos los fragmentos de ARN predominantes del vtRNA2-1/nc886 en los tejidos.

La realización del meta-análisis de sRNA-seq de PRAD-TCGA nos permitió evaluar el perfil de expresión de snc886-5p en el tejido de glándula prostática. En acuerdo con nuestros resultados preliminares en las líneas celulares prostáticas, evidenciamos que snc886-5p aumenta su expresión en el tumor respecto al tejido normal adyacente (Figuras 1A y 1B). Si bien esto podía ser simplemente un cambio secundario sin valor funcional, el hecho de que su expresión se asocia con peores parámetros clínicos de la enfermedad en la cohorte estudiada, lo posiciona más fuertemente como un posible ARN conductor de la neoplasia con efecto funcional (Figuras 1C-D). Estos resultados, en conjunto con los antecedentes de snc886-3p en próstata (Fort et al., 2020), exponen que durante la carcinogénesis prostática ocurriría una disminución de la expresión de snc886-3p y en simultáneo, el aumento de expresión de snc886-5p. Esto sugiere que vtRNA2-1/nc886 podría ser objeto de un cambio de preferencia de brazos "arm switching" durante la carcinogénesis prostática. El "arm switching" implica un cambio en el procesamiento de un precursor de microARNs que conduce a un cambio en la proporción de la producción de los brazos/microARNs 5p (extremo 5' del precursor) y 3p (extremo 3' del precursor) derivados (Pundhir & Gorodkin, 2015a). Es importante destacar que este fenómeno ha sido descrito para otros precursores de microARNs, y es fisiológicamente relevante en varios procesos celulares, incluso en la transición tumoral (Chen et al., 2018b; Kim et al., 2015, 2020; Pundhir & Gorodkin, 2015b). Existen diferentes proteínas reportadas capaces de modificar y/o asociarse al vtRNA2-1/nc886 y/o a los otros vtRNAs que podrían estar involucradas en el fenómeno de "arm switching" (TEP1, DUSP11, SSB, NSUN2, TUTs y DIS3L2 (Burke & Sullivan, 2017; Burke et al., 2016; Hussain et al., 2013; Kickhoefer et al., 1999, 2002; Kim et al., 2015, 2020; Łabno et al., 2016; Sajini et al., 2019; Ustianenko et al., 2016)). De hecho, las proteínas TUTs, que modifican a los vtRNAs (Łabno et al., 2016), fueron directamente involucradas en el fenómeno de "arm switching" de microARNs en cáncer (Kim et al., 2015, 2020).

En concordancia con los resultados aquí presentados encontramos un hallazgo análogo en los datos de un estudio de "profiling" de microARNs de cáncer de tiroides, donde se reportó la expresión diferencial invertida de snc886-3p (disminuye en el tumor) y snc886-5p (aumenta en el tumor), si bien los autores no dan cuenta del fenómeno (Dettmer et al., 2014). Buscando fortalecer nuestra observación realizamos el re-análisis de transcriptomas de sncARNs para determinar la expresión de snc886-5p y snc886-3p en líneas celulares normales primarias (n=37, (McCall et al., 2017)) y líneas celulares tumorales (n=57, (Marshall et al., 2017)). El estudio de sncARNs expresados diferencialmente entre las líneas celulares normales *vs* las líneas celulares tumorales, reafirmó el fenómeno de

cambio de preferencia de brazos o “arm switching” para vtRNA2-1/nc886, y el perfil de expresión oncogénico de hsa-miR-886-5p/snc886-5p. Incluso, nuestros análisis sugieren que existiría un cambio en la tasa de procesamiento/estabilidad de los brazos 5p y 3p derivados de vtRNA2-1/nc886 entre las líneas celulares normales y tumorales analizadas. Globalmente, los datos sugieren que durante la carcinogénesis ocurriría una disminución global de la expresión de snc886-3p y en simultáneo el aumento global de la expresión de snc886-5p (Figuras 3A-D).

Es interesante destacar que los reportes existentes sobre la actividad en cáncer de hsa-miR-886-5p/snc886-5p lo postulan mayoritariamente como OG en cáncer cervical (Kong et al., 2015; Li et al., 2011), oral (Xiao et al., 2012), linfoma (Liu et al., 2013), mama (Zhang et al., 2014), tiroides (Dettmer et al., 2014), vejiga (Khoshnevisan et al., 2015) y mieloma múltiple. Incluso, los ensayos funcionales realizados con hsa-miR-886-5p/snc886-5p respaldan una actividad oncogénica, así como su función microARN donde se validó su capacidad de regular a p53 (Kong et al., 2015; Li et al., 2011; Xiang et al., 2019; Zhang et al., 2014). No obstante, algunos reportes mostraron un perfil TSG para hsa-miR-886-5p/snc886-5p en cáncer de pulmón (Gao et al., 2011) y carcinoma hepatocelular (Han et al., 2012). Contrariamente, la literatura relativa a hsa-miR-886-3p/snc886-3p lo posiciona con función TSG en PrCa (Aakula et al., 2015; Fendler et al., 2011; Fort et al., 2020), vejiga (Nordentoft et al., 2012), mama (Tahiri et al., 2014), colon (Yu et al., 2011), pulmón (Bi et al., 2014; Cao et al., 2013; Gao et al., 2011; Shen et al., 2018) y tiroides (Dettmer et al., 2014; Xiong et al., 2011). Sin embargo, algunos reportes muestran una acción oncogénica de hsa-miR-886-3p/snc886-3p en cáncer renal (Yu et al., 2014), colorrectal (Schou et al., 2014) y de esófago (Okumura et al., 2016). Por lo tanto, la literatura acompaña en mayor medida la observación de un perfil OG para snc886-5p y TSG para snc886-3p en cáncer, lo que se encuentra acorde con los datos de expresión diferencial determinados en nuestros análisis para ambos sncARNs en PrCa. No puede sin embargo descartarse que ejerzan roles diferentes en algunos tejidos.

En suma, estos resultados evidencian un incremento de la expresión de snc886-5p en el tejido tumoral *vs* el tejido normal en próstata humana, así como su asociación con peores parámetros clínicos de la enfermedad, lo que termina sugiriendo su posible función como OG en la próstata. Los datos preliminares en próstata para vtRNA2-1/nc886 (Fort et al., 2018) y snc886-3p (Fort et al., 2020) mostraron su función TSG y la disminución de su expresión durante la carcinogénesis prostática, sin embargo, snc886-5p podría cumplir una función OG ya que aumenta su expresión/estabilidad en el tumor. Finalmente, hipotetizamos que vtRNA2-1/nc886 podría experimentar el fenómeno de “arm switching” en la transición carcinogénica de la próstata y probablemente en otros tejidos. Esto representaría uno de los pocos casos en los que una molécula precursora de pequeños ARNs de síntesis específica posee una función como transcrito de ARN completo y además genera dos moléculas de

ARN con contribuciones funcionales diferentes, es decir, el gen vtRNA2-1/nc886 genera 3 productos que son conductores de la neoplasia, actuando por vías probablemente diferentes.

Link a los archivos suplementarios:

https://drive.google.com/drive/folders/14Q07jJ1wugEcKDyS3eGUiQ8_4717-fVH?usp=sharing

IV. EXPRESIÓN GLOBAL DE VTRNA2-1/NC886 Y SU POSIBLE ASOCIACIÓN CON LOS VTRNAS CANÓNICOS EN EL CÁNCER DE DIFERENTE ORIGEN TISULAR.

***Objetivo específico 2.3*: Determinar el perfil de expresión global de vtRNA2-1/nc886 y su posible asociación con los vtRNAs canónicos en el cáncer de diferente origen tisular.**

Con el fin de explorar la expresión de vtRNA2-1/nc886 globalmente en el cáncer y su relación con los vtRNAs canónicos humanos, realizamos el estudio del perfil de la estructura de la cromatina de sus regiones reguladoras en el set de datos de Pan-Cáncer del TCGA. Basados en la literatura y en los antecedentes de nuestro trabajo, utilizamos el status de la cromatina del promotor de estos genes como marcador subrogado de su expresión. Concretamente, evaluamos la cromatina en la región promotora de los vtRNAs, explorando los datos de accesibilidad y los datos de metilación del ADN, determinados por ATAC-seq y microarreglos de metilación de las muestras de TCGA, respectivamente (*objetivo específico 2.3.1*). Para estudiar si los vtRNAs se encuentran co-regulados a nivel transcripcional, evaluamos la asociación de la accesibilidad de la cromatina de los promotores de los 4 vtRNAs en las muestras del TCGA y comparamos los factores de transcripción que se unen a sus promotores (determinados en análisis de datos de líneas celulares producidos por el consorcio ENCODE). Adicionalmente, abordamos los perfiles de asociación y de correlación entre los diferentes vtRNAs a nivel de accesibilidad de la cromatina en los tejidos tumorales, normales adyacentes y en la transición normal-tumoral para cada origen tisular, buscando descubrir diferencias específicas de tejido (*objetivo específico 2.3.2*). Asimismo, investigamos la asociación de la accesibilidad de la cromatina y la sobrevida de los pacientes a nivel Pan-Cáncer (*objetivo específico 2.3.3*). Finalmente, buscamos relacionar el estado de accesibilidad de la cromatina del promotor de los vtRNAs con el de los promotores de otros genes, para de esta manera, explorar posibles grupos de genes co-regulados a nivel de accesibilidad de la cromatina y su vinculación con vías y procesos celulares (*objetivo específico 2.3.4*). Con los resultados obtenidos, indagamos específicamente en la posible vinculación entre la expresión de los vtRNAs y los subtipos inmunológicos.

El conjunto de estas aproximaciones nos permitió explorar la relación de vtRNA2-1/nc886 con los otros vtRNAs y su relación con el cáncer globalmente. Los resultados se encuentran compilados en un manuscrito científico que se adjunta a continuación y será sometido para su publicación en revista arbitrada.

Artículo científico 3: Fort, R.S., and Duhagon, M.A. (2020). Pan-Cancer chromatin analysis of the human vtRNA genes uncovers their association with cancer biology.

Pan-Cancer chromatin analysis of the human vtRNA genes uncovers their association with cancer biology.

Authors:

Rafael Sebastián Fort [1,3] and María Ana Duhagon [1,2,*]

[1] Laboratorio de Interacciones Moleculares, Facultad de Ciencias, Universidad de la República, Montevideo 11400, Uruguay; rfort@fcien.edu.uy (R.S.F.).
[2] Departamento de Genética, Facultad de Medicina, Universidad de la República, Montevideo 11800, Uruguay.
[3] Departamento de Genómica, Instituto de Investigaciones Biológicas Clemente Estable, Montevideo 11600, Uruguay.
* Correspondence: mduhagon@fcien.edu.uy/mduhagon@fmed.edu.uy (M.A.D.); Tel.: +598-2-525-8618 (ext. 7237)

Abstract

The vault RNAs (vtRNAs) are 84-141-nt eukaryotic RNAs named for their association with the vault particle, a riboprotein complex whose function remains poorly understood. Gene expression studies of the four human vtRNA in large cohorts have been hindered by their unsuccessful sequencing using conventional transcriptomic approaches. Here we infer the landscape of vtRNA expression in cancer from the genome-wide DNA methylation and chromatin accessibility data of The Cancer Genome Atlas (TCGA). VtRNA1-1 has the most accessible chromatin, followed by vtRNA1-2, vtRNA2-1 and vtRNA1-3. Although the vtRNAs are co-regulated by transcriptional factors related to viral infection, vtRNA2-1 is the most independent homologue. VtRNA1-1 and vtRNA1-3 chromatin status does not significantly change in cancer, however, vtRNA2-1 and vtRNA1-2 expression is widely deregulated in neoplastic tissues and is compatible with a broad oncogenic role of vtRNA1-2, and both tumor suppressor and oncogenic functions of vtRNA2-1. Yet, vtRNA1-1, vtRNA1-2 and vtRNA2-1 promoter DNA methylation predicts a shorter patient overall survival cancer-wide. In addition, gene ontology analyses of co-regulated genes identify a chromosome 5 regulatory domain controlling vtRNA1-1 and neighboring genes, and epithelial differentiation, immune and thyroid cancer gene sets for vtRNA1-2, vtRNA2-1 and vtRNA1-3 respectively. Furthermore, vtRNA expression patterns are associated with cancer immune subtypes and vtRNA1-2 expression is positively associated with cell proliferation and wound healing. Overall, our study presents the landscape of vtRNA expression cancer-wide, identifying co-regulated gene networks and ontological pathways associated with the different vtRNA genes that may account for their diverse roles in cancer.

Keywords: vault RNA; vtRNA1-1; vtRNA1-2, vtRNA1-3, vtRNA2-1; nc886; cancer; TCGA; DNA methylation; chromatin accessibility.

Introduction

The vault RNAs (vtRNAs) are a class of eukaryotic middle size non-coding RNAs (84-141 nt) transcribed by the RNA polymerase III, which associates to the vault particle (<5 % of the total mass of the vault particle) (Boivin et al., 2019; Kedersha and Rome, 1986; Kedersha et al., 1991). Although this particle is the largest cellular nucleoprotein complex, its function remains scarcely understood. Most mammals have a single vtRNA gene (i.e., mouse and rat), but the human genome has three copies, annotated as vtRNA1-1 (98pb), vtRNA1-2 and vtRNA1-3 (88pb), which are located in the chromosome region 5q33.1 (the vtRNA1 locus) and transcribe the RNAs that are integral components of the vault particle. Another vault RNA gene in chromosome X, was classified as a pseudogene (vtRNA3-1P) due to the absence of expression in several cell lines and the presence of silencing mutations at the B box element of its promoter (van Zon et al., 2001). Lately, a transcript initially annotated as the human microRNA precursor hsa-mir-886 (Landgraf et al., 2007), was re-classified as another human vtRNA homologue and consequently renamed as vtRNA2-1 (Stadler et al., 2009). VtRNA2-1 is also located in chromosome 5 (5q31.1, locus vtRNA2) at 0.5Mb distance from the vtRNA1 cluster, where is placed between SMAD5 and TGFB1 genes in an antisense direction. Existing evidence indicates that despite being a duplication of the vtRNAs of locus 1, the vtRNA2-1 is neither associated with the vault particle nor co-regulated with the vtRNA1 locus (Lee et al., 2011; Stadler et al., 2009). Nevertheless, the realization that only 5-20% of all the cellular vtRNA transcripts are associated to the vault particle suggests additional roles for the majority of vtRNA transcripts, independent of the vault particle (Kickhoefer et al., 1998; Nandy et al., 2009; van Zon et al., 2001).

Most of the current knowledge of vtRNA function focuses on vtRNA1-1 and vtRNA2-1 roles in viral infection and cancer. Functional studies found that vtRNA1-1 and vtRNA1-2 (but not vtRNA1-3) can interact directly with drugs as mitoxantrone, doxorubicin and etoposide (Gopinath et al., 2005, 2010; Mashima et al., 2008). A recent report demonstrated that p62 protein interacts with vtRNA1-1 and inhibits the p62 dependent autophagy *in vitro* and *in vivo* (Horos et al., 2019). The vault RNAs have also been linked to native immune response, because of their strong upregulation during the infection of Influenza A virus (IAV) and Epstein-Barr virus (EBV) (Amort et al., 2015; Li et al., 2015; Nandy et al., 2009). These studies proposed a viral activation of host

vtRNAs as a mechanism to maintain the inhibition of PKR signaling pathway, representing a viral strategy to circumvent host innate immunity.

Initial reports about vtRNA2-1 (locus vtRNA2) revealed that it is abundant in normal tissues while lowly expressed in cancer cell lines from different tissue origin (breast, melanoma, cervix, lung, oral and prostate), which is consistent with a tumor suppressive role in cancer (Lee et al., 2011; Treppendahl et al., 2012). Moreover, vtRNA2-1 was proposed as a new type of ncRNA functioning as a tumor suppressor gene (TSG) that inhibits PKR, and was consequently renamed as “nc886” (Golec et al., 2019; Jeon et al., 2012a, 2012b; Lee et al., 2011). Then, its anti-proliferative and TSG function was described in prostate (Aakula et al., 2015; Fort et al., 2018; Ma et al., 2020), skin (Lee et al., 2019a), gastric (Lee et al., 2014b) and esophageal (Im et al., 2020; Lee et al., 2014a) and cholangiocarcinoma cells (Kunkeaw et al., 2012). Conversely, a pro-proliferative and anti-apoptotic oncogenic role was proposed for vtRNA2-1 in renal (Lei et al., 2017), ovarian (Ahn et al., 2018), thyroid (Lee et al., 2016), cervical (Li et al., 2017) and endometrial (Hu et al., 2017) tissues. A recent finding proposing a vtRNA2-1/PKR loss mediated doxorubicin cytotoxicity introduced a novel view about its contribution to chemotherapy response (Kunkeaw et al., 2019). In addition, a potential TSG role has been put forward for vtRNA1-3 in Myelodysplastic syndrome (MDS) (Helbo et al., 2015).

Apart from their role as full length RNAs, vtRNAs are precursors of small RNAs. Indeed, small RNAs with microRNA like function were demonstrated to derive from vtRNA1-1 (svRNAs) and to repress the expression CYP3A4, a key enzyme of drug metabolism (Meng et al., 2016; Persson et al., 2009). VtRNA2-1 has also been shown to act as a microRNA precursor in different tissues, serving both as TSG in prostate (Aakula et al., 2015; Fendler et al., 2011; Fort et al., 2020), bladder (Nordentoft et al., 2012), breast (Tahiri et al., 2014), colon (Yu et al., 2011), lung (Bi et al., 2014; Cao et al., 2013; Gao et al., 2011; Shen et al., 2018) and thyroid cancers (Dettmer et al., 2014; Xiong et al., 2011) and as oncogene (OG) in renal (Yu et al., 2014), colorectal (Schou et al., 2014) and esophagus cancer (Okumura et al., 2016) through the repression of specific mRNA transcripts in human cancer.

The vtRNAs transcription is controlled by promoter DNA methylation. Different lines of evidence revealed that the epigenetic control of vtRNA2-1 is complex and owns clinical relevance in several tissues solid tumors including breast, lung, colon, bladder, prostate, esophagus, hepatic

and stomach cancer (Cao et al., 2013; Fort et al., 2018; Lee et al., 2014a, 2014b; Romanelli et al., 2014; Treppendahl et al., 2012; Yu et al., 2020). Intriguing aspects of the epigenetic regulation of vtRNA2-1 locus comprise its dependence on the parental origin of the allele (Joo et al., 2018; Paliwal et al., 2013), and its sensitivity to the periconceptional environment ((Silver et al., 2015) and subsequent independent studies (van Dijk et al., 2018; Richmond et al., 2018)). In addition, vtRNA1-3 promoter methylation was associated with significantly poor outcome in lower risk myelodysplastic syndrome patients (Helbo et al., 2015).

Currently, transcriptomic sequencing is the benchmark technique to study global RNA expression (Stark et al., 2019). Nonetheless, some classes of RNAs are elusive to the standard transcriptomics due to their stable RNA structure and the presence of modified bases or ends, which impair the cDNA synthesis and/or adapter ligation during the sequencing library preparation (Sendler et al., 2011; Zheng et al., 2015). The vtRNAs belong to this group due to their conserved stable stem/hairpin loop secondary structure. The latter, together with the lack of sequencing of 40-200bp-long RNAs in the conventional transcriptomic studies, which are mostly intended for small and long RNAs, probably delayed their study in comparison with other regulatory RNAs. In fact, 50-300 nucleotides long RNAs are considered the black hole of RNA biology (Boivin et al., 2018; Steitz, 2015). Nonetheless, since chromatin accessibility plays a critical role in the regulation of gene expression, at some extent the transcription of an RNA can be inferred from the chromatin status of its promoter (Corces et al., 2018; Duren et al., 2017; Liu et al., 2018; Park et al., 2017b). Since mounting evidence has shown that vtRNAs expression is tightly controlled by chromatin accessibility, dependent on nucleosome positioning and promoter DNA methylation (Ahn et al., 2018; Fort et al., 2018; Helbo et al., 2015, 2017; Lee et al., 2014a, 2014b; Park et al., 2017a, 2017b; Sallustio et al., 2016; Treppendahl et al., 2012), the chromatin structure is a suitable surrogate marker of vtRNA transcription and could be used as a proxy of their expression.

The expression, regulation, and role of the four human vtRNAs in normal and disease conditions are still poorly understood, and available knowledge indicates that they hold diverse tissue specific activities. The availability of genomic data of large sets of human tissues provided by The Cancer Genome Atlas (TCGA), allows the study of the human vtRNAs across 16 tissue types and normal/cancer conditions. Here, we analyze vtRNA genes chromatin of the TCGA

patient cohort withdrawn from two approaches: the assay for transposase-accessible chromatin followed by NGS sequencing (ATAC-seq) to analyze chromatin accessibility (Buenrostro et al., 2013, 2015; Corces et al., 2018; Thurman et al., 2012) and the Illumina Infinium Human Methylation 450K BeadChip to analyze the CpG methylation of DNA (Moran et al., 2016). This led us to determine the patterns of transcriptional regulation of the four human vtRNAs throughout cancer tissues. We also evaluate the association between vtRNA expression and the patient clinical outcome in all the available cancer types. Finally, seeking for functional discoveries, we analyze vtRNA relations with immune subtypes and transcriptionally co-regulated gene programs. Our study reveals specific patterns of expression for each vtRNA that support previous evidence and poses potential new roles and molecular programs in which they may participate across and intra cancer types, increasing the comprehension of the role of the human vtRNAs in health and disease.

Results

VtRNA genes have different chromatin accessibility at the promoter region.

The Cancer Genome Atlas consortium recently incorporated ATAC-seq data for tumor samples of the GDC Pan-Cancer dataset (385 primary tumors samples across 23 cancer types (Corces et al., 2018)). The ATAC-seq strategy is a genome-wide sequencing profiling approximation to chromatin accessibility using the hyperactive Tn5 transposase that simultaneously cut and ligate adapters preferentially to the accessible DNA regions. The counts of sequencing reads in a particular genomic region provides a direct measurement of chromatin accessibility (Buenrostro et al., 2015; Tsompana and Buck, 2014). For those gene promoters regulated by DNA methylation, ATAC-seq is a more direct approximation to chromatin accessibility than promoter CpG DNA methylation measurements because the latter is well correlated but not an exact measurement of chromatin accessibility. Indeed, the effect of DNA methylation on chromatin structure depends on the gene and the distribution of the methylation sites along it. It is also important to mention that gene expression interpretations based solely on chromatin accessibility are blind to post-transcriptional regulatory events such as processing, localization, and stability of the RNA transcript. Nevertheless, since the chromatin status of the different

vtRNA promoters has been positively correlated with the abundance of their transcripts (Ahn et al., 2018; Fort et al., 2018; Helbo et al., 2015; Lee et al., 2014a, 2014b; Park et al., 2017a, 2017b; Sallustio et al., 2016; Treppendahl et al., 2012), ATAC-seq is likely a good surrogate of vtRNA expression. DNA CpG methylation data is available for 746 normal adjacent (across 23 tissues) and 8403 primary tumors (across 32 tissues) tissue samples of the Pan-Cancer TCGA cohort (Supplementary Table 1 and Supplementary Figure 1). The full data is listed in Supplementary Table 1 and the tissue composition of the three datasets of the cohort, comprising tumor ATAC-seq, normal and tumor DNA methylation, is shown in Supplementary Figure 1. The DNA methylation data has 9 more tissue types and a higher number of samples than the others, while the abundance of some tissues is skewed to twice enrichment in 1-4 specific dataset specific tissue types.

Although several reports demonstrated that the DNA methylation of vtRNA promoters is well correlated to vtRNA transcript expression in various tissues (Ahn et al., 2018; Fort et al., 2018; Helbo et al., 2015, 2017; Lee et al., 2014a, 2014b; Park et al., 2017b; Sallustio et al., 2016; Treppendahl et al., 2012), the association between the DNA methylation and chromatin accessibility at their promoters was not previously investigated.

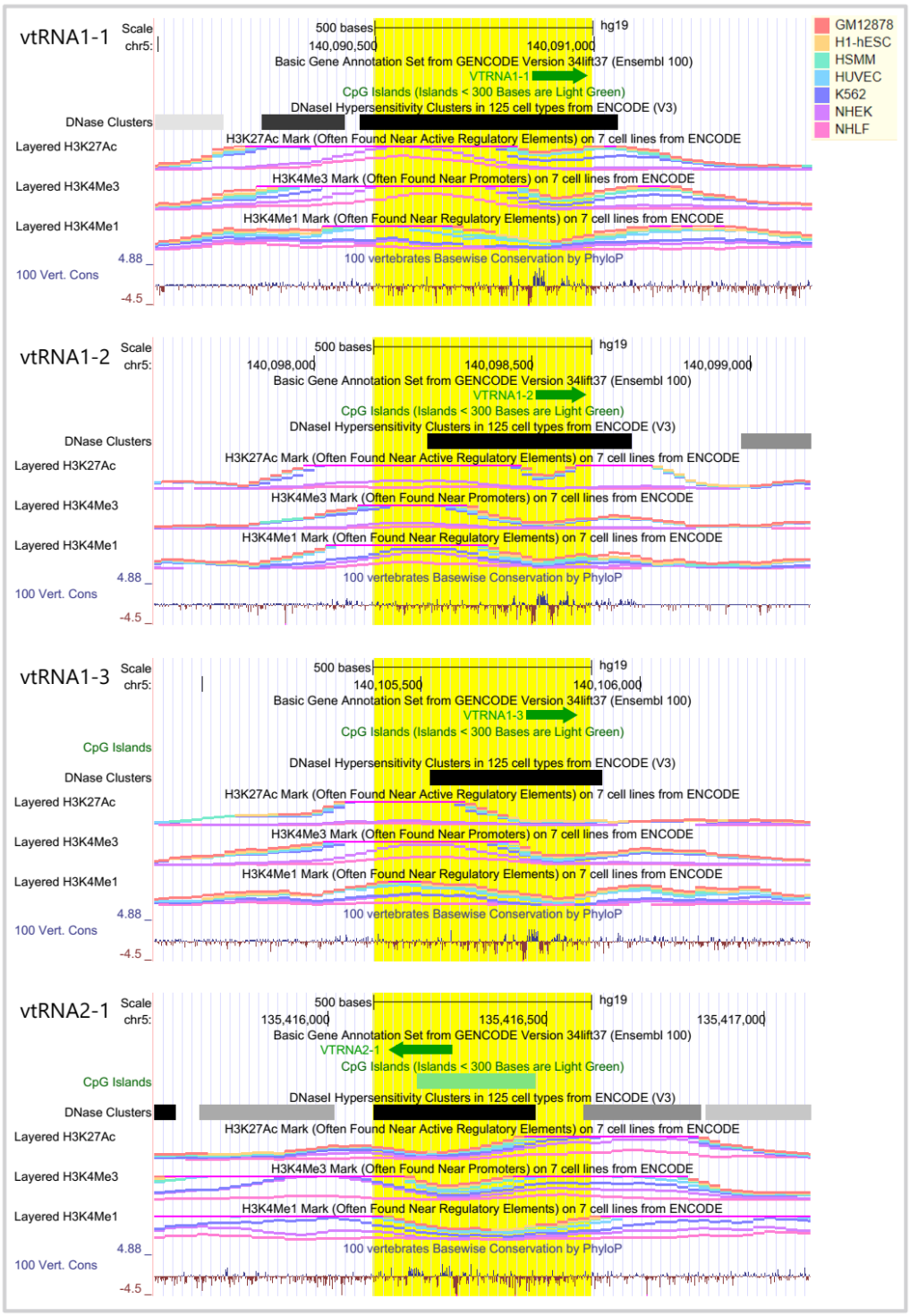

Figure 1. Genomic view of human vtRNA genes epigenetic features. Genomic view of 1.5 kb region of human vtRNA genes in UCSC Genome browser (GRCh37/hg19) centered at the 500bp bin highlighted in *yellow,* which was used for ATAC-seq and CpG methylation analyses. VtRNAs of locus 1 (vtRNA1-1, vtRNA1-2, vtRNA1-3) and of locus 2 (vtRNA2-1) clusters are in the sense and antisense orientation respectively. Several Gene annotation and ENCODE Project tracks for seven cell lines (GM12878, H1-hESC, HSMM, HUVEC, K562, NHEK, NHL) are

displayed: DNA accessibility (DNaseI hypersensitivity clusters (color intensity is proportional to the maximum signal strength)), DNA methylation (CpG islands length greater than 200 bp), histone modification (H3K27Ac, H3K4me1, H3K4me3 marks), conservation of the region in 100 Vertebrates (log-odds Phylop scores). The vertical viewing range of the tracks displays the default settings of the browser for each variable.

To assess the expression of vtRNAs in cancer tissues, we analyzed a 500 bp region, containing the full vtRNA genes, the proximal promoter region and the RNA polymerase III A and B box elements located downstream of the transcription start site (TSS) (Figure 1). Indeed, Vilalta et. al., 1994 demonstrated that the deletion of the 300bp 5´-flanking region of the rat vtRNA transcript largely reduced its transcription greater than 30-fold (Vilalta et al., 1994). As depicted in Figure 1, this region bears epigenetic marks of transcriptionally active chromatin (Li et al., 2007), including histone H3K27ac, H3K4me1, H3K4me3 at the promoters and DNaseI hypersensitivity clusters around the TSS in the cell types compiled by UCSC browser (Goldman et al., 2013). Interestingly, vtRNA2-1 is the only vtRNA immersed in a CpG island and vtRNA1-1 displays the strongest epigenetic marks of transcriptional activity (Figure 1). The analysis of the ATAC-seq values of this 500 bp region of all the TCGA primary tumors reveals that the four human vtRNAs have different levels of chromatin accessibility (Figure 2A). Moreover, the average DNA methylation of the promoters (Figure 2B) in primary tumor samples supports this finding (32 tissues, Supplementary Figure 1 and Supplementary Table 1). VtRNA1-1 promoter has the highest chromatin accessibility and the lowest DNA methylation, showing the smallest dispersion of values among the samples (Ave. 4.1, 0.6 SD) relative to the other three vtRNAs. Meanwhile, vtRNA1-2 (Ave. 2.9, 1.6 SD), vtRNA1-3 (Ave. 1.7, 1.2 SD) and vtRNA2-1 (Ave. 2.5, 1.4 SD) have broader ranges of ATAC-seq and DNA methylation values (Figure 2, Table 1, Supplementary Table 1 and Supplementary Figure 1). A comparison among the vtRNAs shows that the average chromatin accessibility of their promoters is inversely proportional to their average DNA methylation (Table 1 and Figure 2) (relative ATAC-seq values are vtRNA1-1 (4.1) > vtRNA1-2 (2.9) > vtRNA2-1 (2.5) and accordingly, relative DNA methylation are vtRNA1-1 (0.09) < vtRNA1-2 (0.4) < vtRNA2-1 (0.5)). Yet vtRNA1-3 average low chromatin accessibility is not accompanied by a comparatively denser promoter methylation (values 1.7 and 0.22 respectively). Nevertheless, the intra-sample correlation between the ATAC-seq and DNA methylation for the vtRNAs is between -0.24 and -0.78 (see rs-values in Table 1 and Supplementary Figure 2), suggesting that regardless of the relatively smaller average effect of DNA methylation on vtRNA1-3 promoter accessibility, all the vtRNAs are regulated by DNA

methylation to some extent (Table 1). In addition, the CpG DNA methylation negatively correlates with ATAC-seq values in the 500bp of the promoters of the four vtRNAs (Table 1 and Supplementary Figure 2). The strength of the correlation for each vtRNA is higher for the two vtRNAs that have a broader spectrum of DNA methylation, i.e. vtRNA1-2 and vtRNA2-1 (rs = -0.74 and rs = -0.78 respectively) (Table 1 and Supplementary Figure 2B and 2D). Meanwhile, vtRNA1-1 and vtRNA1-3 promoters, which have narrower range of DNA methylation (vtRNA1-1 has also a small range of chromatin accessibility) present a smaller association between both values (rs = -0.24 and rs = -0.54 respectively) (Table 1 and Supplementary Figure 2A and 2C). Technical differences in ATAC-seq and DNA methylation array approaches, as well as naturally occurring non-linear correlation between average DNA methylation and chromatin structure may account for these differences (Corces et al., 2018; Liu et al., 2018). The low ATAC-seq value of the vtRNA3-1P pseudogene (Ave. -1.2, 0.6 SD), represents a proof of concept of the analyses (Supplementary Figure 3 and Supplementary Table 1).

Table 1. Correlation between vtRNA promoters ATAC-seq and DNA methylation in the Pan-Cancer TCGA dataset.

	Average ± SD		Spearman correlation (ATAC-seq vs DNA methylation)	
vtRNA	Promoter ATAC-seq	Promoter DNA methylation	*Rs*	*p-value*
vtRNA1-1	4.1 ± 0.6	0.09 ± 0.07	-0.24	<0.0001
vtRNA1-2	2.9 ± 1.6	0.42 ± 0.20	-0.74	<0.0001
vtRNA1-3	1.7 ± 1.2	0.22 ± 0.15	-0.54	<0.0001
vtRNA2-1	2.5 ± 1.4	0.47 ± 0.21	-0.78	<0.0001

The Spearman correlation was calculated for the 329 primary tumors studied by ATAC-seq and DNA methylation.

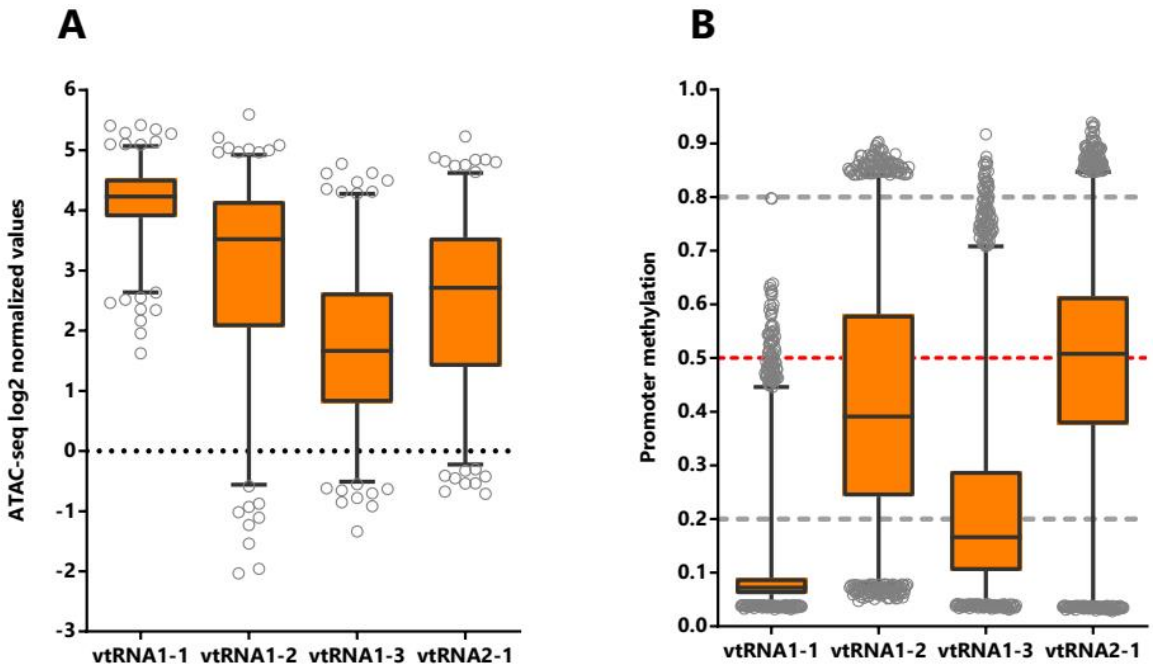

Figure 2. Chromatin accessibility and DNA methylation of the vtRNA promoters. Analysis of vtRNA 500pb promoter region of **A.** Average chromatin accessibility ATAC-seq values for the 385 primary tumors available at the Pan-Cancer TCGA dataset (23 tissues types) and **B.** Average DNA methylation beta-values for the 8403 primary tumors (32 tissues types). Dashed horizontal lines denote unmethylated (bottom gray, average beta-value ≤ 0.2), 50% methylated (middle red, average beta-value = 0.5) and highly methylated (top gray, average beta-value ≥ 0.8) promoter. The box plots show the median and the lower and upper quartile, and the whiskers the 2.5 and 97.5 percentile of the distribution.

Chromatin accessibility, DNA methylation and transcription factor binding at the four vtRNA promoters are correlated.

Aiming to investigate a possible co-regulation of vtRNA transcription, we determined the pairwise correlations in chromatin accessibility and DNA methylation between the four vtRNA promoters. We found that all pairs of vtRNAs, except vtRNA1-2 and vtRNA2-1, shown positive correlations in both datasets (Figure 3A and 3B) (rs-values 0.23-0.41 for ATAC-seq and rs-values 0.20-0.50 for DNA methylation). The unsupervised clustering of these epigenetic marks indicates that the three vtRNAs clustered at vtRNA1 locus (vtRNA1-1, vtRNA1-2 and vtRNA1-3), which are the vault particle associated vtRNAs, are more similar than vtRNA2-1 (Figure 3A and 3B).

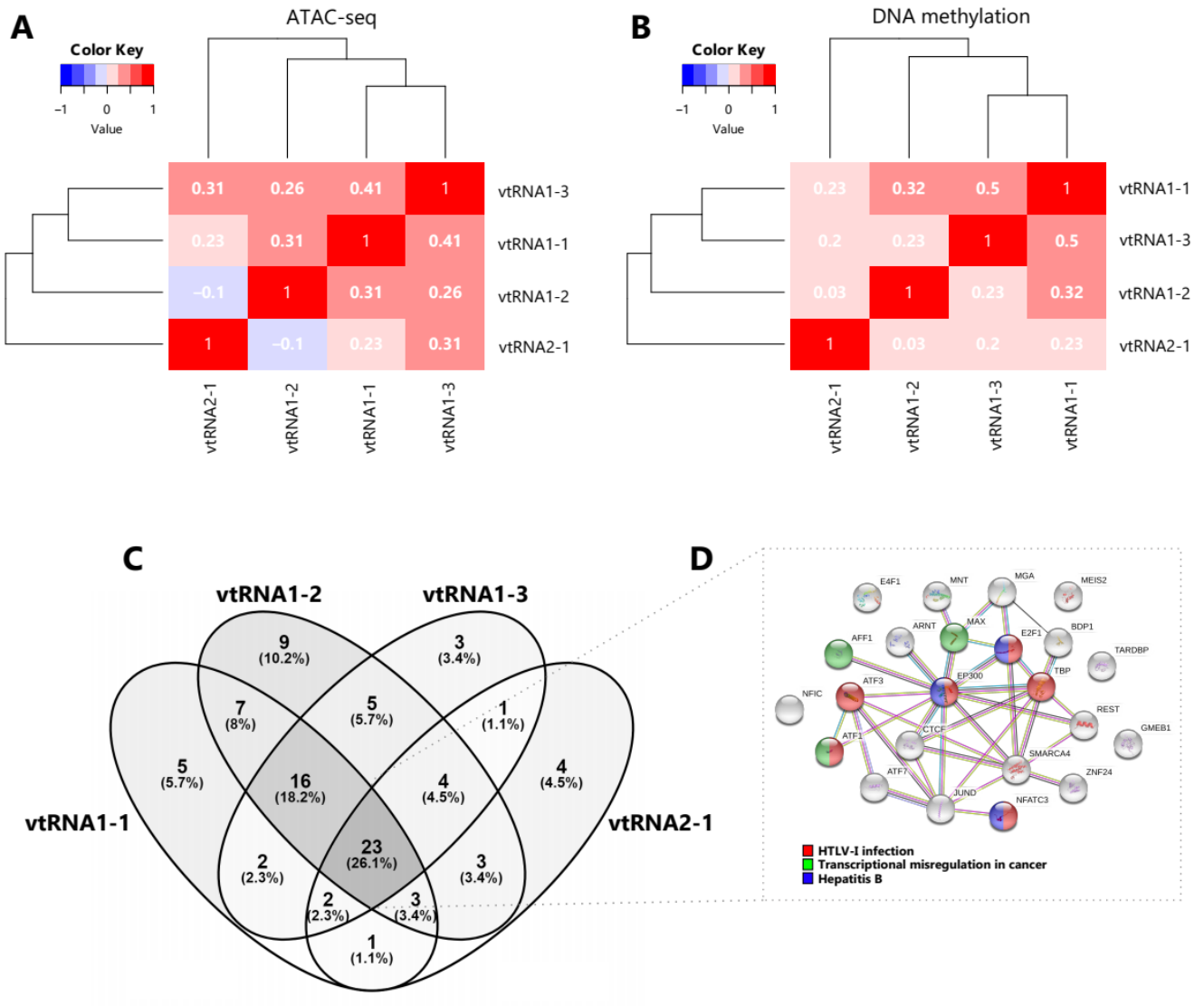

Figure 3. Comparative chromatin accessibility and transcription factor occupancy at the vtRNA loci. A-B Matrix of pairwise Spearman correlations (two-way hierarchical clustering distance measured by Euclidean and Ward clustering algorithms) of vtRNA 500pb promoter region for ATAC-seq data (385 primary tumors samples across 23 tissues) (A) and DNA methylation average beta-values data (8403 primary tumors samples across 32 tissues) (B). **C.** Venn diagram of transcription factors identified as ChIP-seq Peaks by ENCODE 3 project in the cell line K562 (Venny 2.1; https://bioinfogp.cnb.csic.es/tools/venny/index.html). The region for TFs assignment was defined as ±3000 pb from the vtRNA transcript sequence boundaries. **D.** Interaction cluster of the core 23 TFs common to all vtRNAs performed with STRING (Szklarczyk et al., 2017). The colored labels of the top 3 enriched KEGG pathway terms (FDR < 0.05) are indicated.

Given that the chromatin accessibility of a DNA region is partially controlled by transcription and chromatin remodeler's factors (Corces et al., 2018; Klemm et al., 2019), we analyzed transcription factors (TFs) occupancy at a ± 3000 pb region centered at each vtRNA gene. Since there is no such study of the TCGA samples, we investigated the CHIP-seq data of the K562

chronic myelogenous leukemia cell line, which has the richest TFs data at ENCODE dataset (Goldman et al., 2013). We observed that the 4 vtRNAs share a common core of 23 TFs (26%). The 3 members of the vtRNA1 cluster share 16 additional TFs (18%), reaching 39 common TFs (44%), while only 2-4 TFs with vtRNA2-1 (Figure 3C and 3D and Supplementary Table 2). We finally asked whether this common core of TFs is linked to a specific biological process. The STRING enrichment analysis of the core of 23 TFs common to all vtRNAs identified HTLV-I infection (ATF1, ATF3, E2F1, EP300, NFATC3, TBP), Hepatitis B (E2F1, EP300, NFATC3) and Transcriptional misregulation in cancer (AFF1, ATF1, MAX) as the top 3 enriched KEGG pathway terms (FDR < 0.05) (Figure 3C and Supplementary Table 2).

Taken together these findings indicate that the transcriptional activity of the vtRNAs is gene specific, being vtRNA1-1 the most accessible and possibly the most expressed. In addition, the data suggest that the regulatory status of the vtRNA promoters is coordinately controlled, and the three vtRNA1s are more co-regulated among themselves. Yet, the core of TFs shared by the vtRNAs is associated with viral infection and cancer related terms in the myeloid cell line K562.

The vtRNA promoters present gene and tissue specific patterns of chromatin accessibility in primary tumors.

In order to investigate the expression of vtRNAs in different tissues we analyzed the Pan-Cancer TCGA ATAC-seq data discriminating the tissue of origin. As expected, vtRNA1-1 has the highest promoter chromatin accessibility among tissues and the smallest variation (Figure 4A, Supplementary Table 1 and Supplementary Figure 1). Remarkably, low-grade glioma tumor samples (LGG) show a global reduction in chromatin accessibility at the 4 vtRNA promoters (Figure 4A). An opposite pattern is seen in adrenocortical carcinoma tissue (ACC), where the vtRNAs have the highest concerted chromatin accessibility (Figure 4A). Individually, vtRNAs promoter accessibility is maximum and minimum in THCA (4.7) and LGG (3.3) for vtRNA1-1, ACC (4.2) and LGG (0.29) for vtRNA1-2, ACC (3.7) and LGG (0.24) for vtRNA1-3 and KIRC (4.2) and LGG (1.0) for vtRNA2-1 (Figure 4A). VtRNA3-1P reaches a maximum of promoter chromatin accessibility in Testicular Germ Cell Tumors (TGCT) (0.65) with an extremely low average ATAC-seq value and its minimum in PRAD (-1.5) (Supplementary Figure 3C). Remarkably, although vtRNA1-1 and vtRNA1-3 have the highest and lowest promoter

accessibility in the majority of tissues respectively, vtRNA1-2 and vtRNA2-1 are the most variable (vtRNA1-1 SD = 0.34, vtRNA1-2 SD = 1.4, vtRNA1-3 SD = 0.75 and vtRNA2-1 SD = 0.78) (Figure 4A). In addition, in 12 tissues the chromatin accessibility of vtRNA1-2 is higher than vtRNA2-1 (57%) whereas in 9 tissues the chromatin accessibility of vtRNA1-2 is lower than vtRNA2-1 (43%) (Figure 4A).

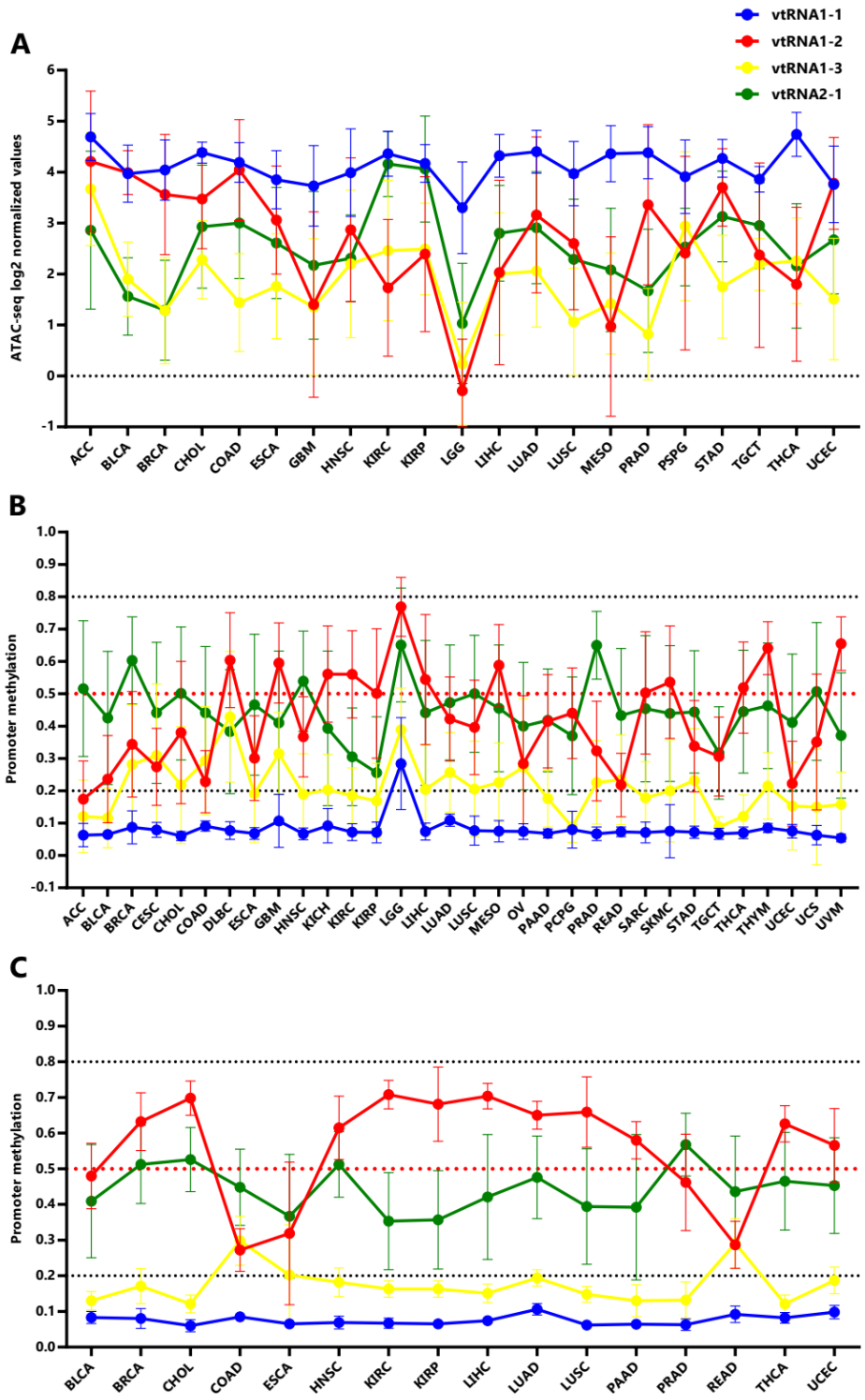

Figure 4. Chromatin accessibility and DNA methylation of the vtRNA promoters in tumor and normal tissues. A. ATAC-seq values for vtRNA promoters in 21 primary tumor tissues. **B.** Average beta-values of promoter DNA methylation for vtRNAs in 32 primary tumors tissues. **C.** Average beta-values of promoter DNA methylation for vtRNAs in 16 normal adjacent tissues. For **A**, **B** and **C**, the charts show the average value and standard deviation of each vtRNAs for the tissues with at least five samples available at Pan-Cancer TCGA dataset.

Using the vtRNAs promoter DNA methylation data, we extended the analysis to 32 primary tumor tissues, incorporating nine more tissues than ATAC-seq samples (DLBC, KICH, OV, PAAD, READ, SARC, THYM, UCS, UVM) (Figure 4B, Supplementary Figure 1) and 16 normal adjacent tissues (Figure 4C, Supplementary Figure 1). Again, the DNA methylation profile mirrors the chromatin accessibility in the individual tissue types (Figure 4). Remarkably, the association between the average vtRNA promoter chromatin accessibility and DNA methylation of the vtRNA1 cluster in each tissue type is higher than that observed for the average of all tissues (vtRNA1-1 rs = -0.28, vtRNA1-2 rs = -0.90 vtRNA1-3 rs = -0.74 and vtRNA2-1 rs = -0.58) (Table 1 and Supplementary Figure 4). The opposite finding for vtRNA2-1 may be explained by the impact of the previously recognized chromatin polymorphisms in the locus (Silver et al., 2015), which may prevail over the tissue specific variation for this gene.

In primary tumor tissues, promoter DNA methylation of vtRNA2-1 is higher than vtRNA1-2 in 17 tissues (53%) and the opposite is observed in 15 tissues (47%) (Figure 4B), while in normal tissues, promoter DNA methylation of vtRNA2-1 is higher than vtRNA1-2 in 4 tissues (25%) and the opposite is observed in 12 tissues (75%) (Figure 4C), indicating that although vtRNA1-2 is more methylated in normal samples, vtRNA2-1 gains methylation in neoplastic tissue, becoming more methylated than vtRNA1-2 (in 7 tissue types: BLCA, BRCA, CHOL, HNCSC, LUAD, LUSC, UCEC). Indeed, the Fisher's exact test identifies a mirrored profile of chromatin accessibility between normal (4 tissues with high vtRNA1-2 and 12 tissues with high vtRNA2-1 from 16 total tissues) and tumor tissues (17 tissues with high vtRNA1-2 and 15 tissues with high vtRNA2-1 from 32 total tissues) for vtRNA1-2 and vtRNA2-1 (p-value = 0.07). Despite this deregulation in transformed tissues, we wondered if the tissue specific differences in vtRNA promoters were explained by their pre-existing status in the normal tissues. The correlation among average vtRNA promoter DNA methylation in normal and tumor tissues suggest that the variation in chromatin accessibility among tissue types is already established in the normal tissue counterparts (vtRNA1-1 rs = 0.53, vtRNA1-2 rs = 0.84, vtRNA1-3 rs = 0.47 and vtRNA2-1 rs = 0.75, Supplementary Figure 5).

VtRNA promoter´s DNA methylation is associated with tumor stage and tissue of origin.

The assessment of differential vtRNA expression from normal to tumor condition at the TCGA cohort can only be performed using DNA methylation dataset since no ATAC-seq analyses were performed in the normal tissues. The average beta-value of CpG sites in the 500bp vtRNAs promoter of normal and tumor tissue evidenced gene specific patterns of deregulation in neoplastic tissues (Figure 5). As depicted in Figure 4, vtRNA1-1 and vtRNA1-3 promoter DNA methylation and chromatin accessibility is low and high tissue-wide respectively, in both normal and tumor tissues (yet, there are highly methylated tumor outliers as LGG, that lack normal counterpart) (Figure 4 and Figures 5A and 5C). Conversely, vtRNA1-2 and vtRNA2-1 revealed significant differences in average promoter DNA methylation among the tissue categories (Figures 5B and 5D). In agreement with previous results the methylation of vtRNA1-2 promoter decreases from normal to tumor samples, while vtRNA2-1´s increases (Figures 5B and 5D and Figure 4).

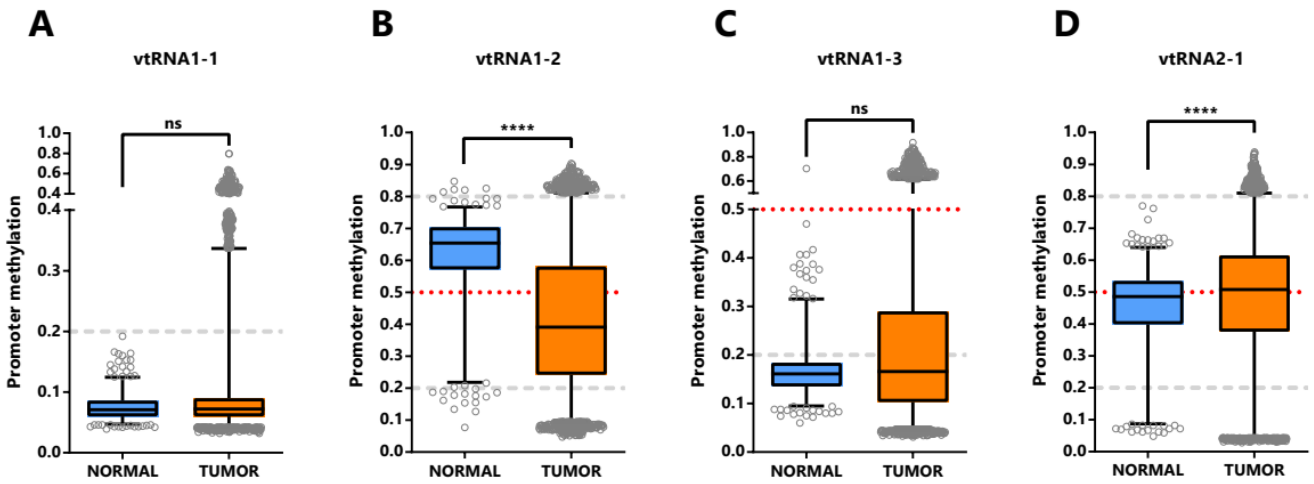

Figure 5. Promoter DNA methylation of vtRNAs in Normal and Tumor tissues of Pan-Cancer TCGA dataset. Average beta-values of promoter DNA methylation of vtRNA1-1 (**A**), vtRNA1-2 (**B**), vtRNA1-3 (**C**) and vtRNA2-1 (**D**), assessed in 746 normal and 8403 tumor tissues respectively. The box plots show the median line and lower and upper quartile and the whiskers the 2.5 and 97.5 percentile. Horizontal grey striped and red dotted lines denote unmethylated (average beta-value ≤ 0.2), 50% methylated (average beta-value = 0.5) and highly methylated (average beta-value ≥ 0.8) promoters. One-way ANOVA multiple test analysis with Sidak as posthoc was performed. **** p-value < 0.0001.

We next asked whether the promoter status of the vtRNAs is deregulated during the normal and tumor transformation of different tissue types. This comparison was restricted to the 16 tissues

with normal samples (with data of at least five samples, Supplementary Figure 1, Supplementary Table 1 and Figure 6). The results revealed that vtRNA1-1 is globally unmethylated in normal and tumor from different tissue origins, but presents small but statistically significant changes in 4 tissue types (OG profile in BLCA, THCA UCEC and TSG in LUSC), whose biological impact remains to be determined (Figure 6A). Similarly, vtRNA1-3 is globally unmethylated, showing larger variability and significant upregulation in BRCA and PRAD, compatible with a TSG function (TSG trends for LIHC p-value = 0.08 and LUSC p-value = 0.09, Figure 6C). In agreement with the literature, vtRNA2-1 presents a TSG pattern of deregulation in PRAD, LUSC and BRCA (Cao et al., 2013; Fort et al., 2018; Romanelli et al., 2014), and an OG pattern in KIRP that has not been previously described (Figure 6D). Finally, a statistically significant dysregulation of vtRNA1-2 promoter DNA methylation across almost all cancer types (13 out of 16 tissues analyzed) poses it as a candidate OG in cancer (Figure 6B).

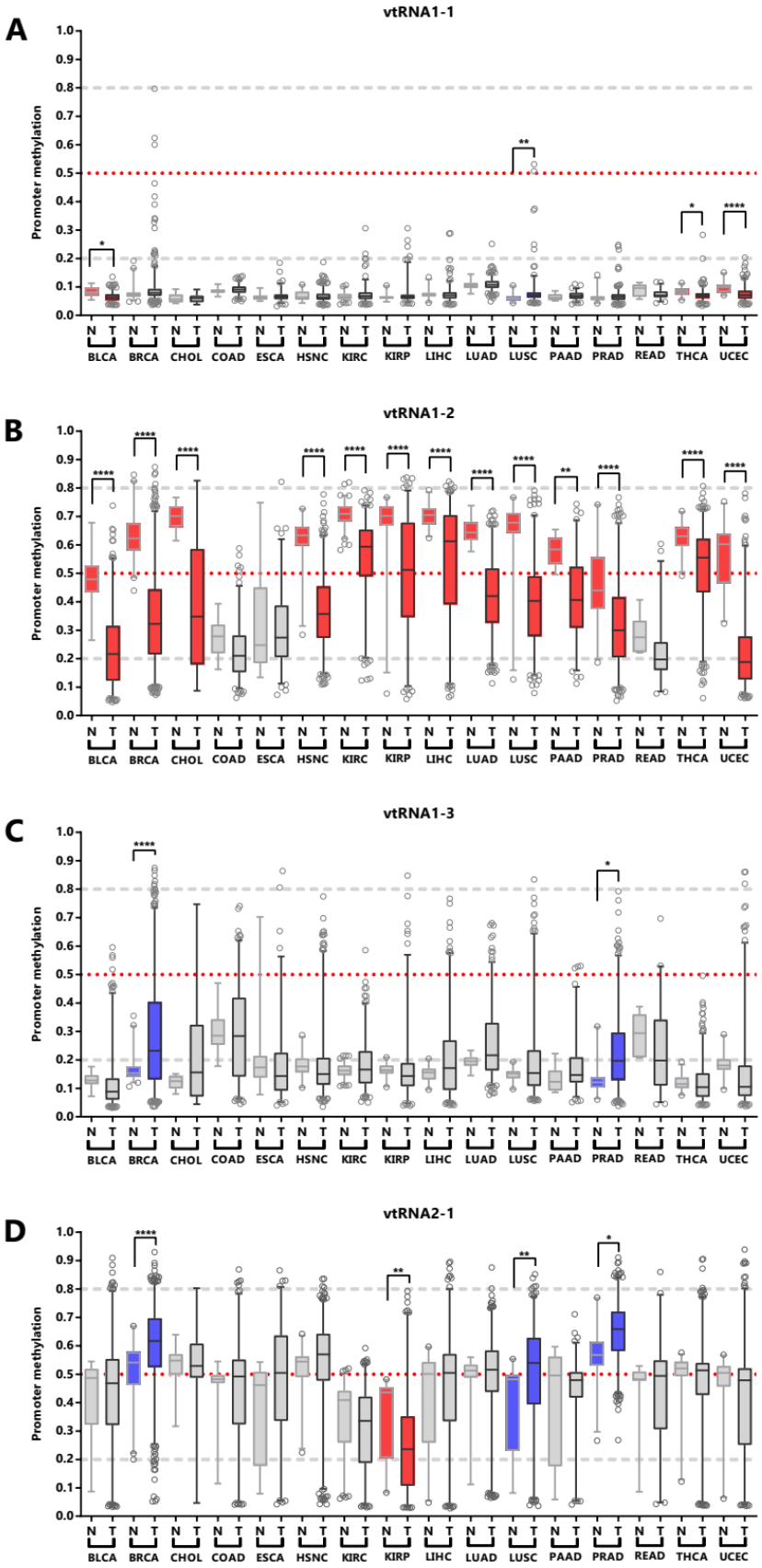
A
vtRNA1-1
Promoter methylation
B
vtRNA1-2
Promoter methylation
C
vtRNA1-3
Promoter methylation
D
vtRNA2-1
Promoter methylation
N T
BLCA BRCA CHOL COAD ESCA HSNC KIRC KIRP LIHC LUAD LUSC PAAD PRAD READ THCA UCEC

Figure 6. VtRNA promoters DNA methylation in Normal vs. Tumor samples. Average beta-values of promoter DNA methylation for vtRNA1-1 (**A**) vtRNA1-2 (**B**), vtRNA1-3 (**C**) and vtRNA2-1 (**D**). Acronyms indicate the tissue condition (normal (N) and tumor (T)). *Blue* and *red colors* indicate an increase or reduction in promoter methylation in tumor vs their normal tissues counterparts, compatible with a TSG and OG function respectively. The box plots show the median and the lower and upper quartile, and the whiskers the 2.5 and 97.5 percentile of the distribution. Horizontal, lines denote the methylation level of the promoters: grey striped bottom and top for unmethylated (average beta-value ≤ 0.2) or highly methylated (average beta-value ≥ 0.8) respectively, and red dotted for 50% methylated (average beta-value = 0.5)) promoters. One-way ANOVA multiple test analysis with Sidak as posthoc was performed. * p-value < 0.05; ** p-value < 0.01; **** p-value < 0.0001.

Overall, the data shows different DNA methylation changes in the vtRNAs promoters upon malignant transformation in several tissues. In addition, the deregulation of each vtRNA occurs mostly in a gene specific direction, where vtRNA1-2 has an OG like epigenetic de-repression while vtRNA2-1 (and to a lesser extent vtRNA1-1, vtRNA1-3) has a TSG like repressive methylation in tumor tissues.

High chromatin accessibility at the promoter of vtRNA1-1, vtRNA1-3 and vtRNA2-1 is associated with low patient overall survival.

Seeking for a possible clinical significance of the chromatin accessibility changes of the vtRNA promoters, we studied its association with the overall survival of patients (Figure 7 and Supplementary Table 3). The analysis of patients stratified by vtRNA promoter accessibility quartiles did not show differences in overall survival (data available at Supplementary Table 3). However, a significantly lower patient survival probability when patient tumors have lower promoter DNA methylation is observed for vtRNA1-1 (p-value = 0.003), vtRNA1-2 (p-value = 0.004) and vtRNA2-1 (p-value = 0.002) (patient stratified in quartiles of the promoter DNA methylation cohort values, Figure 7). Therefore, a lower promoter DNA methylation of vtRNA1-1, vtRNA1-2 and vtRNA2-1, a surrogate of their high expression, might be associated with poor patient overall survival cancer-wide.

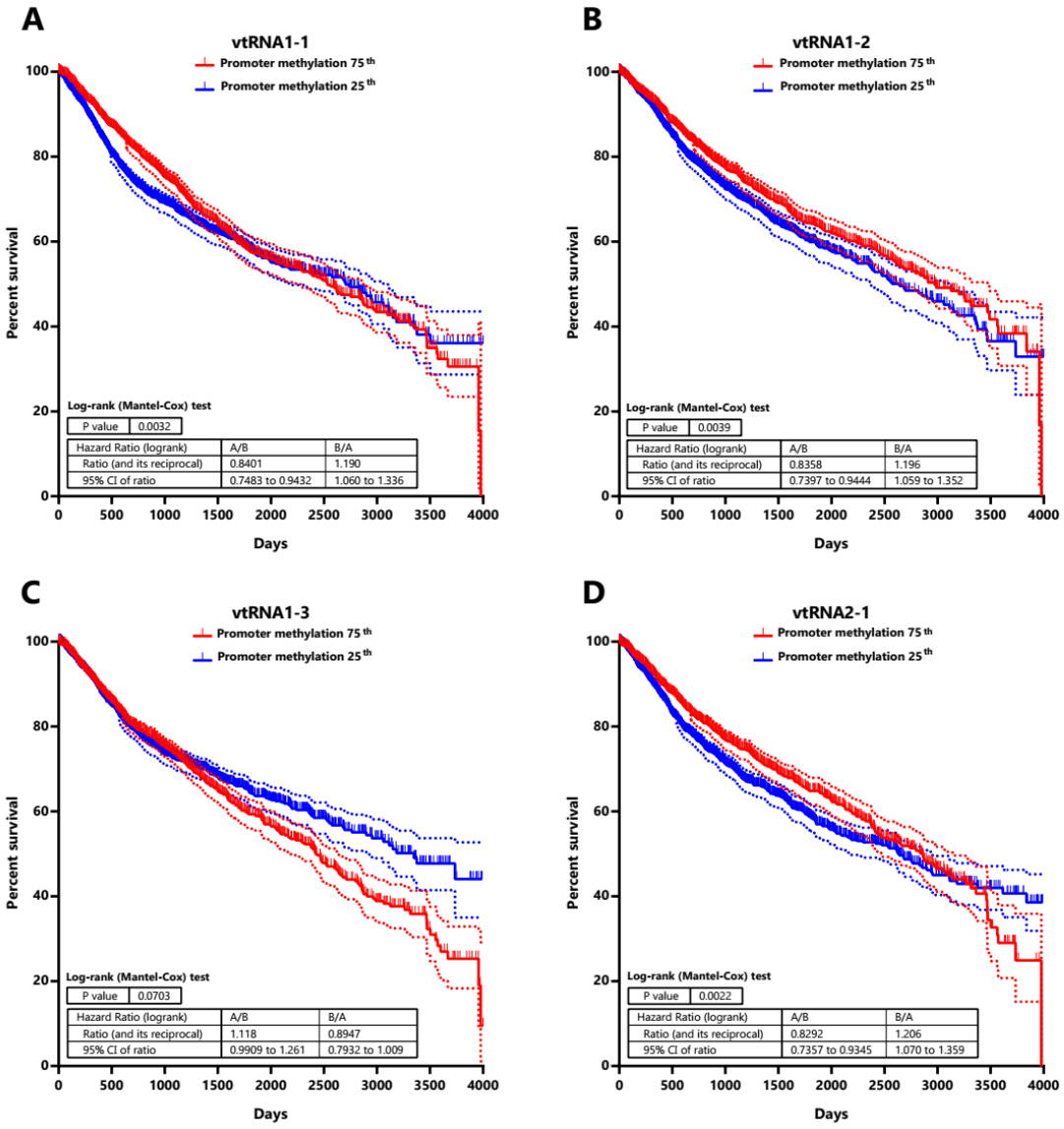

Figure 7. Patient Overall survival relative to vtRNA promoters DNA methylation status in Pan-Cancer TCGA dataset. Kaplan-Meier curves of overall patient survival probability over the time (4000 days) discriminating the primary tumors into two cohorts with relatively higher (75th) and lower (25th) DNA methylation at each vtRNA promoter. Promoter DNA methylation data of the 8060 primary tumors was used to stratify the patients in two quartiles, based on the expression of vtRNA1-1 (**A**) vtRNA1-2 (**B**), vtRNA1-3 (**C**) and vtRNA2-1 (**D**). Patient survival probability of the two groups was analyzed using Log-rank (Mantel-Cox) test. The dotted lines represent the 95% confidence interval for each curve.

Genome-wide chromatin accessibility correlations with vtRNA promoters reveals their link to specific cancer related functions.

Seeking to get insight into the function of the vtRNAs from their transcription regulatory marks, we searched for the genes co-regulated at chromatin level. We calculated the correlation of the ATAC-seq promoter values of each vtRNA and all the individual genes in the 385 primary tumor cohort and selected those showing a Spearman correlation rs ≥ 0.4. Using STRING software analysis, we then investigated their connection with Biological Process categories and KEGG pathways (Szklarczyk et al., 2017). A few enriched terms for the genes correlated with vtRNA1-2, vtRNA1-3 and vtRNA2-1 is identified (FDR < 1×10^{-3}) (Supplementary Table 4). The 191 protein coding genes correlated with vtRNA1-2 are enriched in the Biological Process "Epithelial cell differentiation" (FDR < 1×10^{-4}) (Supplementary Table 4). Meanwhile, the 353 protein coding genes correlated with vtRNA2-1 are enriched in the Biological Processes "Immune system process", "Inflammatory response" and "Immune response" (FDR < 1×10^{-5}) and the KEGG pathways term "Cytokine-cytokine receptor interaction" (FDR < 1×10^{-4}) (Supplementary Table 4). The only 6 protein coding genes correlated with vtRNA1-3 are enriched in the "Thyroid cancer" KEGG pathway term (FDR < 1×10^{-4}). Remarkably, although STRING analysis of the vtRNA1-1 associated 37 protein coding genes did not find enriched process or pathways, 36 of the 37 correlated genes are located at chromosome 5q region. Using the Cluster Locator algorithm (Pazos Obregón et al., 2018), we found a statistically significant non-random clustering behavior for the chromosomal location of the genes co-regulated with vtRNA1-1 (p-value < $1x10^{-10}$). Indeed, when the analysis was extended to 174 protein coding genes with Spearman correlation rs ≥ 0.3, 140 genes of 174 were situated at chromosome 5 (p-value < $1x10^{-10}$). These genes are positioned in particular regions at chr5q31, chr5q35, chr5q23, chr5q14, chr5q32, chr5q34 (FDR < $1x10^{-4}$) (Kuleshov et al., 2016) (Supplementary Table 4). We did not find a similar phenomenon for the other 3 vtRNAs. In summary, vtRNA1-3, vtRNA1-2 and vtRNA2-1 transcription may be co-regulated with genes belonging to specific biological processes located elsewhere, while vtRNA1-1 transcription may be controlled by a locally specialized chromatin domain at chromosome 5q region lacking apparent functional relatedness.

Immune Subtypes associated with the vtRNAs profile.

Taking into account that vtRNAs have been previously related to the immune response (Golec et al., 2019; Li et al., 2015; Nandy et al., 2009), and that we found an association of vtRNA2-1 with immune related terms, we sought to investigate a putative relation between the vtRNAs expression and the six Immune Subtypes defined by Thorsson et al. (Thorsson et al., 2018), compiled at Pan-Cancer TCGA (Supplementary Table 5). These six Immune Subtypes are named because of the foremost immune characteristic, comprising wound healing, IFN-g dominant, lymphocyte depleted, inflammatory, immunologically quiet and TGF-b dominant types (Thorsson et al., 2018). As was expected, mirrored patterns were observed for promoter ATAC-seq and DNA methylation data of the six groups (Figure 8). The immunologically quiet subtype shows a concerted shutdown of all vtRNA promoters (Figure 8), which is largely composed by LGG samples showing low vtRNA ATAC-seq and high promoter methylation average values in LGG tumors (Figures 4A and 4B). The immunological quiet subtype exhibits the lowest leukocyte fraction (very low Th17 and low Th2) and the highest macrophage:lymphocyte ratio (high M2 macrophages) (Thorsson et al., 2018). The remaining subtypes present a similar vtRNA profile except for the inversion of vtRNA1-2/vtRNA2-1 accessibility ratio, which is higher than 1 for the wound healing and IFN-g dominant subtypes while is lower than 1 for the lymphocyte depleted and inflammatory subtypes (Figure 8A). As expected, a mirrored pattern was observed for vtRNA1-2 and vtRNA2-1 at DNA methylation data (Figure 8B). Since the wound healing and IFN-g dominant subtype have high proliferation rate opposite to the lymphocyte depleted and inflammatory subtypes (Thorsson et al., 2018), we evaluated the correlation between vtRNA1-2 and vtRNA2-1 chromatin status and proliferation rate or wound healing status defined by Thorsson et al. (Supplementary Table 5) (Thorsson et al., 2018). A negative correlation between vtRNA1-2 promoter DNA methylation and the proliferation rate ($rs = -0.44$) and wound healing features of the tumors is revealed ($rs = -0.48$) (Supplementary Table 5). These findings suggest that vtRNA transcriptional regulation may be associated with tumor immunity.

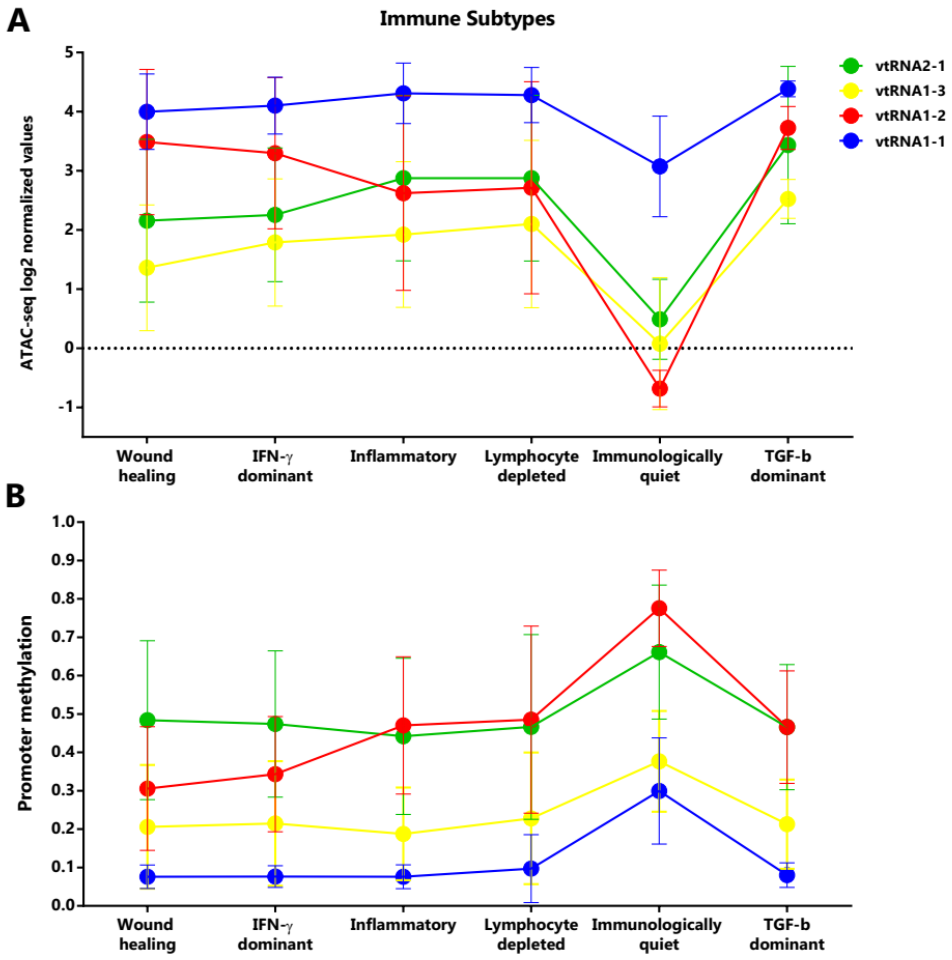

Figure 8. Chromatin accessibility and DNA methylation of vtRNA promoters in the Six Immune Subtypes analyzed in the PANCAN TCGA dataset. A. ATAC-seq values expressed as log2 normalized values for vtRNA promoters grouped in six Immune Subtype: wound healing (105 samples), IFN-g dominant (93 samples), inflammatory (110 samples), lymphocyte depleted (43 samples), immunologically quiet (9 samples), TGF-b dominant (4 samples). **B.** DNA methylation average beta-values for vtRNA promoters grouped in six Immune Subtype: wound healing (1963 samples), IFN-g dominant (2137 samples), inflammatory (2126 samples), lymphocyte depleted (933 samples), immunologically quiet (383 samples), TGF-b dominant (151 samples) (Thorsson et al., 2018). The charts show the average and standard deviation for each vtRNA promoter in each Immune Subtype group.

Discussion

Although important insight into the vtRNA function has been recently gained, the landscape of vtRNA expression in human tissues and cancer was unknown, perhaps for the absence of vtRNA data in transcriptomic studies. Here we used ATAC-seq and methylation arrays data from the

Pan-Cancer TCGA consortium (Weinstein et al., 2013), as surrogate variables to uncover the expression of vtRNAs across multiple cancer types. A limitation of our study is its blindness to post-transcriptional controls of vtRNA expression, such as RNA processing, transport, localization and/or stability. Indeed, there is evidence of vtRNA transcript regulation via RNA methylation by NSUN2, or via its association to other proteins like DUSP11, DIS3L2, SSB, SRSF2 and DICER (Burke et al., 2016; Hussain et al., 2013; Kickhoefer et al., 2002; Łabno et al., 2016; Persson et al., 2009; Sajini et al., 2019). Nonetheless, the chromatin status of the vtRNA promoters has been correlated with the expression of their transcripts in several reports (Ahn et al., 2018; Fort et al., 2018; Helbo et al., 2015, 2017; Lee et al., 2014a, 2014b; Park et al., 2017b; Sallustio et al., 2016; Treppendahl et al., 2012). These evidences unequivocally stand for the use of chromatin structure as a suitable proxy for vtRNA expression.

An integrated genomic view of the regulatory features of the vtRNA genes compiled in UCSC genome browser indicates that the 4 vtRNAs have chromatin signs of active transcription in different cell lines and defines a proximal promoter regulatory region of approximately 500pb (Nikitina et al., 2011; Vilalta et al., 1994). High resolution chromatin accessibility mapping studies by NOMe-Seq of the vtRNA promoters in cell lines validate this assumption (Helbo et al., 2017). Particularly, vtRNA2-1 is singular for being immersed in a CpG island, for lacking the TATA box, DSE or PSE elements characteristic of the others vtRNA promoters, and for bearing a cAMP-response (CRE) element (Canella et al., 2010; Helbo et al., 2017; Nandy et al., 2009). Since ATAC-seq approach is currently the best high throughput method to determine the chromatin accessibility of a DNA region directly (Chen et al., 2016; Sun et al., 2019; Tsompana and Buck, 2014), we interrogated the ATAC-seq data of TCGA samples as a surrogate marker of vtRNA expression (Corces et al., 2018). Although DNA methylation is a less direct and less accurate measurement of chromatin accessibility compared to ATAC-seq, 25 times more TCGA samples have been analyzed by DNA Methylation Arrays, including matched normal tissues samples, thus this dataset is of great significance for the current study. Our analyses revealed that vtRNA1-1 has accessible chromatin and small variation in all the evaluated tissues, which is consistent with its identity as the ancestor vtRNA gene and its significance as the major RNA component of the ubiquitous vault particle (Stadler et al., 2009; van Zon et al., 2001). In addition, vtRNA1-2, vtRNA1-3 and vtRNA2-1, have lower chromatin accessibility at their promoters and

a larger variation among the samples. As expected, the average DNA methylation assessed by microarrays is negatively correlated with the chromatin accessibility assessed by ATAC-seq. Therefore, the landscape of vtRNA chromatin status was corroborated by both approaches. Yet, the low chromatin accessibility of vtRNA1-3 promoter is not reflected by a concomitant high DNA methylation, suggesting that additional regulatory features of this gene, acting in trans or cis, play a major influence in its chromatin structure. As was reported by Helbo et. al. using NOMe-seq assay (Nucleosome Positioning), the chromatin at vtRNA1-3 may be poised for transcription, and still require TFs to achieve physiological levels of transcription (Helbo et al., 2017).

The relative abundance of the 4 vtRNAs determined in the current study has been previously observed in various cell lines, including H157, H1299, CRL2741, WI-38 and NTera-2 (Lee et al., 2011), HSC CD34+, HL60 (Helbo et al., 2015), T24, colorectal RKO, human diploid fibroblasts IMR90 (Helbo et al., 2017) and MCF7 (Chen et al., 2018). Yet, others found different levels of the vtRNAs in MCF7, SW1573, GLC4, 8226, KB, SW620, MCF-7, HeLa, HEK-293 and L88/5 (van Zon et al., 2001), CBL, BL2 and BL41 (Nandy et al., 2009), EBV-negative Burkitt's lymphoma cell lines and A549 (Li et al., 2015) and in LNCaP, PC3, DU145, RWPE-1, HEK, HeLa and MCF-7 (Stadler et al., 2009) cell lines, suggesting that the expression of vtRNAs may differ in laboratory cell lines compared to tissues. Alternatively, the methods used to quantify the vtRNAs are not comparable among the studies.

Seeking to investigate regulatory connections between the vtRNAs as a valuable tool to study their function, we determine the pairwise correlations between the promoters of the vtRNAs. The positive correlations found are compatible with a coordinated transcriptional control of the vtRNAs, that is greater for the three members of the vtRNA1 cluster (specially vtRNA1-1 and vtRNA1-3). The exception is the pair vtRNA1-2 and vtRNA2-1, whose chromatin accessibility and promoter methylation are not linked in the cohort and are indeed negatively associated in some comparisons.

As an alternative approach to investigate the vtRNA transcriptional co-regulation, we analyzed transcription and chromatin remodeling factors associated with their proximal promoter region. In agreement with their higher chromatin correlation, the vtRNA1 cluster have a larger core of

common TFs (39) in comparison with vtRNA2-1 (23 TFs). The divergence of the transcriptional control of vtRNA2-1 was previously recognized given its unique regulatory elements and the complex developmental methylation it undergoes (Canella et al., 2010; Carpenter et al., 2018; Helbo et al., 2017; Nandy et al., 2009). Remarkably, the 23 TFs common to all vtRNAs are related to viral infections and cancer. The upregulation of the four vtRNAs upon viral infection has been reported for several viruses, so it is possible that this core of TFs participate in the coordinated expression of vtRNA during viral infection and related responses (Amort et al., 2015; Li et al., 2015; Nandy et al., 2009). These TFs regulate cell cycle and translational arrest as well as the inhibition of host innate immune response (Attar and Kurdistani, 2017; Ertosun et al., 2016; Horsley and Pavlath, 2002; Jean et al., 2000; Persengiev and Green, 2003; Rohini et al., 2018). Since these processes are also hallmarks of cancer, the dysregulation of the normal function of vtRNAs in viral response may provide a selective advantage for cancer cell to overcome the many sources of stress faced during neoplastic evolution. If that holds true, the core vtRNA TFs may be co-opted in the malignant context to tune vtRNA expression favoring tumor progression. In agreement with that hypothesis, ATF1 and ATF3 were associated with CREB response and increased cell viability (Persengiev and Green, 2003). Likewise, Golec et. al. 2019 showed that altered levels of vtRNA2-1 modulate PKR activation and consequently altered the levels of CREB phosphorylation during T cell activation, which is a prerequisite for IFN-g activity (Golec et al., 2019). Furthermore, E2F1, a cell cycle regulator, was described as a direct transcriptional regulator of vtRNA2-1 in cervical cancer cells (Li et al., 2017). Moreover, it was shown that MYC binding to vtRNA2-1 promoter raises its expression and could be the explanation to the increased levels of vtRNA2-1 in some tumors (Park et al., 2017b). Similarly, TGFB1 provokes the demethylation of vtRNA2-1 promoter and consequently increases its expression in ovarian cancer (Ahn et al., 2018).

Due to its importance for cancer biology, vtRNA2-1 transcriptional regulation was recently more investigated (Yeganeh and Hernandez, 2020). Various studies reported tissue specific roles of vtRNA2-1 in normal (Golec et al., 2019; Lee et al., 2019a; Miñones-Moyano et al., 2013; Sallustio et al., 2016; Suojalehto et al., 2014) and cancer tissue (Ahn et al., 2018; Fort et al., 2018; Hu et al., 2017; Im et al., 2020; Jeon et al., 2012a; Kunkeaw et al., 2012; Lee et al., 2011; Lee, 2015; Lee et al., 2016, 2014a, 2014b; Lei et al., 2017; Li et al., 2017; Ma et al., 2020; Treppendahl et

al., 2012) and epigenetic alterations of the locus have been described in different malignancies (Ahn et al., 2018; Cao et al., 2013; Fort et al., 2018; Helbo et al., 2015, 2017; Joo et al., 2018; Lee et al., 2014a, 2014b; Park et al., 2017b; Romanelli et al., 2014; Treppendahl et al., 2012). Meanwhile, except for Kirsten Grønbæk group´s contributions on the chromatin characterization of vtRNA1-3 and vtRNA1-2 promoters (Helbo et al., 2015, 2017), little is known about the transcriptional regulation and expression of the other vtRNAs. Likewise, to our knowledge, the global landscape of vtRNA expression across different cancer types has not been investigated. Our study shows that, except for vtRNA1-1, which has a high promoter chromatin accessibility and low DNA methylation in all the tissues, the other vtRNA promoters exhibit different levels of chromatin accessibility and DNA methylation among the tissue types. The relative status of the chromatin in different tissues is accurately mirrored by both approaches in the tissues examined by ATAC-seq and Illumina DNA methylation arrays. Interestingly, the same analysis performed in the normal tissue samples reveals that the tissue specific variation in DNA methylation of vtRNA promoters in the neoplastic tissues is already established in their normal tissue counterparts, indicating that the regulation of vtRNA expression is tuned during normal development and cell differentiation.

While there is no apparent concerted modulation of the chromatin accessibility of the vtRNA promoters in most tissues, ACC and LGG tumors seem to be the exception. Concordantly, a global hypomethylation of malignant ACC tumors (Legendre et al., 2016; Rechache et al., 2012), and an aberrantly methylation processes associated to altered DNMTs activity in LGG tumors were reported (Nomura et al., 2019). However, more research is necessary to understand the molecular basis of these observations.

The differential expression of the vtRNAs from normal to primary tumor tissues revealed different patterns depending on tissue origin. The average DNA methylation of the vtRNA1-1 and vtRNA1-3 promoters is not significantly deregulated, whereas vtRNA1-2 and vtRNA2-1 are decreased and increased respectively in tumor tissues. The latter finding favors a candidate OG and TSG function of vtRNA1-2 and vtRNA2-1 in cancer respectively. Indeed, the epigenetic repression of vtRNA2-1 was previously reported by Romanelli et al. in BLCA, BRCA, COAD and LUSC analyzing the same data from TCGA (Romanelli et al., 2014). Furthermore, functional

studies in LUSC, PRAD, ESCA and AML provided experimental support to that hypothesis (Cao et al., 2013; Fort et al., 2018; Lee et al., 2014a; Treppendahl et al., 2012). Yet, vtRNA2-1 has been also proposed as an OG in ovarian, thyroid, endometrial, cervical and renal cancer (Ahn et al., 2018; Hu et al., 2017; Lee et al., 2016; Lei et al., 2017; Li et al., 2017; Yeganeh and Hernandez, 2020). In agreement with the functional data found by Lei et. al. (Lei et al., 2017), we found an epigenetic de-repression of vtRNA2-1 promoter DNA methylation in renal carcinoma (KIRP). Likewise, a closer look at THCA samples, shows an average decrease in the DNA methylation of vtRNA2-1 promoter that supports the OG function described in this tissue (Lee et al., 2016). Unfortunately, normal ovarian, cervical and endometrial tissues are not available at the TCGA. Finally, vtRNA1-2 has an oncogenic pattern of inferred expression between normal and tumor tissues for 13 of 16 tissues analyzed, raising a possible oncogenic function for this RNA.

Our study found also an association of DNA methylation at the promoter with a shorter overall survival for vtRNA1-1, vtRNA1-2 and vtRNA2-1. This is surprising for vtRNA2-1, since it has both TSG and OG roles and TSG compatible expression profiles in 3 cancer types, inferred by DNA methylation of its promoter in tumor vs normal tissues and the average promoter DNA methylation is increased in tumor compared to normal tissue. A higher impact of vtRNA2-1 expression in patient survival in the oncogenic context may justify this discrepancy. On the contrary, the association between vtRNA1-2 low promoter DNA methylation and low patient survival is in agreement with its OG expression in cancer. The lack of survival association with the ATAC-seq values may be due to the small number of patients.

VtRNA expression in individual cancer types, inferred from the epigenetic status of their promoters, has been associated with patient survival in several studies of vtRNA2-1, one of vtRNA1-3 and none for vtRNA1-1 or vtRNA1-2. Low methylation or high expression of vtRNA2-1 promoter was associated with good prognosis or overall survival in lung (Cao et al., 2013), esophageal (Lee et al., 2014a), prostate (Fort et al., 2018), AML (Treppendahl et al., 2012), gastric (Lee et al., 2014b) and liver (Yu et al., 2020). Conversely, a worse prognosis or overall survival association of vtRNA2-1 was reported in thyroid (Lee et al., 2016) and ovarian (Ahn et al., 2018). From these reports, only prostate (Fort et al., 2018) and gastric (Lee et al., 2014b)

studies used the TCGA data. Likewise, the methylation status of the vtRNA1-3 promoter associates with overall survival in the lower risk Myelodysplastic Syndrome patients (Helbo et al., 2015). Additionally, vtRNA1-1 and vtRNA1-2 correlate to chemotherapeutic resistance by direct interaction with drugs (doxorubicin, etoposide and mitoxantrone) and the modulation of vtRNA1-1 confirmed this finding in osteosarcoma cell lines (Gopinath et al., 2005, 2010; Mashima et al., 2008; van Zon et al., 2001). Furthermore, increased levels of vtRNA1-1 were associated with increased proliferation and chemoresistance due to GAGE6 induction in MCF-7 cells (Chen et al., 2018). Besides, Norbert Polacek group showed that vtRNA1-1 expression confers apoptosis resistance in several human cell lines (BL2, BL41, HS578T, HEK293, A549 and HeLa) and revealed it capacity to repressed intrinsic and extrinsic apoptosis pathway (Amort et al., 2015; Bracher et al., 2020). The later findings are in agreement with the lower patient survival associated with high levels of vtRNA1-1 expression cancer-wide observed in our analysis.

Seeking to get insights into the cancer related function of the vtRNAs we performed a genome wide search for genes co-regulated at the level of promoter chromatin accessibility. Remarkably, we identified immune and cytokine related terms for the genes co-regulated with vtRNA2-1. This association agrees with its proposed roles in innate immune modulation via PKR repression or OAS1 regulation and in cytokine production (Calderon and Conn, 2018; Golec et al., 2019; Lee et al., 2019b; Li et al., 2015). Furthermore, vtRNA2-1 has been associated with autoimmune disorders (Renauer et al., 2015; Weeding and Sawalha, 2018) and tumor engraftment in prostate cancer (Ma et al., 2020). This enrichment in viral infection pathways, together with the viral infection involvement of the core TFs common to all vtRNAs, reinforces the hypothesis of the re-utilization of a regulatory RNA induced upon viral response in favor of cancer development at upstream and downstream regulation steps. Additionally, we found a non-random clustering localization at chromosome 5 for genes co-regulated with vtRNA1-1. The chromosome arm 5q and regions chr5q31 and chr5q32-q33 were found frequently deleted in myelodysplastic syndrome (MDS) and acute myeloid leukemia (AML) (Fuchs, 2012; Treppendahl et al., 2012). Furthermore, the modulation of vtRNA2-1 and vtRNA1-3 was previously associated with human bone marrow CD34+ cells, AML and MDS (Helbo et al., 2015; Treppendahl et al., 2012). Yet,

our analysis points to vtRNA2-1 and vtRNA1-2, and to a lesser extent to vtRNA1-1 and vtRNA1-3, as the most relevant players across cancer types.

Support for the involvement of the vtRNAs in the immune responses in the context of cancer came from the association of their chromatin status with the immune subtype categories defined by Thorsson et al. (Thorsson et al., 2018). Our findings suggest a possible role of the vtRNAs in lymphocyte response in tumor samples, since the immunologically quiet subtype shows the lowest leukocyte fraction and vtRNAs promoter chromatin accessibility (Thorsson et al., 2018). Meanwhile, the vtRNA2-1 and vtRNA1-2 expression distinguishes 2 groups among the remaining 4 subtypes. The participation of vtRNA2-1 in the induction of the IFN-g and IL-2 expression in activated T cells through PKR modulation (Golec et al., 2019) goes in agreement with this hypothesis. Although the same study demonstrated that vtRNA1-1 expression was unchanged during T cell activation, it is remarkable that the 5q31-q33 region, comprising the vtRNA1 locus and chromatin co-regulated genes, encodes several cytokines that regulate the differentiation of Th1 and Th2 lymphocytes and has been linked with susceptibility to infections (Jeronimo et al., 2007; Lacy et al., 2000; Naka et al., 2009; Rodrigues et al., 1999). Furthermore, vtRNA2-1 levels were recently associated with macrophages M1/M2 fates in prostate PC3 cell line mice xenografts via TGF-b (Ma et al., 2020), pathways that define the six immune subtypes (Thorsson et al., 2018). Finally, we found that the proliferation rate and wound healing of the tumors are associated with the levels of vtRNA1-2 chromatin accessibility, which reinforces a OG role of vtRNA1-2 in cancer. Nonetheless, the participation of the vtRNAs in immune cells response inside the neoplastic niche needs to be further investigated.

Conclusion

Taken together our analysis reveals the pattern of chromatin accessibility and DNA methylation at the four vtRNA promoters, analyzed by tissue of origin in the TCGA cohort. The agreement between both dataset and previous related literature endorse the use of these variables as surrogates of the vtRNA transcripts expression. The four vtRNAs seem to be co-regulated at the transcriptional level, and TFs involved in viral infection are likely to take part in their coordinated transcription. The pattern of expression in normal vs tumor tissue and the association with cancer cell pathways and patient survival suggest that vtRNA2-1 and vtRNA1-2 are possibly the more

relevant contributors to cancer. The results favor tissue specific TSG and OG roles for vtRNA2-1, a still not investigated oncogenic role of vtRNA1-2 and a limited cancer driver effect of vtRNA1-1/3 in specific tissue types. Lastly, we uncovered new evidence linking the vtRNAs with the immune response, cell proliferation and overall survival in cancer, which guarantees further investigation.

Materials and Methods.

ATAC-seq data

The ATAC-seq data obtained by The Cancer Genome Atlas (TCGA) consortium were retrieved from UCSC Xena Browser (Goldman et al., 2020) on date 03/10/2018. It comprises the genomic matrix TCGA_ATAC_peak_Log2Counts_dedup_promoter with normalized count values for 404 samples (385 primary solid tumor samples across 23 tissues). As is described in UCSC Xena Browser to calculate the average ATAC-seq values a prior count of 5 was added to the raw counts, then put into a "counts per million", then log2 transformed, then quantile normalized; the result is the average value in the file (log2(count+5)-qn values) across all technical replicates and all biospecimens belonging to the same TCGA sample group. The gene promoter for ATAC-seq is defined as a region within -1000 to +100bp from the TSS site. Assignment of promoter peak to gene mapping information derives from the peak summit within the promoter region. Peak location information of the ATAC-seq values for 500 bp gene promoter regions was retrieved from the file TCGA_ATAC_Log2Counts_Matrix.180608.txt.gz. All the analyses were performed for tissues with at least five primary tumor samples (21 tissues), which resulted in the exclusion of CESC (2 primary tumor samples) and SKCM (4 primary tumor samples). Correlations between ATAC-seq and DNA promoter methylation were performed for the 329 primary tumors that are studied by both strategies (Supplementary table 1).

DNA methylation data

The DNA methylation data obtained from The Cancer Genome Atlas (TCGA) consortium was retrieved from UCSC Xena Browser (Goldman et al., 2020) on date 03/10/2018. It comprises the

normalized beta-value of DNA methylation obtained using Illumina Infinium Human Methylation 450 BeadChip arrays of the total (9149 samples) normal adjacent tissues (746 samples across 23 tissues) and primary solid tumors (8403 samples across 32 tissues) of the Pan-Cancer TCGA cohort. The current study is limited to solid tumors since only AML DNA methylation is available at the TCGA. All the analysis was performed for tissues with at least five samples. Normal adjacent tissue comprises 16 tissues, excluding CESC (2 samples), GBM (2 samples), PCPG (3 samples), SARC (4 samples), SKCM (2 samples), STAD (2 samples) and THYM (2 samples). Primary tumors comprise 32 tissues. The normalized promoter average beta-values (500 bp bin) comprise the following CpG sites for vtRNA1-1: cg12532653, cg05913451, cg14633504, cg16615348, cg25602765, cg13323902, cg18296956; for vtRNA1-2: cg21161173, cg13303313, cg00500100, cg05174942, cg25984996, cg11807153, cg15697852; for vtRNA1-3: cg23910413, cg19065177, cg02053188, cg01063759, cg07379832, cg07741016; and for vtRNA2-1: cg16615357, cg08745965, cg00124993, cg26896946, cg25340688, cg26328633, cg06536614, cg18678645, cg04481923 (Supplementary table 1).

Immune Subtypes data.

The data of Immune Subtypes defined by Thorsson et al. (Thorsson et al., 2018) is available at the Pan-Cancer TCGA and was retrieved from UCSC Xena Browser (Goldman et al., 2020) on date 03/10/2018 and from the supplementary material of Thorsson et al. article (Thorsson et al., 2018). ATAC-seq data of vtRNA promoters for the six Immune Subtype comprised a total of 364 samples: wound healing (105 samples), IFN-g dominant (93 samples), inflammatory (110 samples), lymphocyte depleted (43 samples), immunologically quiet (9 samples), TGF-b dominant (4 samples). DNA methylation average normalized beta-values of vtRNA promoters for the six Immune Subtype comprised 7693 samples including wound healing (1963 samples), IFN-g dominant (2137 samples), inflammatory (2126 samples), lymphocyte depleted (933 samples), immunologically quiet (383 samples), TGF-b dominant (151 samples) (Supplementary table 5).

Overall survival analysis.

The Kaplan Meier curve analysis was performed with software GraphPad Prism 6 using Log-ranked Mantel-Cox test. We analyzed the ATAC-seq normalized values and DNA methylation average normalized beta-values for vtRNA promoters and survival data until 4000 days (99% of data). The log-rank statistics was calculated for quartiles of vtRNAs promoter chromatin accessibility comparison groups (25^{th} and 75^{th}) (Supplementary Table 4).

Pathway enrichment and cluster chromosome localization analyses.

The genome wide correlation analysis of promoter chromatin accessibility (ATAC-seq normalized values) for each vtRNA in comparison with all the annotated genes was performed using the genomic matrix TCGA_ATAC_peak_Log2Counts_dedup_promoter retrieved from UCSC Xena Browser (385 primary tumor samples across 23 tissues) (Goldman et al., 2020) on date 03/10/2018. The genes showing a Spearman correlation $r \geq 0.4$ were selected for pathway and cluster location analysis. The pathway enrichment analysis was done using STRING software for the Gene Ontology Biological Process and KEGG pathways categories (Szklarczyk et al., 2017). The cluster localization analysis was performed with two approaches, the Cluster Locator algorithm (Pazos Obregón et al., 2018) and the Enrichr software (Kuleshov et al., 2016).

Statistical Analysis.

Unless specified all the variables are expressed as average value ± standard deviation (SD). Statistical analyses were performed with one-way ANOVA for multiple comparison tests, including Sidak's Honest Significant Difference test as a post-hoc test, as referred in the legend of the Figures. Spearman equations were applied to determine the correlations. All the analyses were done in R software (version 3.6) using libraries ggcorrplot, corrplot, xlsx, heatmap.2 (clustering distance measured by Euclidean and Ward clustering algorithms) and software GraphPad Prism 6. The statistical significance of the observed differences was expressed using the p-value (* $p < 0.05$, ** $p < 0.01$, *** $p < 0.001$, **** p-value < 0.0001). Differences with a p-value of < 0.05 were considered significant.

Supplementary Materials: Supplementary Tables and Figure Legends

Supplementary Figure 1. Data type and tissue sample distribution. Sample distribution per tissue type in the ATAC-seq, DNA methylation, ATAC-seq & DNA methylation and Normal adjacent tissues sample groups. **A.** Number of samples. **B.** Percentage of samples. The color reference, the number of samples of this tissue and the accounted percentage are presented to each tissue. Names references: ACC (Adrenocortical carcinoma), BLCA (Bladder Urothelial Carcinoma), BRCA (Breast invasive carcinoma), CESC (Cervical squamous cell carcinoma and endocervical adenocarcinoma), CHOL (Cholangiocarcinoma), COAD (Colon adenocarcinoma), DLBC (Lymphoid Neoplasm Diffuse Large B-cell Lymphoma), ESCA (Esophageal carcinoma), GBM (Glioblastoma multiforme), HNSC (Head and Neck squamous cell carcinoma), KICH (Kidney Chromophobe), KIRC (Kidney renal clear cell carcinoma), KIRP (Kidney renal papillary cell carcinoma), LGG (Brain Lower Grade Glioma), LIHC (Liver hepatocellular carcinoma), LUAD (Lung adenocarcinoma), LUSC (Lung squamous cell carcinoma), MESO (Mesothelioma), OV (Ovarian serous cystadenocarcinoma), PAAD (Pancreatic adenocarcinoma), PCPG (Pheochromocytoma and Paraganglioma), PRAD (Prostate adenocarcinoma), READ (Rectum adenocarcinoma), SARC (Sarcoma), SKCM (Skin Cutaneous Melanoma), STAD (Stomach adenocarcinoma), TGCT (Testicular Germ Cell Tumors), THCA (Thyroid carcinoma), THYM (Thymoma), UCEC (Uterine Corpus Endometrial Carcinoma), UCS (Uterine Carcinosarcoma) and UVM (Uveal Melanoma).

Supplementary Figure 2. Correlation between ATAC-seq values and promoter methylation values of vtRNAs in Pan-Cancer TCGA dataset. A-D. The correlation was calculated between ATAC-seq data and DNA methylation average normalized beta values data for vtRNAs (vtRNAs1-1 (**A**), vtRNA1-2 (**B**), vtRNA1-3 (**C**) and vtRNA2-1 (**D**)), established in 329 primary tumors samples. The box plots show the median line and lower and upper quartile and the whiskers the 2.5 and 97.5 percentile. Horizontal grey striped and red dotted lines are shown to denote unmethylated (average beta-value ≤ 0.2), 50% methylated (average beta-value = 0.5) and highly methylated (average beta-value ≥ 0.8). Spearman correlation value and the best-fit line (red line) with 95% confidence bands (black dot lines) are shown.

Supplementary Figure 3. Genomic context of human vtRNA3-1P and the evaluated region of ATAC-seq. **A.** Genomic view of the 1.5 kb region of human vtRNA3-1P gene in UCSC Genome browser (GRCh37/hg19) centered at the 500bp of the ATAC-seq. Highlighted in *yellow* is the 500 bp ATAC-seq region used in the posterior analyses. The following Gene annotation and ENCODE Project tracks for seven cell lines (GM12878, H1-hESC, HSMM, HUVEC, K562, NHEK, NHL) are displayed: DNA accessibility (DNaseI hypersensitivity clusters (color intensity is proportional to the maximum signal strength)), DNA methylation (CpG islands length greater than 200 bp), histone modification (H3K27Ac, H3K4me1, H3K4me3 marks), conservation of the region in 100 Vertebrates (log-odds Phylop scores). The vertical viewing range of the tracks displays the default settings of the browser for each variable. **B.** The assay for transposase-accessible chromatin using sequencing (ATAC-seq) values for vtRNAs in different tumors present in PANCAN TCGA dataset (385 tumors samples across 23 cancer types) expressed as log2 normalized values. The box plots show the median and the lower and upper quartile, and the whiskers the 2.5 and 97.5 percentile of the distribution. **C.** The assay for transposase-accessible chromatin using sequencing (ATAC-seq) values for vtRNAs in 21 different tumors with at least 5 tumor samples present in Pan-Cancer TCGA dataset (385 tumors samples) expressed as log2 normalized values. The chart shows the average and standard error for each vtRNAs in each tumor.

Supplementary Figure 4. VtRNA promoter's chromatin accessibility (ATAC-seq and DNA methylation) average values for tumor tissues from Pan-Cancer TCGA dataset. The average vtRNA promoters ATAC-seq and DNA methylation values for each primary tumor tissue type (21 tissues). VtRNA1-1 (**A**), vtRNA1-2 (**B**), vtRNA1-

3 (**C**) and vtRNA2-1 (**D**). The Spearman correlation between averages ATAC-seq and DNA methylation values was calculated for each vtRNA. The chart shows the average and standard deviation for each tissue with at least five samples available at Pan-Cancer TCGA.

Supplementary Figure 5. VtRNA promoter's DNA methylation values for each normal and tumor tissues from Pan-Cancer TCGA dataset. The average promoter DNA methylation beta-values of normal adjacent (Normal) and all primary tumor (Tumor) tissues (16 tissue types) for vtRNA1-1 (**A**), vtRNA1-2 (**B**), vtRNA1-3 (**C**) and vtRNA2-1 (**D**) is shown. The Spearman correlation between tissue averages DNA methylation normalized beta values for each vtRNA was calculated. The chart shows the average and standard deviation for each tissue with at least five samples available at Pan-Cancer TCGA.

Supplementary Table 1. ATAC-seq and DNA methylation data for vtRNA promoters in primary tumors and normal adjacent tissue samples. Excel spreadsheets: ATAC-seq_data_500bp: All ATAC-seq data of vtRNAs promoter (500bp) data for primary tumor samples; DNA_methylation_500bp: All DNA methylation data and ATAC-seq data of vtRNAs promoter (500bp) data for total primary tumor and normal adjacent samples; DNA_methylation_NORMAL: All DNA methylation data of vtRNAs promoter (500bp) data for normal adjacent samples; DNA_methylation_TUMOR: All DNA methylation data of vtRNAs promoter (500bp) data for primary tumor samples; Normal_&_Tumor_matched: All DNA methylation data of vtRNAs promoter (500bp) data for primary tumor and normal adjacent samples.

Supplementary Table 2. VtRNAs Transcription Factors Binding and KEEG enriched terms. Excel spreadsheets: Binding_Factors: Transcription factors identified in the cell line K562 as ChIP-seq Peaks by ENCODE 3 project; KEEG_terms: enriched KEGG pathway terms (FDR < 0.05).

Supplementary Table 3. DNA methylation, ATAC-seq data and associated survival data for primary tumors. Excel spreadsheets: DNA-methylation_Survival_data: All DNA methylation data of vtRNAs promoter (500bp) and survival data for primary tumor samples; ATAC-seq_Survival_data: ATAC-seq data of vtRNAs promoter (500bp) and survival data for primary tumor samples.

Supplementary Table 4. Correlation of ATAC-seq values between vtRNA and all genome promoters in primary tumor samples. Excel spreadsheets: Spearman_correlation: Spearman correlation values of all promoter genes and vtRNAs in primary tumors samples; vtRNA1-1_cluster: Pathway enrichment and cluster chromosome localization data of vtRNA1-1; vtRNA1-2_cluster: Pathway enrichment and cluster chromosome localization data of vtRNA1-2; vtRNA1-3_cluster: Pathway enrichment and cluster chromosome localization data of vtRNA1-3; vtRNA2-1_cluster: Pathway enrichment and cluster chromosome localization data of vtRNA2-1.

Supplementary Table 5. ATAC-seq and DNA methylation data for vtRNA promoters in primary tumors and the associated Immune Subtypes data. Excel spreadsheets: DNA_methylation_data: All DNA methylation data of vtRNAs promoter (500bp) and Immune Subtypes data for primary tumor samples; DNA_methylation_Spearman_corr: Spearman correlation values of DNA methylation data of vtRNAs promoter (500bp) and Immune Subtypes data for primary tumor samples; ATAC-seq_data: All ATAC-seq data of vtRNAs promoter (500bp) and Immune Subtypes data for primary tumor samples; ATAC-seq_Spearman_corr: Spearman correlation values of ATAC-seq data of vtRNAs promoter (500bp) and Immune Subtypes data for primary tumor samples.

Abbreviations:

vtRNA	vault RNA
TCGA	The Cancer Genome Atlas
ATAC-seq	Assay for Transposase Accessible Chromatin with high-throughput sequencing
NoMe-seq	Nucleosome Occupancy and Methylome sequencing
OG	Oncogene
TSG	Tumor Suppressor Gene
TCGA	The Cancer Genome Atlas
TSS	Transcription Start Site
Ave	Average
SD	Standard Deviation
ACC	Adrenocortical carcinoma
BLCA	Bladder Urothelial Carcinoma
BRCA	Breast invasive carcinoma
CESC	Cervical squamous cell carcinoma and endocervical adenocarcinoma
CHOL	Cholangiocarcinoma
COAD	Colon adenocarcinoma
DLBC	Lymphoid Neoplasm Diffuse Large B-cell Lymphoma
ESCA	Esophageal carcinoma
GBM	Glioblastoma multiforme
HNSC	Head and Neck squamous cell carcinoma
KICH	Kidney Chromophobe
KIRC	Kidney renal clear cell carcinoma
KIRP	Kidney renal papillary cell carcinoma
LGG	Brain Lower Grade Glioma
LIHC	Liver hepatocellular carcinoma
LUAD	Lung adenocarcinoma
LUSC	Lung squamous cell carcinoma
MESO	Mesothelioma
OV	Ovarian serous cystadenocarcinoma
PAAD	Pancreatic adenocarcinoma
PCPG	Pheochromocytoma and Paraganglioma
PRAD	Prostate adenocarcinoma
READ	Rectum adenocarcinoma
SARC	Sarcoma
SKCM	Skin Cutaneous Melanoma
STAD	Stomach adenocarcinoma
TGCT	Testicular Germ Cell Tumors
THCA	Thyroid carcinoma

THYM	Thymoma
UCEC	Uterine Corpus Endometrial Carcinoma
UCS	Uterine Carcinosarcoma
UVM	Uveal Melanoma

Author Contributions: Conceptualization, M.A.D.; methodology, R.S.F. and M.A.D.; software, R.S.F.; formal analysis, R.S.F.; investigation, R.S.F. and M.A.D.; resources, M.A.D.; data curation, M.A.D and R.S.F.; writing—original draft preparation, R.S.F.; writing—review and editing, M.A.D.; visualization, R.S.F.; supervision, M.A.D.; project administration, M.A.D.; funding acquisition, M.A.D.
All authors have read and agreed to the published version of the manuscript.

Funding: This study was funded by Agencia Nacional de Investigación e Innovación (ANII), Comisión Sectorial de Investigación Científica (CSIC), Comisión Académica de posgrado (CAP) and Programa de Desarrollo de las Ciencias Básicas (PEDECIBA) from Uruguay.

Conflicts of Interest: The authors declare no conflict of interest.

References:

Aakula, A., Kohonen, P., Leivonen, S.K., Mäkelä, R., Hintsanen, P., Mpindi, J.P., Martens-Uzunova, E., Aittokallio, T., Jenster, G., Perälä, M., et al. (2015). Systematic Identification of MicroRNAs That Impact on Proliferation of Prostate Cancer Cells and Display Changed Expression in Tumor Tissue. Eur. Urol. *69*, 1120–1128.
Ahn, J.H., Lee, H.S., Lee, J.S., Lee, Y.S., Park, J.L., Kim, S.Y., Hwang, J.A., Kunkeaw, N., Jung, S.Y., Kim, T.J., et al. (2018). Nc886 is induced by TGF-β and suppresses the microRNA pathway in ovarian cancer. Nat. Commun. *9*.
Amort, M., Nachbauer, B., Tuzlak, S., Kieser, A., Schepers, A., Villunger, A., and Polacek, N. (2015). Expression of the vault RNA protects cells from undergoing apoptosis. Nat. Commun. *6*, 7030.
Attar, N., and Kurdistani, S.K. (2017). Exploitation of EP300 and CREBBP lysine acetyltransferases by cancer. Cold Spring Harb. Perspect. Med. *7*.
Bi, N., Cao, J., Song, Y., Shen, J., Liu, W., Fan, J., He, J., Shi, Y., Zhang, X., Lu, N., et al. (2014). A MicroRNA signature predicts survival in early stage small-cell lung cancer treated with surgery and adjuvant chemotherapy. PLoS One *9*, 1–8.
Boivin, V., Deschamps-Francoeur, G., Couture, S., Nottingham, R.M., Bouchard-Bourelle, P., Lambowitz, A.M., Scott, M.S., and Abou-Elela, S. (2018). Simultaneous sequencing of coding and noncoding RNA reveals a human transcriptome dominated by a small number of highly expressed noncoding genes. RNA *24*, 950–965.
Boivin, V., Faucher-Giguère, L., Scott, M., and Abou-Elela, S. (2019). The cellular landscape of mid-size noncoding RNA. Wiley Interdiscip. Rev. RNA *10*.
Bracher, L., Ferro, I., Pulido-Quetglas, C., Ruepp, M.D., Johnson, R., and Polacek, N. (2020). Human vtRNA1-1 levels modulate signaling pathways and regulate apoptosis in human cancer cells. Biomolecules *10*.

Buenrostro, J.D., Giresi, P.G., Zaba, L.C., Chang, H.Y., and Greenleaf, W.J. (2013). Transposition of native chromatin for fast and sensitive epigenomic profiling of open chromatin, DNA-binding proteins and nucleosome position. Nat. Methods *10*, 1213–1218.
Buenrostro, J.D., Wu, B., Chang, H.Y., and Greenleaf, W.J. (2015). ATAC-seq: A method for assaying chromatin accessibility genome-wide. Curr. Protoc. Mol. Biol. *2015*, 21.29.1-21.29.9.
Burke, J.M., Kincaid, R.P., Nottingham, R.M., Lambowitz, A.M., and Sullivan, C.S. (2016). DUSP11 activity on triphosphorylated transcripts promotes Argonaute association with noncanonical viral microRNAs and regulates steady-state levels of cellular noncoding RNAs. Genes Dev. *30*, 2076–2092.
Calderon, B.M., and Conn, G.L. (2018). A human cellular noncoding RNA activates the antiviral protein 2'-5'-oligoadenylate synthetase 1. J. Biol. Chem. *293*, 16115–16124.
Canella, D., Praz, V., Reina, J.H., Cousin, P., and Hernandez, N. (2010). Defining the RNA polymerase III transcriptome: Genome-wide localization of the RNA polymerase III transcription machinery in human cells. Genome Res. *20*, 710–721.
Cao, J., Song, Y., Bi, N., Shen, J., Liu, W., Fan, J., Sun, G., Tong, T., He, J., Shi, Y., et al. (2013). DNA methylation-mediated repression of miR-886-3p predicts poor outcome of human small cell lung cancer. Cancer Res. *73*, 3326–3335.
Carpenter, B.L., Zhou, W., Madaj, Z., DeWitt, A.K., Ross, J.P., Grønbæk, K., Liang, G., Clark, S.J., Molloy, P.L., and Jones, P.A. (2018). Mother–child transmission of epigenetic information by tunable polymorphic imprinting. Proc. Natl. Acad. Sci. *115*, E11970–E11977.
Chen, J., OuYang, H., An, X., and Liu, S. (2018). Vault RNAs partially induces drug resistance of human tumor cells MCF-7 by binding to the RNA/DNA-binding protein PSF and inducing oncogene GAGE6. PLoS One *13*, e0191325.
Chen, X., Shen, Y., Draper, W., Buenrostro, J.D., Litzenburger, U., Cho, S.W., Satpathy, A.T., Carter, A.C., Ghosh, R.P., East-Seletsky, A., et al. (2016). ATAC-see reveals the accessible genome by transposase-mediated imaging and sequencing. Nat. Methods *13*, 1013–1020.
Corces, M.R., Granja, J.M., Shams, S., Louie, B.H., Seoane, J.A., Zhou, W., Silva, T.C., Groeneveld, C., Wong, C.K., Cho, S.W., et al. (2018). The chromatin accessibility landscape of primary human cancers. Science (80-.). *362*.
Dettmer, M.S., Perren, A., Moch, H., Komminoth, P., Nikiforov, Y.E., and Nikiforova, M.N. (2014). MicroRNA profile of poorly differentiated thyroid carcinomas: New diagnostic and prognostic insights. J. Mol. Endocrinol. *52*, 181–189.
van Dijk, S.J., Peters, T.J., Buckley, M., Zhou, J., Jones, P.A., Gibson, R.A., Makrides, M., Muhlhausler, B.S., and Molloy, P.L. (2018). DNA methylation in blood from neonatal screening cards and the association with BMI and insulin sensitivity in early childhood. Int. J. Obes. *42*, 28–35.
Duren, Z., Chen, X., Jiang, R., Wang, Y., and Wong, W.H. (2017). Modeling gene regulation from paired expression and chromatin accessibility data. Proc. Natl. Acad. Sci. U. S. A. *114*, E4914–E4923.
Ertosun, M.G., Hapil, F.Z., and Osman Nidai, O.Z.E.S. (2016). E2F1 transcription factor and its impact on growth factor and cytokine signaling. Cytokine Growth Factor Rev. *31*, 17–25.
Fendler, A., Jung, M., Stephan, C., Honey, R.J., Stewart, R.J., Pace, K.T., Erbersdobler, A., Samaan, S., Jung, K., and Yousef, G.M. (2011). miRNAs can predict prostate cancer biochemical relapse and are involved in tumor progression. Int. J. Oncol. *39*, 1183–1192.
Fort, R.S., Mathó, C., Geraldo, M.V., Ottati, M.C., Yamashita, A.S., Saito, K.C., Leite, K.R.M., Méndez, M., Maedo, N., Méndez, L., et al. (2018). Nc886 is epigenetically repressed in prostate

cancer and acts as a tumor suppressor through the inhibition of cell growth. BMC Cancer *18*, 127.
Fort, R.S., Garat, B., Sotelo-Silveira, J.R., and Duhagon, M.A. (2020). vtRNA2-1/nc886 Produces a Small RNA That Contributes to Its Tumor Suppression Action through the microRNA Pathway in Prostate Cancer. Non-Coding RNA *6*, 7.
Fuchs, O. (2012). Important genes in the pathogenesis of 5q- syndrome and their connection with ribosomal stress and the innate immune system pathway. Leuk. Res. Treatment *2012*, 179402.
Gao, W., Shen, H., Liu, L., Xu, J., Xu, J., and Shu, Y. (2011). MiR-21 overexpression in human primary squamous cell lung carcinoma is associated with poor patient prognosis. J. Cancer Res. Clin. Oncol. *137*, 557–566.
Goldman, M., Craft, B., Swatloski, T., Ellrott, K., Cline, M., Diekhans, M., Ma, S., Wilks, C., Stuart, J., Haussler, D., et al. (2013). The UCSC Cancer Genomics Browser: update 2013. Nucleic Acids Res. *41*, D949–D954.
Goldman, M.J., Craft, B., Hastie, M., Repečka, K., McDade, F., Kamath, A., Banerjee, A., Luo, Y., Rogers, D., Brooks, A.N., et al. (2020). Visualizing and interpreting cancer genomics data via the Xena platform. Nat. Biotechnol. *38*, 675–678.
Golec, E., Lind, L., Qayyum, M., Blom, A.M., and King, B.C. (2019). The Noncoding RNA nc886 Regulates PKR Signaling and Cytokine Production in Human Cells. J. Immunol. *202*, 131–141.
Gopinath, S.C.B., Matsugami, A., Katahira, M., and Kumar, P.K.R. (2005). Human vault-associated non-coding RNAs bind to mitoxantrone, a chemotherapeutic compound. Nucleic Acids Res. *33*, 4874–4881.
Gopinath, S.C.B., Wadhwa, R., and Kumar, P.K.R. (2010). Expression of noncoding vault RNA in human malignant cells and its importance in mitoxantrone resistance. Mol. Cancer Res. *8*, 1536–1546.
Helbo, A.S., Treppendahl, M., Aslan, D., Dimopoulos, K., Nandrup-Bus, C., Holm, M.S., Andersen, M.K., Liang, G., Kristensen, L.S., and Grønbæk, K. (2015). Hypermethylation of the VTRNA1-3 promoter is associated with poor outcome in lower risk myelodysplastic syndrome patients. Genes (Basel). *6*, 977–990.
Helbo, A.S., Lay, F.D., Jones, P.A., Liang, G., and Grønbæk, K. (2017). Nucleosome Positioning and NDR Structure at RNA Polymerase III Promoters. Sci. Rep. *7*.
Horos, R., Büscher, M., Kleinendorst, R., Alleaume, A.-M., Tarafder, A.K., Schwarzl, T., Dziuba, D., Tischer, C., Zielonka, E.M., Adak, A., et al. (2019). The Small Non-coding Vault RNA1-1 Acts as a Riboregulator of Autophagy. Cell *176*, 1054-1067.e12.
Horsley, V., and Pavlath, G.K. (2002). NFAT: Ubiquitous regulator of cell differentiation and adaptation. J. Cell Biol. *156*, 771–774.
Hu, Z., Zhang, H., Tang, L., Lou, M., and Geng, Y. (2017). Silencing nc886, a Non-Coding RNA, Induces Apoptosis of Human Endometrial Cancer Cells-1A In Vitro. Med. Sci. Monit. *23*, 1317–1324.
Hussain, S., Sajini, A.A., Blanco, S., Dietmann, S., Lombard, P., Sugimoto, Y., Paramor, M., Gleeson, J.G., Odom, D.T., Ule, J., et al. (2013). NSun2-mediated cytosine-5 methylation of vault noncoding RNA determines its processing into regulatory small RNAs. Cell Rep. *4*, 255–261.
Im, W.R., Lee, H.-S., Lee, Y.-S., Lee, J.-S., Jang, H.-J., Kim, S.-Y., Park, J.-L., Lee, Y., Kim, M.S., Lee, J.M., et al. (2020). A Regulatory Noncoding RNA, nc886, Suppresses Esophageal Cancer by Inhibiting the AKT Pathway and Cell Cycle Progression. Cells *9*, 801.

Jean, D., Tellez, C., Huang, S., Davis, D.W., Bruns, C.J., McConkey, D.J., Hinrichs, S.H., and Bar-Eli, M. (2000). Inhibition of tumor growth and metastasis of human melanoma by intracellular anti-ATF-1 single chain Fv fragment. Oncogene *19*, 2721–2730.
Jeon, S.H., Johnson, B.H., and Lee, Y.S. (2012a). A tumor surveillance model: A non-coding RNA senses neoplastic cells and its protein partner signals cell death. Int. J. Mol. Sci. *13*, 13134–13139.
Jeon, S.H., Lee, K., Lee, K.S., Kunkeaw, N., Johnson, B.H., Holthauzen, L.M.F., Gong, B., Leelayuwat, C., and Lee, Y.S. (2012b). Characterization of the direct physical interaction of nc886, a cellular non-coding RNA, and PKR. FEBS Lett. *586*, 3477–3484.
Jeronimo, S.M.B., Holst, A.K.B., Jamieson, S.E., Francis, R., Martins, D.R.A., Bezerra, F.L., Ettinger, N.A., Nascimento, E.T., Monteiro, G.R., Lacerda, H.G., et al. (2007). Genes at human chromosome 5q31.1 regulate delayed-type hypersensitivity responses associated with Leishmania chagasi infection. Genes Immun. *8*, 539–551.
Joo, J.E., Dowty, J.G., Milne, R.L., Wong, E.M., Dugué, P.A., English, D., Hopper, J.L., Goldgar, D.E., Giles, G.G., Southey, M.C., et al. (2018). Heritable DNA methylation marks associated with susceptibility to breast cancer. Nat. Commun. *9*.
Kedersha, N.L., and Rome, L.H. (1986). Isolation and characterization of a novel ribonucleoprotein particle: Large structures contain a single species of small RNA. J. Cell Biol. *103*, 699–709.
Kedersha, N.L., Heuser, J.E., Chugani, D.C., and Rome, L.H. (1991). Vaults. III. Vault ribonucleoprotein particles open into flower-like structures with octagonal symmetry. J. Cell Biol. *112*, 225–235.
Kickhoefer, V.A., Rajavel, K.S., Scheffer, G.L., Dalton, W.S., Scheper, R.J., and Rome, L.H. (1998). Vaults are up-regulated in multidrug-resistant cancer cell lines. J. Biol. Chem. *273*, 8971–8974.
Kickhoefer, V.A., Poderycki, M.J., Chan, E.K.L., and Rome, L.H. (2002). The La RNA-binding protein interacts with the vault RNA and is a vault-associated protein. J. Biol. Chem. *277*, 41282–41286.
Klemm, S.L., Shipony, Z., and Greenleaf, W.J. (2019). Chromatin accessibility and the regulatory epigenome. Nat. Rev. Genet. *20*, 207–220.
Kuleshov, M. V., Jones, M.R., Rouillard, A.D., Fernandez, N.F., Duan, Q., Wang, Z., Koplev, S., Jenkins, S.L., Jagodnik, K.M., Lachmann, A., et al. (2016). Enrichr: a comprehensive gene set enrichment analysis web server 2016 update. Nucleic Acids Res. *44*, W90–W97.
Kunkeaw, N., Jeon, S.H., Lee, K., Johnson, B.H., Tanasanvimon, S., Javle, M., Pairojkul, C., Chamgramol, Y., Wongfieng, W., Gong, B., et al. (2012). Cell death/proliferation roles for nc886, a non-coding RNA, in the protein kinase R pathway in cholangiocarcinoma. Oncogene *32*, 3722–3731.
Kunkeaw, N., Lee, Y.S., Im, W.R., Jang, J.J., Song, M.J., Yang, B., Park, J.L., Kim, S.Y., Ku, Y., Kim, Y., et al. (2019). Mechanism mediated by a noncoding RNA, nc886, in the cytotoxicity of a DNA-reactive compound. Proc. Natl. Acad. Sci. U. S. A. *116*, 8289–8294.
Łabno, A., Warkocki, Z., Kuliński, T., Krawczyk, P.S., Bijata, K., Tomecki, R., and Dziembowski, A. (2016). Perlman syndrome nuclease DIS3L2 controls cytoplasmic non-coding RNAs and provides surveillance pathway for maturing snRNAs. Nucleic Acids Res. gkw649.
Lacy, D.A., Wang, Z.E., Symula, D.J., McArthur, C.J., Rubin, E.M., Frazer, K.A., and Locksley, R.M. (2000). Faithful expression of the human 5q31 cytokine cluster in transgenic mice. J. Immunol. *164*, 4569–4574.

Landgraf, P., Rusu, M., Sheridan, R., Sewer, A., Iovino, N., Aravin, A., Pfeffer, S., Rice, A., Kamphorst, A.O., Landthaler, M., et al. (2007). A mammalian microRNA expression atlas based on small RNA library sequencing. Cell *129*, 1401–1414.
Lee, Y.S. (2015). A Novel Type of Non-coding RNA, nc886, Implicated in Tumor Sensing and Suppression. Genomics Inform. *13*, 26–30.
Lee, E.K., Hong, S.H., Shin, S., Lee, H.S., Lee, J.S., Park, E.J., Choi, S.S., Min, J.W., Park, D., Hwang, J.A., et al. (2016). Nc886, a non-coding RNA and suppressor of PKR, exerts an oncogenic function in thyroid cancer. Oncotarget *7*, 75000–75012.
Lee, H.-S., Lee, K., Jang, H.-J., Lee, G.K., Park, J.-L., Kim, S.-Y., Kim, S.-B., Johnson, B.H., Zo, J.I., Lee, J.-S., et al. (2014a). Epigenetic silencing of the non-coding RNA nc886 provokes oncogenes during human esophageal tumorigenesis. Oncotarget *5*, 3472–3481.
Lee, K.-S., Park, J.-L., Lee, K., Richardson, L.E., Johnson, B.H., Lee, H.-S., Lee, J.-S., Kim, S.-B., Kwon, O.-H., Song, K.S., et al. (2014b). nc886, a non-coding RNA of anti-proliferative role, is suppressed by CpG DNA methylation in human gastric cancer. Oncotarget *5*, 3944–3955.
Lee, K., Kunkeaw, N., Jeon, S.H., Lee, I., Johnson, B.H., Kang, G.-Y., Bang, J.Y., Park, H.S., Leelayuwat, C., and Lee, Y.S. (2011). Precursor miR-886, a novel noncoding RNA repressed in cancer, associates with PKR and modulates its activity. RNA *17*, 1076–1089.
Lee, K.S., Shin, S., Cho, E., Im, W.K., Jeon, S.H., Kim, Y., Park, D., Fréchet, M., Chajra, H., and Jung, E. (2019a). nc886, a non-coding RNA, inhibits UVB-induced MMP-9 and COX-2 expression via the PKR pathway in human keratinocytes. Biochem. Biophys. Res. Commun. *512*, 647–652.
Lee, Y.S., Kunkeaw, N., and Lee, Y.S. (2019b). Protein kinase R and its cellular regulators in cancer: An active player or a surveillant? Wiley Interdiscip. Rev. RNA e1558.
Legendre, C.R., Demeure, M.J., Whitsett, T.G., Gooden, G.C., Bussey, K.J., Jung, S., Waibhav, T., Kim, S., and Salhia, B. (2016). Pathway Implications of Aberrant Global Methylation in Adrenocortical Cancer. PLoS One *11*, e0150629.
Lei, J., Xiao, J.H., Zhang, S.H., Liu, Z.Q., Huang, K., Luo, Z.P., Xiao, X.L., and Hong, Z.D. (2017). Non-coding RNA 886 promotes renal cell carcinoma growth and metastasis through the Janus kinase 2/signal transducer and activator of transcription 3 signaling pathway. Mol. Med. Rep. *16*, 4273–4278.
Li, B., Carey, M., and Workman, J.L. (2007). The Role of Chromatin during Transcription. Cell *128*, 707–719.
Li, F., Chen, Y., Zhang, Z., Ouyang, J., Wang, Y., Yan, R., Huang, S., Gao, G.F., Guo, G., and Chen, J.-L. (2015). Robust expression of vault RNAs induced by influenza A virus plays a critical role in suppression of PKR-mediated innate immunity. Nucleic Acids Res. *43*, gkv1078.
Li, J.-H., Wang, M., Zhang, R., Gao, W.-L., Meng, S.-H., Ma, X.-L., Hou, X.-H., and Feng, L.-M. (2017). E2F1-directed activation of nc886 mediates drug resistance in cervical cancer cells via regulation of major vault protein. Int. J. Clin. Exp. Pathol. *10*, 9233–9242.
Liu, G., Wang, W., Hu, S., Wang, X., and Zhang, Y. (2018). Inherited DNA methylation primes the establishment of accessible chromatin during genome activation. Genome Res. *28*, 998–1007.
Ma, H., Wang, M., Zhou, Y., Yang, J. jie, Wang, L.Y., Yang, R. hui, Wen, M. jie, and Kong, L. (2020). Noncoding RNA 886 alleviates tumor cellular immunological rejection in host C57BL/C mice. Cancer Med. *9*, 5258–5271.
Mashima, T., Kudo, M., Takada, Y., Matsugami, A., Gopinath, S.C.B., Kumar, P.K.R., and Katahira, M. (2008). Interactions between antitumor drugs and vault RNA. Nucleic Acids Symp.

Ser. (Oxf). 217–218.
Meng, C., Meng, C., Wei, Z., Wei, Z., Zhang, Y., Zhang, Y., Yan, L., Yan, L., He, H., He, H., et al. (2016). Regulation of cytochrome P450 3A4 by small vault RNAb derived from the non-coding vault RNA1 of multidrug resistance-linked vault particle (D.A. Spandidos).
Miñones-Moyano, E., Friedländer, M.R., Pallares, J., Kagerbauer, B., Porta, S., Escaramís, G., Ferrer, I., Estivill, X., and Martí, E. (2013). Upregulation of a small vault RNA (svtRNA2-1a) is an early event in Parkinson disease and induces neuronal dysfunction. RNA Biol. *10*, 1093–1106.
Moran, S., Arribas, C., and Esteller, M. (2016). Validation of a DNA methylation microarray for 850,000 CpG sites of the human genome enriched in enhancer sequences. Epigenomics *8*, 389–399.
Naka, I., Nishida, N., Patarapotikul, J., Nuchnoi, P., Tokunaga, K., Hananantachai, H., Tsuchiya, N., and Ohashi, J. (2009). Identification of a haplotype block in the 5q31 cytokine gene cluster associated with the susceptibility to severe malaria. Malar. J. *8*, 232.
Nandy, C., Mrázek, J., Stoiber, H., Grässer, F.A., Hüttenhofer, A., and Polacek, N. (2009). Epstein-Barr Virus-Induced Expression of a Novel Human Vault RNA. J. Mol. Biol. *388*, 776–784.
Nikitina, T. V, Tischenko, L.I., and Schulz, W.A. (2011). Recent insights into regulation of transcription by RNA polymerase III and the cellular functions of its transcripts. Biol. Chem. *392*, 395–404.
Nomura, M., Saito, K., Aihara, K., Nagae, G., Yamamoto, S., Tatsuno, K., Ueda, H., Fukuda, S., Umeda, T., Tanaka, S., et al. (2019). DNA demethylation is associated with malignant progression of lower-grade gliomas. Sci. Rep. *9*, 1903.
Nordentoft, I., Birkenkamp-Demtroder, K., Agerbæk, M., Theodorescu, D., Ostenfeld, M.S., Hartmann, A., Borre, M., Ørntoft, T.F., and Dyrskjøt, L. (2012). miRNAs associated with chemo-sensitivity in cell lines and in advanced bladder cancer. BMC Med. … *5*, 40.
Okumura, T., Kojima, H., Miwa, T., Sekine, S., Hashimoto, I., Hojo, S., Nagata, T., and Shimada, Y. (2016). The expression of microRNA 574-3p as a predictor of postoperative outcome in patients with esophageal squamous cell carcinoma. World J. Surg. Oncol. *14*, 228.
Paliwal, A., Temkin, A.M., Kerkel, K., Yale, A., Yotova, I., Drost, N., Lax, S., Nhan-Chang, C.L., Powell, C., Borczuk, A., et al. (2013). Comparative Anatomy of Chromosomal Domains with Imprinted and Non-Imprinted Allele-Specific DNA Methylation. PLoS Genet. *9*.
Park, J.-L., Lee, Y.-S., Kunkeaw, N., Kim, S.-Y., Kim, I.-H., and Lee, Y.S. (2017a). Epigenetic regulation of noncoding RNA transcription by mammalian RNA polymerase III. Epigenomics *9*, 171–187.
Park, J.L., Lee, Y.S., Song, M.J., Hong, S.H., Ahn, J.H., Seo, E.H., Shin, S.P., Lee, S.J., Johnson, B.H., Stampfer, M.R., et al. (2017b). Epigenetic regulation of RNA polymerase III transcription in early breast tumorigenesis. Oncogene *36*, 6793–6804.
Pazos Obregón, F., Soto, P., Lavín, J.L., Cortázar, A.R., Barrio, R., Aransay, A.M., and Cantera, R. (2018). Cluster Locator, online analysis and visualization of gene clustering. Bioinformatics *34*, 3377–3379.
Persengiev, S.P., and Green, M.R. (2003). The role of ATF/CREB family members in cell growth, survival and apoptosis. Apoptosis *8*, 225–228.
Persson, H., Kvist, A., Vallon-Christersson, J., Medstrand, P., Borg, A., and Rovira, C. (2009). The non-coding RNA of the multidrug resistance-linked vault particle encodes multiple regulatory small RNAs. Nat. Cell Biol. *11*, 1268–1271.
Rechache, N.S., Wang, Y., Stevenson, H.S., Killian, J.K., Edelman, D.C., Merino, M., Zhang, L.,

Nilubol, N., Stratakis, C.A., Meltzer, P.S., et al. (2012). DNA methylation profiling identifies global methylation differences and markers of adrenocortical tumors. J. Clin. Endocrinol. Metab. *97*, E1004-13.
Renauer, P., Coit, P., Jeffries, M.A., Merrill, J.T., McCune, W.J., Maksimowicz-McKinnon, K., and Sawalha, A.H. (2015). DNA methylation patterns in naïve CD4+ T cells identify epigenetic susceptibility loci for malar rash and discoid rash in systemic lupus erythematosus. Lupus Sci. Med. *2*.
Richmond, R.C., Sharp, G.C., Herbert, G., Atkinson, C., Taylor, C., Bhattacharya, S., Campbell, D., Hall, M., Kazmi, N., Gaunt, T., et al. (2018). The long-term impact of folic acid in pregnancy on offspring DNA methylation: follow-up of the Aberdeen Folic Acid Supplementation Trial (AFAST). Int. J. Epidemiol.
Rodrigues, V., Piper, K., Couissinier-Paris, P., Bacelar, O., Dessein, H., and Dessein, A.J. (1999). Genetic control of schistosome infections by the SM1 locus of the 5q31-q33 region is linked to differentiation of type 2 helper T lymphocytes. Infect. Immun. *67*, 4689–4692.
Rohini, M., Haritha Menon, A., and Selvamurugan, N. (2018). Role of activating transcription factor 3 and its interacting proteins under physiological and pathological conditions. Int. J. Biol. Macromol. *120*, 310–317.
Romanelli, V., Nakabayashi, K., Vizoso, M., Moran, S., Iglesias-Platas, I., Sugahara, N., Simón, C., Hata, K., Esteller, M., Court, F., et al. (2014). Variable maternal methylation overlapping the nc886/vtRNA2-1 locus is locked between hypermethylated repeats and is frequently altered in cancer. Epigenetics *9*, 783–790.
Sajini, A.A., Choudhury, N.R., Wagner, R.E., Bornelöv, S., Selmi, T., Spanos, C., Dietmann, S., Rappsilber, J., Michlewski, G., and Frye, M. (2019). Loss of 5-methylcytosine alters the biogenesis of vault-derived small RNAs to coordinate epidermal differentiation. Nat. Commun. *10*.
Sallustio, F., Serino, G., Cox, S.N., Dalla Gassa, A., Curci, C., De Palma, G., Banelli, B., Zaza, G., Romani, M., and Schena, F.P. (2016). Aberrantly methylated DNA regions lead to low activation of CD4+ T-cells in IgA nephropathy. Clin. Sci. (Lond). *130*, 733–746.
Schou, J. V., Rossi, S., Jensen, B. V., Nielsen, D.L., Pfeiffer, P., Høgdall, E., Yilmaz, M., Tejpar, S., Delorenzi, M., Kruhøffer, M., et al. (2014). miR-345 in Metastatic Colorectal Cancer: A Non-Invasive Biomarker for Clinical Outcome in Non-KRAS Mutant Patients Treated with 3rd Line Cetuximab and Irinotecan. PLoS One *9*, e99886.
Sendler, E., Johnson, G.D., and Krawetz, S.A. (2011). Local and global factors affecting RNA sequencing analysis. Anal. Biochem. *419*, 317–322.
Shen, J., Zhou, W., Bi, N., Song, Y.-M., Zhang, F.-Q., Zhan, Q.-M., and Wang, L.-H. (2018). MicroRNA-886-3P functions as a tumor suppressor in small cell lung cancer. Cancer Biol. Ther. *19*, 1185–1192.
Silver, M.J., Kessler, N.J., Hennig, B.J., Dominguez-Salas, P., Laritsky, E., Baker, M.S., Coarfa, C., Hernandez-Vargas, H., Castelino, J.M., Routledge, M.N., et al. (2015). Independent genomewide screens identify the tumor suppressor VTRNA2-1 as a human epiallele responsive to periconceptional environment. Genome Biol *16*, 118.
Stadler, P.F., Chen, J.J.L., Hackermüller, J., Hoffmann, S., Horn, F., Khaitovich, P., Kretzschmar, A.K., Mosig, A., Prohaska, S.J., Qi, X., et al. (2009). Evolution of vault RNAs. Mol. Biol. Evol. *26*, 1975–1991.
Stark, R., Grzelak, M., and Hadfield, J. (2019). RNA sequencing: the teenage years. Nat. Rev. Genet. *20*, 631–656.

Steitz, J. (2015). RNA-RNA base-pairing: Theme and variations. RNA *21*, 476–477.
Sun, Y., Miao, N., and Sun, T. (2019). Detect accessible chromatin using ATAC-sequencing, from principle to applications. Hereditas *156*, 29.
Suojalehto, H., Lindström, I., Majuri, M.L., Mitts, C., Karjalainen, J., Wolff, H., and Alenius, H. (2014). Altered microRNA expression of nasal mucosa in long-term asthma and allergic rhinitis. Int. Arch. Allergy Immunol. *163*, 168–178.
Szklarczyk, D., Morris, J.H., Cook, H., Kuhn, M., Wyder, S., Simonovic, M., Santos, A., Doncheva, N.T., Roth, A., Bork, P., et al. (2017). The STRING database in 2017: quality-controlled protein–protein association networks, made broadly accessible. Nucleic Acids Res. *45*, D362–D368.
Tahiri, A., Leivonen, S.K., Lüders, T., Steinfeld, I., Aure, M.R., Geisler, J., Mäkelä, R., Nord, S., Riis, M.L.H., Yakhini, Z., et al. (2014). Deregulation of cancer-related miRNAs is a common event in both benign and malignant human breast tumors. Carcinogenesis *35*, 76–85.
Thorsson, V., Gibbs, D.L., Brown, S.D., Wolf, D., Bortone, D.S., Ou Yang, T.H., Porta-Pardo, E., Gao, G.F., Plaisier, C.L., Eddy, J.A., et al. (2018). The Immune Landscape of Cancer. Immunity *48*, 812-830.e14.
Thurman, R.E., Rynes, E., Humbert, R., Vierstra, J., Maurano, M.T., Haugen, E., Sheffield, N.C., Stergachis, A.B., Wang, H., Vernot, B., et al. (2012). The accessible chromatin landscape of the human genome. Nature *489*, 75–82.
Treppendahl, M.B., Qiu, X., Søgaard, A., Yang, X., Nandrup-Bus, C., Hother, C., Andersen, M.K., Kjeldsen, L., Möllgaard, L., Hellström-Lindberg, E., et al. (2012). Allelic methylation levels of the noncoding VTRNA2-1 located on chromosome 5q31.1 predict outcome in AML. Blood *119*, 206–216.
Tsompana, M., and Buck, M.J. (2014). Chromatin accessibility: A window into the genome. Epigenetics and Chromatin *7*, 1–16.
Vilalta, A., Kickhoefer, V.A., Rome, L.H., and Johnson, D.L. (1994). The rat vault RNA gene contains a unique RNA polymerase III promoter composed of both external and internal elements that function synergistically. J. Biol. Chem. *269*, 29752–29759.
Weeding, E., and Sawalha, A.H. (2018). Deoxyribonucleic acid methylation in systemic lupus erythematosus: Implications for future clinical practice. Front. Immunol. *9*, 1.
Weinstein, J.N., Collisson, E.A., Mills, G.B., Shaw, K.R.M., Ozenberger, B.A., Ellrott, K., Sander, C., Stuart, J.M., Chang, K., Creighton, C.J., et al. (2013). The cancer genome atlas pan-cancer analysis project. Nat. Genet. *45*, 1113–1120.
Xiong, Y., Zhang, L., Holloway, A.K., Wu, X., Su, L., and Kebebew, E. (2011). MiR-886-3p regulates cell proliferation and migration, and is dysregulated in familial non-medullary thyroid cancer. PLoS One *6*, 1–11.
Yeganeh, M., and Hernandez, N. (2020). RNA polymerase III transcription as a disease factor. Genes Dev. *34*, 865–882.
Yu, M.C., Lee, C.W., Lin, C.H., Wu, C.H., Lee, Y.S., Tsai, C.L., and Tsai, C.N. (2020). Differential hypermethylation of the VTRNA2-1 promoter in hepatocellular carcinoma as a prognostic factor: Tumor marker prognostic study. Int. J. Surg. *79*, 282–289.
Yu, X.F., Zou, J., Bao, Z.J., and Dong, J. (2011). miR-93 suppresses proliferation and colony formation of human colon cancer stem cells. World J Gastroenterol *17*, 4711–4717.
Yu, Z., Chen, D., Su, Z., Li, Y., Yu, W., Zhang, Q., Yang, L., Li, C., Yang, S., Ni, L., et al. (2014). miR-886-3p upregulation in clear cell renal cell carcinoma regulates cell migration, proliferation and apoptosis by targeting PITX1. Int. J. Mol. Med. *34*, 1409–1416.

Zheng, G., Qin, Y., Clark, W.C., Dai, Q., Yi, C., He, C., Lambowitz, A.M., and Pan, T. (2015). Efficient and quantitative high-throughput tRNA sequencing. Nat. Methods *12*, 835–837.
van Zon, A., Mossink, M.H., Schoester, M., Scheffer, G.L., Scheper, R.J., Sonneveld, P., and Wiemer, E.A. (2001). Multiple human vault RNAs. Expression and association with the vault complex. J. Biol. Chem. *276*, 37715–37721.

Supplementary Figure 1

A

TISSUES	N° Samples			
	Primary Tumor (ATAC-seq)	Primary Tumor (DNA methylation)	Primary Tumor (ATAC-seq & DNA methylation)	Adjacent Normal (DNA methylation)
ACC	9	80	9	0
BLCA	9	415	9	21
BRCA	73	789	42	96
CESC	2	307	2	3
CHOL	5	36	2	9
COAD	37	307	22	38
DLBC	0	48	0	0
ESCA	18	185	18	16
GBM	9	140	9	2
HNSC	8	528	8	50
KICH	0	66	0	0
KIRC	16	322	16	160
KIRP	33	275	33	45
LGG	10	516	10	0
LIHC	17	377	17	50
LUAD	22	469	22	32
LUSC	16	370	16	42
MESO	7	87	7	0
OV	0	10	0	0
PAAD	0	184	0	10
PCPG	9	179	9	3
PRAD	26	502	26	50
READ	0	98	0	7
SARC	0	261	0	4
SKCM	4	104	4	2
STAD	21	395	21	2
TGCT	8	150	8	0
THCA	14	507	14	56
THYM	0	124	0	2
UCEC	12	435	5	46
UCS	0	57	0	0
UVM	0	80	0	0
TOTAL N°	385	8403	329	746

B

TISSUES	Percentages			
	Primary Tumor (ATAC-seq)	Primary Tumor (DNA methylation)	Primary Tumor (ATAC-seq & DNA methylation)	Adjacent Normal (DNA methylation)
ACC	2	1	3	0
BLCA	2	5	3	3
BRCA	19	9	13	13
CESC	1	4	1	0
CHOL	1	0	1	1
COAD	10	4	7	5
DLBC	0	1	0	0
ESCA	5	2	5	2
GBM	2	2	3	0
HNSC	2	6	2	7
KICH	0	1	0	0
KIRC	4	4	5	21
KIRP	9	3	10	6
LGG	3	6	3	0
LIHC	4	4	5	7
LUAD	6	6	7	4
LUSC	4	4	5	6
MESO	2	1	2	0
OV	0	0	0	0
PAAD	0	2	0	1
PCPG	2	2	3	0
PRAD	7	6	8	7
READ	0	1	0	1
SARC	0	3	0	1
SKCM	1	1	1	0
STAD	5	5	6	0
TGCT	2	2	2	0
THCA	4	6	4	8
THYM	0	1	0	0
UCEC	3	5	2	6
UCS	0	1	0	0
UVM	0	1	0	0
TOTAL N°	100	100	100	100

Supplementary Figure 2

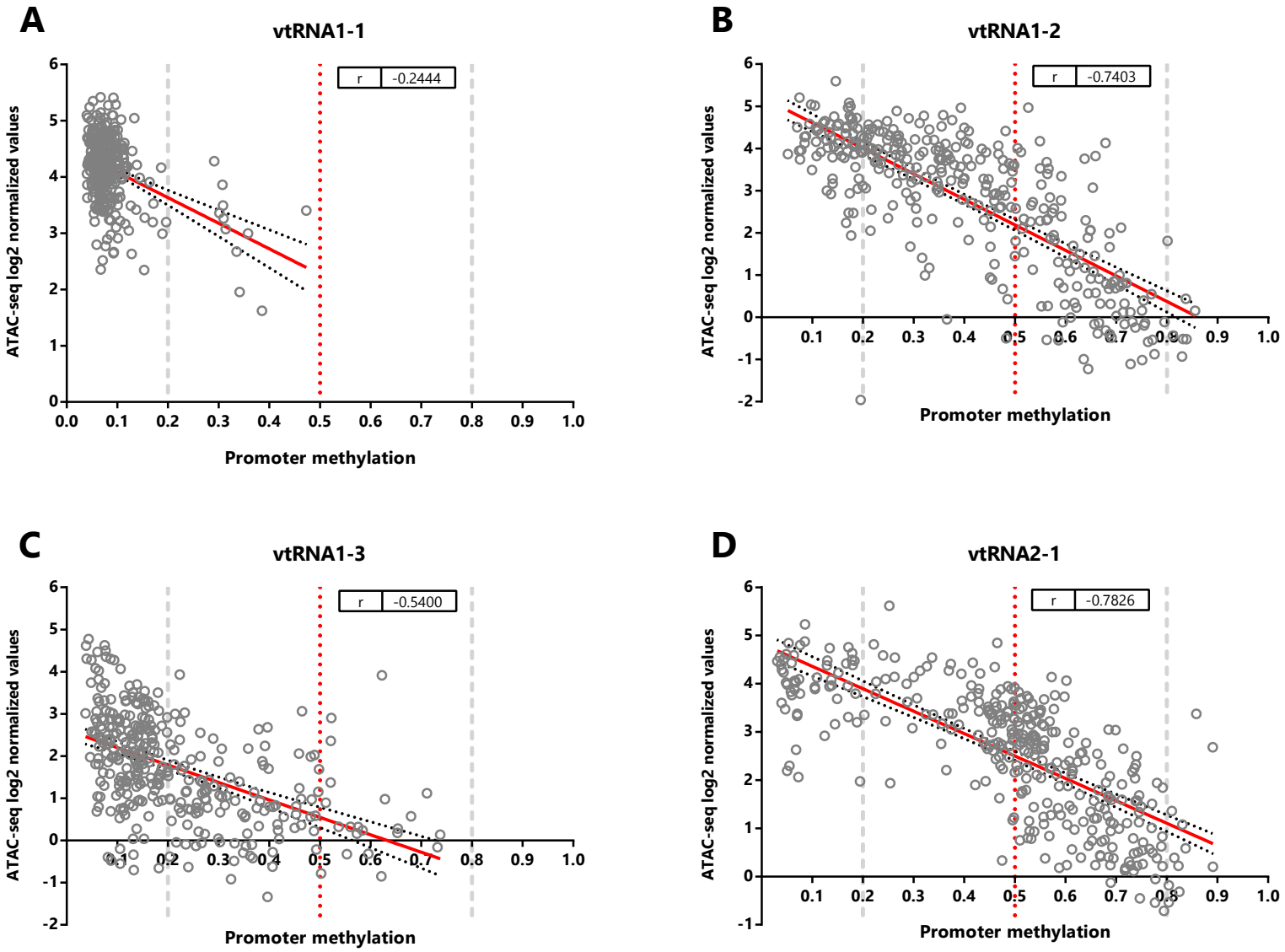

Supplementary Figure 3

A

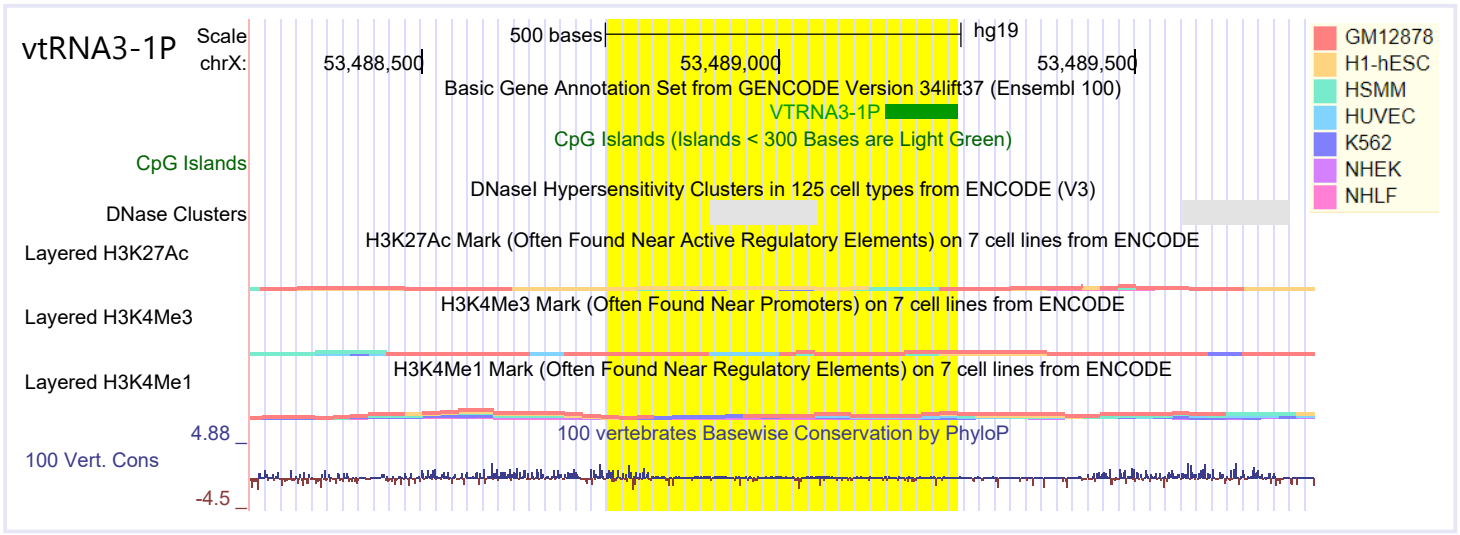

B

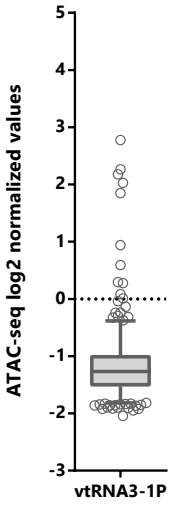

C

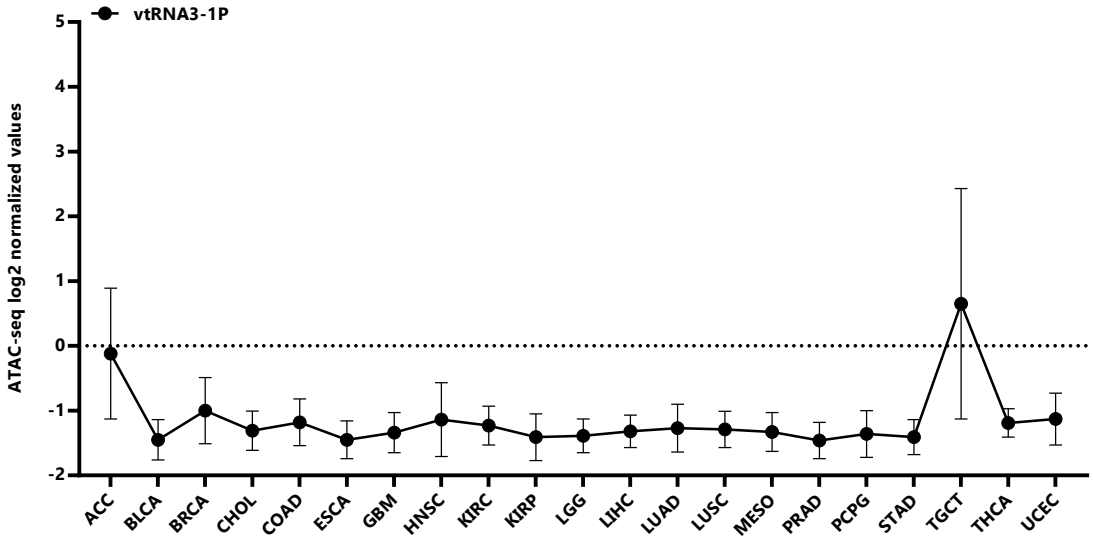

Supplementary Figure 4

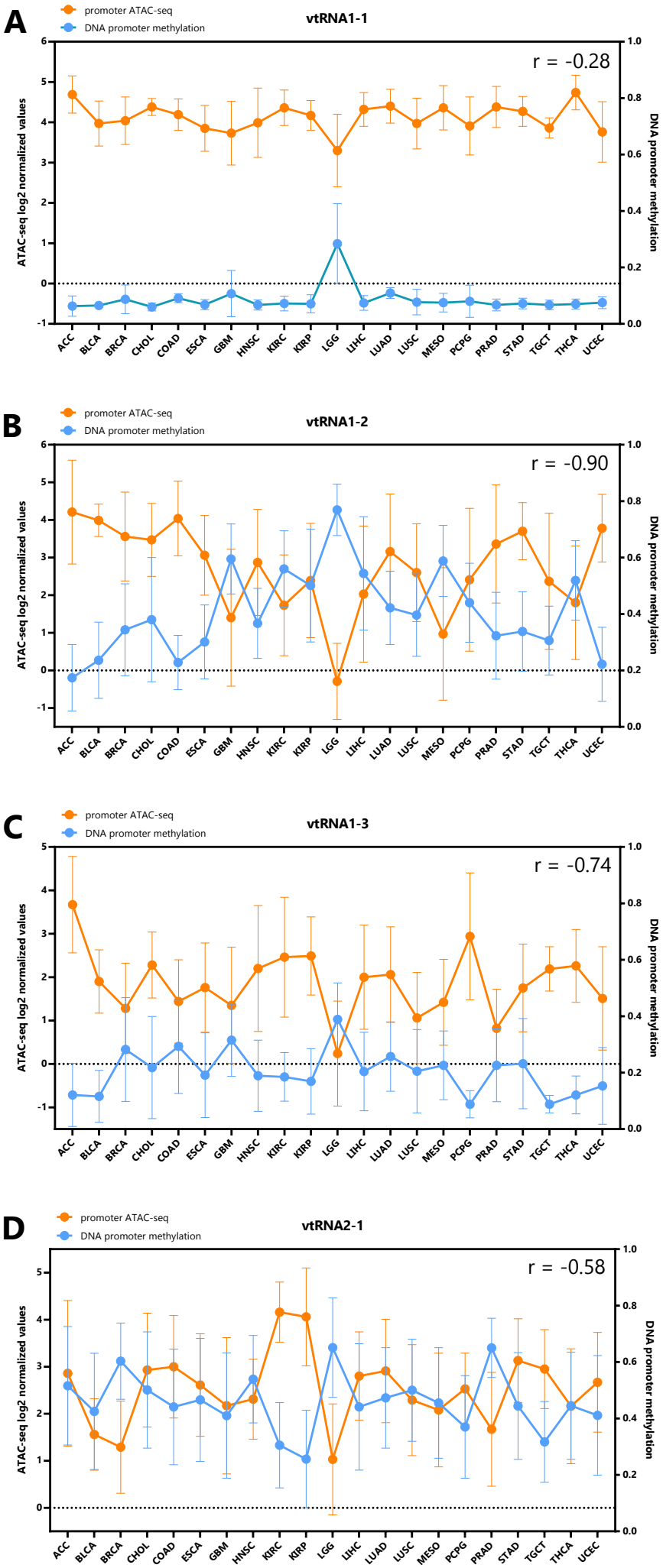

Supplementary Figure 5

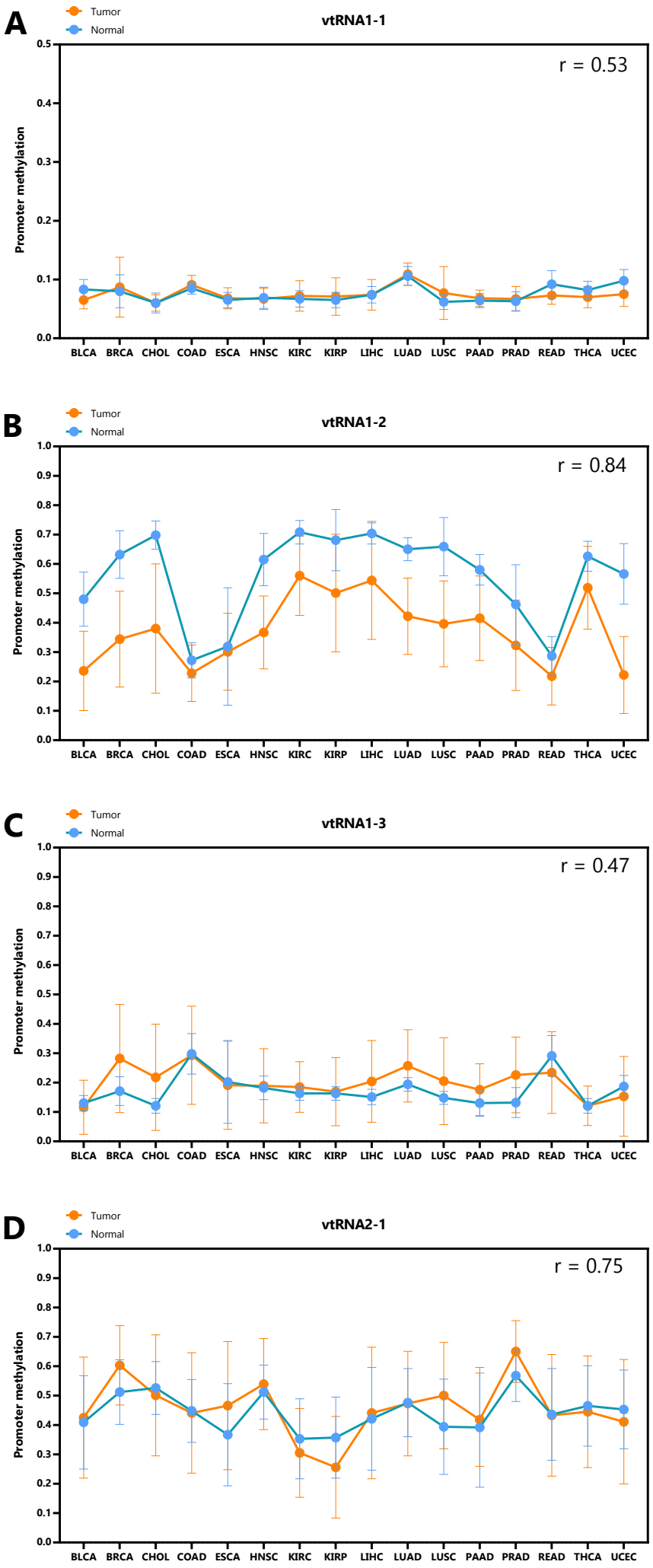

CONCLUSIONES Y PERSPECTIVAS

I. CONCLUSIONES DE OBJETIVOS ESPECÍFICOS.

En este trabajo buscamos aportar en la comprensión del origen de la desregulación de vtRNA2-1/nc886 y sus pequeños ARNs derivados, así como explorar el efecto de la alteración de sus niveles en la biología del PrCa.

Respecto a las implicancias de la desregulación de vtRNA2-1/nc886 en el origen y el mantenimiento del fenotipo tumoral de próstata, ***Objetivo específico 2.1***:

Determinamos que vtRNA2-1/nc886 se expresa en la próstata y que el mismo se encuentra reprimido en muestras de tejido tumoral respecto al tejido normal adyacente de prostactetomías radicales. Conjuntamente, evidenciamos que la metilación del promotor de vtRNA2-1/nc886 correlaciona negativamente con la expresión del transcrito en las líneas celulares de próstata PrEc, DU145, RWPE-1, LNCaP y PC3. Incluso, observamos que el tratamiento de líneas celulares de próstata (DU145, LNCaP, RWPE-1 y PC3) con agentes desmetilantes como 5-aza-citidina, provoca el incremento de los niveles de expresión de vtRNA2-1/nc886. Además, evidenciamos que los niveles de expresión de DNMT3B correlacionan positivamente con los niveles de metilación del promotor de vtRNA2-1/nc886, e incluso con los cambios relativos del mismo en la transición de tejido normal-tumor. La extensión del estudio de los niveles de metilación del promotor de vtRNA2-1/nc886 a las grandes cohortes de pacientes de PrCa, expuso que la metilación del promotor de vtRNA2-1/nc886 incrementa en el tejido tumoral de próstata respecto al tejido normal adyacente o benigno. En el mismo sentido, observamos que los niveles de metilación del promotor de vtRNA2-1/nc886 son aún mayores en muestras de metástasis de próstata. Además, los niveles de metilación del promotor de vtRNA2-1/nc886 mostraron asociación con parámetros clínicos de la patología; concretamente, establecimos que el incremento de los niveles de metilación del promotor de vtRNA2-1/nc886 se asocia con aumentos en los valores de estadificación histológica de Gleason, los valores clínicos T y con la recurrencia de la enfermedad. El conjunto de estos resultados, nos permite decir que vtRNA2-1/nc886 posee un perfil de expresión de tipo TSG y que la metilación de su promotor sería la etiología molecular de su represión en PrCa.

Adicionalmente, los ensayos funcionales de restitución forzada de vtRNA2-1/nc886 en líneas celulares de PrCa (DU145 y LNCaP), revelaron que su sobreexpresión reduce la capacidad invasiva y la viabilidad celular asociada

con un enriquecimiento de células en la fase G2/M del ciclo celular. El ensayo *in vivo* de xenotransplante en seis ratones inmunocomprometidos, confirmó los resultados *in vitro*, mostrando una reducción del crecimiento tumoral de las células que sobreexpresan vtRNA2-1/nc886 respecto al ARN control. Además, el impacto proliferativo se relaciona con los tumores de los pacientes por la asociación del aumento de los niveles de metilación del promotor de vtRNA2-1/nc886 y el aumento de la expresión de los genes de la firma de progresión del ciclo celular (CCP) en las muestras de PRAD-TCGA. Llamativamente, no encontramos asociación entre la actividad inferida de vtRNA2-1/nc886 y la actividad inferida de PKR en muestras clínicas de PrCa de la misma cohorte, lo que sugiere que vtRNA2-1/nc886 podría estar involucrado en la modulación de vías aún no identificadas en células prostáticas. El conjunto de los resultados, expone que vtRNA2-1/nc886 posee una influencia negativa en la viabilidad celular *in vitro* e *in vivo,* así como en la capacidad invasiva en células de próstata, que podrían asociarse con genes asociados a la progresión del ciclo celular.

Respecto a las implicancias de la desregulación de pequeños ARNs derivados de vtRNA2-1/nc886 y su posible contribución en el origen y el mantenimiento del fenotipo tumoral de próstata ***Objetivo específico 2.2*:**

Determinamos que vtRNA2-1/nc886 produce pequeños ARNs derivados en células de próstata y que los mismos poseen características que los posicionan como pequeños ARNs no codificantes con función tipo microARN. De hecho, los análisis de datos experimentales, indican que el procesamiento de los pequeños ARNs derivados de los extremos 5´ y 3´ de vtRNA2-1/nc886, hsa-miR-886-5p/snc886-5p y hsa-miR-886-3p/snc886-3p, respectivamente, son dependientes del procesamiento por DICER e independientes de DROSHA. Asimismo, evidenciamos que la expresión de hsa-miR-886-3p/snc886-3p se correlaciona directamente con la de su precursor vtRNA2-1/nc886 en las líneas celulares y muestras de prostatectomías de una cohorte nacional. Por tanto, al igual que su precursor, hsa-miR-886-3p/snc886-3p experimenta la represión de la expresión en la transición carcinogénica en la próstata, provocada por el incremento de la metilación del promotor del gen. Asimismo, el análisis de datos de experimentos de inmunoprecipitación, mostró la asociación de hsa-miR-886-5p/snc886-5p y hsa-miR-886-3p/snc886-3p con las proteínas Argonautas en la línea celular de próstata de DU145. En particular, observamos un enriquecimiento de hsa-miR-886-3p/snc886-3p en esta fracción. Nuestros ensayos de microarreglos de expresión génica diferencial modulando la expresión de hsa-miR-886-3p/snc886-3p en células de próstata, revelaron que es capaz de reprimir la expresión de genes con sitios complementarios a su región semilla en el 3'-UTR. Incluso, observamos que hsa-miR-886-3p/snc886-3p modularía genes relacionados con la vía del ciclo celular y apoptosis en la línea celular DU145. Complementariamente, evidenciamos que la restitución de hsa-miR-886-3p/snc886-3p utilizando mimics conduce a una reducción de la viabilidad celular, alteración del ciclo celular y un aumento de la apoptosis temprana en líneas celulares modelo de PrCa (DU145, LNCaP y PC3). Adicionalmente,

observamos que la expresión de una lista de posibles genes blanco de acción directa de hsa-miR-886-3p/snc886-3p, se asocia con peor sobrevida libre de enfermedad de PrCa. El conjunto de estos resultados permite hipotetizar que hsa-miR-886-3p/snc886-3p deriva de vtRNA2-1/nc886 y que, al igual que su precursor, poseería una función tipo TSG en células de próstata al reducir la viabilidad celular e incrementar la apoptosis temprana. Hsa-miR-886-3p/snc886-3p sería capaz de modular la expresión de genes que alterarían atributos tumorales, mediante su función tipo microARN en células de próstata, pudiendo contribuir en parte con el fenotipo TSG asociado a su precursor. El mecanismo molecular de acción de la molécula precursora vtRNA2-1/nc886 ocurre probablemente por otra vía independiente.

Llamativamente, la extensión de los análisis de expresión al otro fragmento derivado del extremo 5´ de vtRNA2-1/nc886, hsa-miR-886-5p/snc886-5p, mostraron que éste posee una expresión diferencial opuesta a la de su precursor y a la de hsa-miR-886-3p/snc886-3p en tejidos de próstata. Incluso, la expresión aumentada de hsa-miR-886-5p/snc886-5p en el tejido tumoral respecto al tejido normal adyacente de próstata, se asocia con peores valores clínicos de Gleason y patológicos N y T. Esta relación opuesta de expresión entre hsa-miR-886-5p/snc886-5p y hsa-miR-886-3p/snc886-3p, se extiende al estudiar su expresión diferencial en datos de sRNA-seq de líneas celulares primarias normales y de cáncer disponibles en repositorios de datos transcriptómicos. El conjunto de estos resultados, sugieren que hsa-miR-886-5p/snc886-5p posee un perfil OG en el PrCa, que es inverso al de su precursor vtRNA2-1/nc886 y el pequeño ARN derivado del otro extremo, hsa-miR-886-3p/snc886-3p. Esto sugiere que vtRNA2-1/nc886 sería blanco de un procesamiento diferencial que cambia la preferencia de brazos “arm switching”. Estas hipótesis deberán ser validadas experimentalmente.

Respecto a la evaluación del perfil de expresión global de vtRNA2-1/nc886 y su posible asociación funcional con los vtRNAs canónicos en el cáncer ***Objetivo específico 2.3*****:**

Confirmamos que los niveles de metilación del promotor de los vtRNAs representan una buena aproximación a los niveles de accesibilidad de la cromatina determinados por ATAC-seq en el set de datos públicos de Pan-Cáncer del TCGA. Igualmente, confirmamos que los vtRNAs presentan niveles de accesibilidad de cromatina diferencial entre sí y entre los diferentes tejidos. De hecho, observamos que los vtRNAs del clúster vtRNA1 poseen una mayor coordinación de la accesibilidad de la cromatina y una mayor coincidencia en la ocupación por factores de transcripción en comparación con vtRNA2-1/nc886. El vtRNA1-1, y en menor medida el vtRNA1-3, presentan un estado de accesibilidad a la cromatina ubicua y constante en los diferentes tejidos evaluados y en los estadios tumoral y normal adyacente. Esto coincide con la denominación en la literatura de vtRNA1-1 como el vtRNA ubicuo y con mayor asociación a la partícula vault. En concordancia, nuestros análisis sugieren que los patrones de metilación de los vtRNAs se establecen durante el desarrollo y divergen durante la diferenciación tisular, de

modo que la mayor parte de las diferencias entre tumores de diferente origen se deben a las diferencias preexistentes en los tejidos normales. Por otro lado, observamos que vtRNA2-1/nc886 presenta un aumento del nivel global de metilación en el tejido tumoral respecto al tejido normal adyacente. Incluso observamos que presenta un perfil de expresión TSG en tres tejidos y OG en un tejido, lo que sugiere una regulación tejido específica. Llamativamente, vemos que vtRNA1-2 posee un perfil de metilación global que disminuye en el tejido tumoral respecto al tejido normal adyacente. De hecho, observamos que posee un perfil OG en 13 de 16 tejidos en TCGA. La evaluación de la asociación de accesibilidad de la cromatina y la sobrevida de los pacientes reveló que vtRNA1-1, vtRNA1-2 y vtRNA2-1/nc886 se encuentran globalmente asociados con peor sobrevida a mayores niveles de accesibilidad de la cromatina de su promotor. Llamativamente, revelamos que vtRNA2-1/nc886 estaría co-regulado con genes asociados con la respuesta inmune nativa o la inmunomodulación y que vtRNA1-2 se encuentra asociado con la proliferación y el proceso de herida-cicatrización. De hecho, observamos asociación entre la accesibilidad de la cromatina de los vtRNAs con otros genes que terminan por sugerir que, en conjunto, los vtRNAs podrían encontrarse relacionados globalmente con la respuesta inmune.

II. CONCLUSIÓN GENERAL

Globalmente observamos que los vtRNAs poseen perfiles de expresión diferentes entre sí y entre tejidos, lo que sugiere que podrían tener funciones específicas. Confirmamos que el vtRNA1-1 se encontraría ubicuamente expresado y que el vtRNA2-1/nc886 sería el menos relacionado con los vtRNAs canónicos a nivel de coordinación de accesibilidad de cromatina de su promotor. Asimismo, expusimos que vtRNA2-1/nc886 y vtRNA1-2 poseen perfiles de expresión tejido específicos en cáncer, en gran medida opuestos sugiriendo globalmente perfiles TSG y OG respectivamente. Conjuntamente, los datos de expresión y asociación con otros genes, sugieren que los vtRNAs podrían encontrarse relacionados con la respuesta inmune en cáncer.

Específicamente en la próstata, confirmamos que el vtRNA2-1/nc886 se expresa y que el mismo sería procesado por DICER a pequeños ARNs no codificantes con función tipo microARN, debido a que son capaces de asociarse a las proteínas argonautas y reprimen transcritos con secuencias complementarias a su “seed”. Incluso, evidenciamos que el aumento de la metilación de su promotor (represión epigenética) durante la carcinogénesis prostática sería la etiología de la desregulación de vtRNA2-1/nc886 y hsa-miR-886-3p/snc886-3p. Conjuntamente, mostramos el incremento de hsa-miR-886-5p/snc886-5p en el tejido tumoral de próstata, lo que sugiere que vtRNA2-1/nc886 sufriría el fenómeno de procesamiento diferencial de brazos o “arm switching”. La evaluación de muestras clínicas de PrCa reveló que la represión de vtRNA2-1/nc886/hsa-miR-886-3p/snc886-3p y el aumento

de hsa-miR-886-5p/snc886-5p, se asocian con peores valores clínicos de la enfermedad. Concordantemente, la restitución forzada de vtRNA2-1/nc886 y hsa-miR-886-3p/snc886-3p en líneas celulares de PrCa valida una función TSG para ambas moléculas, asociada a una reducción de atributos tumorales, principalmente de la viabilidad celular. En suma, planteamos que vtRNA2-1/nc886 ejercería su función en PrCa mediante su acción como ARN completo, pudiendo contar con contribuciones adicionales producto de su procesamiento a dos sncARNs, uno supresor de tumor (hsa-miR-886-3p/snc886-3p) y otro que sería oncogénico (hsa-miR-886-5p/snc886-5p), quienes disminuyen y aumentan durante la carcinogénesis respectivamente.

III. PERSPECTIVAS.

Los resultados obtenidos en la presente Tesis dan lugar a diferentes perspectivas, a continuación, se destacan algunas de ellas.

En el contexto del PrCa determinamos la función TSG de vtRNA2-1/nc886 mediante la restitución de su expresión e incluso encontramos una asociación con la firma de genes CCP (Cuzick et al., 2011). Sin embargo, no encontramos asociación con los genes determinados para el *knockout* de vtRNA2-1/nc886 en otros tejidos (Lee et al., 2016, 2014a, 2014b), vinculados con la modulación de PKR y no abordamos profundamente su asociación con un mecanismo molecular en concreto. Resultaría interesante determinar los niveles de expresión/activación de proteínas o reporteros de vías moduladas por vtRNA2-1/nc886 en otros tejidos, por ejemplo, NF-Kb, PKR y/o OAS1 (Calderon & Conn, 2018; Lee, 2015; Lee et al., 2019b). En particular, dada la probable función de vtRNA2-1/nc886 como modulador de la actividad proteína por interacción directa con proteínas blanco, el análisis fosfo-proteómico, así como como el estudio de compañeros de unión directa podrían darnos una imagen completa de efecto directo en el contexto celular. Esto nos permitiría confirmar o descartar su modulación en respuesta a los cambios de expresión de vtRNA2-1/nc886. En este sentido, debido a que se han definido múltiples interactores, vías y procesos celulares asociados a la modulación de vtRNA2-1/nc886 en la literatura, otra opción posible es realizar una evaluación de la expresión génica global alterando los niveles de vtRNA2-1/nc886. Este abordaje ómico, permitiría una mirada global sin tener que enfocarse en ninguna hipótesis concreta. También podríamos vincular los resultados funcionales obtenidos con aquellas vías o efectores moleculares que se relacionen más directamente con los efectos fenotípicos. Además, podríamos relacionarlos con los resultados de expresión génica global obtenidos bajo la modulación de hsa-miR-886-3p/snc886-3p e intentar determinar aportes comunes e independientes de vtRNA2-1/nc886 y hsa-miR-886-3p/snc886-3p en las células de próstata.

Por otro lado, considerando que vtRNA2-1/nc886 es reprimido durante la carcinogénesis prostática, y de forma alternativa a la estrategia utilizada de restitución de vtRNA2-1/nc886 en células de PrCa, sería interesante reprimir la expresión de vtRNA2-1/nc886 en células normales de próstata. De hecho, esto permitiría abordar los posibles efectos funcionales de vtRNA2-1/nc886 en el inicio de la transformación maligna, así como podría dar lugar a efectos diferenciales debido a contextos celulares diferentes, revisado en Lee et al., 2015 y en Yeganeh & Hernandez, 2020.

Otro aspecto a explorar, emerge de la observación de que vtRNA2-1/nc886 posee la capacidad de alterar la capacidad invasiva en células de próstata *in vitro* y disminuye en los tumores metastáticos. Por esto, sería interesante extender el análisis de la modulación de hsa-miR-886-3p/snc886-3p a este fenotipo en el contexto *in*

vivo en modelos de ratón. Esto nos permitiría determinar si hsa-miR-886-3p/snc886-3p participa en este fenotipo, incluso considerando que se ha reportado su participación en este proceso en otros tejidos (Cao et al., 2013; Shen et al., 2018; Xiong et al., 2011).

Por último, el hecho de que vtRNA2-1/nc886 forme parte de una firma epigenética inmune, sumado a su presencia en exosomas y la síntesis de citoquinas, así como antecedentes de la literatura, lleva a pensar que afecte el secretoma celular, produciendo señales que modifican el nicho tumoral, a nivel de las células inmunes, de la matriz o la vasculatura o del estroma. Para investigar esta hipótesis se podría primero evaluar si cambian los niveles de citoquinas secretadas por las células que sobreexpresan o silencian vtRNA2-1/nc886 en cultivo utilizando proteómica o microarreglos de proteínas secretadas, así como ensayos de RT-qPCR o transcriptomas. En segundo lugar, se podría también analizar el efecto del sobrenadante de células que sobreexpresan vtRNA2-1/nc886 sobre otras células. La caracterización de los cambios provocados sería específica para cada atributo y tipo celular estudiado.

La evaluación de los niveles de expresión de hsa-miR-886-5p/snc886-5p revelaron que este presenta un perfil OG opuesto a su precursor y a hsa-miR-886-3p/snc886-3p en células de próstata. Esto estimula la realización de una caracterización funcional de hsa-miR-886-5p/snc886-5p en células de próstata como la que hicimos para hsa-miR-886-3p/snc886-3p. Un primer abordaje podría ser realizar ensayos funcionales para determinar si posee la capacidad de modular la viabilidad celular, utilizando mimics de hsa-miR-886-5p/snc886-5p en células de próstata. Fundamentalmente, esta perspectiva despierta gran interés debido a que en la literatura hsa-miR-886-5p/snc886-5p ha sido reportado como OG en múltiples tejidos (Dettmer et al., 2014; Khoshnevisan et al., 2015; Kong et al., 2015; Li et al., 2011; Liu et al., 2013; Xiang et al., 2019; Xiao et al., 2012; Zhang et al., 2014). En gran medida, esta perspectiva implica explorar una nueva hipótesis que plantea que el procesamiento de vtRNA2-1/nc886 a hsa-miR-886s/snc886s durante la carcinogénesis experimenta un cambio de preferencia de brazos (fragmentos derivados de los extremos 5’ y 3’ de la molécula) “arm switching”, que conllevaría a la disminución del pequeño ARN derivado del extremo 3’ (hsa-miR-886-3p/snc886-3p), al tiempo que provocaría un aumento del pequeño ARN derivado del extremo 5’ (hsa-miR-886-5p/snc886-5p). Entonces, el aumento de expresión de hsa-miR-886-5p/snc886-5p con actividad OG en el tumor promovería atributos pro-tumorales, efectivizando una contribución adicional en la carcinogénesis de próstata, que se suma a las ya reportadas por la pérdida en el tumor para vtRNA2-1/nc886 y hsa-miR-886-3p/snc886-3p.

En conjunto, consideramos que vtRNA2-1/nc886 en conjunto con sus hsa-miR-886s/snc886s derivados podría actuar globalmente en la carcinogénesis provocando tres impactos. Una aproximación útil para analizar si su

efecto es aditivo o de otro tipo, sería modular la expresión de combinaciones de estas tres moléculas (ya sea bloqueo o sobreexpresión) y determinar el efecto funcional.

Respecto a la evaluación de la accesibilidad de la cromatina de los vtRNAs en Pan-Cáncer, sería sugestivo determinar los niveles de expresión mediante RT-qPCR de los vtRNAs en una cohorte de muestras de tejido normal y tumoral. Esto permitiría confirmar las diferencias globales determinadas mediante la accesibilidad de la cromatina. Dado que revelamos a vtRNA1-2 como posible OG de efecto en muchos tipos de cáncer, porque observamos un marcado incremento de la accesibilidad de la cromatina en los tumores, sería especialmente importante confirmar el perfil de expresión tipo OG para vtRNA1-2, que no ha sido determinado y alentaría el estudio de su posible efecto en la carcinogénesis.

AGENCIAS FINANCIADORAS

REFERENCIAS

Aakula, A., Kohonen, P., Leivonen, S.K., Mäkelä, R., Hintsanen, P., Mpindi, J.P., Martens-Uzunova, E., Aittokallio, T., Jenster, G., Perälä, M., et al. (2015). Systematic Identification of MicroRNAs That Impact on Proliferation of Prostate Cancer Cells and Display Changed Expression in Tumor Tissue. Eur. Urol. *69*, 1120–1128.

Abeshouse, A., Ahn, J., Akbani, R., Ally, A., Amin, S., Andry, C.D., Annala, M., Aprikian, A., Armenia, J., Arora, A., et al. (2015). The Molecular Taxonomy of Primary Prostate Cancer. Cell *163*, 1011–1025.

Acunzo, M., Romano, G., Wernicke, D., & Croce, C.M. (2015). MicroRNA and cancer - A brief overview. Adv. Biol. Regul. *57*, 1–9.

Aghdam, S.G., Ebrazeh, M., Hemmatzadeh, M., Seyfizadeh, N., Shabgah, A.G., Azizi, G., Ebrahimi, N., Babaie, F., & Mohammadi, H. (2019). The role of microRNAs in prostate cancer migration, invasion, and metastasis. J. Cell. Physiol. *234*, 9927–9942.

Ahn, J.H., Lee, H.S., Lee, J.S., Lee, Y.S., Park, J.L., Kim, S.Y., Hwang, J.A., Kunkeaw, N., Jung, S.Y., Kim, T.J., et al. (2018). Nc886 is induced by TGF-β and suppresses the microRNA pathway in ovarian cancer. Nat. Commun. *9*.

Amort, M., Nachbauer, B., Tuzlak, S., Kieser, A., Schepers, A., Villunger, A., & Polacek, N. (2015). Expression of the vault RNA protects cells from undergoing apoptosis. Nat. Commun. *6*, 7030.

Arroyo, J.D., Chevillet, J.R., Kroh, E.M., Ruf, I.K., Pritchard, C.C., Gibson, D.F., Mitchell, P.S., Bennett, C.F., Pogosova-Agadjanyan, E.L., Stirewalt, D.L., et al. (2011). Argonaute2 complexes carry a population of circulating microRNAs independent of vesicles in human plasma. Proc. Natl. Acad. Sci. U. S. A. *108*, 5003–5008.

van Balkom, B.W.M., Eisele, A.S., Pegtel, D.M., Bervoets, S., & Verhaar, M.C. (2015). Quantitative and qualitative analysis of small RNAs in human endothelial cells and exosomes provides insights into localized RNA processing, degradation and sorting. J. Extracell. Vesicles *4*, 26760.

Barrios, E., & Garau, M. (2017). Cáncer: magnitud del problema en el mundo y en Uruguay, aspectos epidemiológicos. An. La Fac. Med. *4*, 7–161.

Bartel, D.P. (2004). MicroRNAs: Genomics, Biogenesis, Mechanism, and Function. Cell *116*, 281–297.

Bartel, D.P. (2009). MicroRNAs: target recognition and regulatory functions. Cell *136*, 215–233.

Bartel, D.P. (2018). Metazoan MicroRNAs. Cell *173*, 20–51.

Berezikov, E. (2011). Evolution of microRNA diversity and regulation in animals. Nat. Rev. Genet. *12*, 846–860.

Berezikov, E., Robine, N., Samsonova, A., Westholm, J.O., Naqvi, A., Hung, J.H., Okamura, K., Dai, Q., Bortolamiol-Becet, D., Martin, R., et al. (2011). Deep annotation of Drosophila melanogaster microRNAs yields insights into their processing, modification, and emergence. Genome Res. *21*, 203–215.

Bi, N., Cao, J., Song, Y., Shen, J., Liu, W., Fan, J., He, J., Shi, Y., Zhang, X., Lu, N., et al. (2014). A MicroRNA signature predicts survival in early stage small-cell lung cancer treated with surgery and adjuvant chemotherapy. PLoS One

9, 1–8.

Bolton, E.M., Tuzova, A. V, Walsh, A.L., Lynch, T., & Perry, A.S. (2014). Noncoding RNAs in prostate cancer: the long and the short of it. Clin. Cancer Res. *20*, 35–43.

Bouyssou, J.M.C., Manier, S., Huynh, D., Issa, S., Roccaro, A.M., & Ghobrial, I.M. (2014). Regulation of microRNAs in cancer metastasis. Biochim. Biophys. Acta - Rev. Cancer.

Bracher, L., Ferro, I., Pulido-Quetglas, C., Ruepp, M.D., Johnson, R., & Polacek, N. (2020). Human vtRNA1-1 levels modulate signaling pathways and regulate apoptosis in human cancer cells. Biomolecules *10*.

Brandão, A., Paulo, P., & Teixeira, M.R. (2020). Hereditary predisposition to prostate cancer: From genetics to clinical implications. Int. J. Mol. Sci. *21*, 1–23.

Bray, F., Ferlay, J., Soerjomataram, I., Siegel, R.L., Torre, L.A., & Jemal, A. (2018). Global cancer statistics 2018: GLOBOCAN estimates of incidence and mortality worldwide for 36 cancers in 185 countries. CA. Cancer J. Clin. *68*, 394–424.

Bubendorf, L., Schöpfer, A., Wagner, U., Sauter, G., Moch, H., Willi, N., Gasser, T.C., & Mihatsch, M.J. (2000). Metastatic patterns of prostate cancer: An autopsy study of 1,589 patients. Hum. Pathol. *31*, 578–583.

Burke, J.M., & Sullivan, C.S. (2017). DUSP11 – An RNA phosphatase that regulates host and viral non-coding RNAs in mammalian cells. RNA Biol. *14*, 1457–1465.

Burke, J.M., Kincaid, R.P., Nottingham, R.M., Lambowitz, A.M., & Sullivan, C.S. (2016). DUSP11 activity on triphosphorylated transcripts promotes Argonaute association with noncanonical viral microRNAs and regulates steady-state levels of cellular noncoding RNAs. Genes Dev. *30*, 2076–2092.

Büscher, M., Horos, R., & Hentze, M.W. (2020). 'High vault-age': Non-coding RNA control of autophagy. Open Biol. *10*.

Calderon, B.M., & Conn, G.L. (2017). Human noncoding RNA 886 (nc886) adopts two structurally distinct conformers that are functionally opposing regulators of PKR. RNA *23*, 557–566.

Calderon, B.M., & Conn, G.L. (2018). A human cellular noncoding RNA activates the antiviral protein 2'-5'-oligoadenylate synthetase 1. J. Biol. Chem. *293*, 16115–16124.

Calin, G.A., Dumitru, C.D., Shimizu, M., Bichi, R., Zupo, S., Noch, E., Aldler, H., Rattan, S., Keating, M., Rai, K., et al. (2002). Frequent deletions and down-regulation of micro-RNA genes miR15 and miR16 at 13q14 in chronic lymphocytic leukemia. Proc. Natl. Acad. Sci. U. S. A. *99*, 15524–15529.

Canella, D., Praz, V., Reina, J.H., Cousin, P., & Hernandez, N. (2010). Defining the RNA polymerase III transcriptome: Genome-wide localization of the RNA polymerase III transcription machinery in human cells. Genome Res. *20*, 710–721.

Cao, J., Song, Y., Bi, N., Shen, J., Liu, W., Fan, J., Sun, G., Tong, T., He, J., Shi, Y., et al. (2013). DNA methylation-mediated repression of miR-886-3p predicts poor outcome of human small cell lung cancer. Cancer Res. *73*, 3326–3335.

Castillejos-Molina, R.A., & Gabilondo-Navarro, F.B. (2016). Prostate cancer. Salud Publica Mex. *58*, 279–284.

Chen, J., OuYang, H., An, X., & Liu, S. (2018a). Vault RNAs partially induces drug resistance of human tumor cells MCF-7 by binding to the RNA/DNA-binding protein PSF and inducing oncogene GAGE6. PLoS One *13*, e0191325.

Chen, L., Sun, H., Wang, C., Yang, Y., Zhang, M., & Wong, G. (2018b). miRNA arm switching identifies novel tumour biomarkers. EBioMedicine *38*, 37–46.

Chu, A., Robertson, G., Brooks, D., Mungall, A.J., Birol, I., Coope, R., Ma, Y., Jones, S., & Marra, M.A. (2015). Large-scale profiling of microRNAs for The Cancer Genome Atlas. Nucleic Acids Res. *44*, e3–e3.

Chu, A., Robertson, G., Brooks, D., Mungall, A.J., Birol, I., Coope, R., Ma, Y., Jones, S., & Marra, M.A. (2016). Large-scale profiling of microRNAs for The Cancer Genome Atlas. Nucleic Acids Res. *44*, e3–e3.

Cloonan, N., Wani, S., Xu, Q., Gu, J., Lea, K., Heater, S., Barbacioru, C., Steptoe, A.L., Martin, H.C., Nourbakhsh, E., et al. (2011). MicroRNAs and their isomiRs function cooperatively to target common biological pathways. Genome Biol. *12*, R126.

Cochetti, G., Poli, G., Guelfi, G., Boni, A., Egidi, M.G., & Mearini, E. (2016). Different levels of serum microRNAs in prostate cancer and benign prostatic hyperplasia: Evaluation of potential diagnostic and prognostic role. Onco. Targets. Ther. *9*, 7545–7553.

Costinean, S., Zanesi, N., Pekarsky, Y., Tili, E., Volinia, S., Heerema, N., & Croce, C.M. (2006). Pre-B cell proliferation and lymphoblastic leukemia/high-grade lymphoma in Eμ-miR155 transgenic mice. Proc. Natl. Acad. Sci. U. S. A. *103*, 7024–7029.

Cuzick, J., Swanson, G.P., Fisher, G., Brothman, A.R., Berney, D.M., Reid, J.E., Mesher, D., Speights, V.O., Stankiewicz, E., Foster, C.S., et al. (2011). Prognostic value of an RNA expression signature derived from cell cycle proliferation genes in patients with prostate cancer: a retrospective study. Lancet. Oncol. *12*, 245–255.

De Marzo, A.M., Meeker, A.K., Zha, S., Luo, J., Nakayama, M., Platz, E.A., Isaacs, W.B., & Nelson, W.G. (2003). Human prostate cancer precursors and pathobiology. Urology *62*, 55–62.

De Marzo, A.M., Platz, E.A., Epstein, J.I., Ali, T., Billis, A., Chan, T.Y., Cheng, L., Datta, M., Egevad, L., Ertoy-Baydar, D., et al. (2006). A working group classification of focal prostate atrophy lesions. Am. J. Surg. Pathol. *30*, 1281–1291.

De Marzo, A.M., Platz, E.A., Sutcliffe, S., Xu, J., Grönberg, H., Drake, C.G., Nakai, Y., Isaacs, W.B., & Nelson, W.G. (2007). Inflammation in prostate carcinogenesis. Nat. Rev. Cancer *7*, 256–269.

Dettmer, M.S., Perren, A., Moch, H., Komminoth, P., Nikiforov, Y.E., & Nikiforova, M.N. (2014). MicroRNA profile of poorly differentiated thyroid carcinomas: New diagnostic and prognostic insights. J. Mol. Endocrinol. *52*, 181–189.

Devi, P.U., & Hossain, M. (2000). Induction of solid tumours in the Swiss albino mouse by low-dose foetal irradiation. Int. J. Radiat. Biol. *76*, 95–99.

Devor, E.J., Schickling, B.M., & Leslie, K.K. (2014). microRNA expression patterns across seven cancers are highly correlated and dominated by evolutionarily ancient families. Biomed. Reports *2*, 384–387.

van Dijk, S.J., Peters, T.J., Buckley, M., Zhou, J., Jones, P.A., Gibson, R.A., Makrides, M., Muhlhausler, B.S., & Molloy, P.L. (2018). DNA methylation in blood from neonatal screening cards and the association with BMI and insulin sensitivity in early childhood. Int. J. Obes. *42*, 28–35.

Doldi, V., Pennati, M., Forte, B., Gandellini, P., & Zaffaroni, N. (2016). Dissecting the role of microRNAs in prostate cancer metastasis: implications for the design of novel therapeutic approaches. Cell. Mol. Life Sci. *73*, 2531–2542.

Epstein, J.I., Egevad, L., Amin, M.B., Delahunt, B., Srigley, J.R., & Humphrey, P.A. (2016). The 2014 international

society of urological pathology (ISUP) consensus conference on gleason grading of prostatic carcinoma definition of grading patterns and proposal for a new grading system. Am. J. Surg. Pathol. *40*, 244–252.

Esteller, M. (2011). Non-coding RNAs in human disease. Nat. Rev. Genet. *12*, 861–874.

Eulalio, A., Huntzinger, E., & Izaurralde, E. (2008). Getting to the Root of miRNA-Mediated Gene Silencing. Cell *132*, 9–14.

Farkas, A., Marcella, S., & Rhoads, G.G. (2000). Ethnic and racial differences in prostate cancer incidence and mortality. Ethn. & Dis. *10*, 69—75.

Fendler, A., Jung, M., Stephan, C., Honey, R.J., Stewart, R.J., Pace, K.T., Erbersdobler, A., Samaan, S., Jung, K., & Yousef, G.M. (2011). miRNAs can predict prostate cancer biochemical relapse and are involved in tumor progression. Int. J. Oncol. *39*, 1183–1192.

Ferlay, J., Colombet, M., Soerjomataram, I., Mathers, C., Parkin, D.M., Piñeros, M., Znaor, A., & Bray, F. (2019). Estimating the global cancer incidence and mortality in 2018: GLOBOCAN sources and methods. Int. J. Cancer *144*, 1941–1953.

Fornetti, J., Welm, A.L., & Stewart, S.A. (2018). Understanding the Bone in Cancer Metastasis. J. Bone Miner. Res. *33*, 2099–2113.

Fort, R.S., Mathó, C., Geraldo, M.V., Ottati, M.C., Yamashita, A.S., Saito, K.C., Leite, K.R.M., Méndez, M., Maedo, N., Méndez, L., et al. (2018). Nc886 is epigenetically repressed in prostate cancer and acts as a tumor suppressor through the inhibition of cell growth. BMC Cancer *18*, 127.

Fort, R.S., Garat, B., Sotelo-Silveira, J.R., & Duhagon, M.A. (2020). vtRNA2-1/nc886 Produces a Small RNA That Contributes to Its Tumor Suppression Action through the microRNA Pathway in Prostate Cancer. Non-Coding RNA *6*, 7.

Friedländer, M.R., Mackowiak, S.D., Li, N., Chen, W., & Rajewsky, N. (2012). miRDeep2 accurately identifies known and hundreds of novel microRNA genes in seven animal clades. Nucleic Acids Res. *40*, 37–52.

Friedman, R.C., Farh, K.K.-H., Burge, C.B., & Bartel, D.P. (2008). Most mammalian mRNAs are conserved targets of microRNAs. Genome Res. *19*, 92–105.

Fuziwara, C.S., & Kimura, E.T. (2014). MicroRNA Deregulation in Anaplastic Thyroid Cancer Biology. Int. J. Endocrinol. *2014*.

Gandellini, P., Folini, M., & Zaffaroni, N. (2009). Towards the definition of prostate cancer-related microRNAs: where are we now? Trends Mol. Med. *15*, 381–390.

Gao, W., Shen, H., Liu, L., Xu, J., Xu, J., & Shu, Y. (2011). MiR-21 overexpression in human primary squamous cell lung carcinoma is associated with poor patient prognosis. J. Cancer Res. Clin. Oncol. *137*, 557–566.

Garau, M., Musetti, C., Alonso, R., & Barrios, E. (2019). Trends in cancer incidence in Uruguay: 2002-2015. Colomb. Med. *50*, 224–238.

Golec, E., Lind, L., Qayyum, M., Blom, A.M., & King, B.C. (2019). The Noncoding RNA nc886 Regulates PKR Signaling and Cytokine Production in Human Cells. J. Immunol. *202*, 131–141.

Gopinath, S.C.B., Matsugami, A., Katahira, M., & Kumar, P.K.R. (2005). Human vault-associated non-coding RNAs bind to mitoxantrone, a chemotherapeutic compound. Nucleic Acids Res. *33*, 4874–4881.

Gopinath, S.C.B., Wadhwa, R., & Kumar, P.K.R. (2010). Expression of noncoding vault RNA in human malignant cells and its importance in mitoxantrone resistance. Mol. Cancer Res. *8*, 1536–1546.

Griffiths-Jones, S. (2006). miRBase: microRNA sequences, targets and gene nomenclature. Nucleic Acids Res. *34*, D140–D144.

Griffiths-Jones, S., Hui, J.H.L., Marco, A., & Ronshaugen, M. (2011). MicroRNA evolution by arm switching. EMBO Rep. *12*.

Guerrero, I., & Pellicer, A. (1987). Mutational activation of oncogenes in animal model systems of carcinogenesis (MTR 07217). Mutat. Res. Genet. Toxicol. *185*, 293–308.

Gundem, G., Van Loo, P., Kremeyer, B., Alexandrov, L.B., Tubio, J.M.C., Papaemmanuil, E., Brewer, D.S., Kallio, H.M.L., Högnäs, G., Annala, M., et al. (2015). The evolutionary history of lethal metastatic prostate cancer. Nature *520*, 353–357.

Guo, H., Ingolia, N.T., Weissman, J.S., & Bartel, D.P. (2010). Mammalian microRNAs predominantly act to decrease target mRNA levels. Nature *466*, 835–840.

Guo, L., Zhang, H., Zhao, Y., Yang, S., & Chen, F. (2014). Selected isomiR expression profiles via arm switching? Gene.

Han, Z.-B., Zhong, L., Teng, M.-J., Fan, J.-W., Tang, H.-M., Wu, J.-Y., Chen, H.-Y., Wang, Z.-W., Qiu, G.-Q., & Peng, Z.-H. (2012). Identification of recurrence-related microRNAs in hepatocellular carcinoma following liver transplantation. Mol. Oncol. *6*, 445–457.

Hanahan, D., & Weinberg, R.A. (2011). Hallmarks of cancer: The next generation. Cell *144*, 646–674.

Helbo, A.S., Treppendahl, M., Aslan, D., Dimopoulos, K., Nandrup-Bus, C., Holm, M.S., Andersen, M.K., Liang, G., Kristensen, L.S., & Grønbæk, K. (2015). Hypermethylation of the VTRNA1-3 promoter is associated with poor outcome in lower risk myelodysplastic syndrome patients. Genes (Basel). *6*, 977–990.

Helbo, A.S., Lay, F.D., Jones, P.A., Liang, G., & Grønbæk, K. (2017). Nucleosome Positioning and NDR Structure at RNA Polymerase III Promoters. Sci. Rep. *7*.

Hernandez, D.J., Nielsen, M.E., Han, M., & Partin, A.W. (2007). Contemporary Evaluation of the D'Amico Risk Classification of Prostate Cancer. Urology *70*, 931–935.

Hesse, E., & Taipaleenmäki, H. (2019). MicroRNAs in Bone Metastasis. Curr. Osteoporos. Rep. *17*, 122–128.

Holcomb, I.N., Grove, D.I., Kinnunen, M., Friedman, C.L., Gallaher, I.S., Morgan, T.M., Sather, C.L., Delrow, J.J., Nelson, P.S., Lange, P.H., et al. (2008). Genomic alterations indicate tumor origin and varied metastatic potential of disseminated cells from prostate cancer patients. Cancer Res. *68*, 5599–5608.

Holcomb, I.N., Young, J.M., Coleman, I.M., Salari, K., Grove, D.I., Li, H., True, L.D., Roudier, M.P., Morrissey, C.M., Higano, C.S., et al. (2009). Comparative analyses of chromosome alterations in soft-tissue metastases within and across patients with castration-resistant prostate cancer. Cancer Res. *69*, 7793–7802.

Horos, R., Büscher, M., Kleinendorst, R., Alleaume, A.-M., Tarafder, A.K., Schwarzl, T., Dziuba, D., Tischer, C., Zielonka, E.M., Adak, A., et al. (2019). The Small Non-coding Vault RNA1-1 Acts as a Riboregulator of Autophagy. Cell *176*, 1054-1067.e12.

Hu, Z., Zhang, H., Tang, L., Lou, M., & Geng, Y. (2017). Silencing nc886, a Non-Coding RNA, Induces Apoptosis of Human Endometrial Cancer Cells-1A In Vitro. Med. Sci. Monit. *23*, 1317–1324.

Hussain, S., Sajini, A.A., Blanco, S., Dietmann, S., Lombard, P., Sugimoto, Y., Paramor, M., Gleeson, J.G., Odom, D.T., Ule, J., et al. (2013). NSun2-mediated cytosine-5 methylation of vault noncoding RNA determines its processing into regulatory small RNAs. Cell Rep. *4*, 255–261.

Im, W.R., Lee, H.-S., Lee, Y.-S., Lee, J.-S., Jang, H.-J., Kim, S.-Y., Park, J.-L., Lee, Y., Kim, M.S., Lee, J.M., et al. (2020). A Regulatory Noncoding RNA, nc886, Suppresses Esophageal Cancer by Inhibiting the AKT Pathway and Cell Cycle Progression. Cells *9*, 801.

Jeon, S.H., Lee, K., Lee, K.S., Kunkeaw, N., Johnson, B.H., Holthauzen, L.M.F., Gong, B., Leelayuwat, C., & Lee, Y.S. (2012a). Characterization of the direct physical interaction of nc886, a cellular non-coding RNA, and PKR. FEBS Lett. *586*, 3477–3484.

Jeon, S.H., Johnson, B.H., & Lee, Y.S. (2012b). A tumor surveillance model: A non-coding RNA senses neoplastic cells and its protein partner signals cell death. Int. J. Mol. Sci. *13*, 13134–13139.

Johansen, T. (2019). Selective Autophagy: RNA Comes from the Vault to Regulate p62/SQSTM1. Curr. Biol. *29*, R297–R299.

Joo, J.E., Dowty, J.G., Milne, R.L., Wong, E.M., Dugué, P.A., English, D., Hopper, J.L., Goldgar, D.E., Giles, G.G., Southey, M.C., et al. (2018). Heritable DNA methylation marks associated with susceptibility to breast cancer. Nat. Commun. *9*.

Kedersha, N.L., & Rome, L.H. (1986). Isolation and characterization of a novel ribonucleoprotein particle: Large structures contain a single species of small RNA. J. Cell Biol. *103*, 699–709.

Kedersha, N.L., Miquel, M.C., Bittner, D., & Rome, L.H. (1990). Vaults. II. Ribonucleoprotein structures are highly conserved among higher and lower eukaryotes. J. Cell Biol. *110*, 895–901.

Kedersha, N.L., Heuser, J.E., Chugani, D.C., & Rome, L.H. (1991). Vaults. III. Vault ribonucleoprotein particles open into flower-like structures with octagonal symmetry. J. Cell Biol. *112*, 225–235.

Khoshnevisan, A., Parvin, M., Ghorbanmehr, N., Hatefi, N., Galehdari, H., Ziaee, S.A.M., & Mowla, S.J. (2015). A Significant Upregulation of miR-886-5p in High Grade and Invasive Bladder Tumors. Urol. J. *12*, 2160–2164.

Kickhoefer, V.A., Searles, R.P., Kedersha, N.L., Garber, M.E., Johnson, D.L., & Rome, L.H. (1993). Vault ribonucleoprotein particles from rat and bullfrog contain a related small RNA that is transcribed by RNA polymerase III. J. Biol. Chem. *268*, 7868–7873.

Kickhoefer, V.A., Rajavel, K.S., Scheffer, G.L., Dalton, W.S., Scheper, R.J., & Rome, L.H. (1998). Vaults are up-regulated in multidrug-resistant cancer cell lines. J. Biol. Chem. *273*, 8971–8974.

Kickhoefer, V.A., Stephen, A.G., Harrington, L., Robinson, M.O., & Rome, L.H. (1999). Vaults and telomerase share a common subunit, TEP1. J. Biol. Chem. *274*, 32712–32717.

Kickhoefer, V.A., Liu, Y., Kong, L.B., Snow, B.E., Stewart, P.L., Harrington, L., & Rome, L.H. (2001). The Telomerase/vault-associated protein TEP1 is required for vault RNA stability and its association with the vault particle. J. Cell Biol. *152*, 157–164.

Kickhoefer, V.A., Poderycki, M.J., Chan, E.K.L., & Rome, L.H. (2002). The La RNA-binding protein interacts with the vault RNA and is a vault-associated protein. J. Biol. Chem. *277*, 41282–41286.

Kim, B., Ha, M., Loeff, L., Chang, H., Simanshu, D.K., Li, S., Fareh, M., Patel, D.J., Joo, C., & Kim, V.N. (2015). TUT7 controls the fate of precursor microRNAs by using three different uridylation mechanisms. EMBO J. *34*, 1801–

1815.

Kim, H., Kim, J., Yu, S., Lee, Y.-Y., Park, J., Choi, R.J., Yoon, S.-J., Kang, S.-G., & Kim, V.N. (2020). A Mechanism for microRNA Arm Switching Regulated by Uridylation. Mol. Cell *0*.

Kim, V.N., Han, J., & Siomi, M.C. (2009). Biogenesis of small RNAs in animals. Nat. Rev. Mol. Cell Biol. *10*, 126–139.

Kim, Y.-K., Kim, B., & Kim, V.N. (2016). Re-evaluation of the roles of DROSHA, Export in 5, and DICER in microRNA biogenesis. Proc. Natl. Acad. Sci. U. S. A. *113*, E1881-9.

Kong, L., Hao, Q., Wang, Y., Zhou, P., Zou, B., & Zhang, Y. (2015). Regulation of p53 expression and apoptosis by vault RNA2-1-5p in cervical cancer cells. Oncotarget *6*, 28371–28388.

Konoshenko, M.Y., Lekchnov, E.A., Bryzgunova, O.E., Zaporozhchenko, I.A., Yarmoschuk, S. V., Pashkovskaya, O.A., Pak, S. V., & Laktionov, P.P. (2020). The panel of 12 cell-free microRNAs as potential biomarkers in prostate neoplasms. Diagnostics *10*.

Kral, M., Rosinska, V., Student, V., Grepl, M., Hrabec, M., & Bouchal, J. (2011). Genetic determinants of prostate cancer: A review. Biomed. Pap. *155*, 3–10.

Kunkeaw, N., Jeon, S.H., Lee, K., Johnson, B.H., Tanasanvimon, S., Javle, M., Pairojkul, C., Chamgramol, Y., Wongfieng, W., Gong, B., et al. (2012). Cell death/proliferation roles for nc886, a non-coding RNA, in the protein kinase R pathway in cholangiocarcinoma. Oncogene *32*, 3722–3731.

Kunkeaw, N., Lee, Y.S., Im, W.R., Jang, J.J., Song, M.J., Yang, B., Park, J.L., Kim, S.Y., Ku, Y., Kim, Y., et al. (2019). Mechanism mediated by a noncoding RNA, nc886, in the cytotoxicity of a DNA-reactive compound. Proc. Natl. Acad. Sci. U. S. A. *116*, 8289–8294.

Kuo, W.T., Yu, S.Y., Li, S.C., Lam, H.C., Chang, H.T., Chen, W.S., Yeh, C.Y., Hung, S.F., Liu, T.C., Wu, T., et al. (2016). Microrna-324 in human cancer: Mir-324-5p and mir-324-3p have distinct biological functions in human cancer. Anticancer Res. *36*, 5189–5196.

Łabno, A., Warkocki, Z., Kuliński, T., Krawczyk, P.S., Bijata, K., Tomecki, R., & Dziembowski, A. (2016). Perlman syndrome nuclease DIS3L2 controls cytoplasmic non-coding RNAs and provides surveillance pathway for maturing snRNAs. Nucleic Acids Res. gkw649.

Lam, J.K.W., Chow, M.Y.T., Zhang, Y., & Leung, S.W.S. (2015). siRNA versus miRNA as therapeutics for gene silencing. Mol. Ther. - Nucleic Acids *4*, e252.

Landgraf, P., Rusu, M., Sheridan, R., Sewer, A., Iovino, N., Aravin, A., Pfeffer, S., Rice, A., Kamphorst, A.O., Landthaler, M., et al. (2007). A mammalian microRNA expression atlas based on small RNA library sequencing. Cell *129*, 1401–1414.

Langenberger, D., ??akir, M.V., Hoffmann, S., & Stadler, P.F. (2013). Dicer-Processed Small RNAs: Rules and Exceptions. J. Exp. Zool. Part B Mol. Dev. Evol. *320*, 35–46.

Lee, Y.S. (2015). A Novel Type of Non-coding RNA, nc886, Implicated in Tumor Sensing and Suppression. Genomics Inform. *13*, 26–30.

Lee, E.K., Hong, S.H., Shin, S., Lee, H.S., Lee, J.S., Park, E.J., Choi, S.S., Min, J.W., Park, D., Hwang, J.A., et al. (2016). Nc886, a non-coding RNA and suppressor of PKR, exerts an oncogenic function in thyroid cancer. Oncotarget *7*, 75000–75012.

Lee, H.-S., Lee, K., Jang, H.-J., Lee, G.K., Park, J.-L., Kim, S.-Y., Kim, S.-B., Johnson, B.H., Zo, J.I., Lee, J.-S., et al.

(2014a). Epigenetic silencing of the non-coding RNA nc886 provokes oncogenes during human esophageal tumorigenesis. Oncotarget *5*, 3472–3481.

Lee, K.-S., Park, J.-L., Lee, K., Richardson, L.E., Johnson, B.H., Lee, H.-S., Lee, J.-S., Kim, S.-B., Kwon, O.-H., Song, K.S., et al. (2014b). nc886, a non-coding RNA of anti-proliferative role, is suppressed by CpG DNA methylation in human gastric cancer. Oncotarget *5*, 3944–3955.

Lee, K., Kunkeaw, N., Jeon, S.H., Lee, I., Johnson, B.H., Kang, G.-Y., Bang, J.Y., Park, H.S., Leelayuwat, C., & Lee, Y.S. (2011). Precursor miR-886, a novel noncoding RNA repressed in cancer, associates with PKR and modulates its activity. RNA *17*, 1076–1089.

Lee, K.S., Shin, S., Cho, E., Im, W.K., Jeon, S.H., Kim, Y., Park, D., Fréchet, M., Chajra, H., & Jung, E. (2019a). nc886, a non-coding RNA, inhibits UVB-induced MMP-9 and COX-2 expression via the PKR pathway in human keratinocytes. Biochem. Biophys. Res. Commun. *512*, 647–652.

Lee, R.C., Feinbaum, R.L., & Ambros, V. (1993). The C. elegans heterochronic gene lin-4 encodes small RNAs with antisense complementarity to lin-14. Cell *75*, 843–854.

Lee, Y.S., Kunkeaw, N., & Lee, Y.S. (2019b). Protein kinase R and its cellular regulators in cancer: An active player or a surveillant? Wiley Interdiscip. Rev. RNA e1558.

Lei, J., Xiao, J.H., Zhang, S.H., Liu, Z.Q., Huang, K., Luo, Z.P., Xiao, X.L., & Hong, Z.D. (2017). Non-coding RNA 886 promotes renal cell carcinoma growth and metastasis through the Janus kinase 2/signal transducer and activator of transcription 3 signaling pathway. Mol. Med. Rep. *16*, 4273–4278.

Leinonen, R., Sugawara, H., & Shumway, M. (2011). The sequence read archive. Nucleic Acids Res. *39*.

Leite, K.R.M., Reis, S.T., Viana, N., Morais, D.R., Moura, C.M., Silva, I.A., Pontes, J., Katz, B., & Srougi, M. (2015). Controlling RECK miR21 promotes tumor cell invasion and is related to biochemical recurrence in prostate cancer. J. Cancer *6*, 292–301.

Li, C.C.Y., Eaton, S.A., Young, P.E., Lee, M., Shuttleworth, R., Humphreys, D.T., Grau, G.E., Combes, V., Bebawy, M., Gong, J., et al. (2013). Glioma microvesicles carry selectively packaged coding and non-coding RNAs which alter gene expression in recipient cells. RNA Biol. *10*, 1333–1344.

Li, F., Chen, Y., Zhang, Z., Ouyang, J., Wang, Y., Yan, R., Huang, S., Gao, G.F., Guo, G., & Chen, J.-L. (2015). Robust expression of vault RNAs induced by influenza A virus plays a critical role in suppression of PKR-mediated innate immunity. Nucleic Acids Res. *43*, gkv1078.

Li, J.-H., Wang, M., Zhang, R., Gao, W.-L., Meng, S.-H., Ma, X.-L., Hou, X.-H., & Feng, L.-M. (2017). E2F1-directed activation of nc886 mediates drug resistance in cervical cancer cells via regulation of major vault protein. Int. J. Clin. Exp. Pathol. *10*, 9233–9242.

Li, J.H., Xiao, X., Zhang, Y.N., Wang, Y.M., Feng, L.M., Wu, Y.M., & Zhang, Y.X. (2011). MicroRNA miR-886-5p inhibits apoptosis by down-regulating Bax expression in human cervical carcinoma cells. Gynecol. Oncol. *120*, 145–151.

Litwin, M.S., & Tan, H.J. (2017). The diagnosis and treatment of prostate cancer: A review. JAMA - J. Am. Med. Assoc. *317*, 2532–2542.

Liu, C., Iqbal, J., Teruya-Feldstein, J., Shen, Y., Dabrowska, M.J., Dybkaer, K., Lim, M.S., Piva, R., Barreca, A., Pellegrino, E., et al. (2013). MicroRNA expression profiling identifies molecular signatures associated with anaplastic large cell lymphoma. Blood *122*, 2083–2092.

Lunavat, T.R., Cheng, L., Kim, D.K., Bhadury, J., Jang, S.C., Lässer, C., Sharples, R.A., López, M.D., Nilsson, J., Gho, Y.S., et al. (2015). Small RNA deep sequencing discriminates subsets of extracellular vesicles released by melanoma cells – Evidence of unique microRNA cargos. RNA Biol. *12*, 810–823.

Ma, H., Wang, M., Zhou, Y., Yang, J. jie, Wang, L.Y., Yang, R. hui, Wen, M. jie, & Kong, L. (2020). Noncoding RNA 886 alleviates tumor cellular immunological rejection in host C57BL/C mice. Cancer Med. *9*, 5258–5271.

Mahishi, L.H., Hart, R.P., Lynch, D.R., & Ratan, R.R. (2012). miR-886-3p Levels Are Elevated in Friedreich Ataxia. J. Neurosci. *32*, 9369–9373.

Marshall, E.A., Sage, A.P., Ng, K.W., Martinez, V.D., Firmino, N.S., Bennewith, K.L., & Lam, W.L. (2017). Small non-coding RNA transcriptome of the NCI-60 cell line panel. Sci. Data *4*, 170157.

Martens-Uzunova, E.S., Jalava, S.E., Dits, N.F., van Leenders, G.J.L.H., Møller, S., Trapman, J., Bangma, C.H., Litman, T., Visakorpi, T., & Jenster, G. (2012). Diagnostic and prognostic signatures from the small non-coding RNA transcriptome in prostate cancer. Oncogene *31*, 978–991.

Mashima, T., Kudo, M., Takada, Y., Matsugami, A., Gopinath, S.C.B., Kumar, P.K.R., & Katahira, M. (2008). Interactions between antitumor drugs and vault RNA. Nucleic Acids Symp. Ser. (Oxf). 217–218.

Matoso, A., & Epstein, J.I. (2019). Defining clinically significant prostate cancer on the basis of pathological findings. Histopathology *74*, 135–145.

McCall, M.N., Kim, M.S., Adil, M., Patil, A.H., Lu, Y., Mitchell, C.J., Leal-Rojas, P., Xu, J., Kumar, M., Dawson, V.L., et al. (2017). Toward the human cellular microRNAome. Genome Res. *27*, 1769–1781.

McDonald, A.C., Vira, M., Walter, V., Shen, J., Raman, J.D., Sanda, M.G., Patil, D., & Taioli, E. (2019). Circulating microRNAs in plasma among men with low-grade and high-grade prostate cancer at prostate biopsy. Prostate *79*, 961–968.

McElhinney, J.M.W.R., Hasan, A., & Sajini, A.A. (2020). The epitranscriptome landscape of small noncoding RNAs in stem cells. Stem Cells.

Meng, C., Meng, C., Wei, Z., Wei, Z., Zhang, Y., Zhang, Y., Yan, L., Yan, L., He, H., He, H., et al. (2016). Regulation of cytochrome P450 3A4 by small vault RNAb derived from the non-coding vault RNA1 of multidrug resistance-linked vault particle (D.A. Spandidos).

Mercatelli, N., Coppola, V., Bonci, D., Miele, F., Costantini, A., Guadagnoli, M., Bonanno, E., Muto, G., Frajese, G.V., De Maria, R., et al. (2008). The inhibition of the highly expressed mir-221 and mir-222 impairs the growth of prostate carcinoma xenografts in mice. PLoS One *3*.

Miñones-Moyano, E., Friedländer, M.R., Pallares, J., Kagerbauer, B., Porta, S., Escaramís, G., Ferrer, I., Estivill, X., & Martí, E. (2013). Upregulation of a small vault RNA (svtRNA2-1a) is an early event in Parkinson disease and induces neuronal dysfunction. RNA Biol. *10*, 1093–1106.

Motulsky, H.J., & Brown, R.E. (2006). Detecting outliers when fitting data with nonlinear regression - A new method based on robust nonlinear regression and the false discovery rate. BMC Bioinformatics *7*, 123.

Mouraviev, V., Lee, B., Patel, V., Albala, D., Johansen, T.E.B., Partin, A., Ross, A., & Perera, R.J. (2016). Clinical prospects of long noncoding RNAs as novel biomarkers and therapeutic targets in prostate cancer. Prostate Cancer Prostatic Dis. *19*, 14–20.

Mrazek, J., Kreutmayer, S.B., Grasser, F.A., Polacek, N., & Huttenhofer, A. (2007). Subtractive hybridization

identifies novel differentially expressed ncRNA species in EBV-infected human B cells. Nucleic Acids Res. *35*, e73–e73.

Nandy, C., Mrázek, J., Stoiber, H., Grässer, F.A., Hüttenhofer, A., & Polacek, N. (2009). Epstein-Barr Virus-Induced Expression of a Novel Human Vault RNA. J. Mol. Biol. *388*, 776–784.

Nikitina, T. V, Tischenko, L.I., & Schulz, W.A. (2011). Recent insights into regulation of transcription by RNA polymerase III and the cellular functions of its transcripts. Biol. Chem. *392*, 395–404.

Nolte'T Hoen, E.N.M., Buermans, H.P.J., Waasdorp, M., Stoorvogel, W., Wauben, M.H.M., & 'T Hoen, P.A.C. (2012). Deep sequencing of RNA from immune cell-derived vesicles uncovers the selective incorporation of small non-coding RNA biotypes with potential regulatory functions. Nucleic Acids Res. *40*, 9272–9285.

Nordentoft, I., Birkenkamp-Demtroder, K., Agerbæk, M., Theodorescu, D., Ostenfeld, M.S., Hartmann, A., Borre, M., Ørntoft, T.F., & Dyrskjøt, L. (2012). miRNAs associated with chemo-sensitivity in cell lines and in advanced bladder cancer. BMC Med. … *5*, 40.

Okumura, T., Kojima, H., Miwa, T., Sekine, S., Hashimoto, I., Hojo, S., Nagata, T., & Shimada, Y. (2016). The expression of microRNA 574-3p as a predictor of postoperative outcome in patients with esophageal squamous cell carcinoma. World J. Surg. Oncol. *14*, 228.

Ortega-García, M.B., Mesa, A., Moya, E.L.J., Rueda, B., Lopez-Ordoño, G., García, J.Á., Conde, V., Redondo-Cerezo, E., Lopez-Hidalgo, J.L., Jiménez, G., et al. (2020). Uncovering tumour heterogeneity through PKR and nc886 analysis in metastatic colon cancer patients treated with 5-FU-based chemotherapy. Cancers (Basel). *12*.

Pardini, B., Sabo, A.A., Birolo, G., & Calin, G.A. (2019). Noncoding rnas in extracellular fluids as cancer biomarkers: The new frontier of liquid biopsies. Cancers (Basel). *11*.

Park, J.-E., Heo, I., Tian, Y., Simanshu, D.K., Chang, H., Jee, D., Patel, D.J., & Kim, V.N. (2011). Dicer recognizes the 5' end of RNA for efficient and accurate processing. Nature *475*, 201–205.

Park, J.-L., Lee, Y.-S., Kunkeaw, N., Kim, S.-Y., Kim, I.-H., & Lee, Y.S. (2017). Epigenetic regulation of noncoding RNA transcription by mammalian RNA polymerase III. Epigenomics *9*, 171–187.

Perfetti, A., Greco, S., Bugiardini, E., Cardani, R., Gaia, P., Gaetano, C., Meola, G., & Martelli, F. (2014). Plasma microRNAs as biomarkers for myotonic dystrophy type 1. Neuromuscul. Disord. *24*, 509–515.

Persson, H., Kvist, A., Vallon-Christersson, J., Medstrand, P., Borg, A., & Rovira, C. (2009). The non-coding RNA of the multidrug resistance-linked vault particle encodes multiple regulatory small RNAs. Nat. Cell Biol. *11*, 1268–1271.

Pierce, G.B. (Gordon B., Shikes, R., & Fink, L.M. (1978). Cancer : a problem of developmental biology.

Pillai, M.M., Yang, X., Balakrishnan, I., Bemis, L., & Torok-Storb, B. (2010). MiR-886-3p Down Regulates CXCL12 (SDF1) Expression in Human Marrow Stromal Cells. PLoS One *5*, e14304.

Pritzlaff, M., Tian, Y., Reineke, P., Stuenkel, A.J., Allen, K., Gutierrez, S., Jackson, M., Dolinsky, J.S., LaDuca, H., Xu, J., et al. (2020). Diagnosing hereditary cancer predisposition in men with prostate cancer. Genet. Med.

Pundhir, S., & Gorodkin, J. (2015a). Differential and coherent processing patterns from small RNAs. Sci. Rep. *5*, 12062.

Pundhir, S., & Gorodkin, J. (2015b). Differential and coherent processing patterns from small RNAs.

Quévillon Huberdeau, M., & Simard, M.J. (2019). A guide to microRNA-mediated gene silencing. FEBS J. *286*, 642–652.

Rau, A., Gallopin, M., Celeux, G., & Jaffrézic, F. (2013). Data-based filtering for replicated high-throughput transcriptome sequencing experiments. Bioinformatics *29*, 2146–2152.

Richmond, R.C., Sharp, G.C., Herbert, G., Atkinson, C., Taylor, C., Bhattacharya, S., Campbell, D., Hall, M., Kazmi, N., Gaunt, T., et al. (2018). The long-term impact of folic acid in pregnancy on offspring DNA methylation: follow-up of the Aberdeen Folic Acid Supplementation Trial (AFAST). Int. J. Epidemiol.

Robinson, M.D., & Oshlack, A. (2010). A scaling normalization method for differential expression analysis of RNA-seq data. Genome Biol. *11*.

Robinson, M.D., McCarthy, D.J., & Smyth, G.K. (2010). edgeR: a Bioconductor package for differential expression analysis of digital gene expression data. Bioinformatics *26*, 139–140.

Romanelli, V., Nakabayashi, K., Vizoso, M., Moran, S., Iglesias-Platas, I., Sugahara, N., Simón, C., Hata, K., Esteller, M., Court, F., et al. (2014). Variable maternal methylation overlapping the nc886/vtRNA2-1 locus is locked between hypermethylated repeats and is frequently altered in cancer. Epigenetics *9*, 783–790.

Romano, G., Veneziano, D., Acunzo, M., & Croce, C.M. (2017). Small non-coding RNA and cancer. Carcinogenesis *38*, 485–491.

Rupaimoole, R., & Slack, F.J. (2017). MicroRNA therapeutics: Towards a new era for the management of cancer and other diseases. Nat. Rev. Drug Discov. *16*, 203–221.

Sajini, A.A., Choudhury, N.R., Wagner, R.E., Bornelöv, S., Selmi, T., Spanos, C., Dietmann, S., Rappsilber, J., Michlewski, G., & Frye, M. (2019). Loss of 5-methylcytosine alters the biogenesis of vault-derived small RNAs to coordinate epidermal differentiation. Nat. Commun. *10*.

Sartor, O., & De Bono, J.S. (2018). Metastatic prostate cancer. N. Engl. J. Med. *378*, 645–657.

Schaefer, A., Jung, M., Mollenkopf, H.-J., Wagner, I., Stephan, C., Jentzmik, F., Miller, K., Lein, M., Kristiansen, G., & Jung, K. (2009). Diagnostic and prognostic implications of microRNA profiling in prostate carcinoma. Int. J. Cancer NA-NA.

Schaefer, A., Stephan, C., Busch, J., Yousef, G.M., & Jung, K. (2010). Diagnostic, prognostic and therapeutic implications of microRNAs in urologic tumors. Nat. Rev. Urol. *7*, 286–297.

Scheffer, G.L., Wijngaard, P.L.J., Flens, M.J., Izquierdo, M.A., Slovak, M.L., Pinedo, H.M., Meijer, C.J.L.M., Clevers, H.C., & Scheper, R.J. (1995). The drug resistance-related protein LRP is the human major vault protein. Nat. Med. *1*, 578–582.

Schmiedel, J.M., Klemm, S.L., Zheng, Y., Sahay, A., Blüthgen, N., Marks, D.S., & Van Oudenaarden, A. (2015). MicroRNA control of protein expression noise. Science (80-.). *348*, 128–131.

Schou, J. V., Rossi, S., Jensen, B. V., Nielsen, D.L., Pfeiffer, P., Høgdall, E., Yilmaz, M., Tejpar, S., Delorenzi, M., Kruhøffer, M., et al. (2014). miR-345 in Metastatic Colorectal Cancer: A Non-Invasive Biomarker for Clinical Outcome in Non-KRAS Mutant Patients Treated with 3rd Line Cetuximab and Irinotecan. PLoS One *9*, e99886.

Seok, H., Ham, J., Jang, E.S., & Chi, S.W. (2016). MicroRNA target recognition: Insights from transcriptome-wide non-canonical interactions. Mol. Cells *39*, 375–381.

Shappell, S.B., Thomas, G. V., Roberts, R.L., Herbert, R., Ittmann, M.M., Rubin, M.A., Humphrey, P.A., Sundberg,

J.P., Rozengurt, N., Barrios, R., et al. (2004). Prostate Pathology of Genetically Engineered Mice: Definitions and Classification. The Consensus Report from the Bar Harbor Meeting of the Mouse Models of Human Cancer Consortium Prostate Pathology Committee. In Cancer Research, (Cancer Res), pp. 2270–2305.

Shen, J., Zhou, W., Bi, N., Song, Y.-M., Zhang, F.-Q., Zhan, Q.-M., & Wang, L.-H. (2018). MicroRNA-886-3P functions as a tumor suppressor in small cell lung cancer. Cancer Biol. Ther. *19*, 1185–1192.

Silver, M.J., Kessler, N.J., Hennig, B.J., Dominguez-Salas, P., Laritsky, E., Baker, M.S., Coarfa, C., Hernandez-Vargas, H., Castelino, J.M., Routledge, M.N., et al. (2015). Independent genomewide screens identify the tumor suppressor VTRNA2-1 as a human epiallele responsive to periconceptional environment. Genome Biol *16*, 118.

Stadler, P.F., Chen, J.J.L., Hackermüller, J., Hoffmann, S., Horn, F., Khaitovich, P., Kretzschmar, A.K., Mosig, A., Prohaska, S.J., Qi, X., et al. (2009). Evolution of vault RNAs. Mol. Biol. Evol. *26*, 1975–1991.

Starega-Roslan, J., Koscianska, E., Kozlowski, P., & Krzyzosiak, W.J. (2011). The role of the precursor structure in the biogenesis of microRNA. Cell. Mol. Life Sci. *68*, 2859–2871.

Subramaniam, S., Jeet, V., Clements, J.A., Gunter, J.H., & Batra, J. (2019). Emergence of microRNAs as key players in cancer cell metabolism. Clin. Chem. *65*, 1090–1101.

Tahiri, A., Leivonen, S.K., Lüders, T., Steinfeld, I., Aure, M.R., Geisler, J., Mäkelä, R., Nord, S., Riis, M.L.H., Yakhini, Z., et al. (2014). Deregulation of cancer-related miRNAs is a common event in both benign and malignant human breast tumors. Carcinogenesis *35*, 76–85.

Takamizawa, J., Konishi, H., Yanagisawa, K., Tomida, S., Osada, H., Endoh, H., Harano, T., Yatabe, Y., Nagino, M., Nimura, Y., et al. (2004). Reduced expression of the let-7 microRNAs in human lung cancers in association with shortened postoperative survival. Cancer Res. *64*, 3753–3756.

Tomlins, S.A., Mehra, R., Rhodes, D.R., Cao, X., Wang, L., Dhanasekaran, S.M., Kalyana-Sundaram, S., Wei, J.T., Rubin, M.A., Pienta, K.J., et al. (2007). Integrative molecular concept modeling of prostate cancer progression. Nat. Genet. *39*, 41–51.

Tosar, J.P., Gambaro, F., Sanguinetti, J., Bonilla, B., Witwer, K.W., & Cayota, A. (2015). Assessment of small RNA sorting into different extracellular fractions revealed by high-throughput sequencing of breast cell lines. Nucleic Acids Res. *43*, 5601–5616.

Treppendahl, M.B., Qiu, X., Søgaard, A., Yang, X., Nandrup-Bus, C., Hother, C., Andersen, M.K., Kjeldsen, L., Möllgaard, L., Hellström-Lindberg, E., et al. (2012). Allelic methylation levels of the noncoding VTRNA2-1 located on chromosome 5q31.1 predict outcome in AML. Blood *119*, 206–216.

Tsai, K.-W., Leung, C.-M., Lo, Y.-H., Chen, T.-W., Chan, W.-C., Yu, S.-Y., Tu, Y.-T., Lam, H.-C., Li, S.-C., Ger, L.-P., et al. (2016). Arm Selection Preference of MicroRNA-193a Varies in Breast Cancer. Nat. Publ. Gr.

Ustianenko, D., Pasulka, J., Feketova, Z., Bednarik, L., Zigackova, D., Fortova, A., Zavolan, M., & Vanacova, S. (2016). TUT-DIS3L2 is a mammalian surveillance pathway for aberrant structured non-coding RNAs. EMBO J. *35*, 2179–2191.

Vachon, V.K., Calderon, B.M., & Conn, G.L. (2015). A novel RNA molecular signature for activation of 2'-5' oligoadenylate synthetase-1. Nucleic Acids Res. *43*, 544–552.

Varambally, S., Cao, Q., Mani, R.S., Shankar, S., Wang, X., Ateeq, B., Laxman, B., Cao, X., Jing, X., Ramnarayanan, K., et al. (2008). Genomic loss of microRNA-101 leads to overexpression of histone methyltransferase EZH2 in cancer. Science (80-.). *322*, 1695–1699.

Vickers, K.C., Roteta, L.A., Hucheson-Dilks, H., Han, L., & Guo, Y. (2015). Mining diverse small RNA species in the deep transcriptome. Trends Biochem. Sci. *40*, 4–7.

Vilalta, A., Kickhoefer, V.A., Rome, L.H., & Johnson, D.L. (1994). The rat vault RNA gene contains a unique RNA polymerase III promoter composed of both external and internal elements that function synergistically. J. Biol. Chem. *269*, 29752–29759.

Volinia, S., & Croce, C.M. (2013). Prognostic microRNA/mRNA signature from the integrated analysis of patients with invasive breast cancer. Proc. Natl. Acad. Sci. U. S. A. *110*, 7413–7417.

Wang, D., Qiu, C., Zhang, H., Wang, J., Cui, Q., & Yin, Y. (2010). Human MicroRNA oncogenes and tumor suppressors show significantly different biological patterns: From functions to targets. PLoS One *5*, 1–7.

Wang, J., Lee, J.E., Riemondy, K., Yu, Y., Marquez, S.M., Lai, E.C., & Yi, R. (2020). XPO5 promotes primary miRNA processing independently of RanGTP. Nat. Commun. *11*, 1–17.

Wang, Z., Zhou, D., Cao, Y., Hu, Z., Zhang, S., Bian, Y., Hou, Y., & Li, C. (2016). Characterization of microRNA expression profiles in blood and saliva using the Ion Personal Genome Machine ® System (Ion PGM™ System). Forensic Sci. Int. Genet. *20*, 140–146.

Weidle, U.H., Epp, A., Birzele, F., & Brinkmann, U. (2019). The functional role of prostate cancer metastasis-related Micro-RNAs. Cancer Genomics and Proteomics *16*, 1–19.

Wilczynska, A., & Bushell, M. (2015). The complexity of miRNA-mediated repression. Cell Death Differ. *22*, 22–33.

Wilusz, J.E., Sunwoo, H., & Spector, D.L. (2009). Long noncoding RNAs: functional surprises from the RNA world. Genes Dev. *23*, 1494–1504.

Winter, J., Jung, S., Keller, S., Gregory, R.I., & Diederichs, S. (2009). Many roads to maturity: MicroRNA biogenesis pathways and their regulation. Nat. Cell Biol. *11*, 228–234.

Witte, J.S. (2009). Prostate cancer genomics: Towards a new understanding. Nat. Rev. Genet. *10*, 77–82.

Xiang, P., Liu, Y., Liu, L., Lin, Q., Liu, X., Zhang, H., Xu, J., & Fang, B. (2019). The Biological Function and Clinical Significance of MIR-886-5p in Multiple Myeloma. Acta Haematol. *142*, 208–216.

Xiao, W., Bao, Z.X., Zhang, C.Y., Zhang, X.Y., Shi, L.J., Zhou, Z.T., & Jiang, W.W. (2012). Upregulation of miR-31* is negatively associated with recurrent/newly formed oral leukoplakia. PLoS One *7*.

Xiong, Y., Zhang, L., Holloway, A.K., Wu, X., Su, L., & Kebebew, E. (2011). MiR-886-3p regulates cell proliferation and migration, and is dysregulated in familial non-medullary thyroid cancer. PLoS One *6*, 1–11.

Yeganeh, M., & Hernandez, N. (2020). RNA polymerase III transcription as a disease factor. Genes Dev. *34*, 865–882.

Yu, M.C., Lee, C.W., Lin, C.H., Wu, C.H., Lee, Y.S., Tsai, C.L., & Tsai, C.N. (2020). Differential hypermethylation of the VTRNA2-1 promoter in hepatocellular carcinoma as a prognostic factor: Tumor marker prognostic study. Int. J. Surg. *79*, 282–289.

Yu, X.F., Zou, J., Bao, Z.J., & Dong, J. (2011). miR-93 suppresses proliferation and colony formation of human colon cancer stem cells. World J Gastroenterol *17*, 4711–4717.

Yu, Z., Chen, D., Su, Z., Li, Y., Yu, W., Zhang, Q., Yang, L., Li, C., Yang, S., Ni, L., et al. (2014). miR-886-3p upregulation in clear cell renal cell carcinoma regulates cell migration, proliferation and apoptosis by targeting PITX1. Int. J.

Mol. Med. *34*, 1409–1416.

Yuan, T., Huang, X., Woodcock, M., Du, M., Dittmar, R., Wang, Y., Tsai, S., Kohli, M., Boardman, L., Patel, T., et al. (2016). Plasma extracellular RNA profiles in healthy and cancer patients. Sci. Rep. *6*, 19413.

Zhang, C., Zhang, C., Wang, Q., Li, Z., Lin, J., & Wang, H. (2020). Differences in Stage of Cancer at Diagnosis, Treatment, and Survival by Race and Ethnicity Among Leading Cancer Types. JAMA Netw. Open *3*, e202950.

Zhang, L.-L., Wu, J., Liu, Q., Zhang, Y., Sun, Z.-L., & Jing, H. (2014). MiR-886-5p inhibition inhibits growth and induces apoptosis of MCF7 cells. Asian Pac. J. Cancer Prev. *15*, 1511–1515.

Zhang, X., Zhong, Y., Taylor, N., & Xu, X. (2019). Family history of prostate cancer and age-related trend of testosterone levels among US males: NHANES 2003–2004. Andrology *7*, 288–292.

van Zon, A., Mossink, M.H., Schoester, M., Scheffer, G.L., Scheper, R.J., Sonneveld, P., & Wiemer, E.A. (2001). Multiple human vault RNAs. Expression and association with the vault complex. J. Biol. Chem. *276*, 37715–37721.

Van Zon, A., Mossink, M.H., Scheper, R.J., Sonneveld, P., & Wiemer, E.A.C. (2003). The vault complex. Cell. Mol. Life Sci. *60*, 1828–1837.